Universität Augsburg
Mathematisch-Naturwissenschaftliche
Fakultät

Biomaterials Properties of Polymer Brush and Plasma Polymer Coatings

Dissertation zur Erlangung des Doktorgrades der Mathematisch-Naturwissenschaftlichen Fakultät der Universität Augsburg

vorgelegt von
Annina Marie Steinbach
30. Januar 2014

Mündliche Prüfung abgelegt am 30. April 2014

Erster Gutachter: Prof. Dr. Dirk Volkmer
Lehrstuhl für Festkörperchemie und Materialwissenschaften, Institut für Physik, Universität Augsburg

Zweite Gutachterin: Prof. Dr. Anita Ignatius
Institut für Unfallchirurgische Forschung und Biomechanik, Universität Ulm

Contents

List of Figures

List of Schemes

List of Tables

Abbreviations and Acronyms

ACC Amorphous Calcium Carbonate

ACP Amorphous Calcium Phosphate

AFM Atomic Force Microscopy

AIBN Azobisisobutyronitrile

ALP Alkaline Phosphatase

ATR-IR Attenuated Total Reflectance Infrared Spectroscopy

ATRP Atom Transfer Radical Polymerisation

BCP Biphasic Calcium Phosphate

bpy 2,2'-Bipyridyl

BMP Bone Morphogenetic Protein

BSP Bone Sialoprotein

CaP Calcium Phosphate

CDHA Carbonated/Calcium Deficient Hydroxylapatite

COL I Type I Collagen

DCPA Dicalcium Phosphate Anhydrate

DCPD Dicalcium Phosphate Dihydrate

DIC Differential Interference Contrast

DMF *N*,*N*-Dimethyl Formamide

ECM Extracellular Matrix

EDTA Ethylene Diamine Tetraacetic Acid

EDX Energy-Dispersive X-ray Spectroscopy

ESEM Environmental Scanning Electron Microscopy

FAP Fluorapatite

FCS Fetal Calf Serum

FFT Fast Fourier Transform

GMA Glycidyl Methacrylate

HA Hydroxylapatite

hMSC Human Mesenchymal Stem Cell

HOPG Highly Oriented Pyrolytic Graphite

HR-SEM High Resolution Scanning Electron Microscope

ICP-OES Inductively Coupled Plasma Optical Emission Spectrometry

IR Infrared Spectroscopy

LCST Lower Critical Solution Temperature

METAC 2-(Methacryloyloxy)ethyl Trimethylammonium Chloride

microCP Micro Contact Printing

MMA Methyl Methacrylate

MSC Mesenchymal Stem Cell

NaMA Sodium Methacrylate

NMP Nitroxide Mediated Polymerisation

NMR Nuclear Magnetic Resonance

OCP Octacalcium Phosphate

OEG Oligo(Ethylene Glycol)

OEGMA Oligo([Ethylene Glycol] Methacrylate)

OTES Octyltriethoxysilane

PAA Poly Acrylic Acid

PBS Phosphate Buffered Saline

PDMAEMA Poly(Dimethylaminoethyl Methacrylate)

PDMS Poly(Dimethyl Silane)

PE Poly(Ethylene)

PE-CVD Plasma Enhanced Chemical Vapour Deposition

PEG Poly(Ethylene Glycol)

PHEMA Poly(2-Hydroxyethyl Methycrylate)

PILP Polymer Induced Liquid Precursor

PNIPAm Poly(*N*-Isopropylacrylamide)

PMAA Poly(Methacrylic Acid)

PMETAC Poly(2-[Methacryloyloxy]Ethyl Trimethylammonium Chloride)

PMI *N*-(2,6-Diisopropylphenyl)Perylene-3,4-Dicarbonacidimid

PMMA Poly(Methyl Methacrylate)

PMPC Poly(2-Methacryloyloxyethyl Phosphorylcholine)

POEGMA Poly(Oligo[Ethylene Glycol]Methacrylate)

PPEGMA Poly(Poly[Ethylene Glycol]Methacrylate)

ppH Plasma Polymerised *n*-Heptane

ppMMA Plasma Polymerised Methyl Methacrylate

PPO Poly(Propylene Oxide)

ppS Plasma Polymerised Styrene

PS Polystyrene

PSBMA Poly(*N*-[3-Sulfopropyl]-*N*-Methacryloyloxyethyl-*N*,*N*-Dimethylammonium Betaine)

PSPMA Poly(3-Sulfopropylmethacrylate)

PVPA Poly(Vinylphosphonic Acid)

RAFT Reversible Addition-Fragmentation Chain Transfer Polymerisation

RF Radio Frequency

RGD Arginine–Glycine–Aspartic Acid

ROMP Ring Opening Metathesis Polymerisation

ROP Ring Opening Polymerisation

RT-PCR Real Time Polymerase Chain Reaction

SAM Self-Assembling Monolayer

SBF Simulated Body Fluid

SBMA *N*-(3-Sulfopropyl)-*N*-Methacryloyloxyethyl-*N*,*N*-Dimethylammonium Betaine

SEM Scanning Electron Microscope

SI-ATRP Surface Initiated Atom Transfer Radical Polymerisation

SPMA Potassium 3-Sulfopropyl Methacrylate

TCP Tricalcium Phosphate

TEM Transmission Electron Microscope

THF Tetrahydrofuran

TRIS Tris(hydroxymethyl)aminomethane

VPA Vinylphosphonic Acid

XPS X-Ray Photoelectron Spectroscopy

1 Introduction – Hard Tissue Implants

Prostheses have developed much since the first attempts to substitute the "dead material" bone at the time of the Egyptian, Greek and Roman empires. Humankind has moved on from wood or gold prostheses[1] to titanium, titanium alloys and medical steel. These materials are bone replacements that fit the bill for mechanical stability and biological inertness.[2–4] However, with implants not integrating properly into the bone, it began to dawn upon many performing surgery, working with and researching implants, that bone is by no means dead material having only mechanical-structural functions but a complex living tissue.[5] Moreover, it is constantly rebuilt and remodelled to meet the requirements of the applied load.[5–9] Therefore, the ideal bone replacing material does not only have to meet the mechanical requirements but also has to integrate into the bone or – even better – actively induce bone growth around it.[3]

Data of the U.S. Bone and Joint Decade study[10] illustrate the dimensions of the implant issue. In 2006, 96 % of the almost one million joint replacement procedures in the USA were hip or knee replacements. The authors of the study predict even higher numbers for the decades to come, as people get older and lead less and less active lifestyles. Alarmingly high is the percentage of patients, who have to endure revision caused by implant failure, especially with artificial hips: Approximately 20 % of the primary hip procedures have to be revised, 2006 showing even an unusual 63 % to 65 %.

This rate indicates that titanium as the "material of choice" – as it is in some opinions[11] – can still be improved in several aspects, such as bone adhesion.[2,5] To ameliorate the material, it is essential to take a close look at the causes for implant failure. Main causes for revision surgery are[2,5,10,12,13]

- wear-out of the implant parts
- bacterial infection
- foreign body reaction.

Consequently, better implant integration into the bone and reduced bacterial infection together with the right mechanical behaviour will have a positive impact on the patients' health and overall health care costs.[2,14]

A foreign body reaction and attachment of fibroblasts to a hard tissue implant may lead to a collagenous encapsulation.[2,12,13] This process results in a loosened implant with reduced load-bearing properties likely causing implant failure.[2] Thus, it is essential that a strong contact region forms at the interface between material and bone tissue.[15] As mentioned above, this means that the host tissue should not only tolerate the implant material.[3,15] The implant should also encourage new bone formation by inducing crystallisation of bone mineral, by promoting adhesion of bone cell progenitors and/or by stimulating bone forming cells to deposit bone material.

Following the definition of Williams,[3] this active role of the biomaterial adapting to the demands of the respective tissue implies a material's biocompatibility. More common is the usage of the term biocompatible in a more passive meaning with a material being simply tolerated by the host tissue.[4,15] In these cases, authors also call for bioactive and osteoinductive materials.[5,15] Bioactivity in this context means that the material encourages the precipitation of bone mineral in a biological environment, often by releasing Ca^{2+} and PO_4^{2-} ions.[16,17] Bioactivity results in an enhanced healing process as the bone mineral (or other bioactive material) guides bone cells from the surrounding to the implant.[5,16,18] This process is called osteoconduction and provides a good contact between bone and implant material through bone growth on the implant surface.[5,16,17,19] An osteoinductive implant material even promotes the formation of new bone around the implant by newly recruited and matured bone building cells.[18–20]

1.1 Titanium Implants and Approaches Towards Improving Them

The advantages of titanium and its alloys are the mechanical stability and the good fatigue strength, the high corrosion resistance and the relative inertness.[11,21] The drawbacks of these materials occur when it comes to their longterm behaviour, when they should perform longer than 15 years.[5] The metallic implants do not seem to integrate into the bone as well as they should, they are often recognised by the organism as a foreign body and in some cases they even seem to lead to bone loss around them.[2,5,22]

As outlined above, a good hard tissue implant material should be osteoinductive or at least osteoconductive to prevent a fibrous incapsulation. On this account, a major focus of biomaterials research has been the improvement of the implant surface for interactions with the human host tissue.[23] There are several approaches to improve the healing capabilities of biomaterials by altering the physical, chemical or biological characteristics of the surface.

The physiological environment of cells consists mostly of pores and fibres on the micro- and nanoscale as seen in the basement membrane and the Extracellular Matrix (ECM).[24–26] Moreover, bone material consists of a meshwork of calcified collagen fibers. A micro- or nanotextured surface will consequently affect cell adhesion and proliferation. Bone cell attachment on titanium material was enhanced by nanostructuring the substrate by high pressure torsion.[27] The cell growth and development of bone building cells was enhanced on nanofibres of polycaprolactone and silk.[24,28,29] These nanofibers matched the size of bone mineral crystals, thus mimicking the natural surrounding of bone cells.[24]

Closely related is another important parameter – the surface roughness. On rough surfaces the distribution of focal contacts of the cell to the surface is different from the one on smooth surfaces; the focal adhesions are at the outer edges of the cell and not evenly distributed.[15] In studies, increased surface roughness affected bone building cells positively and through this roughness was anticipated to improve osseointegration.[30] Indeed, increasing the roughness of implant titanium surfaces on a micro- or nanoscale enhanced cell adhesion, integration of implants into the bone and bone formation around the implant.[31,32] The authors attributed this effect to the similarity of the surface structure to the pits that generally form in the bone remodelling process.[31] On surfaces with higher roughness bone building cells also secreted more of a protein that reduces the activity of bone resorbing cells.[30] Roughness even promoted differentiation, *i.e.* the recruitment and maturation of precursor cells into bone building cells.[33] *In vivo* experiments confirmed the cell culture results and showed that rougher implants had a better bone-implant contact.[32] As a drawback, the quantification of roughness is difficult, therefore this phenomenon seems to be quite complex. Apparently, an important aspect of surface roughness is the surface organisation with a fractal construction or some kind of structural order.[15,34]

Roughness itself influences the surface energy (or wettability), which is an additional factor to affect cell behaviour.[15,27,35] Surface energy affects protein adsorption from the omnipresent extracellular body fluid and the conformation of the adsorbed proteins.[15,33] Generally, bone cells prefer hydrophilic surfaces over hydrophobic ones.[36] Protein and cell attachment are both better on hydrophilic surfaces, as is the proliferation of the cells.[27,36–39]

During surgery the bone is unprotected by the surrounding tissue and skin, so bacteria may access the wound around the implant or may be introduced by the implant surface even when an aseptic environment is provided as in the operating rooms.[14] This issue is difficult to address from the outside as there is only a limited selection of an-

tibiotics that can penetrate bone.[40] This difficulty may be solved by the incorporation of antibiotics into implant coatings. Campbell *et al.*[41] incorporated an antibiotic in a Calcium Phosphate (CaP) coating and thus reduced bacterial growth. Zhang *et al.* covalently bound the antibiotics gentamycin or penicillin to surface bound polymer films.[14] Counter-arguments against this strategy arise from the general over-usage of antibiotics, facilitating resistent bacterial strains.[42] The strategy is also challenging, as the exact bacterial strain is not known when the implant is chosen, nor are its resistencies and susceptibilities.[40]

Bacterial growth may also be prevented by anti-fouling surfaces – just like they are used in blood contacting material. Unpropitiously, the anti-fouling surfaces would in most cases also decrease the contact area between bone and implant due to the lack of bone cell adhesion to these surfaces.[43–48] Interesting approaches towards the selective adhesion of bone cells onto bacteria resistent surfaces are made in the field of polymer brushes. These hydrophilic and highly hydrated polymer coatings block the adsorption of proteins and consequently cell adhesion in a quite unspecific way.[43–55] However, they can be functionalised with peptides or proteins promoting cell adhesion.[14,56–58] These peptide sequences and proteins enable bone cells to bind to surfaces that repel (bacterial) cells lacking the receptors for the peptides.[14,57,58]

1.2 Alternatives to Titanium Implants

Next to titanium other materials are explored as possible biomaterial for implant applications. These materials are also object of intensive research aiming at better integration of the biomaterial into bone. Some represent alternatives to the surface modification of the mechanically favourable material titanium but have their own challenges and difficulties.

Ceramics show good bioactivity, as they release the ions needed for bone mineral formation and thus bond to bone tightly.[2,18,21,32,59–61] Yet, they are brittle and thus do not meet the mechanical standards of the metal implants.[21,59,61–63] Therefore a number of techniques was developed and tested to coat the mechanically superior metal implants with the bioactive mineral.[2,22,32,60,61,64–70] The resulting (thus chemically enhanced) bonding between coating and bone was often very good.[21,32,69,71,72] On the other hand, the implant-coating interface stability is of great concern with many of these techniques.[2,61,63,69] A delaminating coating may lead to implant loosening, which in turn may lead to implant failure.[21] As a consequence, a better integrity of the coatings is sought.[61] An example for an approach to a better integrity of the coatings is synthesising thinner coatings, as thin films do not experience as much inner stress as thicker

coatings.[21]

The same problem of the poor mechanical properties of ceramics is addressed with another approach. Similar to the bone substance, the mineral is reinforced by flexible polymers to combine the properties of the two materials in one composite.[22,23,37,73–76] These composites are apt materials for certain dentistry and surgery applications,[22] but still do not match the mechanical standards of load bearing applications and biodegradable polymers pose other difficulties as they may alter the pH in their surrounding or elicit inflammatory responses.[18]

1.3 Résumé of the Current Situation

Although there are drawbacks, when it comes to titanium implants, they are still the best solution for mechanical stability in load bearing applications.[77] Until other more bioactive materials can be modified in their load bearing properties, the currently most suitable approach towards better implants is the modification of the metallic surface. Consequently, the major challenge is modifying the metal's biological properties and thus unite stability and bioactivity.[2,23,59,78] As the surface is the only area in contact with the organism, altering the surface should suffice to ameliorate the bioactivity. Surface modification was consequently the approach of this work.

1.4 Research Goal – An Approach Towards Better Implant Coatings

Striving towards better implants, polymer coatings were synthesised and tested for their potential of improving osseointegration . The approach was a multi-component one and tried to combine the excellent mechanical properties of titanium and titanium alloys as the bulk material with a coating that contained a covalently bound organic matrix mineralised with calcium phosphates. Nanoparticles were intended to be integrated into this coating, which may be loaded with pharmaceuticals to assist wound healing and bone growth.

The approach towards fabrication of these composite materials was based on the use of patterned polymer brushes as a biomimetic macromolecular matrix, the patterns being produced by UV-lithographical destruction of the surface bound initiator. Since carboxylate and sulfate functional groups of extracellular matrix molecules are essential in biomineralisation,[6,79,80] polyelectrolyte brushes with carboxylates and sulfonates as functional groups were fabricated. As an additional biomimetic functional group of the biological environment, some of the polymer brushes contained quaternary amines. The polymer matrix was covalently bound to the test surfaces aiming at overcoming the problem of delaminating coatings.

Since the polymer brushes had several disadvantages as biomaterials especially for implant applications, another technique to produce polymer coatings was introduced: Plasma Enhanced Chemical Vapour Deposition (PE-CVD). For this method, carboxyl esters or purely hydrocarbons were used as monomers in model systems. The polymerisation of the monomers took place in a low temperature plasma and produced thin plasma polymer films. UV-lithography was again the method of choice to introduce patterns by ablating the polymer in the irradiated areas. The plasma polymer coatings were not covalently bound to the substrate but good adhesion was nevertheless ensured.

Chapter 2 describes the two polymer coatings' completely differing synthesis routes, their patterning and analysis.

The pattern of the polymer brushes and plasma polymers provided convenient means to analyse the samples by Differential Interference Contrast (DIC), by profilometry and by Atomic Force Microscopy (AFM) techniques. Apart from these advantages for analysis, the patterns enabled the investigation of the influence of specific patterns formed by the polymer brushes and plasma polymers on the growth of bone cells. The group of Prof. Ignatius (Institute of Orthopaedic Research and Biomechanics, Ulm University) evaluated the cells' morphological response to the materials, their activity and their pro-

liferation ability. To assess the applicability of the coatings as biomaterial, both polymer coatings were additionally tested for their stability and behaviour in physiological conditions by immersion in Simulated Body Fluid (SBF). The experiments were conducted analogously for plasma polymers and polymer brushes to compare both coatings in their biomaterial properties. Chapter 3 discusses the question, if the polymer coatings show the right properties to be used for implant coatings.

As the main interest focused on the improvement of implant surfaces, mineralisation experiments with the bone mineral CaP were conducted as described in chapter 4. The organic matrix (polymer brushes or plasma polymers) was intended to be mineralised with CaP for a certain stealth effect and enhanced osseointegration. Therefore, different mineralisation techniques were evaluated and the mineralisation parameters optimised. The specific aim was examining the influence that the different coatings exert on the mineralisation process. Additionally, immersion in SBF evaluated the *in vitro* bioactivity, *i.e.* the mineralisation-inducing properties, of the mineralised samples and their CaP phase conversion in these simulated physiological conditions. Using an organic matrix did not only aim at a biomimetic mineralisation of the coating, it was intended to provide a covalent link or good adhesion between surface and mineral, as well. The purpose of a good bond was preventing delamination of the CaP coating from the substrate, as delamination is a concern with CaP synthesised with other methods (comp. Section 1.2).

Finally, the selective adsorption of nanoparticles to the polymer brush surfaces was investigated as described in Chapter 5. The nanoparticles were added to the coating to act as future drug carriers for bone formation enhancing agents or antibiotics. Loaded with the proper pharmaceutical agents, the nanoparticles might therefore reduce bone resorption around an implant, enhance bone deposition or work against bacterial infection (comp. Section 1.1). The experiments on nanoparticle adsorption were only conducted with the polymer brushes. Their functional groups were meant to enable the site-selective adsorption of the phosphonate functionalised nanoparticles through electrostatical and specific binding interactions.

The combination of three strategies namely

- biomimetic composition of the coating with a mineralised organic matrix,
- a good link of the coating to the substrate and
- integration of nanoparticles into the coating

was intended work on three issues of titanium implants:

- Foreign body response
- Delamination
- Bone loss and/or bacterial infection

Taken together the multi-component coatings were meant to ensure osteoblast proliferation and finally formation of new bone. The concept is summarised schematically in Figure 1.1 for the polymer brushes and in Figure 1.2 for the plasma polymers.

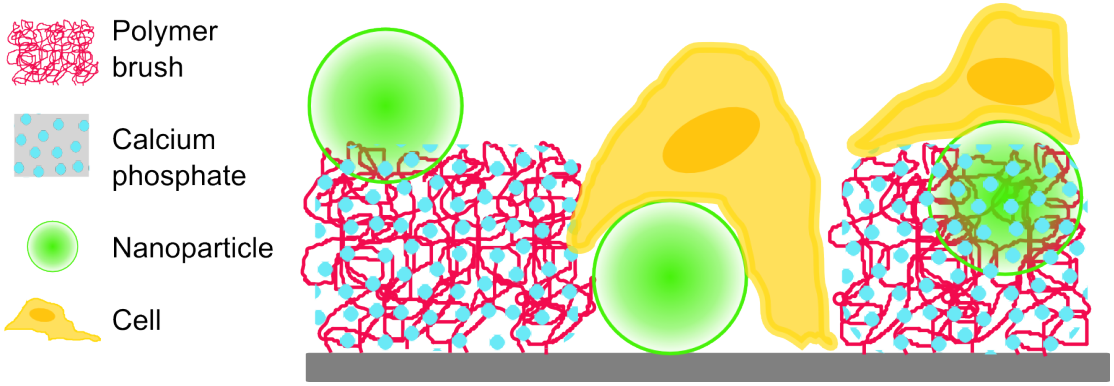

Figure 1.1: Schematic summary of multifunctional coatings intended to enhance bone growth around implants using polymer brushes as an organic matrix; the polymer brush is symbolised by the red lines, CaP by pale blue dots and the nanoparticles by the green spheres, cells are depicted in yellow. Sketch is not drawn to scale.

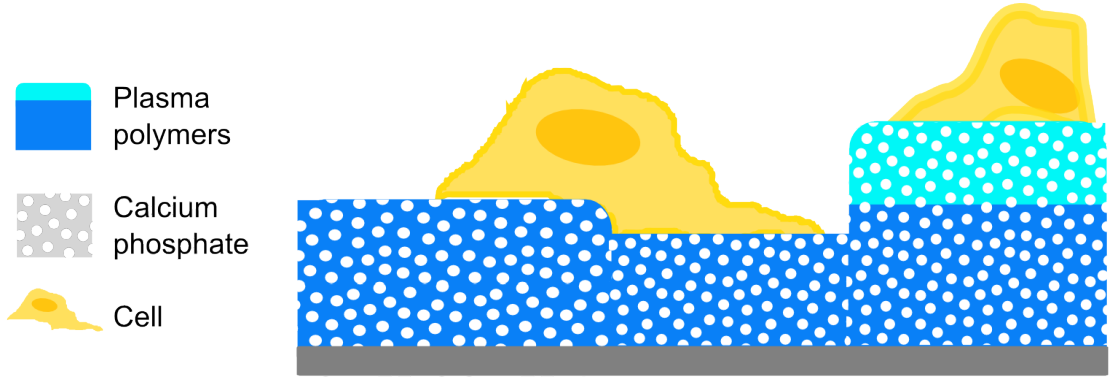

Figure 1.2: Schematic summary of the composite coatings intended to enhance bone growth around implants using plasma polymers as organic matrix for biomimetic implant coatings; the plasma polymers are represented by the blue areas, different shades symbolising different polymers, the CaP mineral is pictured as white dots and the cells in yellow. Sketch is not drawn to scale.

A graphical overview of the work is shown in Figure 1.3 placing the experiments for polymer brushes and plasma polymers next to each other for better comparison.

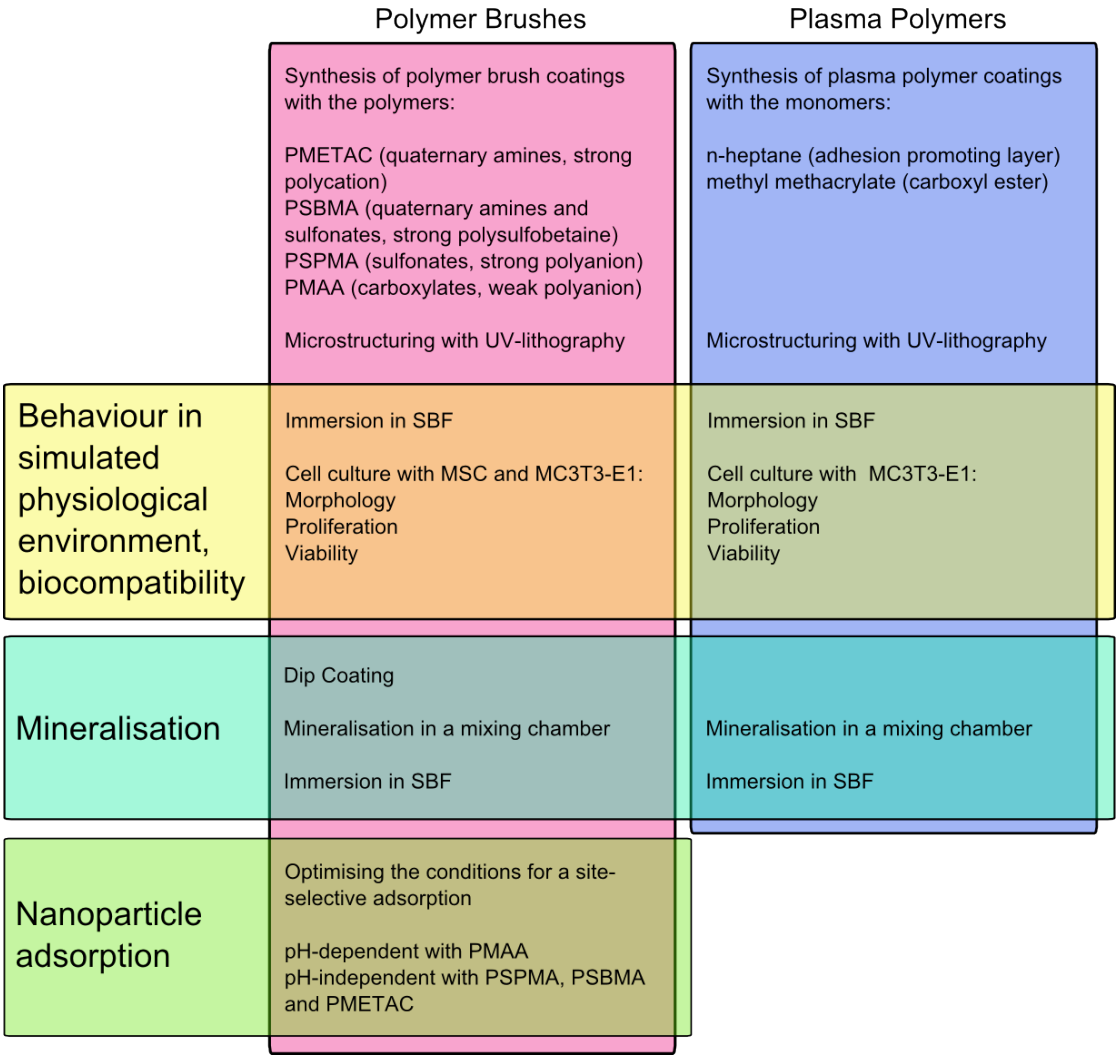

Figure 1.3: Schematic summary of the experiments conducted for this thesis investigating and comparing two different polymer coatings.

2 Patterned Polymer Thin Films – Synthesis and Characterisation*

2.1 Introduction to Patterned Polymer Thin Films

The properties of a surface differ from the ones of bulk material, as this region is the boundary to the surrounding phase. It may contain unsaturated bonds that are reactive or may be contaminated with other material.[15] The surface is also the contact area between an implant and the recipient tissue. It determines the reaction of the tissue to the implant with its chemistry and its physical properties. Thin films may therefore be used to mask the chemical characteristics of a bulk material's surface. In this work, polymer coatings with biomimetic functional groups were intended to accomplish this task in a biological environment.

The following sections describe the synthesis of these polymeric thin film coatings and their characterisation. The first part introduces the theory of thin film coatings made from polymer brushes (Section 2.1.1). To produce these polymer brushes, Surface Initiated Atom Transfer Radical Polymerisation (SI-ATRP) was the method of choice (Section 2.1.1). For the process, the substrates were cleaned and coated with a Self-Assembling Monolayer (SAM) of an appropriate initiator. The initiator layer was patterned by UV-lithography (Section 2.1.3), decomposing the initiator in the irradiated areas. The non-irradiated areas served as starting sites for the controlled polymerisation. Details of the synthesis and the patterning procedures are given in the chapter "Experimental" (Sections 7.2, 7.3 and 7.5).

*Parts of this chapter (text, experimental details and figures) have been published in ref.s 47,48,81:
Sabine Letsche, Annina Steinbach, Manuela Pluntke, Othmar Marti, Anita Ignatius, Dirk Volkmer; "Usage of polymer brushes as substrates of bone cells" *Front. Mater. Sci. China*, **2009**, *3*, 132–144,
Annina Steinbach, Andrea Tautzenberger, Anita Ignatius, Manuela Pluntke, Othmar Marti, Dirk Volkmer; "Coatings from micropatterned sulfobetaine polymer brushes as substrates for MC3T3-E1 cells" *J. Mater. Sci. Mater. Med.*, **2012**, *23*, 573–579 and
Annina Steinbach, Andrea Tautzenberger, Andreas Schaller, Andreas Kalytta-Mewes, Sebastian Tränkle, Anita Ignatius, Dirk Volkmer; "Plasma-Enhanced Chemical Vapor Deposition of *n*-Heptane and Methyl Methacrylate for Potential Cell Alignment Applications" *Appl. Mater. Interfaces*, **2012**, *4*, 5196–5203.

The second strategy to produce polymer thin films – *via* plasma polymerisation – is outlined afterwards (Section 2.1.2). The plasma polymer thin films consisted of an adhesion promoting layer made from Octyltriethoxysilane (OTES) or plasma polymerised heptane, and an outer layer formed by plasma polymerised methyl methacrylate. UV-lithography was used to introduce patterns into the plasma polymer layer by ablating the polymer in exposed areas (Section 2.1.3). A detailed description of the methods can be found in Sections 7.4 and 7.5.

2.1.1 Introduction to Polymer Brush Coatings

Polymer Brushes

Polymer brushes are defined as assemblies of macromolecules chemically tethered at one end to a substrate or interface.[82] They are closely packed and are therefore forced into a non-coiled conformation. Often the polymer brush chains are illustrated as quite stretched. However, as described below in more detail, this likely does not depict the polymer conformation properly. Picturing the polymer chain as more stretched but still looped is probably nearer the truth. Nevertheless, the unique conformation results in interesting properties of polymer brushes that differ greatly from the behaviour of the corresponding bulk material. Especially polyelectrolyte structures, *i.e.* brushes carrying charges, show special and unique properties, such as swelling behavior, complex formation, capacity of ion exchange and autophobic behavior.[82–84]

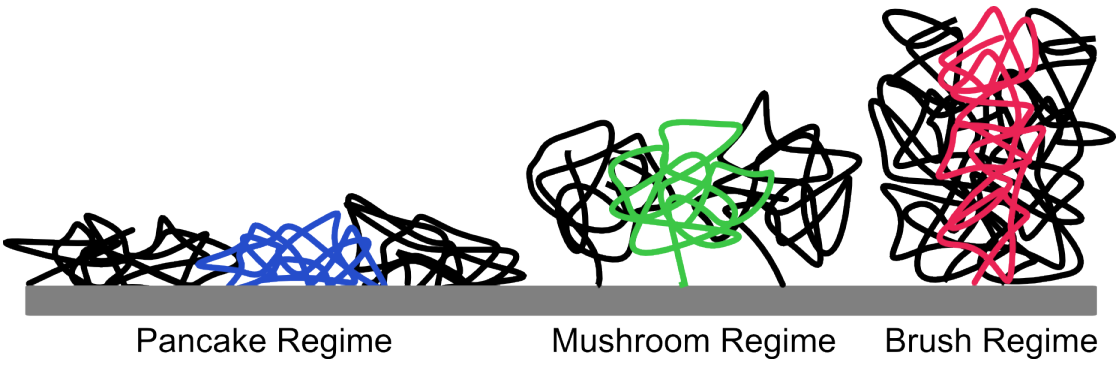

Figure 2.1: Schematic model of the conformational regimes of surface tethered polymer chains. The colours visualise the supposed conformation of a single polymer chain in the respective regime.

Surface-attached polymers can adapt different folding states: “pancake”, “mushroom” and “brush” (Figure 2.1). When the chains interact strongly with the substrate surface and they are given sufficient space (*i.e.* at low grafting densities), they typically fold

into flat "pancake"-like morphologies.[85,86] A so-called "mushroom regime" exists at low grafting densities, if the polymer chains have only weak interactions with the surface and form a random coil.[45,82,87] At higher grafting densities the polymer chains interact with each other and stretch away from the interface to avoid overlapping, thus forming a polymer "brush".[45,82,86,87] In this regime, the distance, at which two polymer chains are anchored to the surface, is smaller than the radius of gyration of the coiled polymer.[83,85]

Two methods to fabricate polymer brushes can be used: "grafting to" and "grafting from".[86] With the "grafting from" method, the synthesis of the polymer chains is at the same time the coating process — the polymer is build starting *from* the surface and growing away from it. "Grafting to" means that polymer chains, which were synthesised prior to the coating process, are deposited onto a surface and attached *to* it. For the "grafting to" approach macromolecules have to diffuse towards the surface and have to find space for adsorption. The first molecules find ample space and adapt a relaxed conformation until the gaps are too small for further adsorption, building a barrier against the adsorption of more molecules.[88] Therefore, the "grafting to" approach yields surface-tethered polymer coatings of lower densities than the "grafting from" method.[83,89]

For the "grafting from" method, not bulky polymers but small monomer molecules have to diffuse to activated initiator sites or growing polymer chains to sustain the surface initiated reaction.[90,91] Starting point is a SAM formed by the initiator molecules that comprise two important functionalities at their two ends. The one end of the initiator starts the polymerisation and therefore has to carry an appropriate group, such as a halogen for Atom Transfer Radical Polymerisation (ATRP), or an Azobisisobutyronitrile (AIBN) unit for Reversible Addition-Fragmentation Chain Transfer Polymerisation (RAFT).[89] The other end has to link the molecule to the surface, so it has to carry functional groups such as alkoxysilanes to bind to glass or silicon,[56,92–94] or thiols to bind to gold surfaces.[45,51,89] For this work, glass was chosen as the model substrate, although for an hard tissue implant application, the proper substrate would be titanium. Glass is an inexpensive abundant material and more convenient for analysis when using light and fluorescence microscopy, as it is transparent, quite in contrast to Ti and its alloys. It has been shown that the chemistry of SI-ATRP was transferable to Ti substrates by growing polymer brushes from silanised Ti substrates.[14] The silanised initiator was coupled to the OH groups of the oxide film on the surface of Ti substrates, just as to the OH-groups on the SiO_2 substrates. Therefore, the chemistry of the glass surface is comparable to the one of the titanium surface and results should be transferable.

A SAM of initiator molecules represents a dense array of possible starting points for polymerisation. The polymer chains growing in a controlled polymerisation at a similar

speed in close neighbourhood to each other (resulting in a low polydispersity) do not have the possibility to adapt a relaxed conformation and are more stretched owing to the sterical hindrance.[95] Consequently, in contrast to the "grafting to" approach, the "grafting from" polymer brushes already grow in a high density. The polymer brush chains do not have to change their conformation for a high density. Therefore the surface-initiated polymerisation approach is widely used, not only because it yields high density polymer brushes, but also because coating and polymerisation is done in one step. Another advantage is the covalent bond to the surface build by the initiator molecule promising high stability.[83] At the same time, the same wide variety of functionalised monomers is available as for the corresponding polymerisation in solution.

Important parameters for the polymer brush performance in the different application fields are molecular weight and grafting density.[44,45] The grafting density influences the conformation of the polymer determining, if mushroom or brush conformation of surface tethered polymers is prevailing.[44,96] It can control the response of charged polymers to ionic solutions.[44] Grafting density as well as molecular weight also influence the film thickness.[44,97] The higher the grafting density and the molecular weight, the thicker the film will be.[44,88] This is formulated in the following equation, which applies to surface tethered polymer films:[44,98,99]

$$h = \frac{M_W \sigma}{\rho N_A}$$

with h as the film thickness, M_W as the molecular weight, σ as the grafting density, ρ as the polymer density and N_A as the Avogadro's constant. Thus, with a constant polymer density, the film thickness increases in direct proportion with the grafting density, or with the molecular weight. In the present work, the grafting density was not varied, so the film thickness was only dependent on the molecular weight of the polymer and thus on the polymerisation time.

When the polymer is functionalised, the functional group density increases with increasing grafting density. This surface coverage and the local concentration of functional groups are major reasons for the wide possible application range of polymer brush films.[44] In addition to hydrophobic and hydrophilic moeties, charged functional groups can be introduced *via* the appropriate monomer. Introducing functional groups directly with the monomer, as it was done in the present work, gives highly functionalised and defined polymers. Thus, it is possible to synthesise polymers carrying a charged group on every segment of the chain, yielding maximally charged polyelectrolyte brushes. If the charge of a polymer chain is constant regardless of the pH of the surrounding solution, the polyelectrolyte is termed a "strong" electrolyte. Is the charge dependent on the conditions of the

solution, the polyelectrolyte is termed "weak".[83,84,98,100,101]

The charges along the polymer brush determine the responsive behaviour to different solvents. Dense and highly charged polyelectrolyte brushes as the ones synthesised and used in this work are in the so-called osmotic regime and respond to osmotic pressure counteracting the elasticity of the polymer.[84,102] In a good solvent, such as aqueous solutions in the case of polyelectrolytes, the chains are more stretched than in the dry state because of the electrostatic repulsion between the charged groups and the osmotic pressure exerted by ions and counterions that infuse into the brush.[98,102,103] Consequently, the response of the system depends on the ionic strength of the solvent and ion species in the solvent.[88,103] Hydrophilic polyelectrolyte brushes are highly hydrated, swollen and flexible in an aqueous environment with low concentrations of small ions.[103,104] High counterion concentrations on the other hand can lead to a collapse of the polyelectrolyte brush, which reduces its height drastically and gives a dense and rigid polymer layer.[82,103,104] This effect can even be irreversible, when the ions in solution allow ionic crosslinking.[104] The contrary happens, when bulky ions are in solution as they cannot infuse the brush due to steric effects and the polymer brushes stay in the swollen state.[103,104] These various conformational responses not only change the height of the polymer brushes but also other properties, such as the hydration state or wettability.[104]

Concluding, polyelectrolyte brush conformation depends in a quite complex way on the polymer's grafting density, its molecular weight, its solvent affinity, the surrounding pH and the solvent's ionic strength.[85,98] The polymer chain conformation and the brush responsiveness may itself be exploited for various applications as described in Section 2.1.4. The degree of stretched conformation, the hydration state and the wettability played a role in the present work during the interaction of bone cells with the polymer thin films (Section 3.2.2). Additionally, the pH-responsiveness of weak polymer brushes was used to control the adsorption of nanoparticles to certain areas of patterned coatings (Section 5.2.2).

Atom Transfer Radical Polymerisation

Before the development of a plethora of controlled "living" polymerisation methods, which make use of an abundance of monomers with a range of functional groups,[89] the desired functional groups were often introduced after the polymerisation.[102,105,106] These post-polymerisation modifications have the disadvantage of yielding less defined polymer films as the modifying reaction only reacts to a certain degree. For the synthesis of polymer brushes, it is therefore necessary to avail oneself of a controlled, living polymerisation technique. Whereas thick polymer coatings can be produced by the conventional free rad-

ical polymerisation, good control of the reaction is provided by the range of techniques that have been evolved to yield well-defined high-molecular-weight polymers with a narrow molecular weight distribution.[82,107,108] Among those are the Ring Opening Polymerisation (ROP), Ring Opening Metathesis Polymerisation (ROMP), living cationic and anionic polymerisation, Nitroxide Mediated Polymerisation (NMP), RAFT and ATRP.[89] ROP has quite long reaction times and ROMP can only be applied to a limited number of monomers with strained ring structures.[82,89,109,110] The living cationic polymerisation has the disadvantage of needing an initiator with a complex synthesis and harsh reaction conditions in a dry box, whereas the anionic polymerisation is slow, elaborate, extremely sensitive to impurities and limited in the range of possible monomers.[82,111,112] NMP limits the choice of substrate as it calls for high reaction temperatures.[82] It is quite ineffective and needs a parallel polymerisation in solution for a surface initiated polymerisation, as does RAFT.[89]

The most commonly used polymerisation method for the "grafting from" technique is therefore ATRP.[82,89,97,107] Compared with the other "living" polymerisation methods, ATRP represents a simple, inexpensive and widely applicable method for controlled radical polymerisation.[97] It is more tolerant towards the usage of monomers carrying functional groups than other "living" polymerisation techniques are.[89,107,108,113] Early studies of the development of the method asked for higher temperatures and dry solvents, used long polymerisation times and partly needed sacrificial initiator in solution for control.[114,115] Later, higher temperatures were found to be unnecessary.[113,114,116,117] Furthermore, the addition of water enhanced the polymerisation rate without loss of the controlled character of the reaction.[89,108,114,116,118] The freedom in choice of solvent opened up the possibility to polymerise a plethora of monomers, including hydrophobic ones.[114] Consequently, monomers with functional groups as diverse as hydrophobic Methyl Methacrylate (MMA),[119] styrene,[120] *tert*-butyl acrylate,[94,121] anionic Sodium Methacrylate (NaMA),[57,83,93,122] Potassium 3-Sulfopropyl Methacrylate (SPMA),[115,123,124] cationic 2-(Methacryloyloxy)ethyl Trimethylammonium Chloride (METAC),[88,125,126] zwitterionic *N*-(3-Sulfopropyl)-*N*-Methacryloyloxyethyl-*N*,*N*-Dimethylammonium Betaine (SBMA),[49,50,126] biologically inert hydroxyethyl methacrylate,[87,118] Oligo([Ethylene Glycol] Methacrylate) (OEGMA)[56] and even glucose-bearing 3-*O*-methacryloyl-1,2:5,6-di-*O*-isopropylidene-D-glucofuranose can be polymerised.[89,127] Nevertheless, ATRP is still not possible for a couple of monomers such as methacrylic acid or acrylic acid, as the acid functionality will poison the ATRP catalyst.[83,108] This shortcoming is alleviated by the use of charged monomers of methacrylic or acrylic acid such as sodium methacrylate or acrylate[93,113,128] or by using

protected monomers such as tert-butylacrylate, which can be subsequently pyrolysed[121] or hydrolysed using HCl.[129]

In the present work, ATRP was the method of choice to produce thin films of polyelectrolyte brushes making use of the robustness and tolerance to many functional groups. Specifically, monomers that mimic biomacromolecules were chosen with the aim to chemically mask implant surfaces to bone cells. Biomacromolecules such as proteins or polysaccharides mainly contain carboxylates, sulfates and amines. Consequently, the ATRP monomers carried a carboxyl group (NaMA), a sulfonate (SPMA), or an amine (METAC). To introduce carboxylic acid functional groups for weak polyelectrolyte brushes, NaMA was used to avoid poisoning of the catalyst. The sulfonate was chosen as the more stable analogue of the sulfate. The amine in METAC also differed from the biological moiety in its being a quaternary one, but had the advantage of a stable and pH independent charge. As a fourth monomer, SBMA was adopted as a zwitterion containing both the sulfonate and the amine group. Zwitterions are found mainly in the cell membrane and promised interesting properties as a surface coating.[49,130]

To start a well controlled ATRP reaction, a fast and effective initiation is essential.[108] The polymerisation initiating group of the trialkoxysilane used in this work is the bromide at the silane opposing end of the molecule (Scheme 2.1). It is a tertiary halide, which is a more effective initiator than secondary or primary alkyl halides. The bromide is also a better choice over the chloride as it has higher activation rates due to its lower bond strength to the alkyl.[108,131]

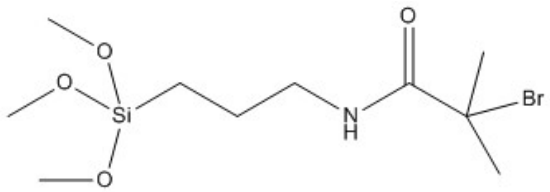

2-bromo-2-methyl-*N*-(3-(trimethoxysilyl)propyl)propanamide

Scheme 2.1: Chemical structure of the trimethoxysilane SI-ATRP initiator.

The initiator used here was a trialkoxysilane (Scheme 2.1) providing a linking group to $-OH$ terminated surfaces. Alkoxysilanes are generally less reactive than chlorosilanes and are therefore less prone to building aggregates and form better controlled SAMs. On the other hand, the reduced reactivity may lead to incomplete layers of the molecule. The higher reactivity of trifunctional silanes compared to mono- or difunctional ones compensates this and leads to SAMs of a sufficient density.[132]

The catalyst of an ATRP reaction is a transition metal that has an appropriate one-

electron redox transition, a suitable halogen affinity and a coordination sphere that can be entered by an additional ligand upon oxidation.[108,133] Although also other transition metals such as Ru or Fe are employed for ATRP, Cu is the most common one and was used in this work.[133] The metal ion is complexed by an organic ligand, often a chelator to ensure strong binding.[108] In the present work, the catalyst system was a Cu(I)/2,2'-Bipyridyl (bpy) complex, which is a robust and low cost system. Wang and Matyjaszewski[134] described this catalyst system in the 1990s, and of course, there have been many enhancements through other more elaborate ligands,[108,133] but as the stress of this work is not on mechanistic details of the polymerisation, this well-proven system was used.

The mechanism of polymerisation is a repetitive atom transfer radical addition with an activation/deactivation cycle[108,134] and is depicted schematically in Figure 2.2. Initially, the surface bound initiator carries the halide as a capping group and can be considered to be "dormant". This halide is transferred to the catalyst complex as a radical, leaving an unpaired electron at the initiator and oxidising at the same time the catalyst system, which it serves as an additional ligand. At the newly formed active radical site at the initiator, radical addition can take place. Is the halide radical transferred back to the end of the growing chain, it caps again the reaction site and the chain returns to the dormant state again. This cycle of active and dormant state, uncapping and capping, and catalyst oxidation and reduction is repeated until the reaction is quenched.

The more the equilibrium is on the side of a dormant chain, the lower is the polymerisation rate and the higher is the control, as side reactions such as coupling or disproportionation are suppressed.[108] As the equilibrium between the dormant and the active state is at the same time an equilibrium between the Cu(I) and the Cu(II) complex, the reaction rate can be influenced by adding Cu(II) along with Cu(I), and by varying their ratio.[14,97,135,136] Before this finding, control over the polymerisation was often achieved by adding a sacrificial initiator to the polymerisation solution. A sacrificial initiator offers a competing reaction that lowers the reaction rate on the surface and thus yields better control.[82] On the other hand, it causes polymerisation in solution that complicates the retrieval of the polymer film and its separation from the bulk polymer.[82,94,108]

As a side note, the polymerisation in solution started by a sacrificial initiator also increases the concentration of the Cu(II) complex during the ATRP cycle by increasing the number of halogen transfers to catalyst complexes. It may therefore not only control the reaction by a concurrence reaction but also by influencing the redox equilibrium of the catalyst.[97] However control is achieved, it leads to a lower polydispersity at the costs of a long polymerisation time.[97,108] The direct addition of Cu(II), on the other hand,

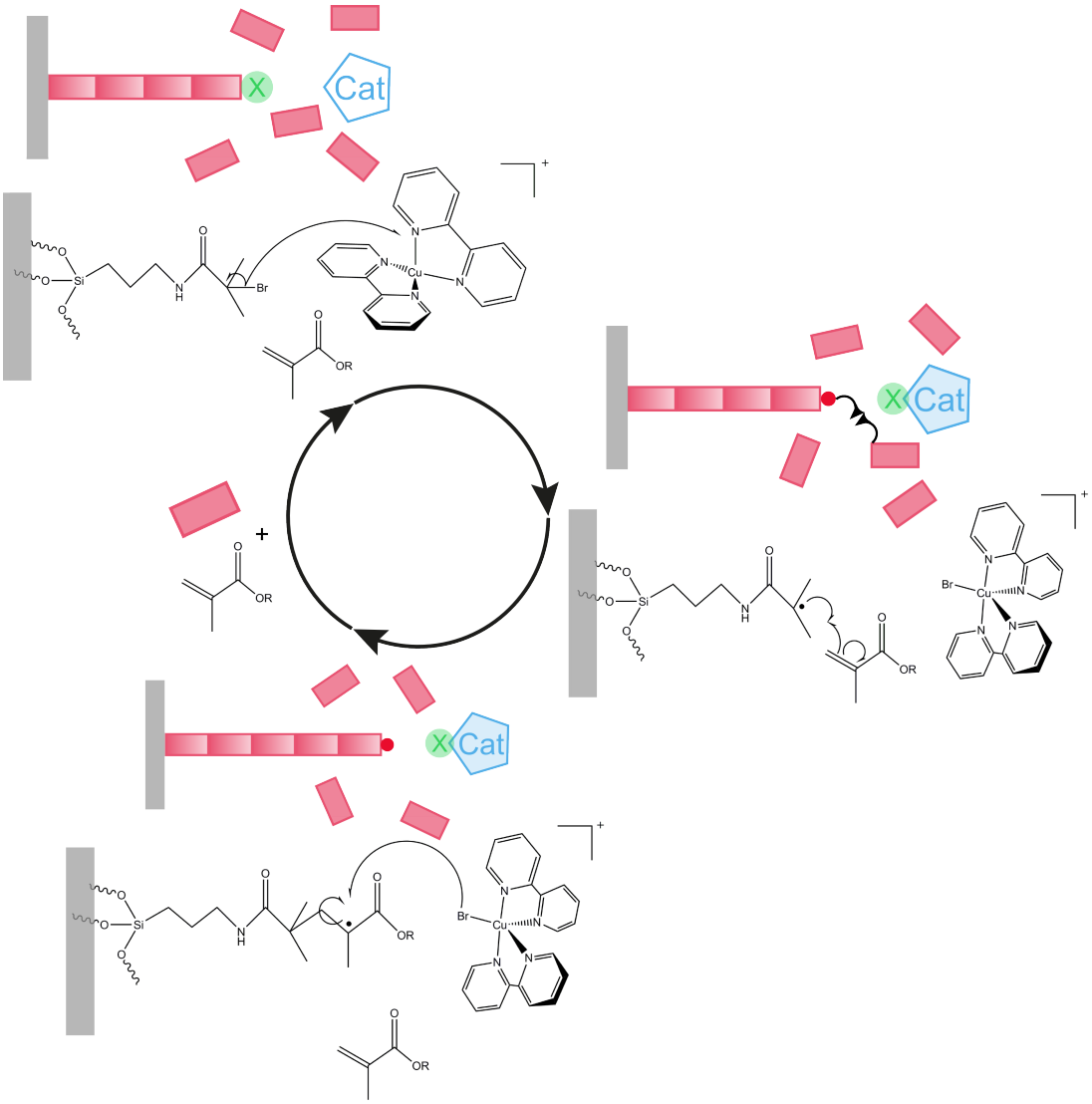

Figure 2.2: Schematic mechanism of the ATRP, the substrate is grey, monomers and the polymer are depicted as pink rectangles, the halide is green and the catalyst system blue. Is the catalyst filled, it indicates its oxidised state. The catalyst complex has then an additional ligand – the capping halide. Below the schematic illustration, the first reaction cycle for the polymerisation of a methacrylate is depicted exemplifying the reaction mechanism for SI-ATRP.

alters the activity of the catalyst instead of enhancing the number of radical sites in solution as a sacrificial initiator does. It is therefore a more practicable route to control the polymerisation and was employed in this work.

2.1.2 Introduction to Plasma Polymerisation

Although plasma processes and polymer deposition are known for more than a century,[137] plasma polymerisation has been studied more intensely only since the 1960s.[138] First of all, the term plasma polymerisation does not fully characterise the method but is commonly used for organic hight molecular weight layers deposited by plasma activation. The method is more correctly described by a plasma enhanced chemical vapour deposition (PE-CVD) of organic compounds.[137] The terms refer to a process that activates the organic molecules in the vapour phase by applying a plasma.[138] The activation is followed by a polymerisation and deposition of the organic compounds onto a substrate yielding a thin film. However, for convenience also in this work the terms plasma polymerisation and plasma polymer are used.

The plasma polymerisation takes place in a chamber, into which the samples are placed for coating (Figure 2.3). The chamber has lines to let in process gasses and the vapour of organic monomers. The pressure in the chamber is controlled by a valve at the gas outlet connected to a vacuum pump. A plasma can be ignited by internal or external electrodes connected to an electric power source, typically with an alternating current with a frequency in the microwave or Radio Frequency (RF) range.[139] The experiments of this work were conducted in a RF plasma (see Section 7.4 for details).

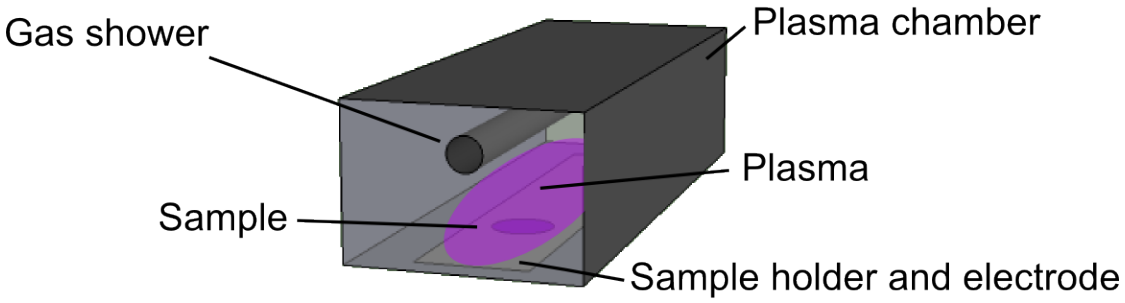

Figure 2.3: Schematic of the plasma polymerisation set-up.

The proceedings during this process are quite complex and subject to research using *in situ* analysis methods such as Langmuir probing and mass spectrometry.[137] In plasma,

there are many reactions and processes happening at the same time, *e.g.* different fragmentations of the organic compounds, generation of energetic electrons, ionisation and collisions of the diverse ionic and radical species.[137,140] There is also always a balance between ablation and deposition from and to surfaces in the plasma chamber.[138,141] Monomers adsorb to the surfaces and react with monomers and fragments activated by the plasma. Polymers or short chains form in the vapour phase and adsorb to the surfaces. At the same time, the surfaces and everything deposited on them are bombarded with ions and radicals from the plasma and are ablated consequently.[138]

Yasuda *et al.*[139] described the polymerisation mechanism in the plasma as an "atomic" mechanism, in contrast to the "molecular" polymerisation mechanism of classical wet chemistry. This means that the monomer molecules are activated in a general way and predictions are difficult, which bonds are cleaved during the reaction, as the whole molecule is in an excited state. Plasma polymerisation in this case results in films that are quite undefined in their molecular weight and chemical structure.[137,138] Since the introduction of milder plasma conditions, the retention of the original moieties has been achieved.[138,142] These mild or soft conditions stand for plasma processes with high pressure, low power in-put and a pulsed plasma. In these conditions, vinyl monomers, for example, are supposed to be cleaved only at the double bond.[138] The milder conditions also reduce other unwanted side reactions, such as sample heating during the plasma process, which is important especially when aiming at biomaterials applications with heat sensitive molecules such as proteins.[138] Less radical species are incorporated into the plasma polymer films resulting in less ageing effects and more stable films. In addition, the degree of cross-linking can be reduced.[143]

The parameters of a plasma polymerisation that have to be optimised for every single monomer are – assuming the reactions take place in the same reactor – the kind of excitation, its frequency and its power, the flow rate of the monomer, the gas pressure, the substrate temperature and its material, size and positioning.[137] This opens a huge parameter space, which makes comparison of different studies difficult and necessitates working on good process optimisation. Generally, placing the substrate outside of the plasma zone reduces the cross-linking of the polymer but also deposition rates.[143] The strive for high deposition rates is often successful when the temperature is low.[137] A lower substrate temperature also helps maintaining the functional groups of the monomer.[143] Deposition rates increase with increasing monomer flow rate until a certain saturation level is reached.[137] For the input power and the gas pressure optima exist, at which deposition is high and ablation does not yet take over.[137] Guerin *et al.*[140] pointed out the different kinds of reaction that may take place in the plasma of the model monomer 2-

propanol. The route of fragmentation that the molecules took in the plasma phase under different conditions directly influenced the plasma polymer film's chemical structure.

A vast improvement of the PE-CVD of organic compounds was the introduction of the pulsed mode. In the pulsed mode, the plasma is ignited in regular time intervals. This periodic on and off of the plasma is defined in the duty cycle. The duty cycle is the ratio $\frac{t_{on}}{t_{on}+t_{off}}$,[138,143] but often this is not sufficient to really specify the conditions. Not only the relative ratio but also the absolute length of the "plasma on" and "off" periods influence the composition of the plasma polymer film.[143] The "plasma on" state provides the activation of the monomers and produces radicals and active ions, just as a continuous plasma does. In between the "plasma on" periods, the "plasma off" periods reduce the concentration of radicals and thus promote the reaction of radicals with monomers while reducing recombination between radicals. This increased reaction rate between radicals and monomers means that during the "plasma off" periods more of the polymer is formed through mechanisms that are comparable to polymerisations of the conventional wet chemistry.[143] The more conventional mechanism preserves more functional groups of the monomers than the constantly activating continuous plasma.[138] Additionally, the deposition rate is greatly increased during the "plasma off" phase, the substrate temperature is lower in the pulsed mode than in the continuous mode, and the plasma induced irradiation is reduced. Another advantage of the pulsed mode is the decreased bombardment of the already formed thin films with ions, which in turn reduces film ablation. The pulsed plasma mode decreases the effective power input, as can be seen in the equivalent average power $< P >= Dutycycle \cdot PeakPower$.[138,143] As the power is only applied in the "plasma on" period, the overall power that the sample and the polymer receive is lower than in the continuous mode.[143] This means less damage to the plasma polymer film and higher peak powers can be applied. The degree of cross-linking is also lower in the pulsed mode than in the continuous mode and governed by the duty cycle.[138,143] All these effects of pulsing the plasma lead to a higher degree of functional groups conservation and chemically more defined films.

When using mild conditions, such as the pulsed plasma mode, with optimised parameters, it is possible to control the functional group density.[142–144] However, plasma polymers still undergo side reactions and suffer from ageing and reorientation in the bulk.[142] During the polymerisation, double bonds and branching and cross-linking structures are still introduced.[145] Radicals remaining in the polymer coatings from the plasma process always react with oxygen and water upon contact with air or in an aqueous environment. Thus, oxygen containing groups are introduced.[137,138,144,145] Additionally to the post-deposition reactions, the functional groups in the polymer film rearrange away from

or towards the interface with air or solvent affected by the wettability and interactions between moieties and environment.[138,142,146] Thus the surface of a plasma polymer coating will undergo changes on the short as well as on the long time scale depending on the surrounding.

For the present work MMA was polymerised in a pulsed plasma, *i.e.* in soft conditions, to preserve the functional group. The choice of Poly(Methyl Methacrylate) (PMMA) was based upon its often being used as a model material for biomaterials research and it being widely applied as bone cement.[35,81,147,148] It is known to be an inert polymer and has been proven to be biocompatible.[81,149] Additionally, spin-coated PMMA films provide a good surface for a protein distribution to encourage cell adhesion.[81,147] Although there is still potential for improvement when it comes to PMMA as bone cement,[148] the monomer MMA seemed to be a good starting point for the synthesis of plasma polymer films. With its double bond, it is suitable for mild PE-CVD conditions and is estimated to give a PMMA-like coating.[81,150] These coatings may be the starting point for further modifications. Controlled hydrolysis, for example, could yield films with a tunable carboxylate content, which could serve as nucleation points for biomineralisation.[151–153]

For biomaterial applications, not only the control over number and type of functional groups is essential but also the adhesion of the films to the substrate.[146] To ensure good adhesion between a plasma polymer thin film and its substrate, it is often necessary to introduce an adhesion promoting layer. This strategy was required and used in the present work to ensure the stability of the Plasma Polymerised Methyl Methacrylate (ppMMA) films. The adhesion promoting layer bridges the chemistry of the substrate and of the desired outer layer. This bridging can be done with a gradient, such as a duty cycle gradient going from high power input for good adhesion to the substrate to low duty cycles for retaining the functional groups of the monomer.[138,143] The gradient can also be formed by monomers going from simple hydrocarbon monomers to monomers carrying the desired moieties.[138] The method used in this work did not involve gradients but quite defined layers. Here, two layers promoted good adhesion in simulated physiological conditions: Plasma Polymerised *n*-Heptane (ppH) and a SAM of OTES (see also Sections 3.1.3 and 3.2.1). ppH formed a simple hydrocarbon layer, which most likely binds to the outer functionalised layer through the ablation and deposition processes during the plasma polymerisation of the outer layer (*i.e.* like a small gradient from ppH to ppMMA). The second possible adhesion promoting layer was assembled in a wet chemical process. Hydroxyl groups on the surface of the activated glass surface reacted with the siloxane groups of OTES forming a covalent bond. The hydrocarbon tail on the other side provided the connection to the outer plasma polymer layer probably through the

same processes as the ppH layer.[138]

2.1.3 Lithography of Polymer Brush and Plasma Polymer Films

To obtain patterned polymer brushes with the "grafting from" method, a host of diverse patterning methods exist to limit polymer growth to defined areas of the substrate. The most popular techniques are Micro Contact Printing (microCP),[114,123,154] photolithography[155] and direct writing approaches such as electron beam or ion beam lithography.[95,156–160] Some lithographical methods pattern polymer films after they were synthesised on the surface or deposited onto it.[147,161] However, often the patterning takes place before the surface initiated polymer film growth by selective application of initiator to the surface, or by destructing or inactivating the initiator in certain areas.[95,122,162,163]

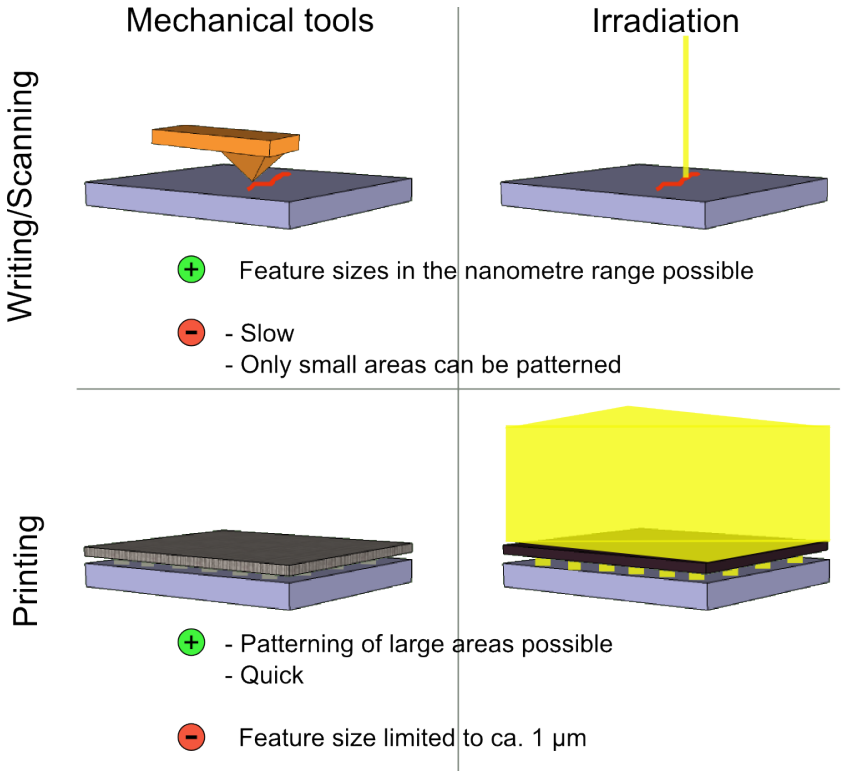

Figure 2.4: Overview of techniques to pattern thin polymer films. Methods that use the writing approach (upper part) scan the surface of the substrate (blue) to pattern it *e.g.* with a cantilever (orange, upper left) or an electron or ion beam (yellow, upper right). These methods yield patterns with very small features but are slow and can only be applied to small areas. Quick patterning of large areas can be achieved by the printing approach (lower part). The feature size of the pattern, however, has a lower limit when using *e.g.* PDMS stamps (grey, lower left) or UV-irradiation (yellow, lower right) through a mask (black, lower right) to pattern surfaces.

The several methods of patterning use either mechanical tools or irradiation to alter certain parts of a surface. Tools and irradiation methods have been developed for a "writing" and a "printing" approach (Figure 2.4). The "writing" approach with a mechanical tool employs a "pencil". An AFM cantilever is often the favourite "pencil" for this approach.[164] It can be used to scrape or press into an existing polymer coating,[165] scratch off parts of a SAM,[166] or deposit a kind of ink.[164] The ink may be, for example, alkane thiols with initiator functional groups, which are applied to certain areas of gold surfaces. Independent of the method, the resolution is always limited by the size of the "pencil". Nevertheless, as most studies employ AFM tips, extremely small pattern sizes even in the nanometre range are possible with this method. The major drawback is its limitation to small areas correlating to the maximum scanner range and the slowness of the scanning or writing method.[167]

The second possibility for the mechanical manipulation of surfaces is the "printing" approach (Figure 2.4, lower left). A heated stamp may be pressed into polymer material[115,161] or it may be loaded with ink.[167] Popular and often used are PDMS stamps for the microCP method.[114,168,169] Here, the resolution of the pattern is limited by the possible pattern size of the stamp, about 1 µm pattern width.[115] Suitable surface-ink pairs are needed[114,123] or polymers that can be processed in the hot embossing method.[115,161] However, all in all this method is quite versatile and covers quickly relatively large areas.

The third possibility belongs to the "irradiation" principle, which is the one employed in the present work. The use of irradiation as focused beam or through a mask with electromagnetic waves of various wavelengths and also ions is reported. Just as the "pencil", the focused beam (Figure 2.4, upper right) scans or writes on the sample surface ablating, activating, or inactivating certain areas.[95,147,156,157,159] The focused beam methods have every advantage and disadvantage of the "writing" techniques described above. They reach high resolutions (even in the nanometre range), especially when using small wave lengths such as electron beams.[95,157,160,170] Although the method has a great scope, it is rather slow and only applicable for small areas.[147,160]

The irradiation equivalent of the printing approach is the irradiation of larger areas through a mask (Figure 2.4, lower right). Generally, the UV-band with its high energy and short wavelength is used.[39,122,171] Advantages of the UV-lithography method are the relatively low costs and the bigger irradiation area. As it is not a scanning method, every "pixel" is irradiated at once, saving time. In contrast to the focused beam methods, such as electron beams and ion beams, there is not need for extremely cost intensive equipment such as an electron microscope. It was the approach chosen for this work, making use of the above mentioned advantages. Additionally, this lithography method was applicable

for patterning both kinds of polymer films, the polymer brush as well as the plasma polymer coatings.

However, the size of the pattern is limited by two factors: by the wavelength and the patterning of the mask. The latter is possible well below the micrometre range using e-beam lithography as it is described by Letsche.[172] Letsche used quartz glass masks with a chrome coating. The UV-light can pass the quartz glass, but not the areas covered by the chrome layer. Nevertheless, the patterning of the substrate is not possible in the nanometre scale, as the wave length of the light being used limits the pattern size. Features in the micrometre range can cause diffraction and produce artefacts as shown in Figure 2.5, even in the UV-range, which was used to pattern the coating here.

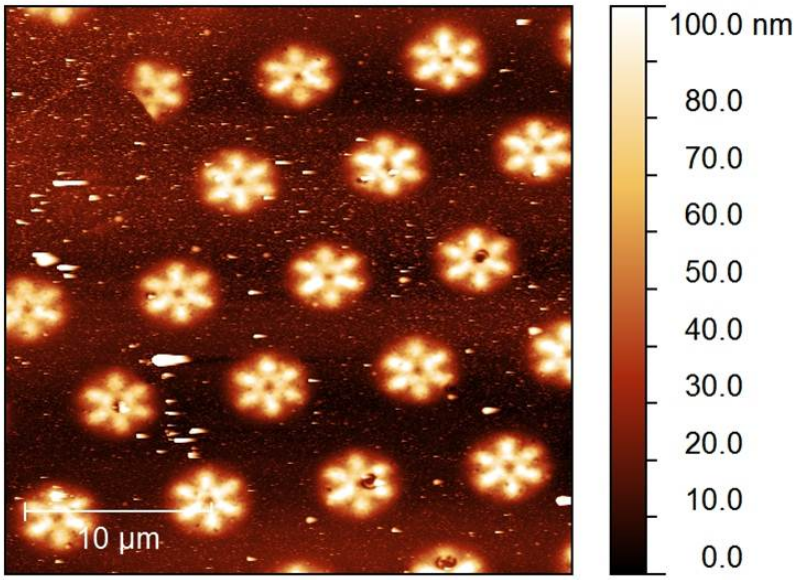

Figure 2.5: AFM topography image of diffraction artefact "flowers" of a polymer brush sample structured by irradiation through a mask with a hexagonal pattern.[173]

To pattern the polymer brush coatings for this work, a SAM of initiator molecules was irradiated though a quartz mask with a patterned chrome layer. As described by Tugulu *et al.*,[122] the initiator molecule was inactivated by decomposition in UV-light. In the non-irradiated areas covered by the chrome layer of the mask, the initiator molecule was intact. In the polymerisation solution, these areas initiated polymer brush growth through the bromide and formed the hills of the pattern. The irradiated areas could not initiate polymerisation and thus formed the grooves.

In contrast to the lithography strategy applied for the polymer brushes, the plasma polymer was synthesised first and then patterned. This process compares to the pat-

terning methods used for spin coated polymer films. Basically, the same methods of patterning can be applied for the already synthesised film as for the polymer brushes. A difference only lies in the necessity of using a developer after the irradiation, may it be an organic solvent, a mixture of solvents[147] or water. The procedure of Ploux *et al.*[39] was the guide for the patterning of the plasma polymer coatings in this work. They described the UV-lithography of plasma polymerised maleic anhydride as a simple and fast patterning method. They irradiated the sample for different time periods with the light of a medium pressure mercury lamp through a mask and developed the polymer film with ultrapurified water.

2.1.4 Comparison of Polymer Brushes and Plasma Polymers and their Application Range

Although both plasma polymerisation and SI-ATRP produce polymer thin films, the two methods differ greatly in their mechanisms and their products.

The initiation through monomers activated by electron impact is far less specific than the initiation by a conventional initiator.[137] The SI-ATRP mechanism initiates even more specific than conventional polymerisation methods a highly controlled polymerisation. Using soft plasma conditions, such as the pulsed plasma mode, it is possible to retain monomer functional groups and control their density.[142–144] Nevertheless, the control over the number and type of functional groups of a plasma polymer surface is still not comparable with that over a polymer brush surface.[140,142,145] Polymer brushes only have the kind of moiety and its exact number per unit that was introduced. In plasma polymers, side reactions during the plasma process, even if minimised, post-process reactions and ageing partly eliminate original functional groups and introduce new moieties.[137,138,142,144,145]

Despite the lower control in the plasma process, plasma polymerisation still has advantages over the SI-ATRP process. The plasma polymerisation is less cost and labour intensive and is by far the faster process.

In spite of the differences in the processes and resulting polymer films, the application range as biomaterials is similar. Surface-attached polyelectrolytes are mostly water-soluble and therefore interesting for biochemical and medical applications[53] as well as for the extensive field of biotechnology.[164] They promise control over important surface properties such as wettability and charge.[82,114] The unique behaviour of polyelectrolyte brushes such as Poly(2-[Methacryloyloxy]Ethyl Trimethylammonium Chloride) (PMETAC) in different solvents and ion solutions makes them candidates for nanoactuators applications or the build-up of microfluidic devices.[82,103,104] In the present work,

this polymer was synthesised and tested as a potential biomaterial and implant coating.

Possible and actual applications for plasma polymers range as well from medical implants over sensors to selectively permeable membranes.[138,143,146] Biosensors and bionanotechnological devices are probably the most important application aimed at for plasma polymers.[78,138,140,146]

Non-fouling applications are anticipated for polyether brushes (Poly(Ethylene Glycol) (PEG) analogues) such as Poly(Oligo[Ethylene Glycol]Methacrylate) (POEGMA) or polyzwitterionic brushes such as Poly(*N*-[3-Sulfopropyl]-*N*-Methacryloyloxyethyl-*N*,*N*-Dimethylammonium Betaine) (PSBMA).[50,51,130] The latter example is a sulfobetaine and was synthesised and examined in this work. Just like the polymer brushes, the plasma polymers are also suggested as possible anti-fouling materials. Especially the plasma analogue of PEG is a promising candidate for protein resistant surfaces.[143]

These anti-fouling functional groups are additionally studied as biocompatible materials exerting control over cell adhesion.[49] Regulating cell adhesion is of interest for a variety of biomedical applications.[43] Whereas implant materials should provide good conditions for the human cells of the target tissue and prevent bacterial colonisation, surfaces for cell arrays or biosensors should direct cell adhesion without interfering with other cell functions.[58,164,174] Polyzwitterionic brushes and other surface tethered polyelectrolytes but also Poly(2-Hydroxyethyl Methycrylate) (PHEMA), POEGMA and Poly(Poly[Ethylene Glycol]Methacrylate) (PPEGMA) are very effective in preventing unspecific protein adsorption.[43–45,50,51,56,87,164,175] This property makes the polymer brushes an interesting material for biomedical and biotechnological applications, such as protein microarrays or diagnostic sensors of lab-on-a-chip techniques.[55,56,82,114,118] Preventing unwanted protein adhesion at some places, but admitting it when wanted, may reduce the background signal on microarrays and thus enhance the detection limits.[82,118]

The polymers deposited in a plasma environment came also into focus for biomaterial applications, quite early.[141,176,177] They were thought suitable for a range of tissues and materials, especially intraocular and contact lenses and materials in contact with blood.[78,177] Drug release, prevention of leaching and corrosion, or a stealth effect for endoprostheses are thought possible as well as usage in the development of lab-on-a-chip devices.[141,176] Plasma polymer films with amine, carboxylate or hydroxyl groups are intensely explored for biomaterial applications and optimised in their stability and retention of functional groups.[138,140,142,144,178]

The polymer brush coatings and plasma polymer films synthesised for this work were examined to answer the question if they were applicable as implant coatings. As written above, the polymers were partly already candidates for other biomaterials applications,

such as the sulfobetaine PSBMA and the quaternary amine PMETAC. Poly(Methacrylic Acid) (PMAA) and the plasma polymer chosen, ppMMA, contained the carboxyl moiety often used in biomaterials.

2.2 Results and Discussion of the Polymer Coatings' Synthesis

2.2.1 Synthesis of Patterned Polymer Brush Coatings

The basic step towards the fabrication of the multi-component coating (comp. Figure 1.1 on p. 8) was the synthesis of patterned polymer brushes of different functionalities *via* SI-ATRP. The procedure started with the activation of the glass substrates (experimental details in Section 7.2), which served as a model surface. In a self-assembly process, the initiator reacted with the activated and oxidised glass to build siloxane links between coating and surface.

The patterning was achieved by UV-lithography through a chrome coated quartz mask containing the respective pattern (Section 7.5). As described by Letsche in detail,[172] the masks were in direct contact with the initiator coated substrates to ensure a good resolution and avoid diffraction.

Upon irradiation, the initiator SAM became more hydrophilic (Figure 3.4 on p. 72). The increasing hydrophilicity might indicate a reaction of the initiator molecules with an active oxygen species during UV-irradiation. UV-light can not only cause a homolytic scission of the bromide bond.[172] Besides this, also the reactive oxygen species that are generated in the deep UV-light[179] could react with the initiator SAM in a photooxidation. It is not known, if only the bromide is cleaved off, or if more of the irradiated molecules is degraded.

To elucidate the surface chemistry of the irradiated initiator SAM, X-Ray Photoelectron Spectroscopy (XPS) measurements were conducted (Figure 2.6). In the spectrum, no Br peaks were detected. The presence of small amounts of N indicated that the amide group was at least partly preserved in the irradiation process.

Fitting the high resolution spectra (Figure 2.7 and Table 2.1) showed that most carbon atoms were bound in an aliphatic environment. 23 % was part of a C=O double bond, just as the residue nitrogen implying that the amide group was at least partly retained.

As expected, most of the oxygen was bound in SiO_2, but also found in a C=O double bond environment. This confirmed the assumptions from the survey spectrum and the C1s fits. However, the surface chemistry of the irradiated areas and the mechanism of the

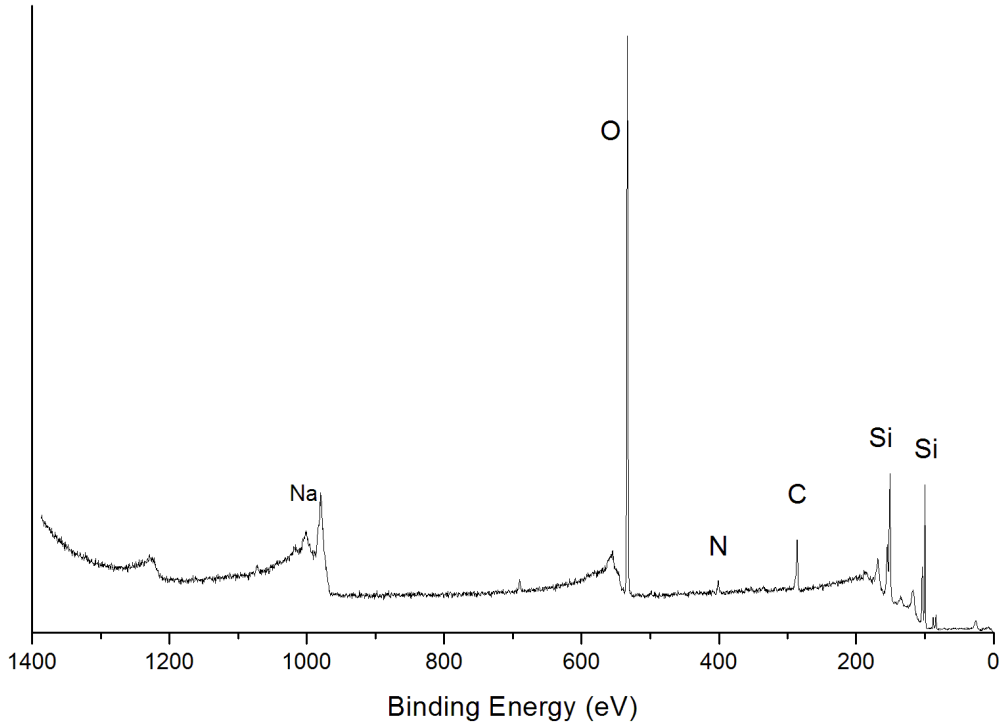

Figure 2.6: XPS survey scan of a Si surface that was coated with initiator and subsequently irradiated. Measurements indicate the presence of N. Elemental composition: 43 % Si, 32 % O, 12 % C and 1.1 % N. Br was not detected. Figure published in ref. 180.

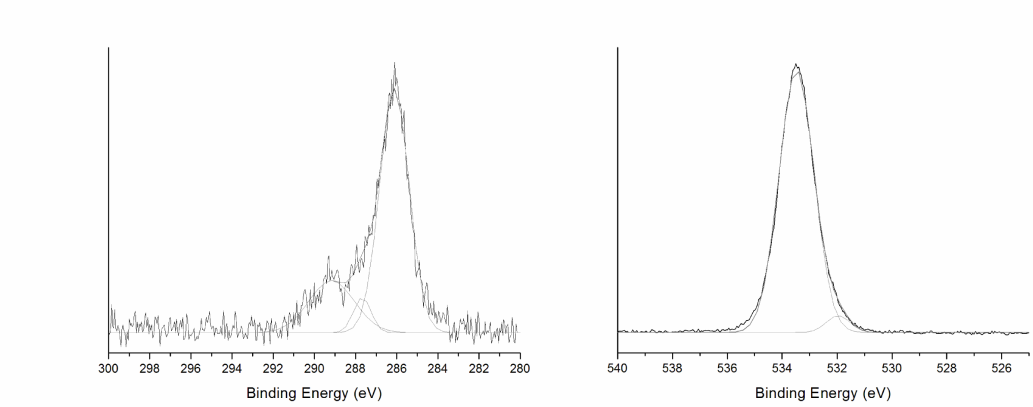

Figure 2.7: High resolution XPS spectra of the C1s (left) and O1s (right) peaks of the Si surface coated with initiator and subsequently irradiated. The C1s peak was fitted with three peaks assigned to (from left to right) a C=O double bond (289.2 eV), an C−O single bond (287.7 eV) and an aliphatic environment (286.1 eV). The O1s peak was found to contain two peaks assigned to the prevailing Si−O environment (533.5 eV) and carbon bound oxygen (532.0 eV). For details see Table 2.1. Figure published in ref. 180.

inactivation could not be fully elucidated. Even if the exact mechanism of irradiating the initiator remained unsolved, the molecule was clearly inactivated as seen by the absence of Br and by the patterns build through the polymerisation (Figure 2.10 and Figure 2.11).

Table 2.1: Values for the binding energy and the areas of the fitted peaks in the high resolution XPS spectra (Figure 2.7) of an irradiated initiator surface.

Element	Peak assignment	Binding energy [eV]	Area [%]
C 1s	C–C/C–H	286.1	70.8
	C–O	287.7	6.02
	C=O	289.2	23.2
O 1s	C=O	532.0	4.09
	Si–O	533.5	95.9

Polysulfonate Brush Coatings

Using SPMA as a monomer with its strong acidic sulfonate group (Scheme 2.2) for the SI-ATRP yields a strong polyelectrolyte, which carries the negative charge nearly over the entire pH range. For the SI-ATRP procedure, the protocol of Masci *et al.*,[124] which describes the polymerisation of SPMA in solution, was adapted for a surface initiated reaction. The details of the reaction and its optimisation are described in my master thesis.[181] The protocol made use of a CuCl/bpy catalyst and of the addition of $CuCl_2$ as a means to control the reaction as it is detailed in Section 7.3.2. The reaction was additionally slowed down and controlled by the choice of a *N*,*N*-Dimethyl Formamide (DMF)/water mixture as solvent instead of pure water.[124] Increasing the monomer content of the polymerisation solution and the polymerisation time compared to ref. 124 produced Poly(3-Sulfopropylmethacrylate) (PSPMA) brushes with a height of up to 30 nm.

The PSPMA brush coatings were employed mainly for cell culture experiments and for nanoparticle adsorption experiments, but they were also tested as a matrix for mineralisation experiments. Their synthesis was additionally used to learn more about the polymerisation and the resulting coating. By comparing the properties of the PSPMA brush films with those of PMETAC, PSBMA and PMAA, a more accurate picture of the polymer brush conformation and its behaviour could be elucidated.

The living character of the polymerisation was shown by self-blocking experiments previously by my-self in good agreement with literature.[108,114,124,181] In a self-blocking experiment, the polymerisation is re-initiated on already synthesised polymer brushes.

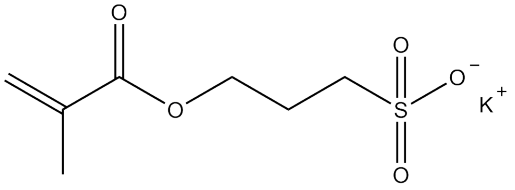

potassium 3-sulfopropylmethacrylate

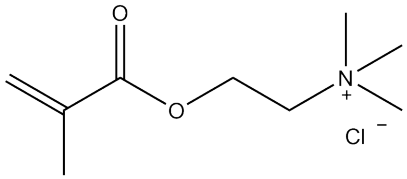

2-(methacryloyloxy)ethyl trimethylamonium chloride

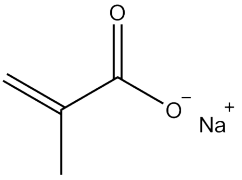

sodium methacrylate

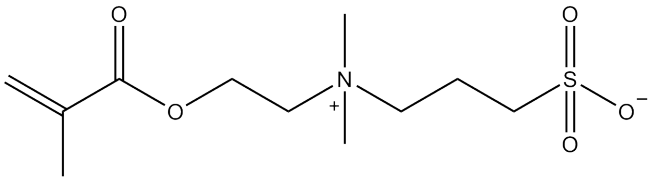

N-(3-sulfopropyl)-*N*-methacryloyloxyethyl-*N,N*-dimethylammonium betaine

Scheme 2.2: Chemical structures of the monomers used for SI-ATRP.

Thus, the preservation of the halide at the end of the polymer is shown, which is a criterion for the livingness of the reaction.[108,182] However, the results from the self-blocking experiment with PSPMA could not absolutely rule out irreversible termination or loss of the active endgroup, contrary to the statement in ref. 181. Although the polymerisation was successfully re-initiated, the height added during the re-initiated polymerisation was lower than the height resulting from the first polymerisation at the same conditions and concentrations.

This apparently lower efficiency of the re-initiation does not necessarily mean that the active endgroups were lost. They could also be buried in the polymer. The swelling properties of the polymer brushes (for details see ref. 173,181) indicate a quite coiled conformation in the dry state. The swelling experiments described therein showed that PSPMA brushes could swell in water about twice their dry height. This would not be possible, if the polymers were already nearly completely stretched in the dry state.

An alternative explanation for the lower efficiency of the re-initiation is that a mixed halide system was used for the polymerisation of SPMA.[108,124] The reaction was started by the highly efficient bromide, but continued by the less efficient chloride. This halide exchange increases the initiation rate over the propagation and thus increases the control over the polymerisation.[108,183] On the other hand, it leaves the ends of the polymers capped by the chloride at the end of the polymerisation and thus lowers the efficiency of the re-initiation.

In summary, PSPMA brushes were synthesised with an ATRP protocol yielding polymer chains that can be re-initiated for a self-blocking polymerisation, showing the living character of the reaction. The lower re-initiation rate can be due to the change of the capping group from $-Br$ to $-Cl$ or the loss of the halide capping group. Alternatively, it can be evidence for a conformation of the polymer chains that is more coiled than the common picture suggests for polymer brushes (as *e.g.* in ref. 122). The synthesis and characterisation of the other polymers PSBMA, PMETAC and PMAA gave additional clues to answer this question.

Polysulfobetaine Brush Coatings

PSBMA is a zwitterion with the constantly positively charged quaternary amine and negatively charged sulfonate (Scheme 2.2). The protocol of Azzaroni *et al.*[49] emerged as a good guide to the reaction.[181] Just like the polymerisation of SPMA, the reaction was catalysed by a CuCl/bpy complex. Control was achieved through the addition of $CuCl_2$ shifting the equilibrium to the capped polymer chain (comp. Section 2.1.1). The mixed halide system consisting of a bromide initiator and chloride copper salts added to the control. Additionally, a mixture of water and the organic solvent methanol provided the right degree of control and reaction rate (comp. experimental details in Section 7.3.1).

The polymer was examined extensively as cell culture substrate, as mineralisation matrix and as template for nanoparticle adsorption. PSBMA contained negative as well as positive charges. It thus offered unusual possibilities for interactions with other molecules and particles.

The water contact angle measured for biocompatibility and stability experiments (comp. Figure 3.4 on p. 72) showed that the PSBMA brushes used here were hydrophilic with a contact angle of $20°\pm9°$. Previous measurements (comp. ref. 181) implied that the brushes synthesised following the same protocol were less hydrophilic (water contact angle $36°\pm3°$). Although the reaction conditions were kept constant for all polymerisations, the contact angle seemed to have varied between different experiments.

The PSBMA zwitterions have an extremely high dipole moment. The dipole moment results in the groups interacting strongly intra- and intermolecularly, forming bridges to other chains or loops connecting different parts of one chain.[49] To break these interactions and make the polymer soluble, high temperatures or ionic solutions are necessary.[49–51,184,185] Due to the strong interactions, polymer brushes build from these polymers may form extremely dense, supercollapsed layers, depending on the molecular weight of the polymer and the electrostatic environment.[49,185] Azzaroni *et al.*[49] found that PSBMA brushes showed two regimes depending on the film thickness, *i.e.* the mo-

lecular weight of the polymer. Below a thickness of 50 nm, the PSBMA brushes were not in a collapsed state, the inter- and intramolecular interactions were low, resulting in hydrophilic coatings. After a transient linear rise of the contact angle, the polymer chains of 100 nm or more were supercollapsed interacting strongly intramolecularly and thus excluding the water. According to the authors, in water, solvation antagonises the electrostatic effect and the hydration of the polymer chains causes the brushes to swell. Consequently, hydration and electrostatic binding are antagonists determining properties of the PSBMA brushes.

Azzaroni *et al.*[49] measured a water contact angle of about 12° when brushes were 50 nm or less. Previous measurements of my own samples in ref. 181 gave a contact angle of 36°±3° corresponding to a height of about 60 nm in ref. 49. This height was in agreement with AFM measurements at the time (60 nm to 100 nm). The brushes with the contact angle of 20°±9° on the other hand were probably at the lower end of the transition regime. The lower contact angle indicated a lower dry height of the PSBMA brushes of this specific experiment. On the whole, contact angle measurements of the PSBMA brushes suggested the brushes synthesised for this work being in the non-associated regime (comp. ref. 49). In this regime, the polymer brush coatings were hydrophilic, could be hydrated and swell.

In a set of experiments, the polymerisation was stopped after various time periods. These experiments were performed on glass and silicon substrates in parallel. AFM scans were used to determine the height of the polymer brush film.

The height plotted over the polymerisation time (Figure 2.8) showed a linear relation of thickness *vs.* time in the section with the data of the first 20 min to 30 min. A linear increase of the film thickness over the reaction time indicates a good control over the reaction.[97,99,114] Therefore, the reaction seemed to have a controlled character in the beginning of the polymerisation. After that time, the slope slowly begins to level. This behaviour is observed in many studies on different SI-ATRP reactions and seems to be quite common.[93,99,108,186] It is a sign that the controlled character of the reaction is lost and an irreversible chain termination takes place, even if only in small numbers.[99,108,114,186] Consequently, the polydispersity rises in this period.[99]

Just as the lower re-initiation rate in the self-blocking experiments with PSPMA did, the non-linear relation of thickness *vs.* time for longer polymerisation time suggested that irreversible chain termination did occur. On the other hand, it does not rule out the possibility that the active ends were simply buried in the brush and poorly accessible for monomers and catalyst. This possibility should have had a similar effect on chain growth.

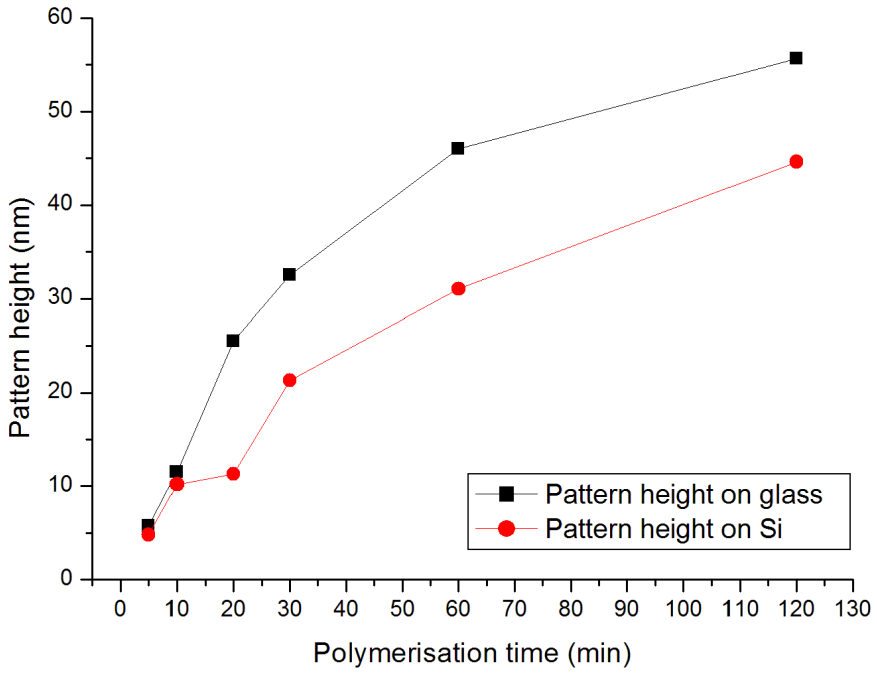

Figure 2.8: PSBMA brush height over the polymerisation time as measured in AFM scans. The line serves to guide the eye. A linear section in the beginning of the curve implies a controlled polymerisation, levelling off a loss of control. Even though the substrates shared pretreatment and the reaction solution, the height on the silicon wafer differs from the one on glass indicating that on the two substrates brushes are not necessarily equal.

Despite the common picture of a really "brush-like" polymer brush with polymers in a very stretched conformation standing separated next to each other (as depicted *e.g.* in ref. 122), particle tracking micro-rheology measurements conducted by Pluntke and Paust with PSBMA and PMAA brushes synthesised for this work suggested another picture. The polymer brushes acted more as a network implying a more coiled and entangled conformation of the polymer brushes (compare also Figure 2.1 and Outlook of ref. 173).

Concluding, probing the brush height at different time points of the polymerisation showed that the controlled character of the reaction was lost after about 30 min reaction time. The loss of control can be explained by employing the conventional reasoning that irreversible chain termination took place. Alternatively, it may be argued that the conformation of the polymer brush is more coiled than is usually anticipated. The network of polymers might bury the chain ends in the coating making them less accessible for the reactants leading to an apparent termination. In this case, the low re-initiation rate (as for PSPMA) and the levelling off of height increase over time (as for PSBMA) might give information about the conformation of the polymer brushes.

A second finding of these experiments was the differing brush height on the two substrates, glass and silicon. The substrates for this experiment shared the pretreatment and the reaction solution, so all parameters should have been kept constant. The polymerisation on glass was therefore not necessarily equal to the reaction on silicon. This should be considered when the substrate is changed to use a wider range of analysing methods as it is generally done.[56,93,187] The difference in film thickness might be caused by a lower density of the initiator SAM on the silicon substrates. A differing surface chemistry and less efficient activation prior to the initiator coating might provide fewer anchorage sites for the silane. As all other reaction conditions were kept constant, this seems the most feasible explanation. This observation should also be considered when transferring these findings to titanium substrates.

Polyamine Brush Coatings

The monomer METAC is a constantly charged quaternary amine (Scheme 2.2). It was polymerised *via* ATRP, just as the other monomers, but different conditions had to be chosen to accelerate the reaction for this apparently less reactive monomer. Additionally, a pretreatment of the METAC solution was necessary (experimental details in Section 7.3.3). The monomer METAC was provided as a 75 wt% aqueous solution. Whereas in ref. 88,167,188,189 no treatment is mentioned, Cheng *et al.*[97] and Zhou *et al.*[163] mention treatment with aluminium oxide or elution through a neutral alumina plug. Luo *et al.*[190]

and Yan *et al.*,[191] on the other hand, purified a similar reagent by washing it with ether. In the present work, after skipping the pretreatment or after the pretreatment with ether, no sign of successful polymerisation could be observed. Experimentally, the purification by Al_2O_3 treatment, however, proofed to be the most effective method. The procedure consisted of making a slurry of the monomer solution and neutral Al_2O_3 and by subsequently sucking off the purified solution.

As outlined above in Section 2.1.1, a crucial parameter for ATRP is the ratio of monomer to active copper species (Cu^+), to inactivating copper species (Cu^{2+}) and to ligand (bpy). The influence the two copper species have on this specific polymerisation of METAC was examined by Cheng *et al.*[97] The authors reported that a high Cu(I)/Cu(II) ratio increased the polymerisation rate but lead to high polydispersity. In literature, ratios of [monomer]:[Cu(I)]:[Cu(II)]:[bpy] of 100:2:0.1:5[88,188,189] and 40:1.1:0.11:2.7[103] are given. In the present work, ratios of 100:3:1:7, 100:2:0.1:5 and 100:2:–:4 were tried, decreasing the amount of Cu(II), the last approach omitting the inactivating copper species altogether.

Respresentative DIC micrographs of the patterned coatings resulting from these optimisation eyperiments are shown in Figure 2.9. The faintest pattern can be seen in Figure 2.9a. The coating was prepared with the inhibiting Cu^{2+} ions added to give a 100:2:0.1:5 ratio. A clear improvement was the abolishing of this copper species resulting in a ratio of 100:2:–:4 (Figure 2.9b), as can be seen by comparing Figure 2.9a and b. As stated above and studied by Cheng *et al.*,[97] this measure likely reduced the control and raised the polydispersity. As the perfect control over the reaction was not in the focus of this work but the application as a means to direct cell and nanoparticle adsorption, this deficit was traded against the higher polymer film thickness. The material contrast produced by charge and functionalisation of the patterned polyelectrolyte was in the centre of interest and was provided by this reaction as the results in the following chapters will show.

Next to the ratio of Cu^+ to Cu^{2+} ions, a second parameter to optimise was the reaction time. Polymerisations for 1 h or 2 h did not yield a coating that could be seen under the microscope. In cases like this, the samples were scratched with the pointy end of tweezers to find traces of a polymer films through scratches on the surface even if patterns were not discernible. For the PMETAC samples with a short polymerisation time, also then no sign of a polymer film was found. The increase of polymerisation time from 18 h to 24 h is visible by comparing Figure 2.9 e and f indicating that the increase of polymerisation time caused an increase in apparent film thickness. Nevertheless, the polymerisation seemed to vary from batch to batch, as Figure 2.9b, d and e were prepared basically under the same

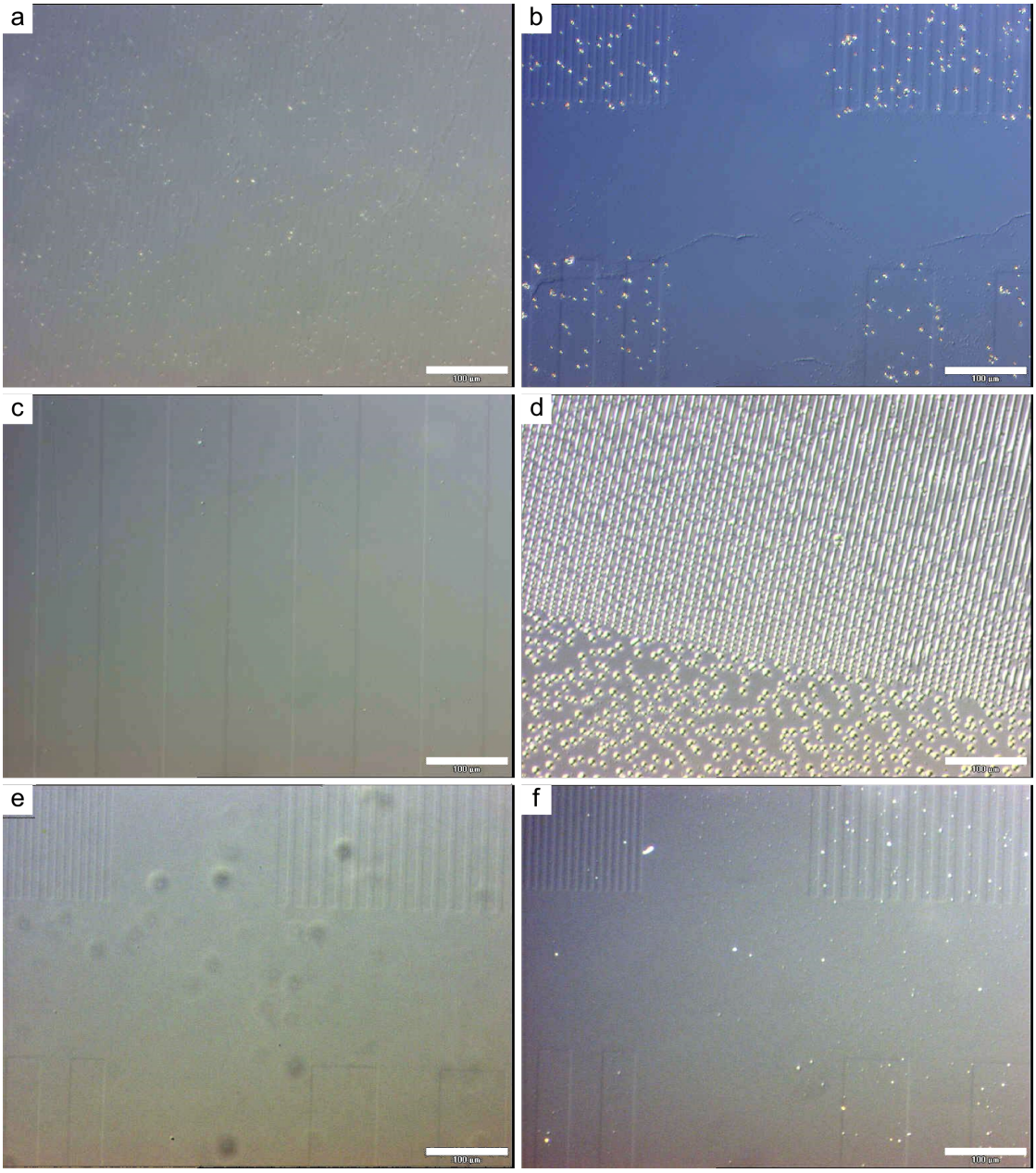

Figure 2.9: DIC micrographs of PMETAC coatings prepared following the protocol given in Section 7.3.3. Between the experiments the ratio of [monomer]:[Cu^+]:[Cu^{2+}]:[bpy] and the reaction time were varied; a: ratio 100:2:0.1:5 polymerised for 18 h, b: ratio 100:2:–:4 polymerised for 18 h, c: no slurry, only sucked through Al_2O_3 ratio 100:2:–:4 polymerised for 16 h, d: ratio 100:2:–:4 polymerised for 18 h pattern was only visible as the water condensation pattern, e: ratio 100:2:–:4 polymerised for 18 h, f: ratio 100:2:–:4 polymerised for 24 h; scale bars 100 µm; pictures were modified to enhance contrast.

conditions, but differed in material contrast of the structure when analysed by DIC. As is shown in Figure 2.9d, the pattern was partly only visible under the microscope through the water condensation pattern. When increasing the humidity of the air locally around a sample, the water condensed preferably on the areas covered with PMETAC and not in the grooves. The condensation pattern reproduced the pattern of the polymer brush and was used to detect the thin film when the optical material contrast was not good enough to be adequately enhanced by the DIC.

A third measure to increase the film thickness was increasing the water content of the reaction solution. This generally serves to accelerate the reaction[89,108,114,116,118] and diminishes the decelerating effect of poor solubility of a monomer in the solvent[114] comp. Section (2.1.1). In the experiments, these changed reaction conditions assisted with accelerating the polymerisation, but, at the same time, presumably meant loss of control and a higher distribution of molecular weight.[97,124]

In conclusion, the polymerisation of METAC produced only very thin coatings as first analyses by DIC light microscopy indicated and AFM measuremnets described below confirmed (Figure 2.11). The polymerisation of METAC was very likely not under good control as soon as a feasible reaction rate was achieved. Besides eliminating the Cu^{2+} ions and raising the polymerisation time to 24 h, the solvent ratio was raised from water:methanol 1:4 to 1:1. However, this seemed acceptable with regard to the requirements of the coating: These extremely thin polymer film changed the surface energy considerably. Water contact angle measurements revealed the hydrophilic properties of the PMETAC brushes with a contact angle of $11°\pm3°$. The polycationic brush is therefore comparable to the polyanionic brush ($17°\pm6°$[181]) in its hydrophilicity.

Polycarboxylate Brush Coatings

NaMA is a smaller molecule than the ones described before (Scheme 2.2 on p. 32) and with its carboxylate group yields a weak polyelectrolyte (comp. Section 2.1.1). The polymerisation of NaMA was described by Tugulu *et al.*[93] and adapted and refined by Letsche.[172] For this work, the synthesis protocol (7.3.4) was simply adopted to expand the range of polymers for ensuing experiments described in the following chapters.

The polymerisation reaction of NaMA was marked by the formation of polymer in solution, additional to the surface initiated polymerisation. The by-product "bulk polymer" is a sign for the lack of control in this reaction.[114] Although the outer experimental conditions, such as the strength of vacuum during the freeze-pump-thaw cycles and exclusion of oxygen, were similar for all monomers, polymerisation in solution took place only for NaMA. Bulk polymerisation occured even before adding the catalyst, but adding the

copper species accelerated the polymerisation even more. The most likely radical starter was residual oxygen in the monomer solution during the degassing process. Before the addition of the catalyst, a free radical polymerisation was highly probable. After the addition of the copper species, also other mechanisms were possible.

NaMA seemed to be much more prone to radical reactions than the derivatives used. A reason for the apparently higher reactivity might be the ability of the carboxylate groups to complexate the Cu^+ ions of the catalyst. Carboxylate functional groups in general and specifically PMAA brushes are known for their good affinity to Cu^+ ions.[83] Jones *et al.*[192] studied the SI-ATRP of the monomer Glycidyl Methacrylate (GMA) and observed an accelerated reaction rate. The authors ascribed this to a complexation of Cu^+ ions by the epoxide moeties that changed the catalyst structure, accelerated the reaction rate and caused a loss of control. Therefore, complexation could play a role in the increased polymerisation rate and loss of control.

The optimisation and refinement of the polymerisation would go beyond the scope of a thesis aimed at the *application* of polymer thin films. The following issues (comp. Section 7.3.4), however, might be addressed in future works concentrating on the synthesis: First, degassing the unsolved monomer before it can react in aqueous solution might reduce bulk polymerisation in solution. Ascertaining that the NaMA was not already partly polymerised could be part of this approach. Second, a change of solvent from water to an organic solvent/water mixture could improve control. The catalyst system might, third, be changed from a pure bromide to a mixed system[108] by employing the chloride salts instead of the bromide salts. Fourth, a change of ligand could stabilise the catalyst system and make a complexation by the PMAA brush more unlikely. A fifth way of regaining the control could be the optimisation of the Cu(I)/Cu(II) ratio.

2.2.2 Characterisation of Patterned Polymer Brush Coatings

After the synthesis and washing procedures, the patterned polymer brush coatings were routinely examined through the light microscope in the DIC mode. A clear structuring and homogeneous surface showed a successful coating of the glass samples as it is presented in Figure 2.10.

A part of the produced samples were observed more closely with AFM measurements to provide the dry height of the polymer layer (measurements described in detail by Pluntke[173]). Examples for these topographical measurements are shown in Figure 2.11.

The PSPMA brushes produced following the protocol given in Section 7.3.2 usually were about 30 nm high. The dry height of PSBMA brushes was ca. 50 nm after the polymerisation procedure described in Section 7.3.1. At the lower end of the scale was the

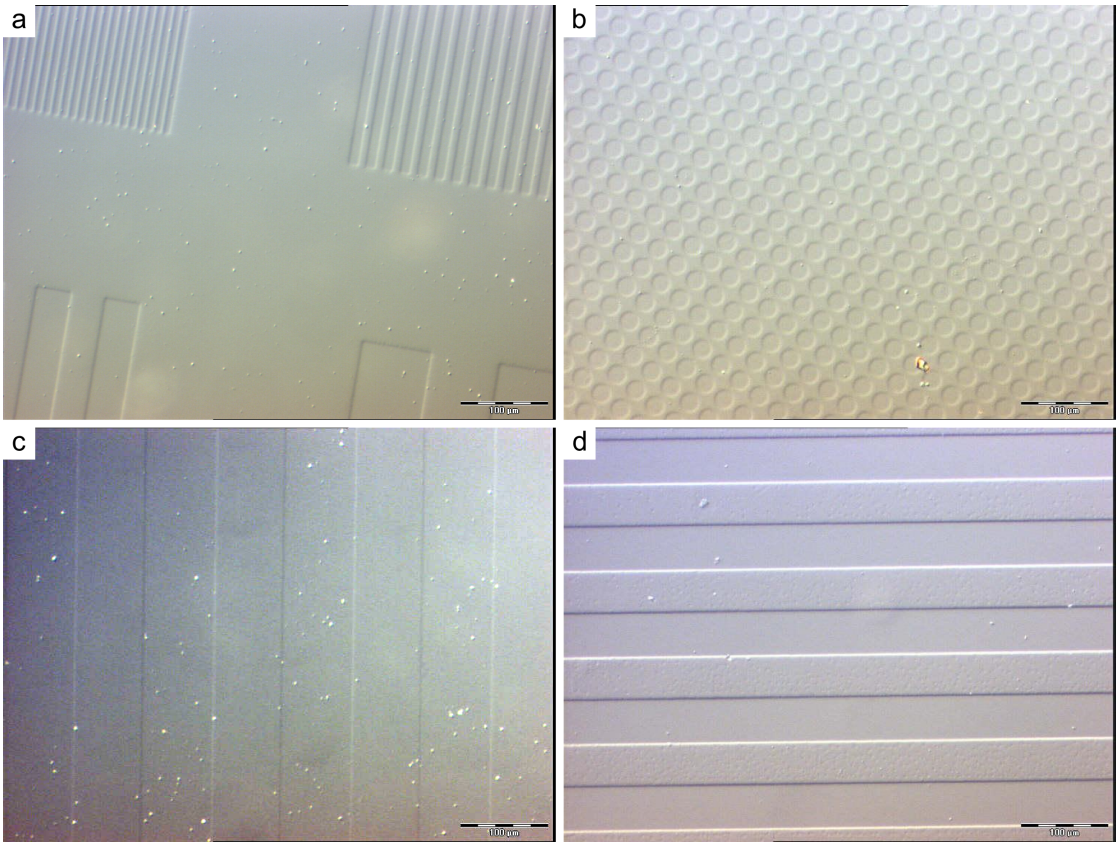

Figure 2.10: DIC micrographs of the polymer brush coatings obtained from the four different monomers SPMA (a), SBMA (b), METAC (c) and NaMA (d) following the reaction conditions listed in Table 2.2 and described in detail in Section 7.3; scale bars 100 µm.

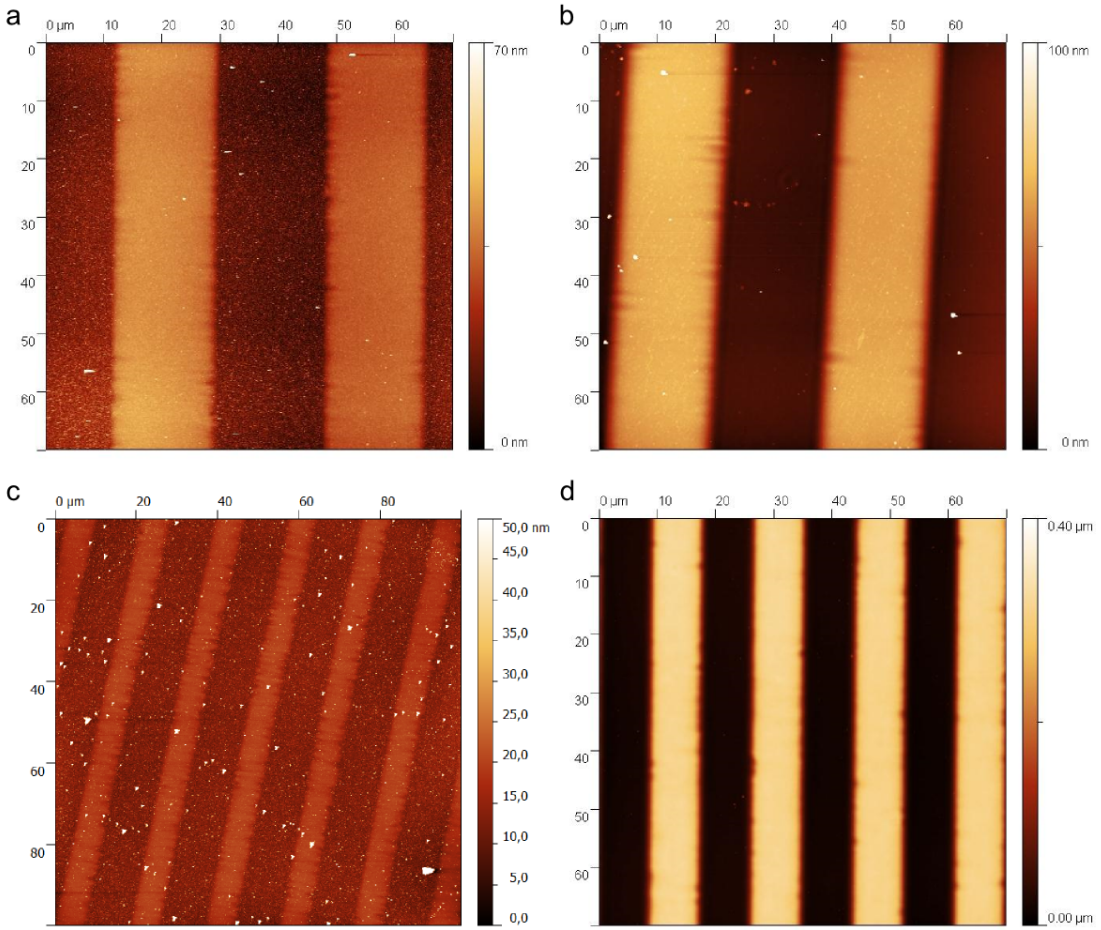

Figure 2.11: Typical AFM topographies of the polymer brush coatings obtained from the four different monomers SPMA (a), SBMA (b), METAC (c) and NaMA (d).

thickness of the PMETAC brushes with 10 nm, despite the efforts to accelerate the polymerisation (comp. Section 7.3.3). The protocol in Section 7.3.4 yielded PMAA brushes with 300 nm height. The values and the corresponding reaction conditions yielding the polymer brush films are listed in Table 2.2.

Table 2.2: Dry height of the four different polymer brush films synthesised and used in this work as measured from AFM scans, listed with the corresponding height when swollen in water, the polymerisation time and the relative concentration ratios of the main reactants during the polymerisation. ··· – no data. For the detailed reaction procedure compare Section 7.3.

Polymer	Dry height	Height in water	Polymerisation time	Ratio [monomer]: $[Cu^+]$:$[Cu^{2+}]$:[bpy]
PSPMA	30 nm	60 nm	14 h to 16 h	75:1:1:5
PSBMA	50 nm to 60 nm	120 nm	2 h	50:1:0.1:2.5
PMETAC	10 nm	···	24 h	100:2:—:4
PMAA	300 nm to 400 nm	2 µm	30 min	200:2:0.4:5

From these measurements it can be seen that the weak polyelectrolyte PMAA reached the highest coating thickness with the shortest polymerisation time. At the same time, the polymerisation was the least controlled one. The lowest polymer brushes, on the other hand, were produced in a very slow polymerisation. As it is described by Matyjaszewski *et al.*,[108] every ATRP monomer has its own unique equilibrium constant. Reactivity, control and conditions are in a singular interplay for every polymerisation system, although the general rules (Section 2.1.1) do apply. This was confirmed by the reactions conducted for this work. Although the outer conditions and the catalyst system were the same for all monomers used, the reactivity differed greatly. Even adjusting the molar ratios of the catalyst components and the solvent did not compensate for the differing reactivity, the resulting polymer films differed in thickness, *i.e.* in polymer chain length.

Another reason for the polymer specific brush heights might be the type of the monomer's charge. Strong polyelectrolytes carry a charged group on every segment of the polymer chain constituting a high charge density usually evaded by chemical systems. It is known for weak polyelectrolyte systems that the density of the functional groups changes the moieties' pK_a. A polycarboxylic system thus evades extreme charge densities by increasing the pK_a when the functional group density is high.[83] This regulating possibility does not exist for systems with a fixed charge. If there is a limit for the functional group density, strong polyelectrolyte systems need other way to prevent exceeding this limit. Lowering the chain length lowers the number of charge bearing groups in the polymer chain. A limit of the functional group density might therefore lead to a restricted polyelectrolyte brush growth and thus lower the polymer brush height. Alternatively,

the counter-ions binding to the functional group might compensate the charge. However, these counter-ions increase the sterical stress in such a system[188] eventually restricting polymer chain growth as well.

Whereas the dry height and topological AFM scans give information about the polymer chain growth and the pattern, the following experiments in cell culture, the mineralisation and the adsorption of nanoparticles were conducted in aqueous solution. To provide a better picture of the polymer brushes in this aqueous environment, AFM scans in deionised water were conducted as shown in Figure 2.12 (see also ref.s 47,48,173).

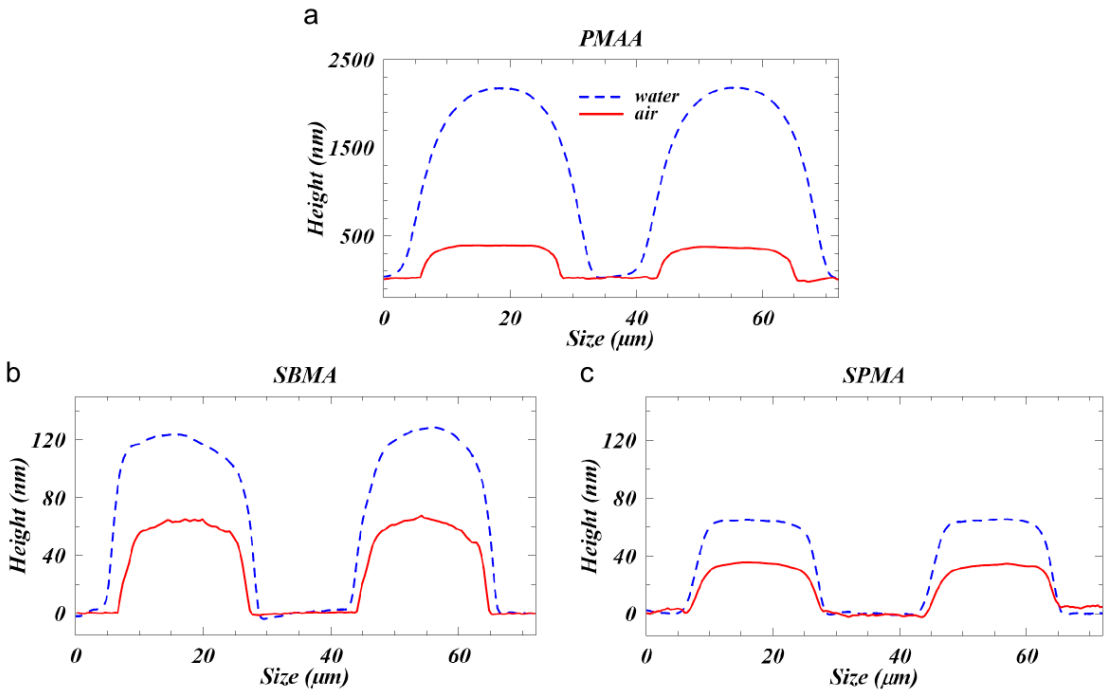

Figure 2.12: Profile of patterned PMAA (a), PSBMA (b) and PSPMA brushes (c) in the dry state (continuous red line) and swollen in water (dashed blue line) as measured with AFM; figure published in ref. 47.

The PMAA brushes were swelling in water about five times their dry height. This enormous height difference compared to the dry film affirms the revised conception of the polymer brush picturing the chains not as nearly stretched but as quite coiled. It also shows the good hydration and solubility of the polycarboxylate in water. Following the argumentation of Cheng *et al.*,[97] the immense swelling behaviour exhibited by these brushes additionally suggests a high polydispersity. A high polydispersity implies the existence of shorter polymer chains as well as very long ones, which can stretch much higher when solvatised than the shorter chains. This was shown for PMETAC brushes

in ref. 97 but should apply to the present PMAA brushes as well.

The PSBMA brush line patterns swelled to about twice their dry height and were softer in these conditions than in their dry state. Azzaroni *et al.*[49] observed a similar swelling behaviour in comparable PSBMA brushes with a dry thickness of 50 nm. When the PSBMA brushes in their study were higher (90 nm), the film height only increased slightly in water due to the PSBMA brush's collapsed state in the associated regime as described in Section 2.2.1. The authors reasoned that longer polymer chains, *i.e.* thicker PSBMA layers, had a different conformation because they had more groups *per* chain that were able to bind. The higher number of functional groups made an intra- and intermolecular binding more probable and caused a collapse of the brushes.

For the thin polymer brush films of the present work, on the other hand, the following should apply:[49]

- The interaction of a sulfonate group with water is better than the one with a quaternary amine
- The high dielectric constant of water stabilises the strong dipole moment of the zwitterion moieties
- Steric hindrance prevents the formation of ion pairs between the zwitterion moieties

Hydration and swelling in water is consequently favoured, if the PSBMA brushes are in the non-associated regime. The PSBMA brushes swelling to twice their height in water thus supported the assumption from the contact angle measurements (Section 2.2.1) of the PSBMA brushes being in the non-associated regime. The hydrophilic property and the good swelling, *i.e.* hydration, imply strongly that the PSBMA brushes were in the non-collapsed state.

Just as the PSBMA brushes, the PSPMA brushes swelled in water to twice their dry height. This affirms good hydration and the hydrophilic character of the polymer which was exhibited in a low contact angle of 17°.[181] The height increase is less than for the PMAA coating, which confirms the assumption of a quite slow and controlled polymerisation. A better control of the reaction through the addition of Cu(II) provided polymer brushes with a lower swelling ability as a sign of lower polydispersity.[97]

Returning to the question, if the low re-initiation rate in the PSPMA self-blocking experiments and the plateau in the polymerisation time-dependent height of PSBMA were due to chain termination or owing to polymer chain ends being buried in the film: The polymerisation with the highest reaction rate and lowest control (PMAA) lead to polymer films with a high apparent polydispersity concluded from the great difference

between dry film height and film height in water. The polymers PSBMA and PSPMA resulted from reactions with a lower rate and better control, and seemed to have a lower polydispersity. A difference in control of the reactions did not change the accessibility of the polymer chain ends but nevertheless caused differing swelling behaviour, indicating differing polydispersity. Therefore, high polydispersity was probably due to irreversible chain termination and not due to inaccessible polymer chain ends. Consequently, improving the control did indeed lead to fewer irreversible chain termination events.

In summary, the synthesis of polyelectrolyte brushes from a range of functional groups was successful. The strong polyelectrolyte PSPMA brush carrying sulfonate groups was produced in a slow and well controlled polymerisation. The PSPMA coatings were about 30 nm thick, hydrophilic ($17°\pm6°$[181]) and increased the height in water to about twice the dry height. The sulfobetaine SBMA was also polymerised in a controlled reaction to yield a polyzwitterionic brush. The dry height of ca. 50 nm doubled in water indicating good hydration and hydrophilic properties ($36°\pm3°$[181] and $20°\pm9°$ in more recent measurements for this work). Polycationic PMETAC brushes only reached a height of 10 nm despite several measures to increase the polymerisation rate sacrificing means of control over the reaction. The resulting polymer coating was very hydrophilic with a water contact angle of $11°\pm3°$. The weak polyelectrolyte PMAA formed the thickest polymer layers in this work with about 300 nm height. It was the least hydrophilic with a water contact angle of $46°\pm4°$,[181] but swelled in water to about five times its dry height. The swelling behaviour, speed of reaction and polymerisation in solution indicated poor control of the polymerisation reaction.

2.2.3 Synthesis and Characterisation of Plasma Polymer Coatings

The method of PE-CVD with organic precursors was established in the Chair of Solid State Chemistry, University of Augsburg, by Schaller and Kalytta-Mewes. It is described in detail in ref. 81.

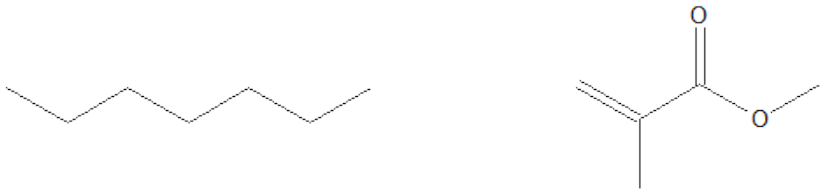

n-heptane methyl methacrylate

Scheme 2.3: Chemical structure of the precursor molecules used for the synthesis of plasma polymer thin films with PE-CVD.

The system consisted of an adhesion promoting layer (see also Section 2.1.2 and 3.2.1 on adhesion promoting layers) and a coating of ppMMA (Scheme 2.3). Either a SAM of OTES served as an adhesion promoting layer or a ppH coating prepared by PE-CVD of *n*-heptane (Scheme 2.3). This ppH layer was patterned and tested on its own, or with an additional layer of ppMMA deposited on top of it and patterned (Figure 2.13).

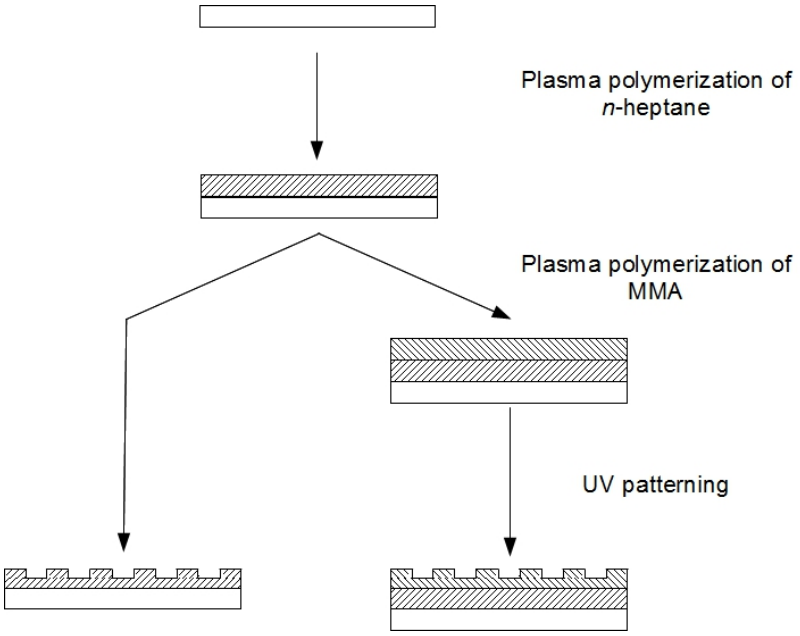

Figure 2.13: Schematic overview of the plasma polymer layer synthesis. On plasma cleansed glass slides, an adhesion promoting layer was introduced. This layer was patterned and tested on its own (left) or an additional layer was deposited on top of the first layer by PE-CVD of MMA (right). Also this two layer system was patterned and tested; figure published in ref. 81.

To track the polymerisation reaction of MMA, Attenuated Total Reflectance Infrared Spectroscopy (ATR-IR) measurements were used (Figure 2.14). The signal of the MMA double bond at $1638\,\mathrm{cm}^{-1}$ is well-defined for the monomer, but disappears after the PE-CVD process. At the same time, the alkane bond signals between $2800\,\mathrm{cm}^{-1}$ and $3000\,\mathrm{cm}^{-1}$ increase. This indicates a successful polymerisation reaction of the C–C double bonds under the formation of alkane structures.

The ester signal served as a sign for the integrity of the functional group. Although quite mild conditions were sought for the plasma polymerisation to avoid the cleavage of MMA,[81,138] fragmentation still may occur. The ester signal at $1726\,\mathrm{cm}^{-1}$ decreased slightly upon plasma polymerisation, but still was pronounced. As ATR-IR does not yield quantitative information and is extremely sensitive to the position of the sample, additional measurements were necessary.

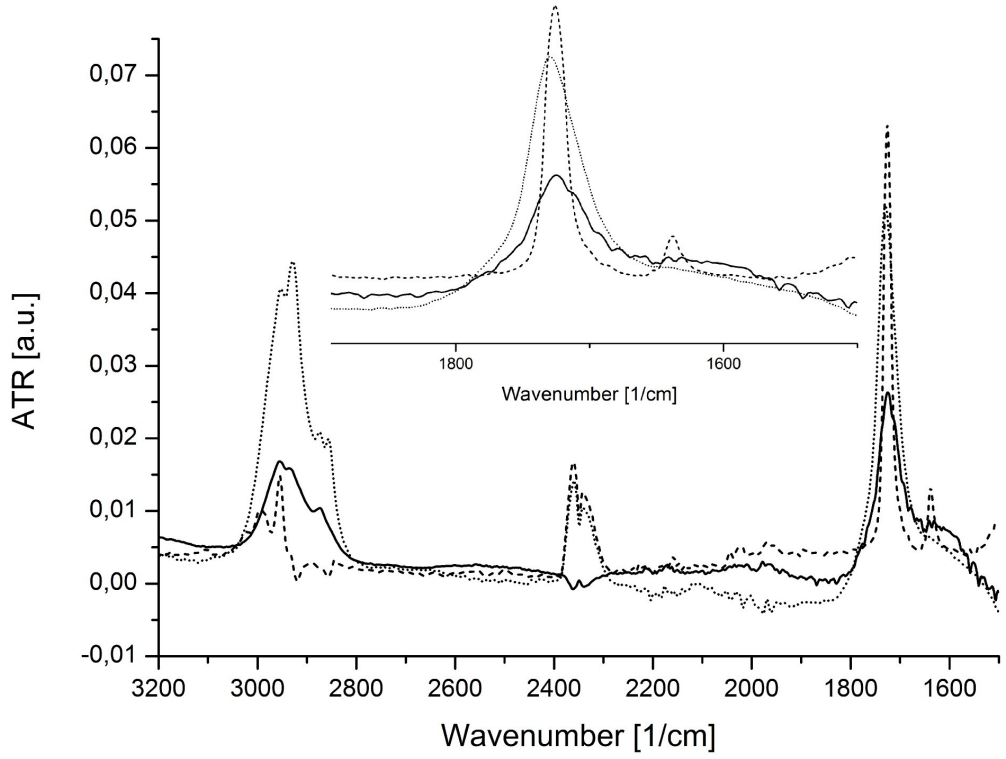

Figure 2.14: ATR-IR spectra of the monomer MMA (dashed line), the resulting ppMMA coating (dotted line) and the ppMMA coating after an immersion in SBF for 21 d (solid line). The discussion of the immersion experiments is in Section 3.2.1. Figure published in ref. 81.

Fits of high resolution XPS spectra allowed for a closer look at the surface chemistry of the plasma polymerised coating. The O 1s signal can be fitted with two curves representing a single and a double bond environment at 538.1 eV and 536.8 eV, respectively (Figure 2.15 and Table 2.3).[81] In a conventional PMMA coating the ratio of double to single bond environment should be 1:1. In the present ppMMA film slightly more than half (56.9 %) of the oxygen was in a double bond environment. This can be explained by a certain loss of the ester moiety, which is well known in literature for the plasma polymerisation of MMA.[150] The functional group is cleaved by a plasma induced scission between the carboxyl C and the O of the methoxy group.

In the high resolution C 1s spectrum, the scission is represented by an additional curve for a carbonyl C at 291.9 eV (Figure 2.15 and Table 2.3). The other peaks – the alkyl peak at 289.6 eV, the methoxyl peak at 291.0 eV and the carboxyl peak at 293.6 eV – are analogue to the spectrum of the "conventional" PMMA and other ppMMA coatings.[150] It should be mentioned that the values of the binding energies are slightly shifted compared to literature. This is probably due to a charging of the sample despite using the conductive Highly Oriented Pyrolytic Graphite (HOPG) as a substrate instead of glass. The relative peak positions, however, are consistent with literature values.[150]

Table 2.3: Values for the binding energy and the areas of the fitted peaks in the high resolution XPS spectra (Figure 2.15) of ppMMA coatings on HOPG substrates.

		Before irradiation		After irradiation	
Element	Peak assignment	Binding energy [eV]	Area [%]	Binding energy [eV]	Area [%]
C 1s	C–C/C–H	289.6	73.5	289.7	54.1
	C–O	291.0	12.7	291.1	17.1
	C=O	291.9	5.7	292.1	10.0
	O–C=O	293.6	8.1	293.7	15.3
O 1s	C=O	536.8	56.9	537.1	72.6
	C–O	538.1	43.1	538.2	27.4

Taken together, the ATR-IR and XPS measurements show that the plasma polymerisation of MMA was successful. Part of the functional group might have been lost in the plasma process as indicated by the excess of oxygen in a double bond environment, but the major part was still intact.

The ppH and ppMMA were subsequently patterned *via* UV-lithography irradiating for up to 45 min (Figure 2.16). Already in the DIC micrographs of the patterned ppMMA coatings, a time dependence of pattern height was apparent (Figure 2.16). It is also clearly visible that the patterning process yields an even and uniform surface.

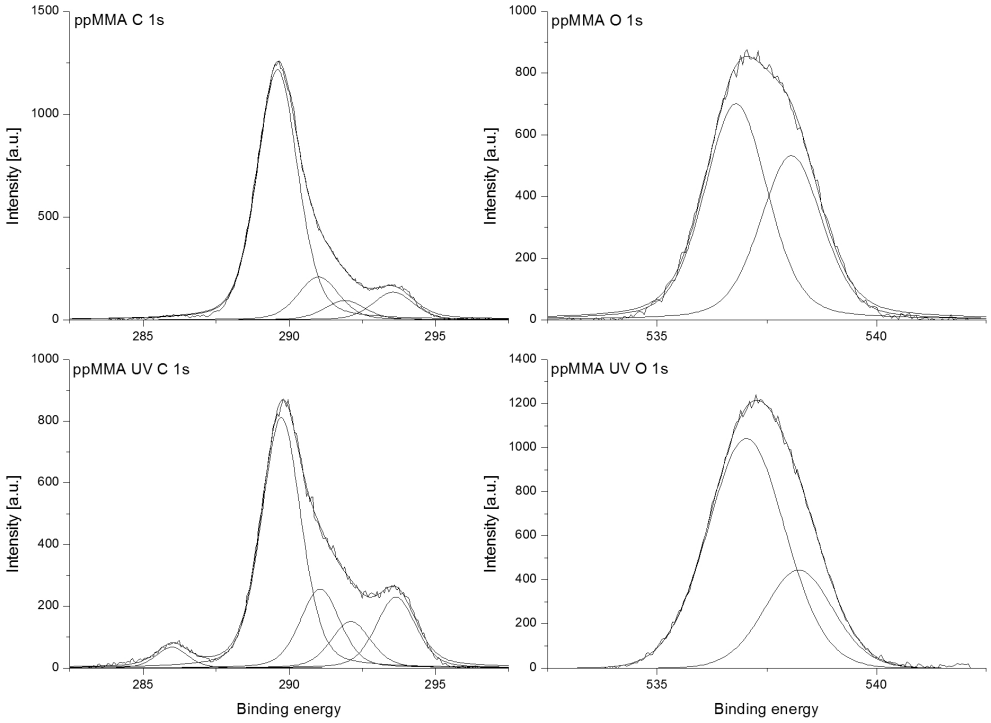

Figure 2.15: XPS spectra of ppMMA coatings on conductive HOPG substrates (above) and the same coating after 20 min of deep UV-irradiation (below); the high resolution spectra of the C 1s signal (left) and the O 1s signal (right) were fitted. Figure published in ref. 81.

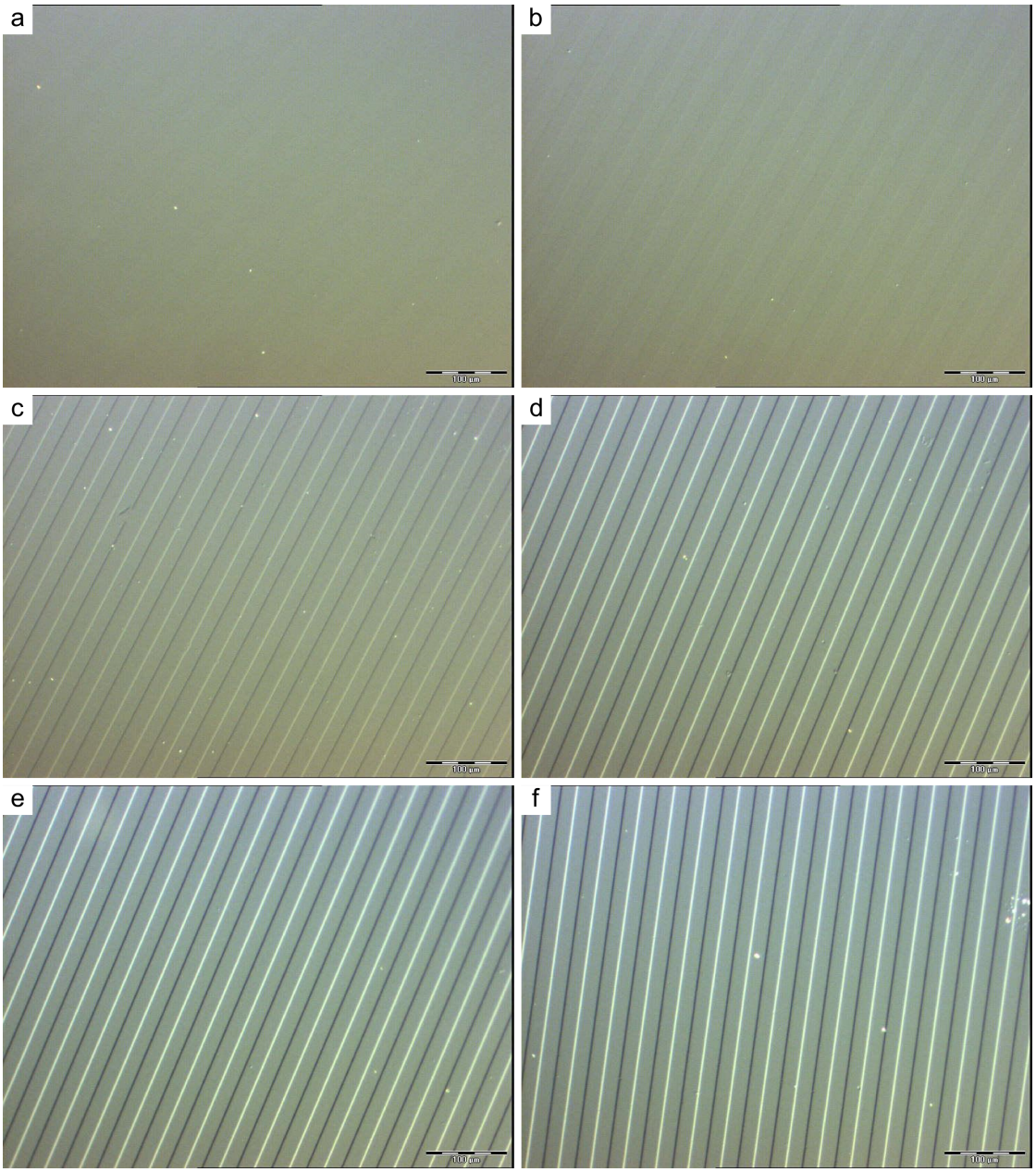

Figure 2.16: DIC micrographs of patterned ppMMA coatings with OTES as adhesion promoting layer prepared following the protocol given in Section 7.4. These coatings were irradiated through a mask with 20 µm lines for 2.5 min (a), 5 min (b), 10 min (c), 20 min (d), 30 min (e) and 45 min (f) as described in Section 7.5; scale bars 100 µm.

To examine the patterned coatings more closely, AFM scans were conducted (Figure 2.17). These measurements confirmed the conclusions drawn from the DIC micrographs. The patterns were even and uniform, even down to a line width of 1.25 µm (Figure 2.17a).

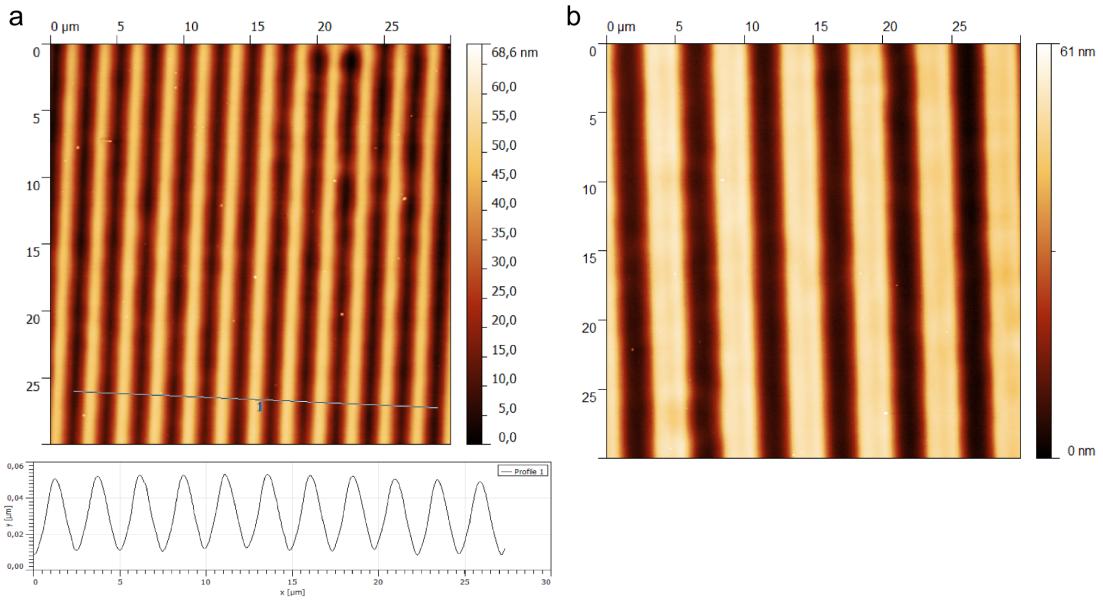

Figure 2.17: AFM topologies of patterned ppMMA coatings with OTES as adhesion promoting layer after 20 min (a) and 30 min (b) irradiation through a mask with line patterns of different sizes. (a) shows the smallest structure produced with a line width of 1.25 µm. For details of the preparation please compare Sections 7.4 and 7.5.

In a series of experiments, the dependence of the pattern height on irradiation time was investigated measuring the profile with a profilometer (Figure 2.18). After a linear increase of the pattern height over irradiation time, the height seems to level off and might even reach a saturation value. Reasons for this decreased height gain could be a photo reaction as described in ref. 39. The authors observed a decrease after 30 min irradiation time and ascribed this to "parasite irradiation in dark areas due to diffraction by the edge of the grating or induction of other reactions such as cross-linking". Alternatively, degradation debris in the grooves might screen lower layers from the irradiation and thus protect them from ablation.

In the present case, the maximum pattern height also correlated to the film thickness, as other experiments in our group showed.[193] After an irradiation of 45 min and above, the complete ppMMA film was removed in the irradiated areas. When OTES was the adhesion promoting layer, further ablation was impossible as the silane monolayer could not exceed 1 nm thickness – well below the accuracy of the measurements. In this case, the

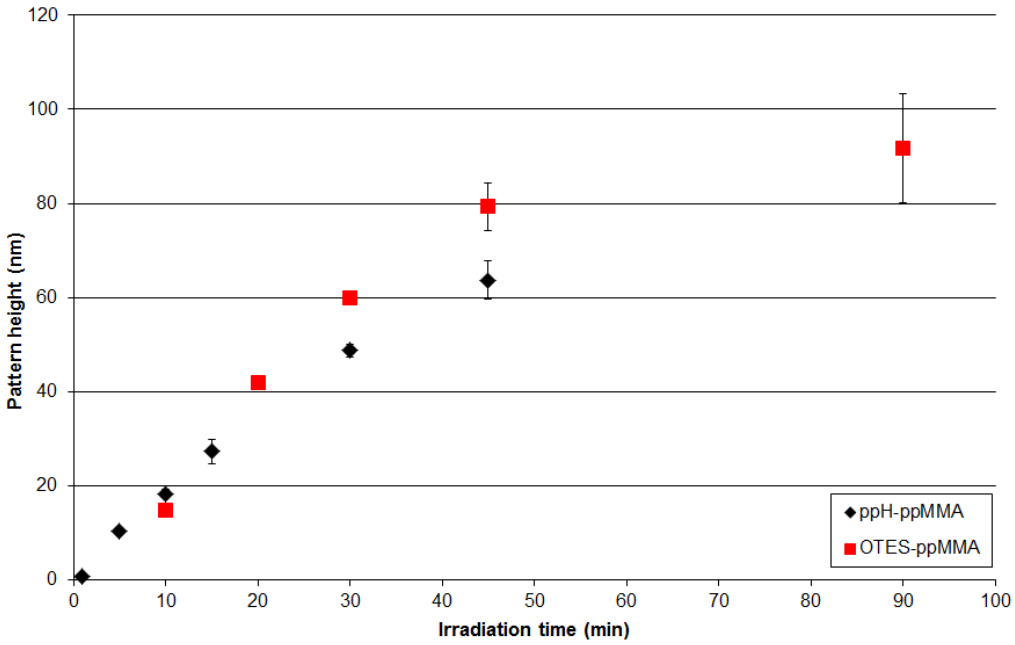

Figure 2.18: Dependence of plasma polymer pattern height, as measured with a profilometer, on the irradiation time. The samples correspond to the ones in Figure 2.16 and were prepared and measured as described in the Sections 7.4, 7.5 and 7.8.3.

higher variability of the pattern height at longer irradiation times reflected the variability of the ppMMA film thickness.

When ppH was the adhesion promoting layer, the ablation could indeed continue as the plasma polymer layer was considerably thicker than the OTES SAM. However, the ablation rate for ppH was considerably lower than the one of ppMMA. After 30 min irradiation, the pattern height of ppH coatings was only about 8 nm,[81] whereas the ppMMA patterns reached a height of 45 nm (ppH-ppMMA) or 60 nm (OTES-ppMMA). It is known that the "conventional" analogue of ppH, Poly(Ethylene) (PE), resists UV-degradation well, as it lacks chromophoric groups[194] and does not absorb UV-light over 200 nm wavelength to a great extent.[195] PMMA on the other hand is ablated by photo-induced ester decomposition and a photo-oxidation process. Although the short ester side group prevents excessive UV-degradation, the polymer is nevertheless known to form acid groups and to possibly form cross-links.[196] Transferring these findings to the plasma polymer analogues explains the higher ablation rate of ppMMA in UV-light compared to that of ppH.

How the UV-light degraded the plasma polymers, remains to be discussed. The energy of the 250 nm band of the UV-lamp alone is sufficient to break single C–C bonds (348 kJ mol^{-1}).[145] However, during irradiation, the polymer was most likely oxidised by the oxygen in air and the ozone that forms in the deep UV-light.[179] Before rinsing, there were already pattern steps of a few nanometre height, but the step height of the structure was multiplied by the rinsing step. The increase of the step height during the rinsing step indicates that organic debris molecules that formed during the lithography were removed. Therefore, oxidation was not complete, the whole polymer was not directly oxidised to CO_2. Next to the oxidative degradation, a photo-induced mechanism cannot be excluded. The degradation might be caused by both mechanisms, as further experiments by Andreas Schaller showed that UV-irradiation under inert gas reduced the pattern height significantly, but did not prevent patterning altogether.[193] Although one must add that there still was residual oxygen present, which might have been sufficient to cause the ablation. Further experiments are still necessary to clarify the degradation mechanism.

A second aspect of the lithography is the change in surface properties it induces. Irradiation makes the surfaces more hydrophilic. This wettability contrast is clearly visible in Figure 2.19, where the square areas were exposed to the UV-light. In these areas water was retained, whereas it was repelled in the non-irradiated regions.

XPS measurements provided a more detailed picture of the changes in surface chemistry during irradiation (Figure 2.15 and Table 2.3). The oxygen content rose from 21.5 % to

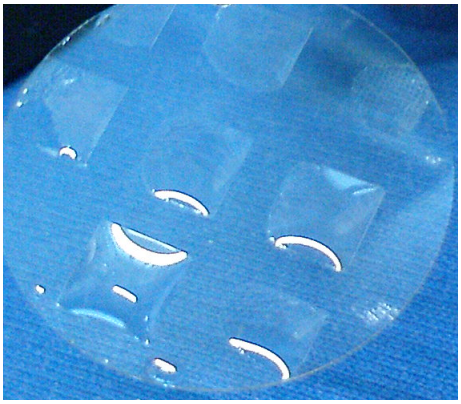

Figure 2.19: Hydrophilic-hydrophobic contrast of a patterned sample after UV-irradiation.

29.0 % during the irradiation. This increase supports the assumption of an oxidative process involving reactive oxygen species formed in the UV-light. Analysis of the C 1s peak backs this up with a rise of the oxygen binding C species from 26.5 % to 42.4 % due to the UV-irradiation. At the same time the binding environment of the O species changed greatly from 56.9 % in a double bond environment before to 72.6 % after irradiation. The excess of O in a double bond environment suggests a loss of the methoxy group degrading the ester and yielding carbonyl moieties. As a short side note, the additional peak at 286 eV in the C 1s spectrum in Figure 2.15 is probably due to a scratch in the coating and can be ascribed to the HOPG substrate.

Concluding, ppMMA layers were successfully deposited onto glass substrates with two different adhesion promoting layers – the silane OTES and the plasma polymer of *n*-heptane. During the plasma process, the major part of the ester functionality was preserved. The ppMMA coating was patterned with a UV-lithography process up to 90 nm pattern height. The dependence of pattern height on irradiation time was examined and found to be linear only in the first 40 min, levelling off after this time. The UV-ablation process was probably due to reactive oxygen species developing in the UV-light. During the irradiation time, the surface chemistry changed considerably becoming more hydrophilic and exhibiting a greater oxygen content. In the irradiated areas, carbonyl moietes presumably prevailed, as XPS measurements suggest.

2.3 Comparison of the Two Coating Procedures

Whereas the polymer brushes are strictly defined linear polymers with a specific chemistry, plasma polymer coatings can contain more chemical groups than the ones intro-

duced by the monomer. Although the development of new methods allowed for quite good chemical control, cross-linking and loss of functional groups takes place even under mild conditions such as pulsed plasma.

For the industrial production of implants, plasma polymers have the great advantage of a simple and fast synthesis, which is easily converted into a process chain, as the already commercially available systems show.[138] If the substrate activating steps are also carried out as a plasma method, there is no need to move or handle samples between the different procedure steps, which saves time and workforce.[143] No solvents are needed, which makes the plasma polymerisation environmentally friendly and economic.[138,143]

The highly controlled polymerisations that produce the polymer brushes are elaborate in several ways. It is necessary to work under inert conditions. The coating process requires several steps, between which handling of every single sample is necessary. This makes the method time- and labour-intensive and thus not effective enough to be attractive for industry. Additionally, the yield in relation to the monomer is extremely low, yielding a coating in the nanometre range after introducing grams of the monomer. SI-ATRP also needs organic solvents for a good control, which adds to the drawbacks, as they are environmental disadvantageous and have to be disposed of, which causes additional costs.

In respect of biomaterial applications, the use of organic solvents in the polymer brush synthesis is also problematic. Methanol is toxic and DMF is harmful. Without being sure that no solvent remains in the polymer brush, one cannot consider these coatings safe for medical uses. Even when a polymerisation protocol is used that does not need an organic solvent, as in the PMAA brush synthesis, there is still the possibility of bound copper ions and the bpy ligand remaining in the polymer film. Both are harmful or toxic, as well, and might negatively affect bone cell growth and viability. For an easier catalyst removal, the copper complex could be immobilised onto spheres and thus even retrieved for a better economical balance.[108] In addition to these partly solved issues, the capping halogen group at the end of the polymer is considered harmful in biomaterials as well. It should be removed in additional post-polymerisation reactions adding to the uneconomic character of SI-ATRP.[108]

However, also the plasma polymerisation technique has some drawbacks in this aspect. The mild polymerisation conditions that make sure the functional groups are retained also cause some unpolymerised monomers to be integrated into the coating. This integration is problematic for a whole range of monomers, especially of acrylates and methacrylates as they could react with tissue in a patients body. Basically, residue monomers would evoke similar concerns as the use of *in situ* polymerising bone cement, which is hardened

during the operation. (Wherein the *in situ* polymerisation poses an additional issue due to the high temperatures developing in the process.) To get rid of residue monomers, the coated substrates could be placed in vacuum to evaporate them, in case the monomers are volatile enough. Alternative monomers might also solve the biocompatibility problem for biomaterials applications. Using biomolecules such as maleic anhydride is a popular and promising approach and deserves further research.[39,197]

In spite of these concerns, biocompatibility experiments in cell culture conducted for this work did not show signs of toxicity for these materials, as will be described in the following chapter. However, carefull testing and long-term research will be necessary to eliminate the possibility of introducing traces of harmful substances into biomaterial. Chemically, the resulting polymers were nevertheless good candidates for a biomaterial that mimics biological polymers. Furthermore, they provided model systems for the analysis of the influence the different functional groups had on cell growth, on mineralisation and on nanoparticle adsorption.

3 Applicability of the Polymer Coatings as Biomaterials*

3.1 Introduction to Biomaterials Testing

3.1.1 Bone Cells

Mesenchymal Stem Cell (MSC) are adult stem cells.[198,199] They can be isolated from the bone marrow, placenta, cord blood and the adipose tissue.[198,200–202] They differ from embryonic stem cells in being already committed to the mesenchymal lineage.[9] Therefore, MSC are called multipotent since they are still able to differentiate into a variety of mesenchymal cell types, such as osteoblasts, adipocytes and chondroblasts, or to myocytes, stromal cells, fibroblasts as well as neuronal and endocrine cells.[9,198–201,203] Because of these properties, they are interesting subjects of research to regenerative medicine and tissue engineering.[198,202,204]

Differentiation *in vitro* has to be induced by supplements added to the cell culture medium. Cell medium supplemented with dexamethasone or retinoic acid, 1,25-$(OH)_2$-vitamin D_3, β-glycerophosphate and ascorbic acid are employed to induce osteoblast differentiation.[9,77,199] However, also other factors influence MSC differentiation or may influence it, such as cell density, mechanical properties of the surrounding, cytokines or other autocrine and paracrine factors.[199]

For some experiments, Human Mesenchymal Stem Cell (hMSC) were used for their being close to the *in vivo* genotype and phenotype, as they are not transformed by oncogenes or viruses.[201] Additionally, due to their undifferentiated state, the influence

*Parts of this chapter (text, experimental details and figures) have been published in ref.s 47,48,81:
Sabine Letsche, Annina Steinbach, Manuela Pluntke, Othmar Marti, Anita Ignatius, Dirk Volkmer; "Usage of polymer brushes as substrates of bone cells" *Front. Mater. Sci. China*, **2009**, *3*, 132–144,
Annina Steinbach, Andrea Tautzenberger, Anita Ignatius, Manuela Pluntke, Othmar Marti, Dirk Volkmer; "Coatings from micropatterned sulfobetaine polymer brushes as substrates for MC3T3-E1 cells" *J. Mater. Sci. Mater. Med.*, **2012**, *23*, 573–579 and
Annina Steinbach, Andrea Tautzenberger, Andreas Schaller, Andreas Kalytta-Mewes, Sebastian Tränkle, Anita Ignatius, Dirk Volkmer; "Plasma-Enhanced Chemical Vapor Deposition of *n*-Heptane and Methyl Methacrylate for Potential Cell Alignment Applications" *Appl. Mater. Interfaces*, **2012**, *4*, 5196–5203.

of external parameters on differentiation can be tested.

From MSCs that are located in the bone marrow, osteoblasts develop. They are the bone building cells. The factors promoting this differentiation are, amongst others, transforming growth factor-β, bone morphogenetic protein and parathyroid hormone. The differentiated osteoblasts are located on the bone surface as a tightly connected cell layer and secret the organic bone matrix, the osteoid, onto this surface. They are not only active during embryogenesis but also in adults, maintaining and remodelling the bone.[9,205] After this secretory phase, the osteoblasts undergo apoptosis or become surrounded by bone tissue and further differentiate into osteocytes.[9,205]

In their secretory phase, the osteoblasts secret the bone ECM proteins, which consist mainly of type I collagen as the main structural protein in bone (see also Section 4.1.2). The other proteins are the non-collageneous proteins: proteoglycans, glycoproteins, γ-carboxylated proteins, phosphoproteins and regulating enzymes. These are involved in the regulation of bone mineralisation, of cell adhesion and differentiation and of cell activity and function.[205] Osteoblasts are also responsible for mineralising the collagen matrix. They form vesicles with a precursor mineral, which they secret into the osteoid where the mature mineral develops.[206] Thus, the osteoblasts account for the secretion of nearly all the components of the bone and are therefore of great interest in almost every aspect of bone research.

As osteoblastic markers in research, osteocalcin, osteopontin, periostin, Bone Sialoprotein (BSP), Alkaline Phosphatase (ALP) and Type I Collagen (COL I) are used.[9,77,207–211] For this work, ALP staining was used as a marker of osteogenic differentiation. Active osteoblasts produce ALP as an early marker, which takes part in the early mineralisation.[77]

Besides hMSCs, a pre-osteoblastic cell line was used to test the polymer coatings for their applicability as biomaterials. Due to the immortalisation, these cells can be used in much higher passages than stem cells, but this immortalisation also changes their metabolism and regulation.[9] Yet, it is a good model system.

The MC3T3-E1 cell line was established by Kodama *et al.* in 1981 and further described by the same group in Sudo *et al.*[212] They characterised the MC3T3-E1 as osteoprogenitor cells, which were able to differentiate into osteoblasts and even further into osteocytes. Sudo *et al.* also showed the cell line's ability to mineralise the collagen fibril matrix they secreted *in vitro*. The authors observed different differentiation stages in cell culture, which were arranged similar to the *in vivo* situation. Also the deposited mineral seemed to correspond to the bone substance, so Sudo *et al.* recommended their cell line as a model system for bone-related studies. MC3T3-E1 cells indeed were em-

ployed for a number of cell culture biocompatibility studies of the materials, *e.g.* in ref.s 27,44,46,161,213–215. *In vitro*, they correspond to mature osteoblasts in their phenotype, but cannot mineralise without the additives of osteogenic cell culture medium.[9]

Finally, there are the bone resorbing cells, the osteoclasts. They are in close interplay with the osteoblasts constantly remodelling and maintaining the bone.[9,205,216] They are a possible target for pharmaceuticals on implants inhibiting the bone resorbing function, such as calcitonin and bisphosphonates, which are already used clinically against pathological bone resorption.[205,216]

3.1.2 Biomaterials and Osteoblasts

The Interaction between Osteoblasts and Patterned Materials

Topographical patterns with a certain orientation induce the alignment of cells, including osteoblasts, and direct their movements.[15,26,38,39,147,157,161,168,217–221] Micropatterned substrates with lines ranging from 5 µm to 10 µm width elicited osteoblast and MSC alignment and contact guidance.[161,218,220] Bone cells were described to exhibit contact guidance on substrates with grooves deeper than 1.6 µm.[15,218,220,222] Nevertheless, it was shown that also nanoscale features can influence osteoblast behaviour as well as alignment, function and proliferation.[5,24,215,223–228]

The reason for this behaviour might be the similarity to the natural environment of osteoblasts,[5,215,221,224,227] as osteoblasts follow osteoclasts on their way through the bone matrix on traces with a "complex micro and nanotopography".[33] Although the topographical environment around osteoblast is so complex,[5,7,33,224] simple geometrical patterns, such as linear ones, can influence cell behaviour in a positive way.[217,218,222] Eisenbarth *et al.*[217] pointed out the better adhesion behaviour of aligned cells over non-oriented ones. The aligned cells had a higher density of focal contacts and a favourable organisation of the cytoskeleton. An alignment of cells lead to the production of aligned ECM, especially COL I, as Zhu *et al.*[228] and Wang *et al.*[218] showed. In mature bone, the ECM is aligned, organising the bone mineral and reflecting the material's anisotropic properties.[228–233] Thus, provoking the alignment of ECM proteins on a biomaterial through microstructures might improve bone growth on the biomaterial and consequently osseointegration.[228,229]

Besides the topographical pattern, the surface chemistry influences cell growth. Cell adhesion, and consequently their proliferation and differentiation capacity, always depends on the composition and the conformation of the underlying layer of adsorbed proteins.[15] The proteins' conformation in turn depends on the physicochemical charac-

teristics of the surface.[142,234,235] Keselowsky *et al.*[236] investigated the effect of functional groups such as methyl, hydroxyl, carboxylate and amine groups on fibronectin adsorption and consequently its impact on cell adhesion. They found that hydroxyl groups outperformed the other functionalities with the methyl groups as the least preferred surface. Healy *et al.*[237] presented both methyl and amino surfaces on substrates that were functionalised in a linear pattern. Bone cells preferably spread on the amino functionalised surface and mineralised it subsequently. As James *et al.*[13] observed, the increase of carboxylate groups on implanted polymer pins improved the integration into the surrounding tissue by chelating Ca^{2+} ions. These Ca^{2+} ions are the foundation for the build-up of hydroxyapatite and connect the biomaterial to the bone.

Zapata *et al.*[36] found an optimum of the size of a pattern, when they fabricated substrates of demixed poly(ϵ-caprolacton)/poly(D,L-lactide) (PCL/PDLA) blends by phase separation. The MC3T3-E1 osteoblast-like cells adhered preferably on the PDLA islands, bridging the PCL parts. At places where the distance was too large, this bridging caused stress on the cytoskeleton resulting in reduced proliferation. The earliest and highest maximum in cell growth was observed at a structure of 21 µm to 33 µm.

Concluding, there is strong evidence that cells are affected by both topography and chemistry of surfaces. The effect can influence cell growth and activity in a positive way.

Cell Culture on Polymer Brushes

The polymer brushes were used in the first place for their anti-bacterial properties. They prevent protein adsorption to surfaces quite effectively. It is well known that protein adsorption is a prerequisite for cell adhesion and it was shown in a number of studies that polymer brushes successfully prevent both protein adsorption and bacterial adhesion.[53,82] Zwitterionic polymer brushes such as the PSBMA brushes in particular turned out to be effective inhibitors of protein adsorption and biofilm formation.[50,51,238] Important parameters to control the cells' interaction with the surfaces are brush length and density.[45,87,239,240] The higher the density and the molecular weight of the polymer brush, the more effective is the prevention of protein adsorption.[44,45,50,52,87,239]

For eukaryotic cell array applications, also the multitude of possibilities to pattern the polymer brush coatings (Section 2.1.3) is a great advantage, as cells and proteins can thus be conducted accurately to specific areas of a surface. Studies on the use of polymer brushes for cell culture with eukaryotes are rare,[43,46,47] but Iwata et al.[43] showed that fibroblast adhesion could be restricted by the zwitterionic phosphorylcholine brush Poly(2-Methacryloyloxyethyl Phosphorylcholine) (PMPC). Tomlinson *et al.*[46] showed the connection between polymer brush length, fibronectin adsorption and cell adhesion

with gradient polymer brushes. When the polymer chain length was high, less fibronectin adsorbed and consequently less cells adhered to the substrate.

Next to the selective spacial adsorption, the selective adhesion of cells in time is a major application of polymer brushes. The thermoresponsive Poly(*N*-Isopropylacrylamide) (PNIPAm) is well known as substrate for cell culture in tissue engineering.[241] The polymer's Lower Critical Solution Temperature (LCST) is at approximately 32 °C, at which temperature its wettability changes from hydrophilic to hydrophobic.[53,54,169,175,241] Cells are cultured at temperatures above the LCST, mostly at 37 °C, when the polymer brush is hydrophobic and not hydrated and therefore allows for protein adsorption and cell adhesion.[53,54,175,241] At confluence, the coated substrate with the cells is brought below the LCST to room temperature, and the PNIPAm properties drastically change.[175,241] The polymer brush suddenly becomes soluble in the aqueous environment and becomes extremely hydrated. In this hydrated state, no cell adhesion is possible and the confluent cells detach as a cell sheet.[54,175,241] The advantage over the conventional enzymatic method is the preservation of the cell-cell contacts and ECM, which is pivotal for tissue engineering applications.[54,241] A similar switching behaviour to the PNIPAm films was shown for PSBMA brushes, but at a higher temperature regime.[49]

To enable adhesion of only a specific wanted cell type, there are approaches that combine the anti-protein adsorption behaviour of the polymer brushes with the possibility of coupling them with bioactive peptides or proteins that are promoting cell adhesion.[56,58] A famous example is the Arginine–Glycine–Aspartic Acid (RGD) peptide.[58,242] It was shown in several studies that RGD-functionalised polymer brushes support adhesion and growth of different cell types.[243–245] Also collagen I was already successfully coupled to PHEMA brushes and this surface showed better osteoblast adhesion than uncoated Ti did.[14] Good biocompatibility and cell adhesion are ascribed to collagen I.[14,246] This behaviour may be partly due to the peptide sequence GFOGER (glycine-phenylalanine-hydroxyproline-glycine-glutamate-arginine) in collagen I, which also promotes cell attachment.[58,242]

For this work, unmodified patterned and unpatterned polymer brushes were tested in cell culture on hMSC and MC3T3-E1 cells. Their morphology was observed and the expression of proliferation and apoptosis markers was analysed at mRNA level to test their viability. For, although it is known that cell adhesion on patterned polymer brush substrates can be restricted to the groove areas, little is known about cell function in this situation.

Cell Culture on Plasma Polymers

Many plasma polymer systems were tested on their influence on a range of cells from neurons to epithelial cells and fibroblasts.[146] Here, I will concentrate on the impact these thin films have on osteoblasts. Schröder *et al.*[247] used plasma polymerised allyl amine to coat titanium substrates with implanted copper ions. The plasma polymer protected osteoblasts from direct contact to the copper, improved their adhesion and controlled the release of copper ions, which inhibited bacterial growth. Similarly, Ploux *et al.* tried to give an edge to osteoblast over bacteria adhesion by using patterned plasma polymerised maleic anhydride for cell culture. Due to the negative charge on the UV-patterned areas, this system succeeded in reducing bacterial proliferation and enhancing osteoblast adhesion. Besides the acidic maleic anhydride, a plasma co-polymer of acrylic acid and the hydrocarbon octa-1,7-diene provided a good surface for osteoblast-like ROS 17/2.8 cells.[248] The optimum acid concentration on these surfaces for the cell adhesion was determined to be 3 %.[142] Substrates made only from the hydrocarbon, on the other hand, performed poorly in supporting cell attachment.[248] In contrast, Grinevich *et al.*[249] found hydrocarbon plasma polymers in a nanocomposite with titanium to be comparable to glass or standard cell culture plastic substrates in supporting the same cell line. Quite common are coatings from plasma polymerised hexamethyldisiloxane, which are cost effective and bioinert. To enhance their biocompatibility and interaction with cells, they are modified using plasma techniques[250] or mineralisation methods.[251] No additional modification is necessary when choosing the popular positively charged plasma polymerised allyl amine coatings. These coatings even enhanced MC3T3-E1 cell adhesion compared to titanium surfaces.[252] To stay with the amines, similar to the PNIPAm brushes, plasma polymer films from the same monomer were thermoresponsive as well. They might therefore be used in tissue engineering in the same way as the polymer brush system.[253,254]

In this work, ppMMA was the coating of choice as described in Section 2.1.2 and published in ref. 81. ppMMA was chosen since it was shown to be bioinert.[149] It is additionally a promising precursor to surfaces with carboxylate functionalisation. It will be even possible to adjust the degree of functionalisation by adjusting the degree of hydrolysis. To preliminarily test the coatings' potential relevance for hard tissue implants, pre-osteoblastic MC3T3-E1 cells were grown on these materials and examined for their morphology light microscopically as well as for proliferation and viability at mRNA level.

3.1.3 Simulated Body Fluid

Simulated body fluid (SBF) is a salt solution corresponding to the human body fluid in its salt ions and their concentrations (comp. Section 7.6.3). It is buffered typically at a physiological pH 7.2 to 7.4 with a Tris(hydroxymethyl)aminomethane (TRIS)/HCl buffer. Kokubo *et al.*[255] famously developed this solution to mimic the effect that implantation experiments had on biomaterials. They presented therefore an *in vitro* alternative to animal experiments. It is mostly used to preliminary test new materials for their ability to induce biomineralisation (often referred to as bioactivity in this context). SBF offers the possibility to screen biomaterials *in vitro* prior to *in vivo* experiments, thus reducing costs and wastage of animals. At the same time, it is a model to investigate biomineralisation itself, being close to the *in vivo* situation but yet controlled. Consequently, a plethora of studies make use of this method in various ways, *e.g.* ref.s 60,64,66,73,256–262.

A point of criticism against this testing of bioactivity is the static nature of the SBF mineralisation set-up. Mostly, the substrates are immersed in the solution for a period in the range of weeks without the turn-over of a biological system. Additionally, the (mineralisation controlling) proteins are not present, so their contribution to the biomineralisation process is left out. Consequently, *in vitro* and *in vivo* experiments might diverge.[60] Usually, the SBF results overestimate the material's bioactivity due to the lack of inhibitory proteins. When additional Ca^{2+} and PO_4^{3-} are introduced by the material, it might add to this overestimation because of the higher effective ion concentration in a static system. Nevertheless, the SBF *in vitro* bioactivity test is a valid method to preliminarily screen materials for their biomaterial behaviour. Its simplicity and cost effectiveness outweigh the tendency to overestimate a material's ability to initiate biomineralisation.

In the present work, the SBF immersion was also used to test the different coatings' stability in simulated physiological conditions and thus to detect delamination at an early stage.

3.2 Results and Discussion of the Applicability of the Polymer Coatings as Biomaterials

3.2.1 Stability in Simulated Body Fluid and Bioactivity Testing

The first important point of polymer thin films in biological and especially medical applications is the integrity of the coatings. Immersion in SBF as a simple model for the

physiological environment served as a test for the stability of the films that were described in the previous chapter (Chapter 2). As stated above, immersion in SBF has the advantage of being at the same time a test for mineralisation inducing properties.

Polymer Brush Stability in SBF

Patterned polymer brush substrates were immersed in SBF for 21 d. Light microscopy in the DIC mode showed that after this period on most samples the pattern was not visible any more, as is shown by way of example in Figure 3.1b. Even after scratching the surface with a pair of tweezers, no sign of the polymer coating was detected. This implies the coatings' delaminating in an ion containing environment already after three weeks.

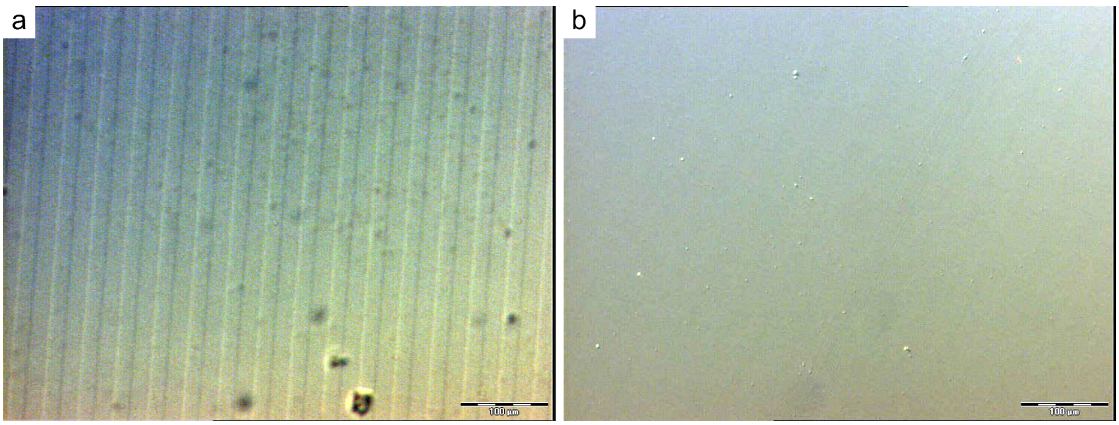

Figure 3.1: PSBMA brush subtrates with a linear pattern with 20 µm line width prepared as described in Section 7.3.1 (a); after immersion in SBF for 21 d (comp. Section 7.6.3) (b) no pattern is discernible any more; scale bars 100 µm.

Although polymer brush chains are presumably not "completely" stretched (comp. Section 2.2.2), they are yet in a restricted conformation. When the grafting density is high enough, the polymer chains have less space available than their radius of gyration (comp. Section 2.1.1). Consequently, conformational stress is acting on the molecules. In addition, especially the strong polyelectrolytes are highly charged, carrying charged groups on every segment of the polymer chain. In the ionic solution, counter-ions enter the polymer film and the hydrated brush swells. This process can increase the conformational stress of the polymer chains in the brush.

Sheiko *et al.*[263] showed that purely conformational stress caused by a high density of polymer chains was indeed able to cause the cleavage of C–C bonds. This finding can probably be transferred to the present case implying a scission of the polymer back

bone under increased conformational stress in ionic solution. As the authors of ref. 263 found the cleavage of C–C bonds at a high density of polymer chains, it might not be the brush's swelling but its collapse to cause polymer brush decomposition. Also Choi *et al.*[123] suggested that polymer brushes might be not stable in ionic solutions. They observed a greater height loss in solutions with high ionic strength than anticipated and reasoned that the collapse of the brush might cause degradation.

The authors of the latter study[123] proposed that the most likely bond to be disrupted of a PSPMA brush coating on gold was the Au–S bond that bound the polymer to the surface, and not the carbon backbone. This observation is supported by the publications of the García group[58] and of Deng and Zhu,[264] both working on Au–S surface-linked polymeric systems. In the polymer brush system of the present work, the polymer brushes were connected to the surface with Si(s)–O–Si bonds. The siloxane bond is stronger than the C–C bond, but there is still the possibility that it was nevertheless the linkage to the surface and not the polymer chain that was breaking.

The trifunctional alkylsilanes are anticipated to build a covalent attachment to the activated glass surface, which carries hydroxyl groups. They are theoretically able to bind to the surface with two siloxane bonds per molecule.[265] Consequently, the polymer brush degradation could happen at two strong siloxane bonds or at one slightly less strong C–C bond. In this case, the choice would be easy and make the scission at the backbone more likely. The situation, however, is more complicated and also other authors argue that the osmotic and steric stress might promote hydrolysis of the siloxane bond.[92] Trifunctional alkylsilanes have two possible alternative reactions: vertical polymerisation and horizontal polymerisation.[265] Vertical polymerisation may happen in the presence of water and leads to agglomerates of alkylsilanes, which are poorly linked to the surface. Horizontally polymerised alkoxysilanes are increasingly linked to their neighbouring molecules as well as to the surface.[266] In both cases, the number of siloxane bonds to the surface per polymer chain is significantly lower than in the case of pure covalent attachment. It might consequently be more probable that the linkage to the surface was the weak spot for polymer brush stability. In this case, one siloxane bond would be cleaved affecting several polymer brush chains around. An argument for this scenario is the polymer brushes tendency to delaminate in patches (Figure 3.3 and ref. 172). It seems more likely that one siloxane link to the surface was broken releasing steric stress of several polymer chains than breaking one C–C bond per chain.

Plasma Polymer Stability in SBF

Just like the polymer brush coatings, the plasma polymerised film was not stable at first. The pure ppMMA layers on glass completely delaminated after 21 d immersion in SBF. Delamination was similarly observed in water by Daw *et al.* with plasma polymer coatings made from acrylic acid and 1,7-octadiene, when the coating was produced with more than 60 % of the acid.[142] Generally, acid, ester and other hydrophilic groups seem to prevent good adhesion to glass surfaces in an aqueous environment. Plasma polymers are commonly thought to have poor adhesion properties on glass, when they are in contact with a good solvent.[144] This is the case when hydrophilic groups are immersed in an aqueous solution. It might be worth noting the parallel to the equally highly functionalised polymer brushes with their high sterical stress that is evaded by the coatings degradation.

One possibility of improving the stability of highly functionalised coatings is a "dilution" of functional groups by co-polymerisation with a hydrocarbon.[142,144] Another possibility of improving the plasma polymer coating's stability is the introduction of an adhesion promoting layer, such as an alkylsilane.[144] This was the route taken here. Different adhesion promoting agents were introduced as an additional layer between glass and ppMMA coating: Plasma Polymerised Styrene (ppS), ppH and OTES. OTES is just like the ATRP initiator an alkylsilane that conveys a direct covalent bond to the surface by building siloxane bonds on activated glass or metals. These covalent bonds are stronger and more difficult to break than the mere electrostatic or hydrophobic interactions that are possible between glass and plasma polymer. The plasma polymers ppS and ppH on the other hand are hydrophobic. Water is therefore not a good solvent for these polymers and consequently, these two coatings should adhere better to the glass substrate when immersed in aqueous solutions. The ppMMA layer on top of the adhesion promoting layer should be well linked to it, as both materials react in the plasma through the ablation/deposition processes.

After immersion in SBF, ppH and OTES did indeed prevent delamination, whereas ppS failed as an adhesion promoting layer. Why the hydrophobic ppS failed and at which interface might deserve additional investigations but this question was not pursued in the present work. As ppH and OTES seemed to be suitable adhesion promoting layers, they were further examined. Therefore, ppH-ppMMA and OTES-ppMMA coatings patterned with different irradiation times were immersed in SBF for 21 d. Before and after the immersion, the pattern height was determined to make sure that the coating did not become thinner instead of delaminating.

The height of ppMMA with OTES and ppH as an adhesion promoting layer did not

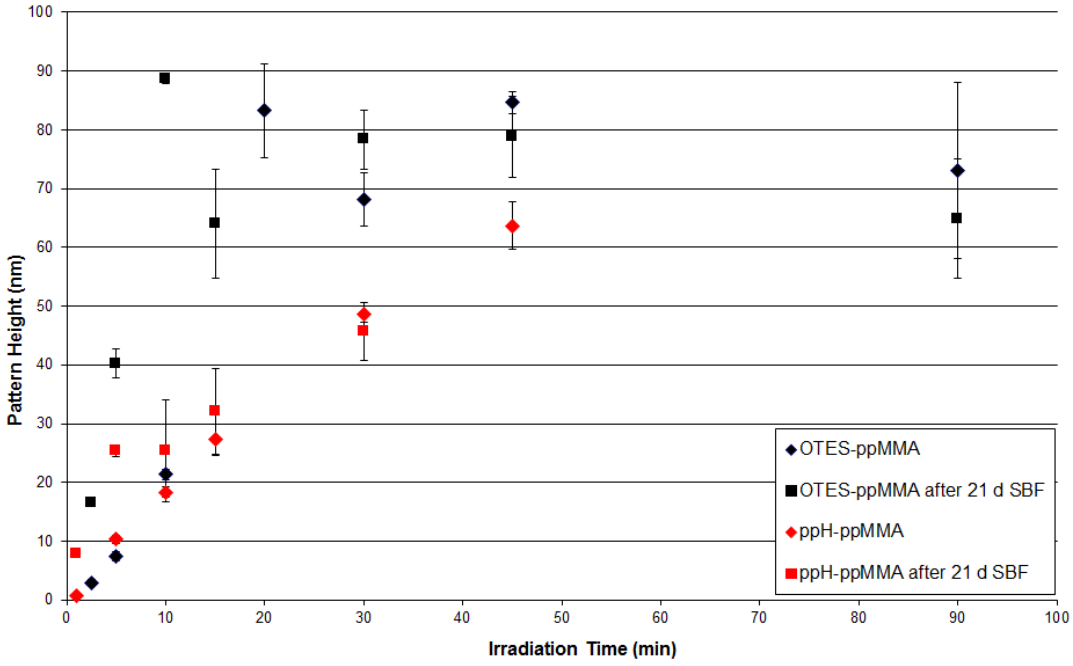

Figure 3.2: Pattern height of ppH-ppMMA and OTES-ppMMA coatings (comp. Section 7.4) as measured with a profilometer in dependence on the irradiation time before and after immersion in SBF for 21 d (comp. Section 7.6.3). OTES-ppMMA before immersion (black diamonds), OTES-ppMMA after immersion (black squares), ppH-ppMMA before immersion (red diamonds) and ppH-ppMMA after immersion (red squares).

decrease during the immersion time. On the contrary, it was partly higher after immersion in SBF than before (Figure 3.2). The height increase is not in agreement with the results of Förch *et al.*,[138,143] who observed a height reduction of a plasma polymer layer after immersion in a good solvent. They ascribed the decreasing height to residual monomers being washed out of the coating. An explanation for this divergence might be the monomers' differing vapour pressure. MMA has a high vapour pressure resulting in a high desorption rate during plasma polymerisation. A high desorption rate leads to films with fewer residual monomers.[140] Consequently, fewer monomers can be extracted during immersion. Alternatively, the height increase might be simply due to residual water in the sample, as they were not thoroughly dried at higher temperatures and in vacuum. Further studies with a sound drying protocol would be necessary to exclude this possibility.

An open question remains why the siloxane connection to the surface was stable enough for the plasma polymer, but not for the polymer brushes. The stability might be linked with the density of the polymer coating. Förch *et al.*[138] observed in their experiments mentioned above that upon immersion in a solvent the plasma polymer layers had a reduced density as monomers and oligomers were extracted from the coatings.[143] The conformational stress of the polymer layer might be reduced in the case of the plasma polymer by the density lowering extraction process taking place, when the polymers are placed in aqueous environment. The extraction process cannot take place with the polymer brushes as – at least theoretically – there is no incorporation of monomer or oligomers. Additionally, the plasma polymer layers might have a lower density in the first place. This seems plausible as the plasma polymerisation mechanism does not have the defined and densely grafted initiatior groups which control the polymer density. In the plasma reaction, there is no controlling force that might drive the system into building a high density layer with conformational stress. Therefore, the plasma polymer layers should have less tension to begin with than the polymer brush systems.

Polymer Brush Stability in Cell Culture Medium

To go a step closer to the physiological system, the polymer brush substrates were immersed in cell culture medium for 7 d. Figure 3.3 shows light micrographs of these samples made in the DIC mode.

For a good part, the unpatterned polymer brush films still seemed to coat the substrates after a week's immersion (Figure 3.3b). In some cases, however, square or geometrically formed areas had delaminated, as shown in Figure 3.3a. The delamination of such regular patches as in Figure 3.3a might imply some degree of cross-linking or entanglement.

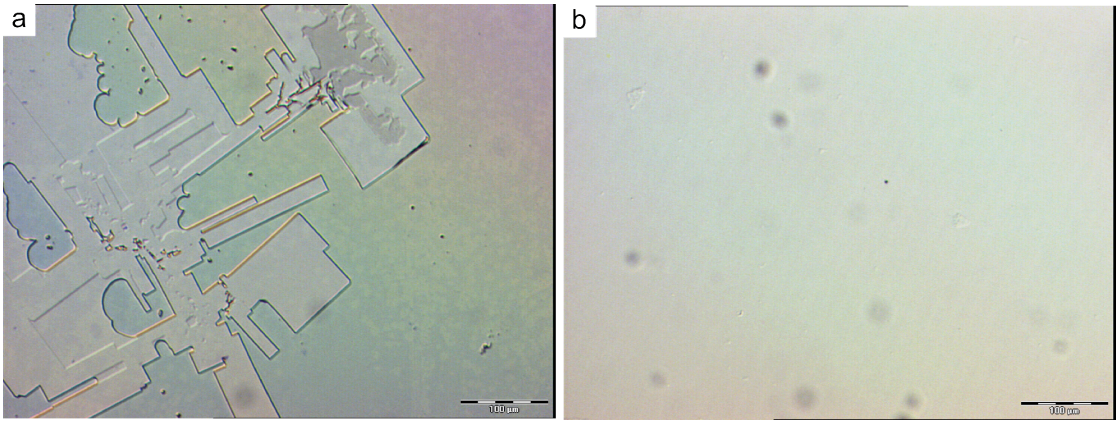

Figure 3.3: DIC micrographs of PSPMA brush substrates (comp. Section 7.3.2) after one week in cell culture medium.

This agrees with the measurements of Pluntke[173] mentioned in Section 2.2.1 suggesting the polymer brushes acting as a network. Tugulu *et al.*[92] showed that cross-linking did not increase a coatings resistance to delamination in cell culture medium, it was, on the contrary, counterproductive. The delamination in patches also supports the hypothesis of the initiator building horizontal polymeric structures and thus lowering the number of anchoring points to the surface. The patches might therefore reflect the horizontal network of polymerised initiator molecules and the network character of entangled polymer chains.

As the cell culture experiments were conducted for a period of three weeks, unpatterned polymer brush substrates were immersed in cell culture medium additionally for 21 d. Prior and after the immersion, contact angle measurements showed changes of the surface chemistry that presented itself to the cells in the cell culture experiments (Figure 3.4). Next to the polymer brush surfaces, also initiator, or more exactly irradiated initiator covered surfaces were in contact with cells. Therefore, these additional samples were included.

Apparently, all the examined surfaces became more hydrophilic in cell culture medium. At the same time, the variation of the values increased for all samples. This suggests that the surface chemistry was less defined after immersion. Most likely, proteins from the cell culture medium adsorbed to the different surfaces exposing their hydrophilic groups to the aqueous surrounding. These modified surfaces presenting hydrophilic proteins should be suitable for cell adhesion, but at the same time, the structuring effect of the polymer brush pattern could be lost.

The non-irradiated initiator's surface chemistry had the greatest change during im-

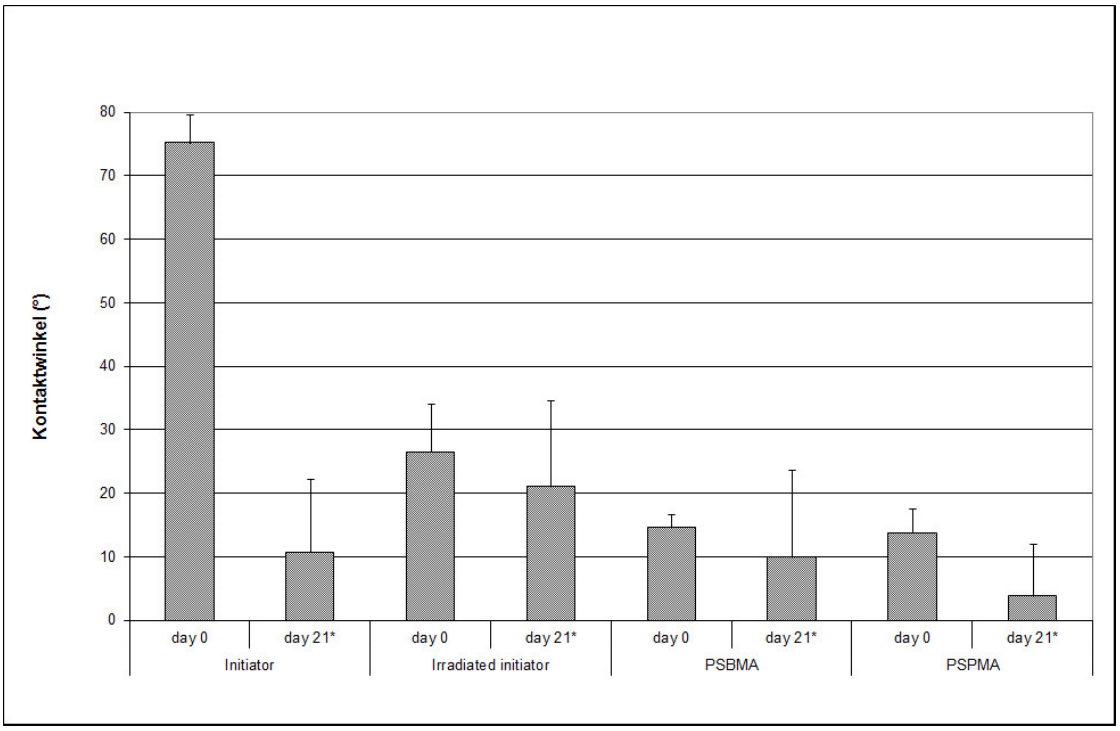

Figure 3.4: Water contact angles of polymer brush surfaces before (day 0) and after exposure to cell culture medium for 21 d (day 21), values indicated with an asterisk (*) are based on fewer measurements, as in these cases the substrates were too hydrophilic for a stable drop to form at several measurements. If no stable drop was formed, a contact angle of 0° was assumed.

mersion in cell culture medium. Chemically, the surface chemistry could have changed through a nucleophilic substitution. Water, which was present in great excess, could substitute the bromide at the end of the alkylsilane molecule and thus render the surface more hydrophilic. This reaction might have added to the surface properties changing effect of the proteins in the cell culture medium.

The changes of the plasma polymer surfaces in cell culture medium have not been examined as thoroughly as the polymer brush surfaces, yet. This should be the subject of further investigations. Yet, preliminary cell culture experiments (Section 3.2.3) gave some insight into the behaviour of the plasma polymer coatings in simulated physiological environments. Despite the promising stability tests in SBF, the formation of cracks (Figure 3.8c and h) and cavities (Figure 3.8j, o and t) was observed on the sample with larger patterns. Nevertheless, the pattern on all specimens was still visible at day 21. Accordingly, no delamination took place. The signs of instability were only observable on samples with a larger pattern width. As the smaller patterns allowed for an easier lateral dilatation,[138] the irregularities suggest strains in the layers swelling in an ion containing aqueous environment. The cracks and cavities could also be caused by monomers and oligomers that were extracted from the polymer coating when surrounded by an aqueous solution.[138] The latter should affect the surfaces irrespective of the pattern size. Therefore strains in the swelling surfaces seem more likely.

3.2.2 Cell Growth on Polymer Brushes

In a series of experiments, hMSC were cultured on the four different polymer brush substrates. Part of the experiments were described in detail in ref. 181. Figure 3.5 gives an overview of the cells' behaviour on these surfaces.

On unpatterned polymer brush substrates, such as in Figure 3.5a, b, e and f, cell adhesion was poor. Especially on the thicker PMAA brushes with the considerable swelling ability, the greatest part of the cells was rounded and floating suggesting that they were not able to attach to the surface. The few cells that were attached to the surface, had an extremely elongated morphology (Figure 3.5a and h). The chemistry of the PMAA brushes is unlikely to be the reason for this unfavourable behaviour of the cells, as studies suggest that growth and behaviour of cells including osteoblast-like cells are improved on negative charged surfaces, especially carboxylate functionalised ones.[142]

The reason for the diminished cell adhesion and growth might be the mechanical properties of the polymer coating. The PMAA brushes swelled to approximately five times their dry height in aqueous environments (Section 2.2.2). The swelling of the polymer brush substrates rendered them rather soft as Plunkte could show with AFM mea-

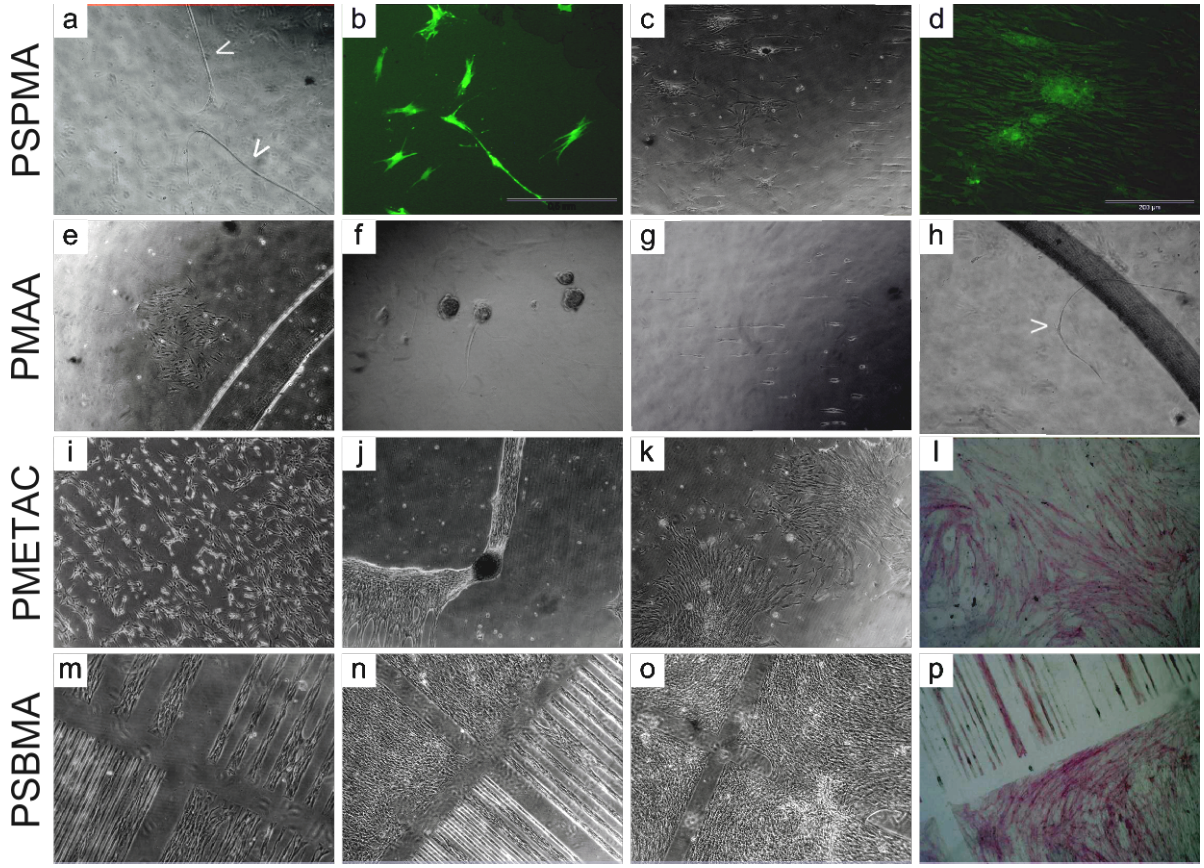

Figure 3.5: Light micrographs of hMSC growth on polymer brush coatings with different functional groups, heights and swelling behaviour: unpatterned PSPMA brushes after one week in cell culture (a), fluorescence micrograph of hMSC after 7 d of cell culture on unpatterned PSPMA brushes dyed for viability with the fluoresceine diactate/IP staining (b), hMSC on a PSPMA brush substrate after 3 d in cell culture (c), fluorescence micrograph of hMSC after one week of cell culture on PSPMA brushes with linear patterns of different sizes dyed for viability with the fluoresceine diactate/IP staining (d), cells on unpatterned PMAA brushes after 12 d in cell culture (e) and on day 1 (f), hMSC on PMAA brush substrates with linear patterns on day 3 (g,h), hMSC on PMETAC brush substrates with linear patterns on day 3 (i), on day 7 (j), on day 10 (k) and after 24 d in cell culture (l) with the hMSC stained for osteogenic differentiation with the ALP staining, hMSC on PSBMA brushes with linear patterns on day 3 (m), on day 10 (n), on day 24 (o) and after 24 d in cell culture (p) with hMSC stained for osteogenic differentiation with the ALP staining. Comp. also ref.s 181 (a–h) and 267 (i–p) and Sections 7.3 and 7.9.

surements.[173] It is well known that osteoblasts need a firm surface for proliferation.[268] As Deschamps *et al.*[269] reported, bone marrow cells preferred even hydrophobic, hard substrates over hydrophilic soft ones, although they generally prefer hydrophilic surfaces. Consequently, the softness of the swollen polymer brushes might hamper cell adhesion.[173,181] Osteoblasts are sensitive to the mechanical properties of their environment and their biochemical pathways and also gene expression are directly linked *via* the cytoskeleton to the mechanical sensors, the focal contacts.[15] Engler *et al.*[270] reported lineage commitment of MSC solely due to the elasticity of the cell culture substrate. The stem cells on very soft substrates differentiated into neurons, whereas the stiffest substrates induced differentiation into osteoblasts. The mechanical properties of the substrate therefore probably have a high impact on MSC and bone cell fate and behaviour.

Alternatively, there are arguments that the mechanical properties of thin polymer brushes are not the cause for the reduced cell interaction and adhesion, but their hydrophilicity and high surface mobility.[14] Singh *et al.*[45] argued that the chain mobility was the main cause for diminished protein adsorption on polymer brush substrates and consequently reduced cell adhesion. It is known that long and mobile polymer chains with a high chain mobility are easily hydrated and more hydrophilic than shorter polymer brush chains.[54] Bhat *et al.*[44] cultured MC3T3-E1 cells on PHEMA brush density and molecular weight gradients and correlated the cell morphology with the fibronectin adsorption. The authors found that high and dense brushes diminished fibronectin adsorption and drastically reduced cell adhesion in these regions. The cells on the high density regions showed an extremely stretched morphology, whereas on areas with a high fibronectin coverage, cell adhesion was higher and morphology normal.[44] The elongated morphology of the hMSC on unpatterned PSPMA and PMAA substrates resembled the descriptions of Bhat *et al.* of cells on surfaces with low fibronectin coverage. The surface coverage and the local concentration of the (hydrophilic) functional groups played a main role according to the authors.[44] Mizutani *et al.*[54] studied the tissue engineering application of the temperature dependent collapsing behaviour of PNIPAm as cell culture material to produce cell sheets. They suggested that the hydration was the key point that prevented protein adsorption.

Hydration and chain mobility indeed seem to be a major factor for the inhibition of protein adsorption.[130,271–274] In a comparison of theoretical and experimental data, Singh and Husson[55] studied the adsorption thermodynamics of peptides adsorbing to different polymer substrates. The authors found that for charged polymer brushes dehydration penalties have to be considered. Chen *et al.*[130] reported in their study on highly protein resistant zwitterionic phosphorylcholine SAMs that the betaines are bin-

ding water through electrostatic binding in contrast to the hydrogen bonds used by PEGs or Oligo(Ethylene Glycol) (OEG) covered surfaces. They are therefore able to bind a significantly higher amount of water. These considerations of Chen *et al.* are in agreement with the observations of Chang *et al.*,[50] who synthesised Poly(Propylene Oxide) (PPO)-block-PSBMA chains and physisorbed them to surfaces to study their influences on protein adsorption. They observed a lower protein adsorption on the zwitterionic PSBMA covered surfaces than on the non-charged PEG covered surfaces. Concluding, these findings make it probable that the diminished cell adhesion is caused mainly by low protein adsorption on highly hydrated polymer brushes. The mechanical properties might be only peripheral for cell behaviour upon initial contact and adhesion, although of great importance for the long term development of cells.

On the patterned polymer brush substrates, the cells had the choice between the hydrophilic, hydrated and soft polymer brush areas and the grooves, which presented the irradiated initiator surface (Figure 3.4). In agreement with literature, the bone cells did not grow on polymer brushes but in the grooves.[43,46,47] As described above, the cells were not able to adhere to the polymer brush areas and evaded the unfavourable surface colonising the solid and rather hydrophilic grooves.

The cells growing on patterned substrates in the presence of the polymer materials affirmed that the chemistry of the polymer itself was not the reason for the poor cell growth. It was the prevention from adhesion and not toxicity of the material that restricted cell colonisation. These considerations are supported by the viability staining revealing with the green colour (Figure 3.5b and d) that the adherent cells were viable on unpatterned as well as patterned substrates. It is also visible that, although the patterned PSPMA substrates did restrict cell adhesion to the grooves and aligned the cells, hMSC were nevertheless able to overgrow the pattern after one week in cell culture (Figure 3.5d). As the PSPMA brushes were only about 20 nm high and most probably degraded in the ionic environment (Figure 3.3), they might have lost their anti-fouling properties over time. The surface also underwent changes in its chemistry as the contact angle measurements had shown (Figure 3.4). Additionally, adhering cells are known to actively modify their surrounding by secreting ECM proteins.[205] These factors probably lead to a loss of influence of the PSPMA brush on the cell growth over the culturing time.

hMSC had most problems colonising on the PMAA brush substrates (second row in Figure 3.5). As on the unpatterned substrates also on the patterned ones, the cell number was lower than on PSPMA brush substrates.[181] The chemistry of the surface was unlikely the reason for the poor cell adhesion, as carboxylates are generally a good

substrate for osteoblasts.[13,142,236] The PMAA chains were very long and, as already mentioned, had an enormous swelling ability. In a good solvent, the polymer brush chains might therefore not only increase in height but also extend into the groove areas on the patterned substrates.[173] At the same time, they would also extend the anti-fouling properties to the grooves of smaller patterns hampering cell attachment. If the cells were not able to attach to the substrate in the beginning, they probably have been washed off the coated glass slide by the cell culture medium and attached to the surface of the multi-well plates used. Thus, they would be lost for the colonisation of the polymer brush substrates, even if the anti-fouling properties of the polymer brush reduced over the time in cell culture.

In preliminary experiments, cells were also grown on PMETAC brushes. Here hMSC growth differed greatly from the one on the other polymer brushes. Unlike on the other polymer substrates, the cells were occupying those areas of the patterned substrates that were carrying the brush coatings. This lead to less clear reflection of the polymer brush pattern by the cell distribution (Figure 3.5i) or to cell growth almost exclusively *on* the polymer brush areas (Figure 3.5j). After a longer period in cell culture, cell growth became completely undirected (Figure 3.5k and l). One possible explanation is the extremely small film thickness. The film might not be thick enough to prevent protein adsorption. As described in Section 3.1.2, with polymer brush height the anti-adhesion effect increases.[43–45,50,52,87,239] On the other hand, Mizutani *et al.*[54] showed cell detachment because of hydration of PNIPAm brushes with a dry height of 1.8 nm – about 1/5 of the PMETAC brushes. However, also in said study,[54] cell adhesion decreases with increasing polymer brush thickness.

A possible explanation of the effect could be the positive charge of the PMETAC polymer, as cells are negatively charged.[237] Early theories on cell adhesion argued that charge and physico-chemical interactions were the means of cell attachment.[275,276] However, as we know nowadays that the picture is more complicated and involves a set of adhesion proteins, this argumentation seems short-sighted.

Generally, a positive effect of amino groups on biomaterials is observed and known.[247] The polyamine poly-L-lysine finds widespread use as a coating material for cell culture plates. MC3T3-E1 cell number and viability on Poly(Dimethylaminoethyl Methacrylate) (PDMAEMA) brushes very clearly exceeded the ones on PMAA brushes.[277] In cell culture of primary bone cells mineralisation was even enhanced on positive charged areas over hydrophobic ones.[15,237] At the same time, quaternary amines are known for their anti-bacterial and anti-fungal properties comparable to antibiotics. On the other hand, there is also a cytotoxic effect on fibroblasts observed for polycations in solution.[278] The

cytotoxic effect is thought to be caused by a disruption of the negatively charged cell membrane that leads to cell necrosis.[14,278–281] Primary amines are said to be more toxic than quaternary amines, like PMETAC, although there are exceptions to the rule.[278] Studies suggest that at least three binding points are necessary to elicit the effect, so long, flexible and branched polymers have a higher effect than linear and rigid ones.[278,280,282] The PMETAC chains might be conformationally hindered in the brush and therefore act as a rigid polymer. Additionally, only the surface of the polymer film is in contact with the cells, so the chains might have the effect of a short polymer.

However, this does not adequately explain why the polyamines have a positive effect on cell adhesion when bound to a surface, and why they have a negative one when in solution. The probably most plausible explanation for this effect is the cells' not having a direct contact with the surface polymer. The polyamines more likely have an indirect effect through the adsorption of proteins. It is known that amino groups on biomaterials promote protein binding.[138] Healy *et al.* observed that cell attachment organised according to a chemically patterned surface with areas of positively charged head groups, only when plasma proteins were present.[237] This observation strongly suggests a pivotal role for plasma proteins to convey the positive effect of polyamines on cell adhesion. Others noticed that osteoblasts cultured on positively charged substrates spread in an extreme way, quite contrary to the negatively charged surface.[15,276,283] The extreme spreading of osteoblasts on surfaces carrying a positive charge was correlated to a differing protein adsorption by Shelton *et al.*[276] The authors assigned one band of the protein profile, seemingly responsible for the osteoblast spreading, to fibronectin, which seemed to adsorb only to surfaces with positive charge. Also the presence of vitronectin seemed necessary for bone cell spreading on positively charges regions.[15,284]

In summary, the PMETAC brush coatings were probably too thin to effectively prevent protein adsorption to the surface. Their positive charge facilitates the adsorption of a protein profile favourable for cell adhesion, probably including fibronectin and vitronectin from the serum. Therefore, the cell distribution pattern on the PMETAC substrates reflected not as clear the pattern of the coating as the cells on the other polymer brush substrates. The effect partly even resulted in an inverse cell distribution pattern compared to the other polymer brush coatings. On day 10, no influence of the PMETAC brush on cell alignment or distribution was visible anymore, probably owing to the cells' active modification of their surrounding combined with polymer brush degradation. The osteogenic differentiation was not hampered as shown by the alkaline phosphatase staining (Figure 3.5l).

As PSBMA very effectively directed hMSC adhesion and distinctly restricted it to the

grooves (last row of Figure 3.5), these substrates were studied more closely. In a set of experiments, the osteogenic cell line MC3T3-E1 was also cultured on these substrates and their proliferation examined at the mRNA level. These experiments were published in ref. 48.

As mentioned above, zwitterionic molecules are especially applicable to prevent protein adsorption. Chen *et al.*[130] ascribed this property to the better hydration through electrostatic interactions between the ionic groups and water molecules than through hydrogen bonds between ether groups (in PEG) and water. The authors also wrote that the balanced charge of molecules like PSBMA chains was essential for good protein resistance. Other factors seemed to be the molecules' density, which had to be close to cell membrane density, and a low net dipole moment, which can be minimised by antiparallel arrangement of the betaine groups in a flexible polymer chain.

These theoretical considerations agree with the observation that the PSBMA brush substrates had the clearest distribution pattern of the cells (Figure 3.5). At the same time, the cell density in the grooves also seemed comparable to the control substrates indicating no harmful influence on the cells. The osteogenic differentiation was likewise not prevented as the alkaline phosphatase staining showed (Figure 3.5p).

Figure 3.6 shows representative light micrographs of MC3T3-E1 cells in cell culture on standard cell culture plastic, glass surfaces and patterned PSBMA substrates. Micrographs taken on day 1, at the beginning of the cell culture experiments, are in the left column, the ones taken on day 21, at the end of the experiments, in the right column. The control substrates (Figure 3.6, first and second row) illustrate normal cell growth and morphology. By day 21, the cells were confluent and displayed their spindle-shaped morphology. On the patterned PSBMA brush substrates (Figure 3.6, third and last row), the MC3T3-E1 cells seemed slightly more elongated and aligned along the linear pattern. Although, the smaller pattern with 10 µm line width did align the cells and seemed to direct them to the grooves, it was nevertheless partly overgrown on day 21 (Figure 3.6g). The MC3T3-E1 cells probably were able to bridge the 10 µm distance between the more favourable attachment sites of this smaller pattern. The larger PSBMA pattern, in contrast, restricted cell growth for the greatest part to the grooves even over 21 d of cell culture. This polymer exhibited the best stability properties of the tested polymer brushes. Additionally, it showed that the cells were not so well able to bridge the greater 50 µm distance between groove areas, although there were cases of this bridging visible in the centre of Figure 3.6h.

Analysing the samples in the Scanning Electron Microscope (SEM) provided a closer look at the cell morphology (Figure 3.7). One can see the spindle-shape of the MC3T3-E1

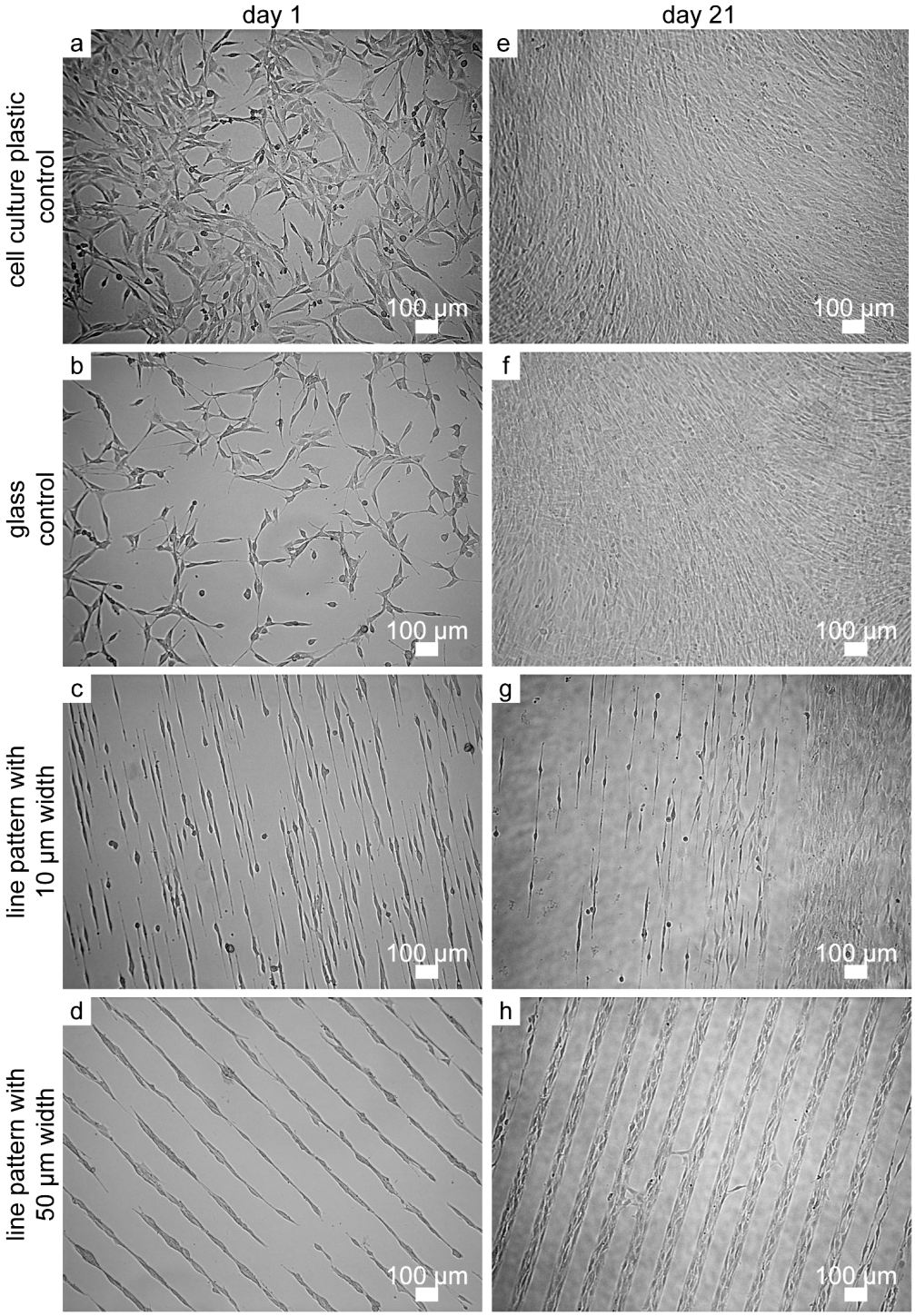

Figure 3.6: Morphology of MC3T3-E1 cells *in vitro* on day 1 (a-d) and day 21 (e-h) on the cell culture plastic control (first row), the glass control (second row), on PSBMA brush substrates with a 10 µm line pattern (third row) and with a 50 µm line pattern (last row). Figure published in ref. 48, see also ref. 267.

cells, slightly elongated on the patterned substrates. The triangles in Figure 3.7 mark areas where the deposition of ECM by the cells became apparent.

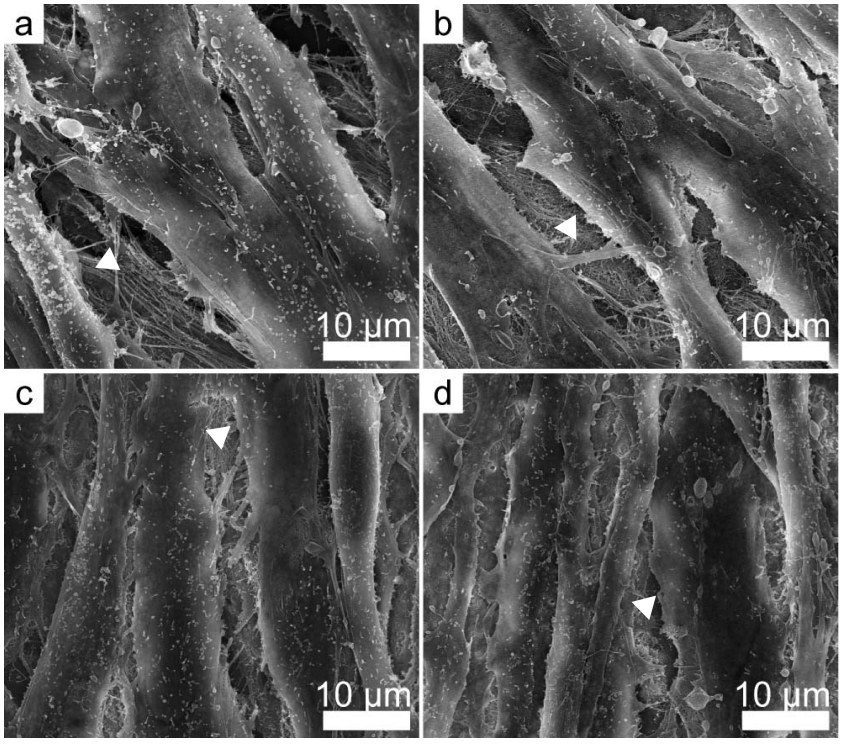

Figure 3.7: Morphology of MC3T3-E1 cells as seen in the SEM after 21 d of cell culture in expansion medium on cell culture plastic (a), glass (b), PSBMA brush substrates with a 10 µm line pattern (c) and with a 50 µm line pattern (d). Figure published in ref. 48, see also ref. 267.

To learn more about the viability of the MC3T3-E1 cells on the patterned PSBMA substrate, the mRNA expression of two proliferation markers and an apoptosis marker was analysed in preliminary experiments.[48] The proliferation markers *antigen identified by monoclonal antibody Ki-67* and *histone H4* are associated with the cell cycle of proliferating cells.[211,285] The apoptosis marker *tumor protein p53* was identified as a tumour suppressor gene. Its protein inhibits cell division of stressed cells and can initiate apoptosis.[286] Should the patterned PSBMA substrates provide an unfavourable environment for the cells and cause cell stress, the level of *Ki-67* and *H4* mRNA expression would be decreased and the level of *p53* mRNA increased compared to the standard cell culture substrate. Within the measuring accuracy, the analysis of the viability and proliferation of MC3T3-E1 cells at mRNA level showed that the patterned PSBMA surfaces were not detrimental for cell proliferation and did not cause elevated levels of apoptosis (comp. ref. 48).

3.2.3 Cell Growth on Plasma Polymers

To compare the effect of ppMMA coatings on cells with the polymer brushes, MC3T3-E1 cells were cultured on patterned ppH-ppMMA substrates. Additionally, to ensure that the adhesion promoting layer itself had no detrimental effect on the cells, patterned ppH substrates were included into the study as an one layer system. The patterns consisted of lines with either 10 µm or 50 µm line width, just like the PSBMA substrates in the MC3T3-E1 cell study.

Plasma polymers are more cross-linked than polymer brushes and contain several different functional groups, even with more modern and mild methods[138] (comp. Sections 2.1.4 and 2.2.3). The degree of cross-linking directly influences their properties, including their properties as biomaterials. The monomer MMA (Scheme 2.3 on p. 46) is not ionic and should therefore be less hydrated in an aqueous environment than the tested polyelectrolyte brushes. Heptane (Scheme 2.3 on p. 46) as a simple alkane is hydrophobic. Contact angle measurements showed that its plasma polymer had a lower surface energy and a lower polar component than ppMMA (Table 3.1). A reduced hydration should make the plasma polymers more suitable for protein adsorption and thus cell adhesion, including bone cell adhesion.

Table 3.1: Surface energy in $mN\,m^{-1}$ of ppH and ppMMA with their dispersive and polar components. Measurements through the courtesy of DataPhysics Instruments GmbH.

	ppH	ppMMA
Total surface energy	36.2	43.1
Dispersive component	35.6	40.9
Polar component	0.6	2.2

MC3T3-E1 cells were indeed well able to adhere to these surfaces, as can be seen in Figure 3.8 and Figure 3.9. The cells were colonising the substrates and spreading on them from day 1 on (Figure 3.8a–e). On day 3, it became apparent that the cells were aligning along the pattern although the height difference between grooves and ridges was only in the nanometre range (comp. Figure 3.8f with g–j). A marked preference of either groove or ridge, however, was not evident. Only on the larger patterned substrates, especially with the ppH surface, one might perceive such a preference (Figure 3.8h and j). From day 7 on, all tested substrates were covered by a confluent cell layer comparable to the plastic control (Figure 3.8k–t).

As is described in Section 2.2.3 the patterning process introduced a difference in surface chemistry between these two regions as well as the height difference. The irradiated areas were more oxidised and were thus more hydrophilic presenting a surface that osteoblasts

are anticipated to prefer over hydrophobic ones. In the beginning (day 3), the MC3T3-E1 cells on the larger pattern seemed to prefer either the grooves or the hills (Figure 3.8h and j). This preference may be attributed to the different surface chemistry, presuming that the cells probably chose the irradiated, oxidised grooves as the more favourable substrate. The reasoning that the cells were anticipated to colonise the grooves rather than the hills is supported by findings concerning the topography: As Alaerts *et al.*[147] found, the strength of attachment of cell protrusions was higher on concave surfaces than on flat ones, which in turn was greater than on convex surfaces. The grooves consequently had the double advantage of having a more oxidised surface and a concave one. According to Britland *et al.*[26] these two parameters, surface chemistry and topography, act synergistically on cell alignment.

In the SEM, there was no obvious difference in morphology between the cells on the control substrate and on the patterned substrate. The cells were growing to confluence on all substrates displaying a spindle-shaped morphology. A good degree of ECM production was visible as well (Figure 3.9) on the control substrate just as on the plasma polymer surfaces.

Real Time Polymerase Chain Reaction (RT-PCR) results confirmed the unaffected proliferation (ref. 81). As in Section 3.2.2, the mRNA expression of the marker of apoptosis (*p53*) and the two proliferation markers (*Ki-67* and *H4*) in cells on the patterned substrates was compared with the expression of cells on the control substrate, which was set at 1. With these results, also at the mRNA level, no harmful influence of the polymer coatings was detected. The expression levels of both the proliferation markers and the apoptosis marker of the cells on the plasma polymer substrates were comparable to the levels of the cells on the control substrate (comp. ref. 81).

Adhesion probably affects proliferation and differentiation.[15,77] Especially on implant surfaces, the proliferation of the bone building cells in turn is of great importance, as it is linked to a fast integration of endoprostheses.[287] Osteoblasts first proliferate in cell culture until they reach confluence, after which proliferation stops and differentiation is initiated.[9,77] Good proliferation leads to a high cell density, which is wanted to encourage differentiation of osteoblasts, which depends among other factors on cell-cell contacts and a certain cell density.[77,198,288,289] It is also known, that cell-cell contacts are beneficial for the viability of MC3T3-E1 cells[290] and that osteoblast cultures require confluency for mineral production.[9] Therefore, a coating material for implants should promote the good proliferation rate and cell density we observed for these plasma deposited polymers.

As described in Section 3.1.2, in several studies, osteoblasts reacted positively to geometrical patterns such as linear ones.[168] The aligned cells had a better adhesion beha-

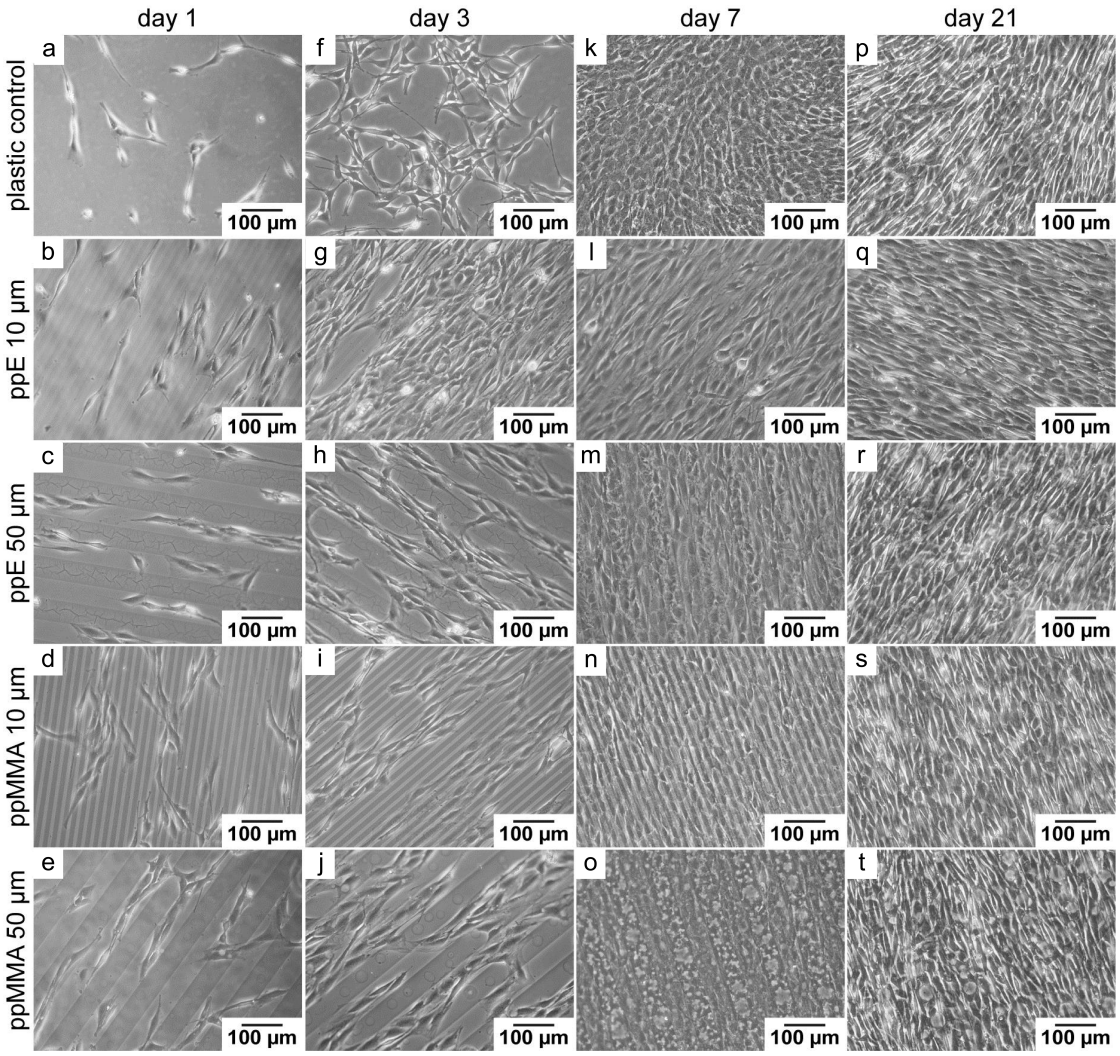

Figure 3.8: Cell morphology as seen through a light microscope on day 1 (a-e), day 3 (f-j), day 7 (k-o) and day 21 (p-t), on the plastic control, the ppH coating with 10 µm and 50 µm line width and the ppMMA coating with 10 µm and 50 µm line width (rows from top to bottom). Published in ref. 81 in cooperation with Tautzenberger and Ignatius.

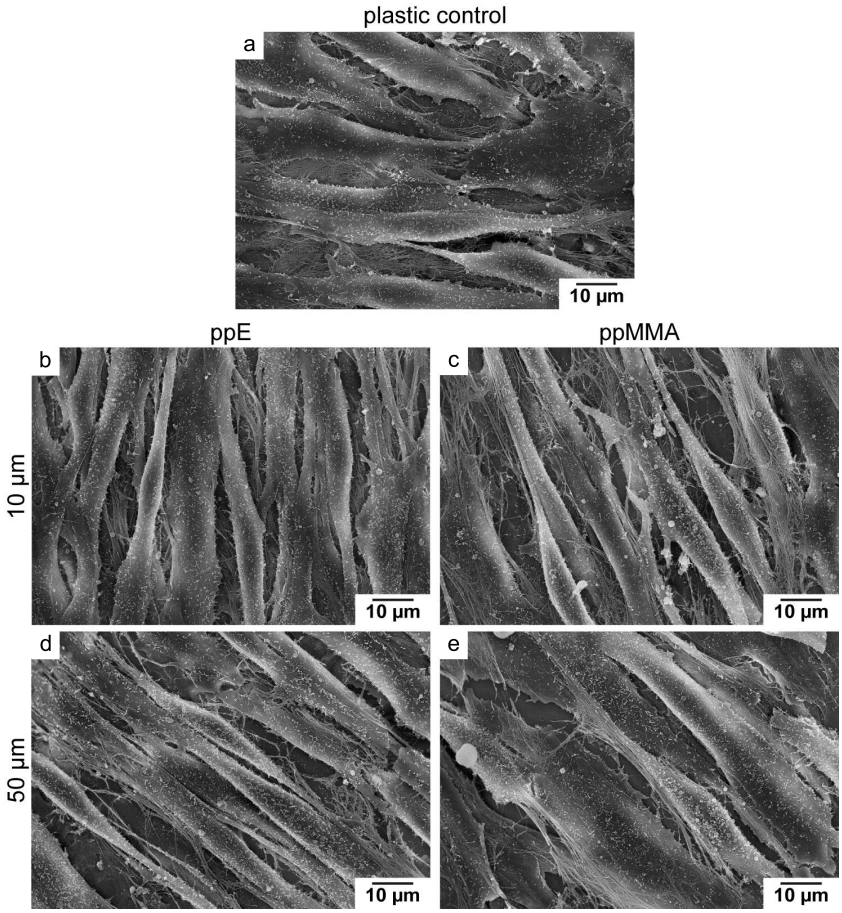

Figure 3.9: Cell morphology on day 21 as seen by SEM; a: On the control substrate; b: On a patterned ppH substrate with 10 µm line width; c: On a patterned ppMMA substrate with 10 µm line width; d: On a patterned ppH substrate with 50 µm line width; e: On a patterned ppMMA substrate with 50 µm line width. Published in ref. 81 in cooperation with Tautzenberger and Ignatius.

viour[217] and their orientation also seemed to determine the orientation of the collagenous matrix they secret, as Wang *et al.*[218] pointed out for MC3T3-E1 cells in ligaments and tendons. The authors also suggested that the aligned collagen matrix had an influence on the tissue's mechanical properties and on a successful healing process. Not only in ligaments and tendons, collagen fiber alignment plays a major role, also mineralisation[9,230,231] as well as the mechanical properties[228,232] in bone rely on proper collagen orientation. With these findings in mind, the observed osteoblast alignment may eventually improve osseointegration.[229,291] However, to elucidate the ideal kind of patterning or grooving for optimised mineralisation, the studies concerning the beneficial effects of topography would have to be more uniform.[9]

In summary, the tested plasma polymer coatings were not detrimental for cell adhesion and proliferation. The pattern did not restrict cell growth to certain areas as the polymer brushes did, but might nevertheless be useful as there is evidence for beneficial effects of linear patterns on osteoblast mineralisation.

3.3 Potential Biomaterials Applications of the Synthesised Materials

Summarising the properties of the here synthesised and tested materials, one can evaluate the applicability of the polymer brush and plasma polymer coatings. The polymer brush films were highly functionalised, exhibited a strong swelling capacity and were well hydrated in an aqueous environment. The good hydration was very likely the reason for the polymer brushes' ability to prevent cell adhesion through inhibiting protein adsorption. As cell adhesion depends on the proteins that can adsorb to a surface, especially fibronectin and vitronectin, a protein adsorption preventing surface like the polymer brushes lack this aspect of a good implant material.[14] This cell adhesion restricting property, however, may be exploited for other applications such as protein or cell based sensor arrays.

Another issue regarding the suitability of the material as endoprostheses coatings is the insufficient stability in a simulated physiological environment. However, there are approaches to work on this point. Tugulu and Klok[92] investigated the stability of PPEGMA brushes in cell culture medium and suggested that the stability could be improved by reducing the polymer brush density. A reduced polymer brush density resulted in lesser conformational stress, but would consequently also reduce the anti-fouling properties as outlined in Section 3.1.2. Consequently, the stability has to be balanced against the prevention of protein adsorption for each application. The same authors point out that

polymer brushes grown from the ill-defined alkylsilane layers are less stable than those anchored to the surface *via* alkyl thiol initiators. For longterm biomaterial applications, it might be useful to think about an alternative chemistry to link the polymer films to the surface. Additionally, other polymerisation techniques such as the surface-initiated photografting and photopolymerisation[292] might offer improved stability.

Evaluating the SI-ATRP method as it is, the high time and effort costs come into mind. Synthesising a batch of samples could take up to half a week active preparation time and two more days of washing (dialysis) and analysis. Concluding, the system will probably work best for short-term applications and sophisticated systems such as lab-on-a-chip or microarrays. In these applications, the effective prevention of protein adsorption and cell adhesion while not interfering with cell viability may be exploited. For these advanced nanosystems also the high production costs might be justified.

The plasma polymer coatings on the other hand exhibited other properties and provoked different cell reactions. The production is significantly less elaborate and much more suited for greater scale industrial production. Especially with ppH as an adhesion promoting layer they seemed to be interesting for future applications, as all steps in the process took place in the plasma reactor. OTES on the other hand needed an additional self-assembly step in solution, requiring more effort and equipment.

Plasma polymer coatings did not interfere with cell proliferation and adhesion. Consequently, the material might be useful for tissue engineering. As stated in ref. 81, the feasibility of further functionalising the here produced polymers with the low temperature plasma technique opens up numerous possibilities. By introducing nitrogen-containing groups additional anti-bacterial properties[14,281] could be realised as well as better proliferation and differentiation[293] or linkage to adhesion peptides or specific bioactive agents.[294,295] Alternatively, treating the ppMMA surface with a SO_2 plasma leading to sulfate or sulfonate groups might also bring about a reduction of bacterial adhesion while maintaining osteoblastic cell function.[296] It may also serve as model systems for the dependence of cell-matrix interactions, although its surface chemistry is not as well defined as the one of the polymer brushes (Section 2.3).

4 Mineralisation of the Polymer Coatings

4.1 Introduction to Mineralisation and Bone

4.1.1 Calcium Phosphates

Next to calcium carbonate and silica, calcium phosphate belongs to the most ubiquitous minerals in nature. It is the main inorganic component in bone and teeth of Vertebrata and is therefore also of high importance in biology and medicine.[297] Several modifications do exist, which are listed in Table 4.1. Generally, CaPs are soluble in acids and less soluble in neutral or basic aqueous solutions. As a rule of thumb, the higher the Ca/P ratio and the lower the water content in the mineral, the more insoluble it becomes in aqueous solutions.

Table 4.1: Calcium orthophosphate phases and their chemical formulas, comp. ref.s 22,297.

Calcium phosphate phase	chemical formula	Ca/P ratio
ACP	$Ca_xH_y(PO_4)_z \cdot nH_2O$	1.20–2.20
Brushite or DCPD	$CaHPO_4 \cdot 2\,H_2O$	1.00
Monetite or DCPA	$CaHPO_4$	1.00
OCP	$Ca_8(HPO_4)_2(PO_4)_4 \cdot 5\,H_2O$	1.33
TCP (α and β phase)	$Ca_3(PO_4)_2$	1.50
HA	$Ca_{10}(PO_4)_6(OH)_2$	1.67
FAP	$Ca_{10}(PO_4)_6F_2$	1.67
CDHA (bone mineral/biological apatites)	$Ca_xMg_yNa_z(PO_4)_m(CO_3)_nF_aCl_bOH_c$	1.61–1.71

Amorphous Calcium Phosphate (ACP) is the metastable, initial phase when CaP precipitates from solution and can be found in the development of biogenic mineral.[22,297] It has the spherical morphology typical for amorphous phases.[297] ACP as a CaP "phase" – if it may be called a phase at all – is rather undefined; the Ca/P ratio and water content may vary depending on environmental parameters.[22,297] In 1989, Christoffersen *et al.*[298] have described ACP "subphases" as distinct steps in the CaP mineralisation with their own morphologies and solubilities: ACP1 and ACP2.[299] ACP1 consists of spheres with a "bubble" structure visible in the Transmission Electron Microscope (TEM). ACP2

was first described by Christoffersen *et al.* as a separate amorphous phase. It occurs in the transformation process from ACP1 to Hydroxylapatite (HA) before Octacalcium Phosphate (OCP) emerges and has a distinct morphology. The authors attributed a more flaky and less spherical morphology to the ACP2 phase, which was also observed in a biomineralisation context by the Addadi group.[206]

Dicalcium Phosphate Dihydrate (DCPD) predominantly precipitates from CaP solutions with a low pH (≤ 6.5).[297,300–302] It is less often found in nature than other CaP phases. As geological or biogenic mineral it is found in kidney stones[303] or in caves with bat guano.[74,304] Its being less common might be due to the DCPD phase's metastability. Consequently, it has been discussed as transitionary phase in HA mineralisation.[297,302,305] Dicalcium Phosphate Anhydrate (DCPA) is the anhydride of DCPD, equally less common and is generated when removing the crystallisation water through heating.[297]

OCP is controversially discussed to be a precursor phase in biomineralisation. Its crystallographic structure is similar to HA, which makes it to a good candidate as a precursor with an easy conversion to HA.[297] On the other hand, it has not been proven to be present in studies on *in vivo* mineralisation.[306]

The α- and β-Tricalcium Phosphate (TCP) phases only form at high temperatures above 1125 °C and 800 °C, respectively.[22] Mg containing β-TCP (whitlockite) is found in pathological calcifications, but not in healthy bone mineral and not as its pure phase.[22,297] Nevertheless, it found widespread use as successful bone substitution ceramic, often in combination with HA as the so-called Biphasic Calcium Phosphate (BCP).[22,73,307] α-TCP in contrast is solely a high temperature phase and metastable at room temperature and quite soluble in water. Its impact on biomaterials research is therefore limited.[22]

HA is the thermodynamically most stable CaP phase and the one least soluble in water. It is also the mineral phase most similar to the inorganic substance in bone, making it a common biomaterial for hard tissue applications.[22] Nevertheless, it is more defined and less substituted than the biological apatite and thus differs from it.[297] In Fluorapatite (FAP) the OH^- is substituted by F^- resulting in a hard mineral that resists better dissolution in acids. In biological apatites, dentin contains most F^- reinforcing the teeth.[22]

As the biological apatite, Carbonated/Calcium Deficient Hydroxylapatite (CDHA) is non-stoichiometric and thus most difficult to define. This apatite is highly substituted: Ca^{2+} is replaced by Na^+, K^+, Mg^{2+} or Sr^{2+}, or even left out, resulting in a vacant place in the crystal lattice; HPO_4^{2-} or CO_3^{2-} may be found instead of PO_4^{3-}; F^-, Cl^- and CO_3^{2-}, or again vacancies, often substitute OH^-. Further, CDHA contains more water than the other apatites making it better soluble in an aqueous environment.[9,22,297] The exact

composition also differs and depends on the organism, the tissue – *e.g.* dentin differs from bone – and even the nutritional situation of the organism.

4.1.2 The Material Bone

The Components

Biominerals are generally composites made of organic and inorganic components.[6,308] Bone is no exception. The combined organic and inorganic composite materials build up a structure with unique mechanical properties, uniting the elasticity of the proteins with the hardness of the mineral.[6,309] The organic part additionally acts as a controlling component on the biomineralisation process regulating mineral phase, crystal orientation and size.[6,308,310–312]

The organic part of the bone consists mainly (about 90 %) of collagenic proteins, of these especially type I collagen.[9,15] Collagen is a fibrous protein forming a fibril out of three peptide chains. This triple helix is 300 nm long with a diameter of 1.5 nm. The collagen triple helices are arranged in long bundles or fibrils lined up longitudinally to build long "strings". In the fibril, the collagen helices lie parallel to each other and are shifted against each other so that the gap regions between the collagen helices are staggered.[5,7,22] Collagen is often regarded as a passive template with little effect on mineralisation itself.[313,314] However, there is evidence that this role for collagen is not entirely true. Collagen seems to partly direct the biomineralisation through its charge.[315,316]

A small fraction (about 10 %) of the bone mass are the non-collagenous proteins.[15] Although they are few in numbers, they are yet important for the biomineralisation process as well as for metabolic regulation, cell-matrix and cell-cell interactions.[9,313] These matrix proteins and proteoglycans are often acidic (i.e. negatively charged), containing mainly aspartic acid (i.e. carboxylates), phosphates and sulfates bound to polysaccharides.[2,6,79,313,317,318] These functional groups are known to bind Ca^{2+} ions and are consequently often discussed to affect biomineralisation greatly.[6,79,80,319] Examples for important non-collagenous proteins are osteocalcin, osteonectin, bone sialoproteins, osteopontin, fibronectin and Bone Morphogenetic Protein (BMP).[15,318] There is a great number and variety of these non-collagenous proteins, although they constitute only a small amount of the organic bone matrix[320] Among the most significant and best studied of these proteins are the BMPs.[18,33,321] The BMP family is a group of proteins vital for the build-up of embryonic and adult bone, inducing osteogenesis (even in muscle tissue when applied with the right delivery system).[18,321] It is therefore of great interest for regenerative orthopaedic surgery.[18]

As described above, a highly substituted, Ca^{2+}-deficient HA is the main inorganic component of bone.[9,298] HA crystals have the crystallographic space group $P6_3/m$ and are hexagonal symmetric about the c axes.[322] In bone, the mineral consists of plate-shaped crystals and is aligned to collagen fibrils along the crystallographic c axes.[9,322] They are preferably coplanar positioned at the gap region of the collagen fibrils, building stacks of mineral plates with collagen sandwiched between them (Figure 4.1).[322]

While non-biogenic HA crystals measure hundreds of micrometre, the biogenic CDHA crystals have a typical size of only $50 \times 25 \times 4$ nm.[7,22] The biogenic CDHA is therefore often referred to as poorly crystalline. The small crystal size might be partly due to the compartimentisation through the collagen fibrils.[22] Another mechanism might be the binding of the non-collagenous proteins, which often inhibit crystal growth.[22,318] However built, the nanocrystals are probably one of the causes for the unique mechanical properties of the nanocomposite bone.[5]

The Hierarchical Build-Up

The properties of bone are not only dictated by the components of the material but also by the structural build-up.[313] The composite build-up and the hierarchical superstructure are the cause for the singular mechanical properties of the material bone.[322] The components self-assemble during biomineralisation with defined hierarchical structures.[6] This self-assembly was thought to be a sign for strong cellular control.[322] There is, however, still discussion about the extent of cellular control over the biomineralisation of bone. It could also be an acellular self-assembly, orchestrated by the non-collagenous proteins and the collagen matrix.[206]

While the mechanism of self-assembly is still unclear, the hierarchical structure of bone is known (Figure 4.1). On the lowest level, the CDHA nanocrystals are sandwiched between collagen in the mineralised fibrils. The collagen matrix with the aligned crystals form an anisotropic material of parallel flexible strings reinforced with hard and brittle platelets. On the next organisational levels, the mineralised fibrils are bundled and further arranged to withstand the external forces acting on bone. Depending on the type of bone this arrangement can be in a parallel, a woven, a plywood-like structure or in a radial symmetry. The respective arrays of fibrils are then organised in the osteon. An osteon is a concentrically organised structure in the bone, a cylinder, around which several layers of mineralised collagen fibres are arranged. The second highest levels of the hierarchy is the spongy and the solid bone. The interior of the bone is usually filled with light and sponge-like bone material and is surrounded by the solid one. In the spongy bone, the (anisotropic) fibres are aligned along the axes of external forces to withstand

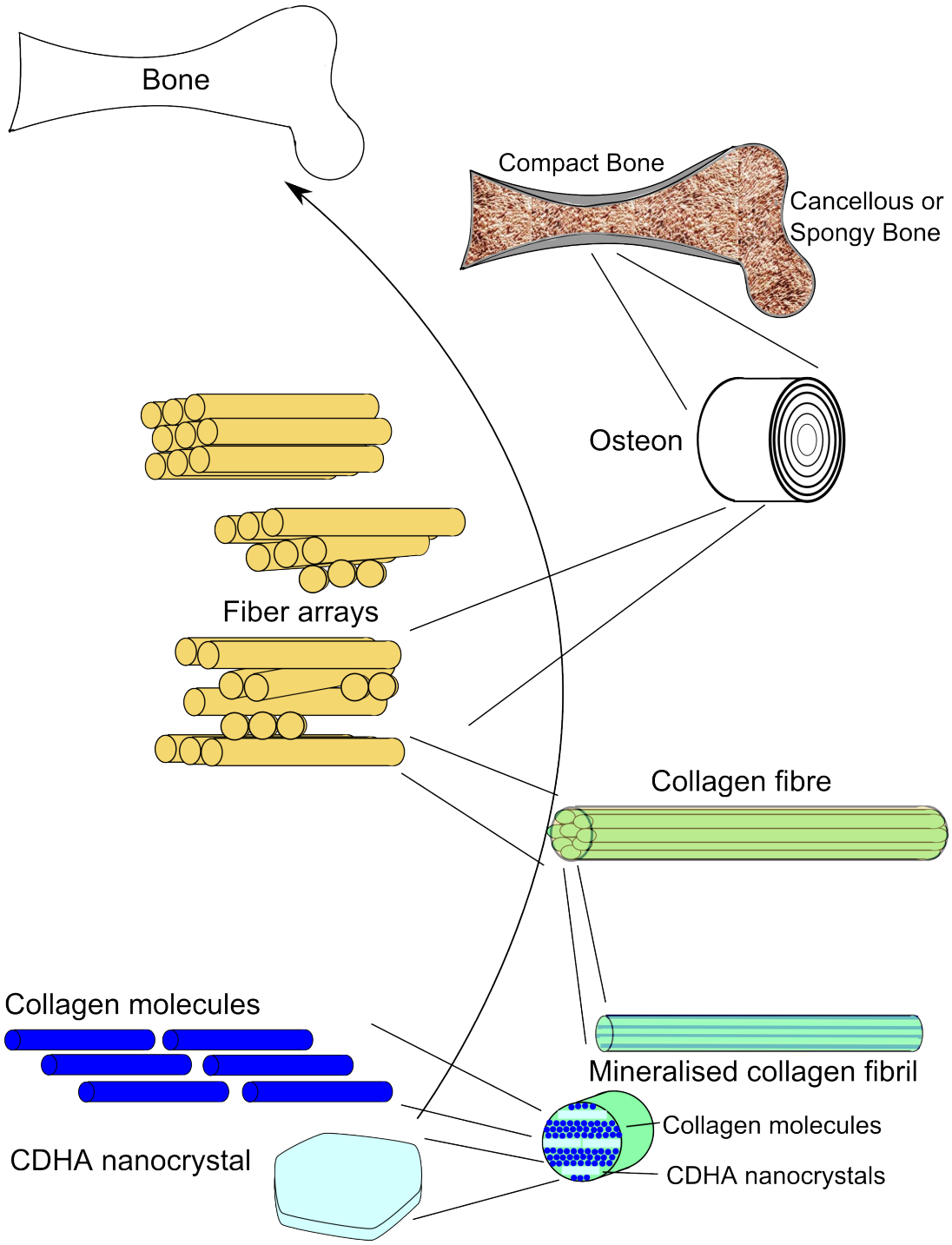

Figure 4.1: The hierarchical structure of bone. The main components (collagen and CDHA nanocrystals) are arranged in seven hierarchical levels to build the though yet elastic composite material bone. Comp. ref.s 5,7,22.

these forces. This build-up provides stability at a relatively low weight. The highest level of organisation is finally the whole bone.[7]

4.1.3 Biomineralisation in Bone

As written above, soluble acidic macromolecules and a collagen fibre template are involved in the production of calcified biomaterials. The insoluble collagen's main task is the spatial control, building the structural matrix[320] and directing the crystallising CaP to the right areas.[315,316] The collagen matrix therefore provides a scaffold and compartiments for the biomineralisation. The build-up is quite consistent with the concept of mesocrystals as a basic principle of biomineralisation propagated by the Cölfen group:[320] aligned nanoparticulate HA crystals separated by an organic collagen matrix.

Beside collagen, the bone-specific non-collagenous proteins regulate, inhibit, or promote calcium phosphate crystallisation.[318,323,324] Their common feature is their having acidic groups, mostly carboxylates, and exhibit hydroxyapatite binding ability.[2,6,79,313,317,318] Ions and molecules with the ability to bind specific crystal faces are associated with an anisotropic crystal growth. They are able to lower the surface energy of crystal faces and thus slow down crystal growth on the specific face modifying the crystal's morphology. The soluble components can even control which polymorph is crystallising.[320] Sulfates such as chrondroidin sulfate probably play a major role in biomineralisation.[80,320] They reduce interfacial mismatches and thus support the build-up of tough and ordered composite materials.[319,320]

Many studies suggest since decades that biogenic highly ordered mineral structures form *via* an amorphous precursor.[206,320,325,326] Xu *et al.*[320] point out the plausibility of the amorphous precursor phase being stabilised by the soluble biomacromolecules and then moulded into the template. The current concept of the biomineralisation of bone was summarised by Cölfen in 2010:[315] Soluble anionic polyelectrolytes bind CaP clusters in solution forming mineral droplets. (Compare this to the concept of Polymer Induced Liquid Precursor (PILP) introduced by Gower and co-workers.[327,328]) The mineral droplets are then directed to the gap region of the collagen matrix probably by electrostatic interactions between the negatively charged soluble polyelectrolytes and the positive charge on the collagen fibrils located primarily at the gap region. From there, the mineral infiltrates the collagen matrix and solidifies in an amorphous phase. The ACP finally converts into the oriented hexagonal CDHA nanoplatelets.

Still pending is the question whether the ACP is converted directly to CDHA in bone minerals[299,329,330] or *via* an intermediate phase, may it be another amorphous phase (ACP2)[206] or OCP[331,332] or both.[298] It is also argued whether the conversion comes

about by dissolution and re-crystallisation or by direct solid phase conversion.[299,329] The results of Abbona *et al.* suggest that at a basic pH and higher supersaturations, the ACP1 directly converts to HA; a process that seems to be mediated by an ion exchange with solution during the crystal rearrangement.[299] Also the conversion of ACP1 to ACP2 has been described as solution-mediated.[298] Although the process is most likely solution mediated, a complete dissolution and re-crystallisation could not be observed.[329]

Next to the collagen matrix, the soluble proteins and the mineral itself, bone cells play a major role in the bone mineralisation and remodelling process. Osteoblasts produce the soluble proteins as well as the collagen matrix. After the collagen matrix is assembled, it is mineralised with the help of the non-collagenous proteins.[313,333] *In vitro* experiments with microstructured substrates showed that aligned cells deposited also an aligned collagen matrix.[218] This suggests the osteoblasts' introducing the anisotropic properties of bone through the arrangement of the collagen matrix. The cells that line the border of bone formation in mice were found to contain vesicles with calcium phosphate granules.[206,212,334] Mahamid *et al.* observed an amorphous and disordered calcium phosphate phase in intracellular vesicles of osteoblasts with a curiously low Ca/P ratio of 0.75[206] (comp. to the values given in Table 4.1). The cells seemed to actively accumulate the ions from blood serum in specialised vesicles. In the organism, osteoblasts build up a barrier between bone and blood by forming a cell sheet on the bone forming surface.[206,334–336] The mineral precursor phase is probably secreted by exocytosis and enters the collagen matrix to crystallise there.[206,316] The mineral content as well as the crystallinity of bone increases with bone maturation suggesting the osteoblasts continuing to deposit mineral.[306,322]

4.1.4 Calcium Phosphates as Biomaterials

As HA is similar to the mineral phase in bone, it suggests that ceramics made of this and other CaP phases are good bone substitutes and implant coatings.[77] Many techniques have been developed to coat especially titanium surfaces with CaP. Among those are pulsed laser deposition,[61] different ion beam techniques,[69] sputtering processes[68] and electrospraying.[60] For those coatings, one of the crucial points for a good biomaterial is their long-term stability. Here, many hydroxyapatite coatings fail to meet the requirements.[2,337] The sputtering methods, such as right angle magnetron sputtering, improved the hydroxyapatite coatings over the ones deposited by plasma spraying, but there is still potential for improvement.[338] Another possible approach is the mineralisation in solution. This can be an electrochemical assisted deposition[67] or a surface-induced one. A great advantage of solution methods is the coating process's being independent of

the geometry of the substrate, *i.e.* it is not a "line of sight" process. Campbell *et al.*,[2] for example, used alkylsilane SAMs with sulfonates as functional groups to mineralise even porous titanium substrates. Mao and co-workers[339] adsorbed Ethylene Diamine Tetraacetic Acid (EDTA) on titanium substrates to provide nucleation sites for a biomimetic calcium phosphate coating.

In the high temperature synthesis methods, the non-natural phases α- and β-TCP can develop. These minerals and combinations of them with HA were tested and turned out to be biocompatible and osteoconductive.[77] However, HA exhibits poor resorption properties; HA scaffolds for bone replacement were found not to be resorbed even after 5 years after implantation.[77,340] Thus, it was still a foreign body in the organism and not part of the constant remodelling process in bone.[16] Buser *et al.*[32] discovered on the other hand that the areas where a plasma sprayed HA coating on Ti implants was resorbed, bone-implant contact was low. This poses the still not completely answerable question which CaP phase or mixture of CaP phases is the ideal biomaterial. Should the phase be resorbable or stable? The answer is probably simple and at the same time difficult to realise: The phase should resorb in the right speed, not too quickly causing defects in the material, nor too slowly constituting a foreign body.[16] ACP for example is a quite undesirable CaP phase for a biomaterial due to its fast dissolution rate in aqueous environment.[2] BCP as a mixture of HA and TCP is quite promising, as it combines different dissolution rates, which can thus be adjusted by adapting the mixing ratio.[22,73,307]

Another possibility to enhance the osteoinductivity of HA and other CaP phases is the combination with other ions or proteins. The osteoinductive properties of HA are improved, when the mineral is doped with Si.[66,77,258,341] The doping charges the surface negative (SiO_4^{4-} *versus* PO_4^{3-}), changes the microstructure, enhances the solubility and thus enhances cell adhesion.[77,342] A second example is the BMP delivery system of Gao *et al.*,[321] which induces more bone, when the basic material is HA and not TCP, and when both collagen IV and BMP are present.

4.1.5 Biomimetic Mineralisation

It is not only of interest to study possible substitutes for bone to make use of in medicine. Also materials scientist are trying to use biomineralisation principles to design new materials.[308,320] The studies on biomineralisation and those on biomimetic mineralisation often cross-fertilised each other bringing a better understanding of biomineralisation and thus better means to copy its principles.[308]

Some groups such as Bradt *et al.*[313] tried to mimic the *in vivo* situation as closely

as possible *in vitro* by mixing Ca^{2+} and HPO_4^{2-} in the presence of collagen and polyaspartate, which served as a model for the acidic non-collagenous proteins. With these components the authors obtained a gel in which the HA crystal were integrated and bound. Without polyaspartate, in contrast, the crystals were clustered and only loosely associated to the fibrils.[313]

The influence of additives, like the polyaspartate, on mineralisation has been studied for decades. Polyanions revealed themselves to be dose-dependent inhibitors of crystal growth (type I inhibitors) or nucleation and phase transformation (type II inhibitors).[79,343,344] Mueller *et al.*[343] found evidence for different binding sites on HA crystals in the competitive binding behaviour of polyanionic peptides and the polycationic spermine. These binding sites were speculated to be the Ca^{2+} and PO_4^{3-}, respectively. In these experiments, the anions also turned out to be more effective inhibitors than the cations. At the same time, good binding correlated with inhibition, although not linearly.[343] Also polyaspartate was found to delay the transformation from ACP to HA.[313]

On the other hand the negatively charged groups such as sulfonates and carboxylates are good chelators of Ca^{2+} ions and might therefore stimulate crystal nucleation in some cases by accumulating cations.[2] Generally, they are of interest due to their crystallisation affecting properties. Consequently, there is a number of studies especially on $CaCO_3$ examining the effect of natural or synthetic polymers, surfaces or monolayers with these moieties on biomineralisation.[6,79,319,345,346] Especially sulfate groups seems to be more potent than other groups in inducing $CaCO_3$ nucleation and face-selective crystallisation.[6]

The control over the crystallisation in particular is in the spotlight of materials scientists. It is often sought to influence mineralisation with additives such as synthetic or biologic macromolecules or Langmuir-Blodgett films with headgroups in defined distances facing the ion solution. In biomimetic approaches it was shown that Langmuir-Blodgett films with calcium carboxylate head groups forming a grid pattern affected calcium phosphate nucleation, crystal growth and morphology.[59,347] The aimed for HA was built only in the presence of the carboxylate head groups.[347] Dey *et al.*[256] observed with cryoTEM methods in detail the mineralisation of HA with a preferred [110] orientation under a monolayer of arachidic acid.

The geometrical arrangement of these acidic groups of the monolayers was for a long time thought to influence mineral growth and phases.[79] To achieve a certain phase, it was suggested that the pattern of the functional groups should match the crystal lattice as much as possible.[347,348] Volkmer and co-workers showed with their work on $CaCO_3$ mineralisation under layers of different calixarenes[349–352] that the assumption of a purely

epitaxial mechanism is not fully valid.[348] Following their work, it seems more likely that matching charge densities and dipole moments caused directional growth of specific $CaCO_3$ phases under the various monolayers. Similar to the static lock-and-key principle as a model for protein interactions, which had to be modified to the more dynamic induced-fit model to provide a better picture of the biological interactions, also a solely epitactic model seems to be too static to fully describe the interactions between organic matrix and mineral.

The group then passed on to other biomimetic mineralisation techniques and studied the influence of acidic polymers and peptides on $CaCO_3$ crystallisation.[353–358] Using Poly Acrylic Acid (PAA), they produced highly oriented laminated calcite platelets strongly resembling nacre.[353,354] Their thin polycrystalline calcite films originated from an amorphous phase serving as a template for epitaxial overgrowth of calcite platelets.

These experiments with calcium carbonate were paralleled with studies on calcium phosphate. Casse *et al.*[359] illustrated that a well-defined (yet non-crystalline) interface, even a rather flexible matrix like an amphiphilic poly(acrylic acid)-block-poly(*n*-butylacrylate) block copolymer film, was able to serve as a template for nucleation controlling calcium phosphate mineralisation. Moreover, the block copolymer film at the air/water interface also acted as a tool for the 2D arrangement of CaP particles in a near-crystalline order. Suzuki *et al.*[360] worked on the mineralisation of phosphate groups containing polymers. They highlight the importance of the number of functional groups, the degree of cross-linking of the polymer and the accessibility of the functional groups.

Volkmer and co-workers showed that a metastable Amorphous Calcium Carbonate (ACC) film was formed when using PMAA brushes as a template.[122] The polyelectrolyte brushes thereby represented a highly functionalised mineralisation matrix with a large number of carboxylate groups stabilising the amorphous phase. After thermal treatment, the amorphous film transformed into a thin polycrystalline calcite film. With this work the authors combined surface bound polyelectrolyte brushes with the biomineralisation topic. In the same group, Letsche[172] mineralised not only calcium carbonate in the PMAA brush template, but also CdS and ZnS as well as PbS, CoS, CuS, Fe_xS_y, Fe_xO_y, SnS, TiO_2 and ZnO. These minerals formed nanoparticles in the organic matrix, some completely impregnating the polymer brush.

Also other groups used the polymer brush system as a mineralisation template. The Huck group successfully prepared magnetic nanoparticles in PSPMA brushes[123] and gold nanoparticles in PMETAC brushes.[361] Boyes *et al.*[362] used surface initiated block-copolymers to synthesise Ag and Pd nanoparticles.

In the present work, the polymer brush and plasma polymer coatings prepared as

described in Chapter 2 were mineralised with CaP. This important biomineral has the potential to increase the biocompatibility of the polymer films and might even render them bioactive. The influence of the two polymer coatings on biomineralisation was examined reassessing the usefulness of the biomimetic functional groups in the polymer films.

4.2 Results and Discussion of the Mineralisation of Polymer Thin Films

4.2.1 Dip Coating Mineralisation

The dip coating experiments were simple immersions of substrates in the respective ion solutions. In the process, the substrates were standing upright to make sure that mineral deposited on the substrate was due to heterogeneous mineralisation on the surface. Had the substrates been lying on the bottom of the vessel, also crystals nucleated homogeneously in solution could have dropped on the substrates non-specifically. Consequently, the upright position ensured that a possible effect on mineralisation was caused by the coatings.

The most straight forward method for biomineralisation is the immersion in SBF, which was conducted as well as immersion in 1.5 SBF (comp. for example ref. 64). The immersion in SBF is the one of the acellular biomineralisation methods without the use of proteins that most closely mimicks the *in vivo* situation as described in Section 3.1.3. As shown in Section 3.2.1, even after 21 days in SBF, there was no mineral to be found on polymer brush coatings. On the contrary, the polymer brush films delaminated.

Next to the immersion in SBF, also more elementary solutions containing only $CaCl_2$ and HPO_4^{2-} with Na^+ or K^+ as counterions were applied. Most solutions were not successful in building up mineral on the polymer brush substrates. For the parameter range used, compare Section 7.6.1. An exception to the failing dip-coating experiments was the immersion of a micropatterned PSBMA coated substrate in a 20 mM $CaCl_2$ solution with the dropwise addition of a 12 mM K_2HPO_4 solution while constantly stirring for 30 min. Following the protocol of Liu *et al.*,[64] this procedure was repeated twice. This experiment was also conducted with lower $CaCl_2$ concentrations (10 mM and 5 mM), but always adding a K_2HPO_4 of a matching concentration to give the HA Ca/P ratio of 1.67. This mineralisation method was supposed to result in poorly crystalline HA.[64]

With the highest concentration of 20 mM $CaCl_2$/12 mM K_2HPO_4, copious amounts of mineral was found on patterned PSBMA substrates, but the distribution was not

constricted to either polymer coated areas or groove regions (Figure 4.2a and b).

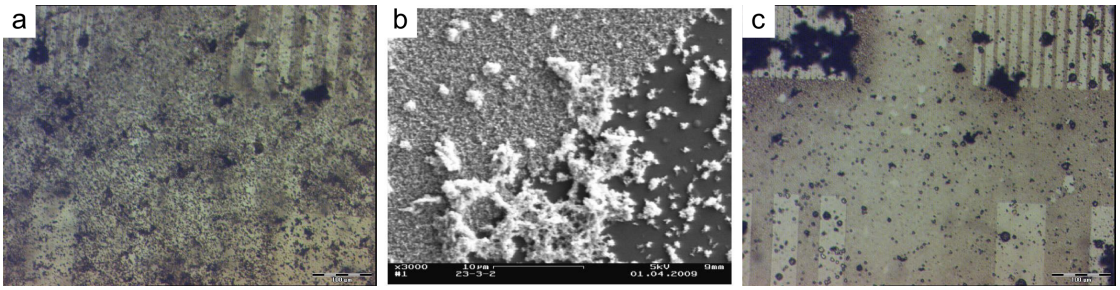

Figure 4.2: PSBMA coated samples with linear patterns after mineralisation with a dip coating procedure described in ref. 64; light micrograph of the sample mineralised in a 20 mM $CaCl_2$ solution with the dropwise addition of a 12 mM K_2HPO_4 solution (a), corresponding SEM micrograph (b) and light micrograph of a sample mineralised with halved concentrations under the same conditions (c), comp. Section 7.6.1.

There seemed to be a slight difference between the mineralisation on polymer brush regions and grooves, but big clusters formed throughout the substrate. Therefore the concentrations were halved and the substrate was immersed in 1 mM $CaCl_2$ solution prior to the mineralisation to try and impregnate the polymer brushes with Ca^{2+} ions. Impregnating the polymer brush in the $CaCl_2$ solution aimed at a higher local Ca^{2+} ion concentration in these regions and, as a result, a more specific mineralisation limited to the polymer brush regions. Nevertheless, even with the lower concentration there still were large clusters, which build unspecifically on the sample (Figure 4.2c). When trying to remove the large clusters by rinsing the sample with water, also the more specific small CaP particles were removed. This being possible shows that a good bonding between the mineral and the polymer matrix was not achieved with this method. The partly unspecific distribution suggests at the polymer not acting as a true template for mineralisation here. It did not seem as if the PSBMA matrix was able to build up strong bonds to the Ca^{2+} ions linking the inorganic and organic components of the system. After further reducing the concentrations to 5 mM $CaCl_2$/3 mM K_2HPO_4 solutions, no signs of cristallisation were observed.

Generally, dip-coating experiments were not successful in mineralising polymer brush regions specifically, either showing an abundance of unspecific mineralisation clusters or no signs of mineralisation at all. One reason for this behaviour might be the nucleation inhibiting effect that polyelectrolytes can have.[79,343,344] The polyelectrolyte brushes might indeed have bound the ions but at the same time inhibited precipitation as it is described for the PILP effect.[327,328] The biomimetic polyelectrolytes could indeed take the role of the polyanionic proteins during the mineralisation of bone as described in 4.1.3.

However, the mineralisation process requires also an insoluble matrix like the collagen scaffold, which was lacking in the mineralisation system of this work.

A disadvantage of this static dip-coating method is the lack of supply of "fresh" ions, which contrasts the *in vivo* situation with its open system. When the mineral precipitates during the dip-coating process, it inevitably reduces the ion concentration in solution. *In vivo*, the ion concentrations are always regulated and held constant. At the same time, there is a constant movement of the body fluid. This situation is better represented by the mineralisation in a mixing chamber. In this system, a pump constantly transports a supply of ions through the mixing chamber and the concentrations are held approximately constant. Therefore, above all, experiments were conducted in a mixing chamber better representing the physiological situation. They are described in the following section.

4.2.2 Mineralisation of Polymer Brush Substrates in a Mixing Chamber with an External Pump

During the mineralisation in the mixing chamber, an external pump transported a Ca^{2+} and a HPO_4^{2-} solution from their storage vessels to the mixing chamber. Shortly before the mixing chamber, the two solutions met and mixed, forming a supersaturated CaP solution. By this, the mineral was likely to precipitate in the mixing chamber and not in the tubing system and the solution entering the mixing chamber had a defined concentration.

A series of experiments was conducted with varying concentrations, flow rates and times. For the parameter range covered please see Section 7.6.2. The mineralisation was carried out with substrates coated with PSBMA, both unpatterned and patterned with circular holes that had a diameter of 20 µm. Uncoated, cleansed glass cover slips were used as control substrates to see a possible effect of the coating on the mineralisation.

After mineralisation, there was almost always a colourless precipitate visible on all types of substrates, which – at best – had the "eye" form of the mixing chamber (Figure 4.3). This precipitate film seemed to be thinner or paler on uncoated glass than on PSBMA coated substrates (Figure 4.3 and Figure 4.4 comparing d and e). In agreement with literature,[2] mineralisation was more even at lower supersaturation. Correspondingly, the time needed to mineralise a sample increased strongly with decreasing ion concentration.

The results of the mineralisations of PSBMA substrates with a 5 mM CaP solution for 1.5 h at a flow rate of 0.8 ml min^{-1} were examined more closely. On the patterned PSBMA samples, the distribution of the CaP precipitate was oriented along the pattern, *i.e.* the mineral reproduced the pattern of the polymer. This mineral pattern was clearly visible

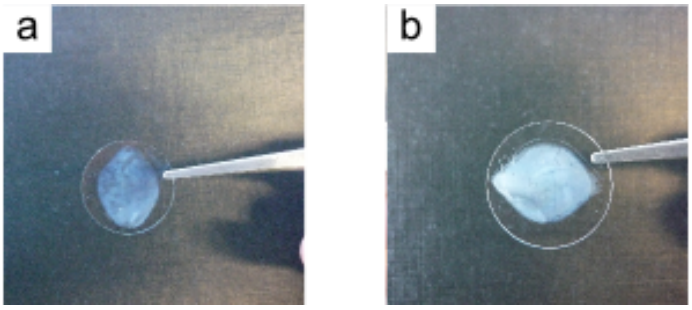

Figure 4.3: CaP precipitate on glass (a) and PSBMA brush substrates (b) after mineralisation in a mixing chamber.

in the light and electron microscope (Figure 4.4 and Figure 4.5). Energy-Dispersive X-ray Spectroscopy (EDX) confirmed the mineral to contain Ca and P and not the counterion elements Na and Cl (Figure 4.7).

Although the pattern was reproduced, it was partly the "positive" and partly the "negative" of the polymer brush pattern (Figure 4.4a and b). Sometimes the distribution pattern even changed from one area to another area on the same sample (Figure 4.4c). Even though there were examples for a "positive" and a "negative" distribution, on most samples, the polymer brush region seemed darker than the holes when analysed in the light microscope in DIC mode, as in Figure 4.4a. This seemed to be a sign that the polymer brush areas carried more mineral than the holes. In the SEM however, it became obvious that for these samples the contrary was the case (Figure 4.5). The samples were more heavily mineralised in the holes than on the polymer brush coating. This deception might be due to an increased light scattering in areas with many small particles compared to the areas where a closed layer of CaP had grown.

The SEM analyses (Figure 4.5) revealed the mineral's precipitating as small round particles of several hundred nanometre diameter. The round morphology was a sign for an amorphous phase, making ACP1 the most likely phase.

The solutions with low ion concentrations ($< 2.5\,\mathrm{mM}$) did not mineralise the PSBMA coatings. The higher supersaturation used in the experiments just described (Figure 4.4 and Figure 4.5) might on the other hand have caused ACP to nucleate homogeneously in solution.[2,299] In this case, the polymer brushes might have filtrated the nucleation seeds and small clusters from the solution. The clusters might have arranged along the pattern depending on the streaming movement of the solution. In the holes of the pattern they would have been more protected from the stream of the solution than on the polymer brush areas. At the same time, the clusters on the PSBMA areas would be prevented from growing and be seperated/dispersed by the polyzwitterions binding to it, as it is

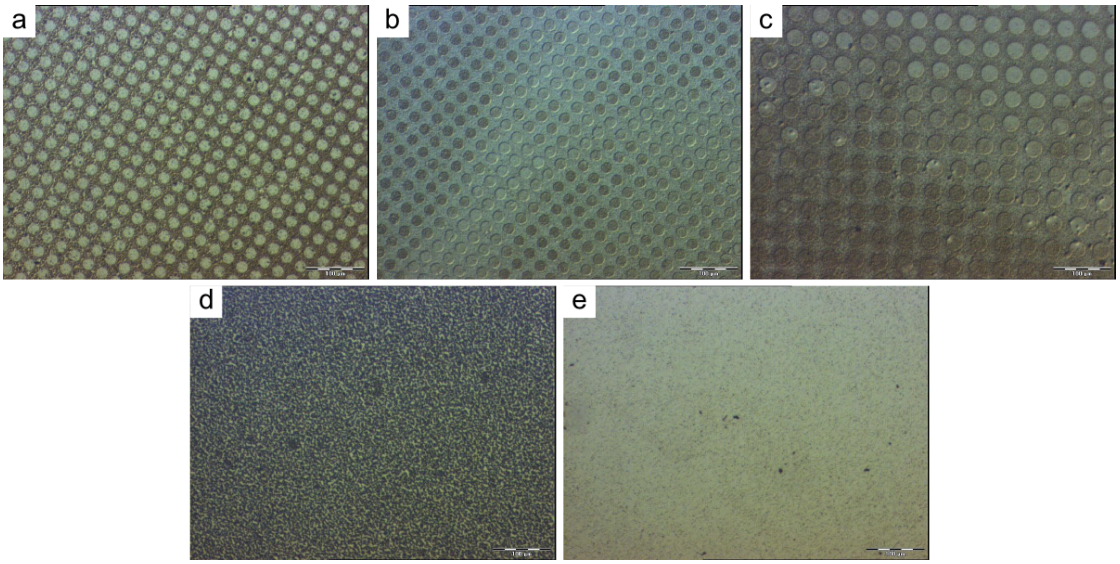

Figure 4.4: Light micrographs of patterned PSBMA (a-c), unpatterned PSBMA (d) and glass control samples (e) made in the DIC mode. Samples were mineralised in a mixing chamber with a 5 mM CaP solution for 1.5 h with a flow rate of $0.8\,\mathrm{ml\,min^{-1}}$. The dark and light areas show differences in the mineral deposition and reproduce the pattern introduced by the polymer brush coating (a-c). The unpatterned (d) and the glass substrate (e) are mineralised homogeneously.

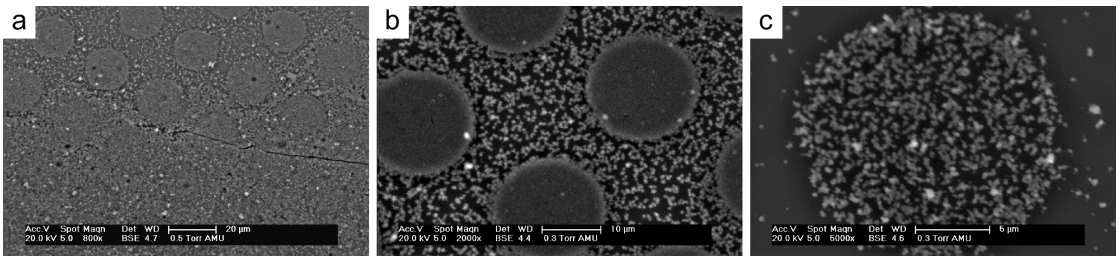

Figure 4.5: SEM micrographs of a patterned PSBMA brush coated sample mineralised as stated in Figure 4.4 show that the mineral distribution is denser in the round "holes" in the PSBMA coating than on the polymer brush areas.

described for peptides by Mueller and Sikes.[343]

The small mineral clusters getting caught in the patterned polymer brush coating might also account for the greater amount of mineral on the PSBMA samples compared to the glass control. Next to this profane mechanical reasoning, the polyelectrolytes might nevertheless enhance the local Ca^{2+} concentration in the vicinity of the substrate surface and thus accumulate mineral while at the same time inhibiting ACP particle growth. A third possible explanation for the difference between glass and PSBMA surfaces is a stronger bond of mineral particles to the ionic groups of the polymer than to a glass surface. In this case, the coating would not influence mineral nucleation but simply better bind homogeneously nucleated mineral clusters.

Ngankam *et al.*[363] examined the influence of polyelectrolyte films, assembled by the layer-by-layer technique, on CaP nucleation. They observed an enhanced nucleation on negatively charged as well as positively charged polyelectrolyte surfaces and proposed two possible mechanisms:

- The polyanion might increase the H^+ concentration near the surface, analogue the polycation might bind OH^- to the surface, and thus both surfaces might change the local pH
- The polyanion might be a good chelator for Ca^{2+} ions, polycations analogue for HPO_4^{2-}

In the present work, the polyelectrolyte was zwitterionic and seemed to increase the amount of CaP on the surface as well. As both, H^+ and OH^-, could find equally well binding partners in the polyzwitterion PSBMA, the pH was unlikely to change. The first explanation of Ngankam *et al.* therefore seems less probable than the second one: The positive amine and the negative sulfonate groups presumably bound Ca^{2+} and HPO_4^{2-} ions in their vicinity, thus providing nucleation sites on the substrate. This explanation seems quite likely and would ascribe a nucleation enhancing property to the polyelectrolytes.

To elucidate the CaP phase that precipitates on the PSBMA and the control samples, the mineral was analysed with TEM (Figure 4.6). The "bubbly" morphology seen in the TEM micrographs and the round form of the clusters in the SEM micrographs are signs for the mineral's consisting of ACP1 (comp. ref.s 65,299). Additionally, in the Fast Fourier Transform (FFT) pictures, there were no signs for electron diffraction. The electron beam, however, induced a clearly visible transition to a crystalline mineral. This beam induced phase transition prevented closer examination with electron diffraction. EDX analyses of these samples showed that the Ca/P ratio varied between 1.4 and 1.6

(for a typical spectrum see Figure 4.7). This Ca/P ratio is within the range of 1.20–2.20 given for ACP.[297]

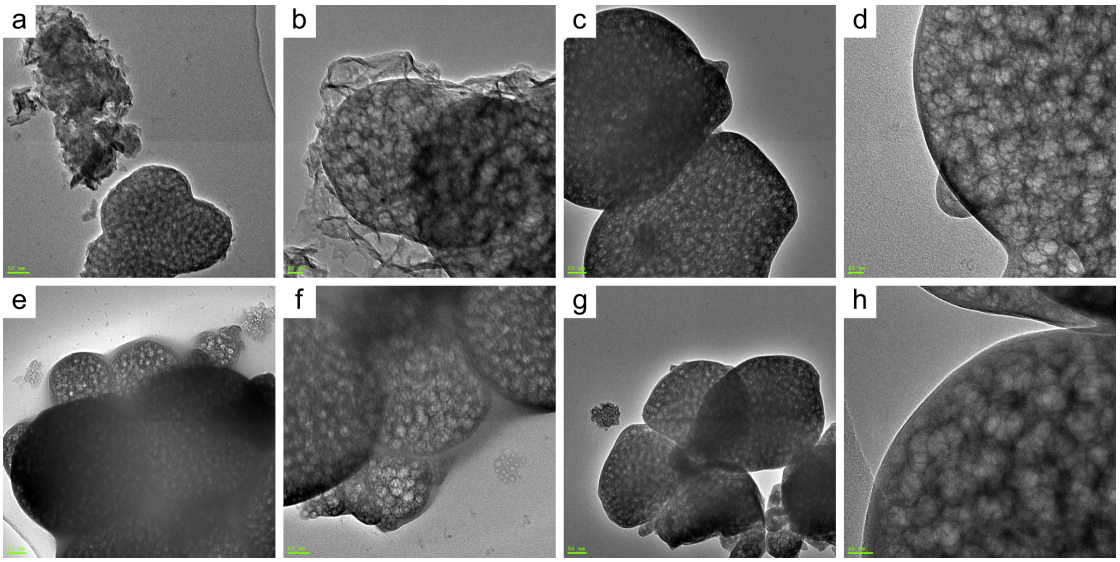

Figure 4.6: CaP precipitate as seen in the TEM after mineralisation of glass control and PSBMA coated substrates; mineral precipitated from solution (a, b), mineral found on the glass control (c, d), unpatterned PSBMA samples (e, f) and PSBMA samples patterned with round holes with 20 µm diameter (g, h).

Analysis with ATR-IR revealed similar spectra for the mineral on the coated samples, the control surface and the precipitate from solution (Figure 4.8). Band positions are listed in Table 4.2 and compared to literature values. The very broad band in the region around 3200 cm^{-1} is usually assigned to water and matches the high water content of ACP.[65] The bands at 1010 cm^{-1} and 545 cm^{-1} can be assigned to PO_4^{3-} vibrations and, being broad without being splitted, are indicative for an amorphous phase.[63,65,255,298] Bands at 875 cm^{-1} and 1400 cm^{-1} to 1700 cm^{-1} show the presence of CO_3^{2-}.[63,65,66,262] If these ions are incorporated into the mineral biomimetically, however, remains unclear in these measurements.[213] Summarising the results of TEM, EDX and ATR-IR, the notion based on other publications[299] and the Ostwald's rule that the first phase to precipitate should be ACP was confirmed.

Noticeably, despite the Infrared Spectroscopy (IR) spectra's being similar throughout the samples and controls and showing an amorphous character, the morphology of the mineral gravitationally precipitated from solution (not heterogeneously on a substrate) was not uniform (Figure 4.6a and b). Next to the typical "bubbly" ACP1, also a crinkled morphology was visible. The other morphology could reflect a conversion from ACP1 to ACP2, the latter being described by Eanes *et al.*[331] as "wrinkled and/or curved rather

Table 4.2: ATR-IR peak positions of the mineral precipitated gravitationally and on different samples in a mixing chamber after 1.5 h mineralisation with a 5 mM CaP solution at pH 7.4 in comparison with the position of IR vibration bands specified in literature.

	Measured band positions [cm^{-1}]				Band positions in literature [cm^{-1}]	
Substrate	From solution	Glass	Micropatterned PSBMA	Non-patterned PSBMA	ACP in ref. 65	ACP in ref. 63
Assignment						
PO_4^{3-}	545	544	544	544		
CO_3^{2-}	877	874	875	875	874	
PO_4^{3-}	1010	1012	1010	1012	1050	
CO_3^{2-}					1419	1400–1500
CO_3^{2-}	1540–1760	1550–1750	1540–1765	1520–1780	1587	
H_2O	3230	3225	3205	3235	3400	

Element	O K	Al K	**P K**	**Ca K**	Cu K
Weight %	31.5	1.5	**12.4**	**24.9**	29.7
Atomic %	56.0	1.6	**11.4**	**17.7**	13.3
Net Integral	215	21.6	**147**	**250**	199
Background	0.16	0.60	**0.20**	**0.24**	0.32
Error	0.97	3.13	**1.17**	**0.90**	1.00
P/B	1343.5	36.0	**735.6**	**1041.5**	623.1

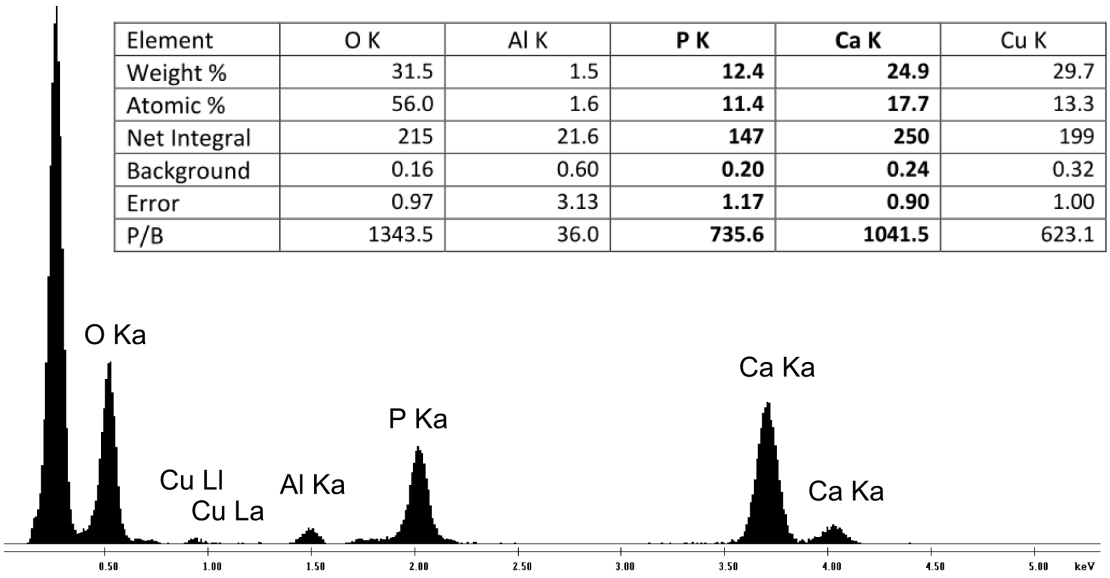

Figure 4.7: Typical EDX spectrum of the mineral precipitating on a control substrate after 1.5 h of mineralisation in a 5 mM CaP solution. The inset is a table of the element distribution of this sample.

than smooth and flat" as cited in ref. 298. Comparing the TEM micrographs in ref. 331 with Figure 4.6a and b, the morphology in Figure 4.6b on the rim of an ACP1 cluster agreed well with the micrograph by Eanes *et al.*. However, for the occurence of ACP2, the mineralisation conditions should have been more acidic according to Abbona *et al.*[299] The morphology in Figure 4.6a also differed from the one described by Eanes *et al.*[331] Nanocrystalline HA exhibited a similar morphology in other studies, *e.g.* in ref. 213,259,319. With the prevailing slightly basic mineralisation conditions, the HA phase seems very likely.[299] Together with the amorphous character of the IR spectra, the second phase occuring in the TEM micrographs is probably poorly crystalline HA.

Why could this additional morphology be found in the mineral sample, which was uninfluenced by the polymer brush coating? The PSBMA brushes are polyelectrolytes and as written above, polyelectrolytes are known to inhibit the transformation of ACP into crystalline phases.[364] Therefore, also in this case, the polyelectrolyte could have provided a larger number of nucleation sites, but at the same time prevented a phase transformation and preserved the ACP1. A counter-argument arises from Figure 4.6c and d showing the mineral on the glass control. On these samples without the inhibiting effect of a polyelectrolyte, also only the ACP1 morphology was observed. It might therefore be simply the size difference between the mineral nucleated on a surface and the gravitational

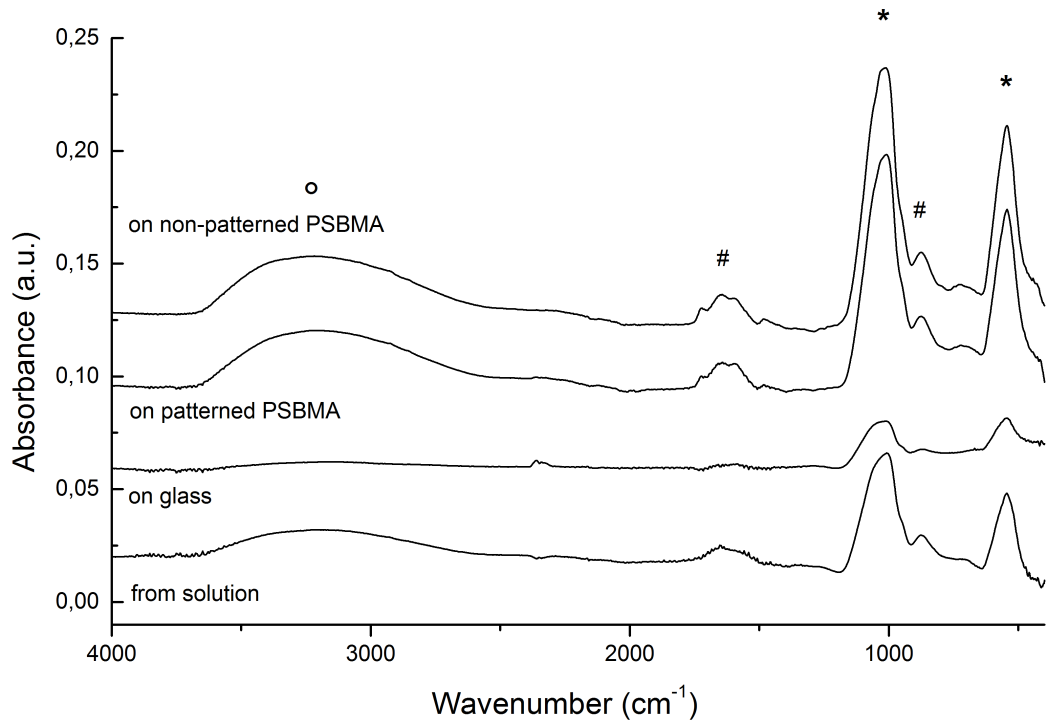

Figure 4.8: ATR-IR spectra of the mineral precipitated after 1.5 h from a 5 mM CaP solution and found (from bottom to top spectrum) on the bottom of the mixing chamber, on a control glass slide, on a micropatterned PSBMA sample and a non-patterned PSBMA one. Bands labelled with $\circ$ are assigned to water, # to CO_3^{2-} and $*$ to PO_4^{3-}.

precipitation. The latter were larger than the clusters on the different surfaces. Larger mineral clusters from poorly crystalline HA might have been washed away from the surfaces by the ion solution flow.

4.2.3 Immersion of Mineralised Polymer Brush Samples in Simulated Body Fluid

Mineralised glass and PSBMA samples were subsequently immersed in SBF for a period of 7 d or 21 d. Already after 7 d of immersing the samples, the P content of the SBF as determined by Inductively Coupled Plasma Optical Emission Spectrometry (ICP-OES) was lower than before, indicating that mineralisation took place. The initial P content of $7.924\,\mathrm{mg\,l^{-1}}$ decreased to $3.647\,\mathrm{mg\,l^{-1}}$ after 7 d of immersion and levelled off to $3.138\,\mathrm{mg\,l^{-1}}$ after 21 d.

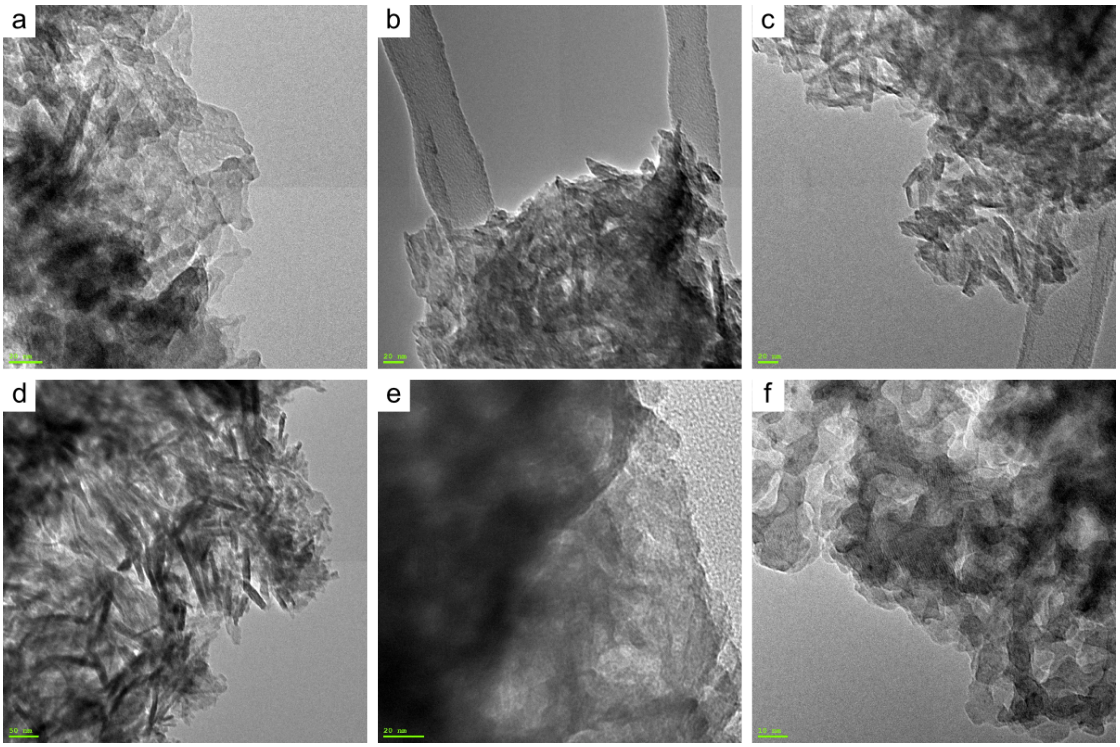

Figure 4.9: TEM micrographs of the CaP phases prevalent on mineralised samples after 7 days immersion in SBF on uncoated glass substrates (a, d), on unpatterned PSBMA brush substrates (b, e) and PSBMA brush coatings patterned with circular holes of 20 µm diameter (c, f).

After the same period, a phase transformation became evident when examining the ensuing mineral in the TEM (Figure 4.9). Again, there was no difference visible between the polymer brush samples and glass. The mineral still seemed to be amorphous in

the FFT mode of the TEM. In Figure 4.9f, it is visible that ordered, crystalline areas developed under the influence of the electron beam. The conversion took again place at high magnifications, as the intensity was higher, when the beam hit a smaller area. The morphology of the CaP after immersion in SBF in Figure 4.9 strongly resembles the one in Figure 4.6a. Comparison with the TE micrographs in the ref.s 213,259,319 shows evidence that this phase could be nanocrystalline HA.

The Ca/P ratio of the mineral, which was determined with EDX, is another indicator for the emerging phase. Before immersion in SBF, the Ca/P ratio of the amorphous samples varied between 1.4–1.6. After the immersion, the mineral on glass and on the patterned sample had a Ca/P ratio of 1.73, whereas the unpatterned PSBMA sample had a ratio of 1.57. HA has a theoretical ratio of 1.67. Factoring in the accuracy of the EDX measurement, which is always only a spot check, the Ca/P ratio of the mineral on glass and patterned coating suggests a HA phase. Poorly crystalline HA is a desirable phase for biomaterials as it is similar to the natural CaP phase in bone (comp. 4.1.2). The Ca/P ratio on the unpatterned sample increased, too, during immersion, but was still lower. Although the lower value might be due to the inaccuracy of the method, it might still also be due to the unpatterned sample only offering polyelectrolyte as an mineralisation surface. The PSBMA brush could therefore have slowed down the conversion from ACP to HA on the whole sample.

SBF contains Mg^{2+} ions, which are known to slow down the transformation from ACP1 to ACP2.[298] However, the ACP1 phase was clearly neither preserved by the Mg^{2+} content nor by the polyelectrolyte. Another major parameter to influence transformation kinetics is temperature.[206] At 15 °C mineralisation can take a completely different route than at 42 °C, preferring the crystallisation of DCPD over that of HA.[298] During the immersion in SBF, the temperature was constant at 37 °C, favouring the transformation to HA.

ATR-IR analysis showed a change of the spectra before and after the immersion (Figure 4.10). The PO_4^{3-} vibration band at 550 cm^{-1} was split in the sample after immersion and more defined than before immersion. The broad band around 3400 cm^{-1} assigned to incorporated H_2O was decreased. These are characteristics for a spectrum of HA. Overall the spectrum agrees well with the data from literature for HA and less with the bands reported for the also likely OCP phase as compared in Table 4.3.

On the other hand, a defined OH^- band could not be detected at 3400 cm^{-1}. This might be due to the reaction of the OH^- ions with CO_2, consuming the OH^- ions and thus reducing the signal. The reduced signal might consequently be covered by the broad H_2O band. The reaction $CO_2 + OH^- \longrightarrow HCO_3^-$ therefore could account for the CO_3^{2-}

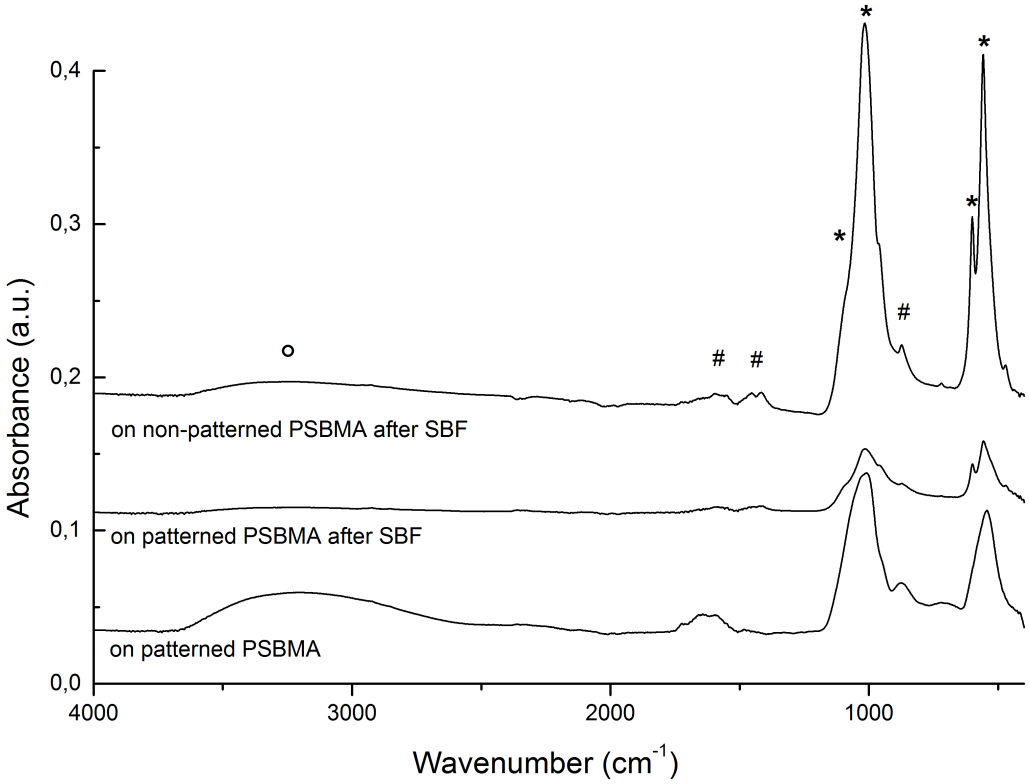

Figure 4.10: ATR-IR spectra of the mineral found (from top to bottom spectrum) on mineralised samples with non-patterned and micropatterned PSBMA coatings after immersion in SBF for 7 d. For comparison the spectrum of a micropatterned sample before the SBF immersion is included. Bands labelled with ∘ are assigned to water, # to CO_3^{2-} and ∗ to PO_4^{3-}. The conditions for the mineralisation before the immersion are given in Section 4.2.2.

Table 4.3: ATR-IR peak positions of PSBMA samples mineralised in a mixing chamber for 1.5 h with a 5 mM CaP solution at pH 7.4 and subsequently immersed in SBF for 7 d in comparison with the position of IR vibration bands specified in literature.

	Measured band positions [cm^{-1}]		Band positions in literature [cm^{-1}]				
Substrate	Micropatterned PSBMA	Non-patterned PSBMA	HA in ref. 65	HA in ref. 313	HA in ref. 16	OCP in ref. 16	OCP in ref. 313,365
Assignment							
PO_4^{3-}	557	557		566	570	530	559
PO_4^{3-}	600	600		602	601	603	599
PO_4^{3-}					631		
OH^-			630	630			630
CO_3^{2-}	871	874	874				
PO_4^{3-}	shoulder	(965)	964	959	954	954	962
PO_4^{3-}	1016	1016	1026	1037		1031	1025
PO_4^{3-}							1035
PO_4^{3-}							1055
OH^-					1030		
PO_4^{3-}			1094	1094	1081	1070	1075
PO_4^{3-}	shoulder	shoulder				1105	1105
CO_3^{2-}	1450	1415/1454	1419				
CO_3^{2-}	1600	1600	1587				
H_2O	3260	3270					
OH^-			3570		3562		

signals.

Concluding, the measurements indicate that the 7 d immersion in SBF likely caused a transformation of the mineral from ACP1 to nanocrystalline carbonated HA.

Next to the mineralisation, the immersion also caused part of the coatings to delaminate, revealing again an inappropriate instability of the polymer brush films. After immersion in SBF for 21 d, the mineralised polymer brush coatings delaminated even more and nearly completely (Figure 4.11) upon soft rinsing with water. The detachment is clearly visible macroscopically (Figure 4.11a and c) as well as under the light microscope (Figure 4.11b and d). The loss of the coating made further analysis of the coatings immersed for 21 d impossible.

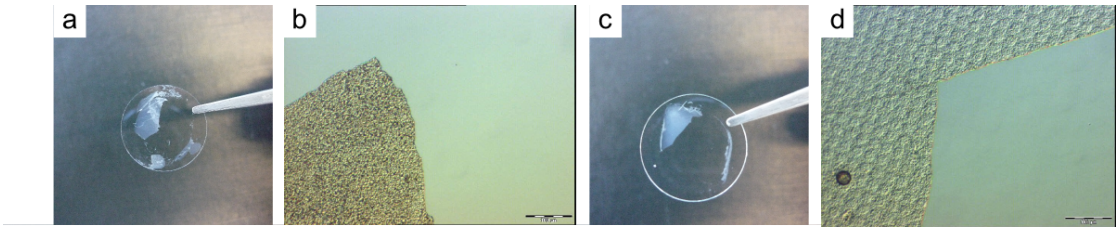

Figure 4.11: Delamination of mineralised PSBMA coatings unpatterned (a, b) and with a pattern consisting of holes with a 20 µm diameter (c, d) after 21 days in SBF.

A recent study of Löbbicke *et al.*[277] reported mineralisation of PDMAEMA and PMAA brush substrates. The authors do not mention problems with the long-term stability of their polymer brush coatings and their composites. They were, however, using gold coated substrates, linking the surface and the polymer *via* the stable S−Au bond. The thiol functionalised SAMs do not build cross-linked structures like the trimethoxysilanes, which might increase the number of achorage sites to the surface and thus the films' stability (comp. 3.2.1).

The authors of the study found evidence that MC3T3-E1 cells on mineralised polymer brush substrates had a strongly increased viability compared to the pure polymer brush surfaces. However, neither cell number nor viability on the mineralised PDMAEMA and PMAA brushes were higher than on the cell culture plastic control. Also neither the CaP amount nor its phase (which could not be elucidated unambiguously) had an obvious influence on the cells in the study. If the mineralisation of the polymer brush surfaces in the present work might lead to increased osteoblast viability still remains to be examined.

In summary, the mineralisation of the PSBMA brush covered samples in the mixing chamber produced an ACP layer. This CaP layer rendered the material more bioactive in terms of its promoting the build-up of a presumably biomimetic carbonated nanocrys-

talline HA coating after 7 d immersion in SBF. Comparing these results to the immersion of the unmineralised PSBMA films in SBF (comp. 3.2.1), the mineralisation was a clear improvement of the coating's bioactivity for biomaterials applications. However, the lack of stability of the present system over a longer immersion period (21 d) is a strong argument against the usage of polymer brushes as hard tissue implant coatings despite the favourable CaP layer after immersion in SBF.

4.2.4 Mineralisation of Plasma Polymer Substrates in a Mixing Chamber with an External Pump

To compare the mineralisation behaviour of the two classes of polymer films, the mineralisation protocol in the mixing chamber was tested on the plasma polymer films as well. The DIC micrographs in Figure 4.12 show a close mineral film after 1.5 h of mineralisation in the mixing chamber in a 5 mM CaP solution.

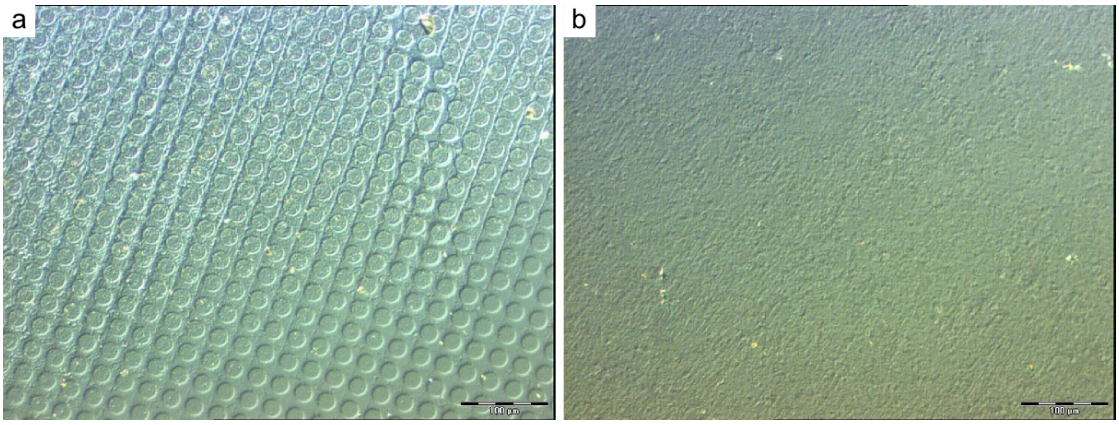

Figure 4.12: DIC micrograph of patterned (a) and non-patterned (b) ppH-ppMMA coatings mineralised in the mixing chamber with a 5 mM CaP solution for 1.5 h. Scale bars 100 µm.

Similar to the PSBMA coatings, the ppH-ppMMA films build-up an CaP layer that had the morphology of ACP1 when analysed in the TEM (Figure 4.13). The Ca/P ratio as determined with EDX was 1.59–1.66 and thus slightly higher than the one of the mineral formed on the PSBMA substrates, but also in the region of ACP (comp. Section 4.2.2).

In Figure 4.13c, it seems as if the mineral at least on this patterned sample was bound to or integrated into the polymer coating. The ACP clusters appears to be still embedded into a polymer matrix, which was visible as a grey layer with low contrast, additional to the carbon coating of the TEM grid. These are quite promising results, as a strong binding of the mineral to the coating probably indicates good stability of the composite.

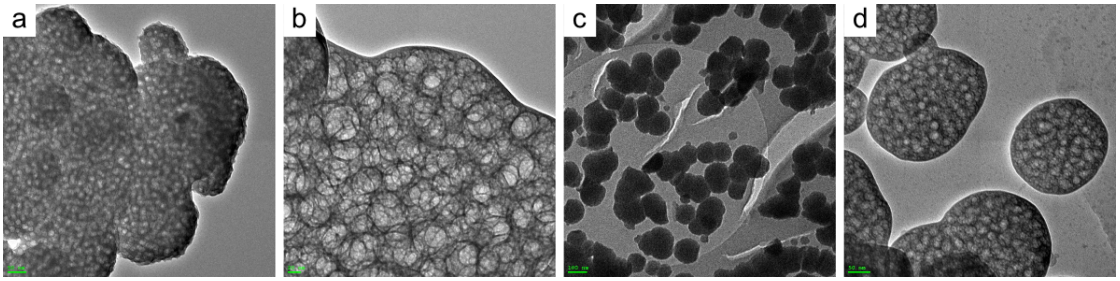

Figure 4.13: TEM micrographs of the CaP precipitate on mineralised ppH-ppMMA films without patterning (a, b) and with a pattern consisting of holes with a 20 µm diameter (c, d).

ATR-IR analysis showed that the spectra of the resulting mineral agreed with the data reported for ACP (Figure 4.14 and Table 4.4). They correlated well with the spectra obtained for the mineral that formed on the PSBMA substrates (Figure 4.8). Small differences, however, do exist:

- For the micropatterned ppH-ppMMA sample an additional band at 804 cm^{-1} could be detected.
- The bands in the range of CO_3^{2-} have a different fine structure. This can be attributed to the ester groups of the polymer matrix. The broadness of this band might be due to a varying chemical environment. Additionally, hydrolysis of the ester cannot be excluded.
- Yet another additional peak at 2960 cm^{-1} can be assigned to the polymer's alkane moieties (comp. Section 2.2.3).

Concluding, the plasma polymer films were mineralised with ACP1, as evidenced from ATR-IR and TEM, when following the protocol used to mineralise the PSBMA brush substrates. Thus, the plasma polymer just as the polymer brush did not change the first phase to precipitate from a 5 mM CaP solution after 1.5 h in a mixing chamber. TEM micrographs suggest a good binding between the mineral and the polymer.

4.3 Comparison of the Two Polymer Coatings' Influence on Mineralisation

Despite their different chemistries and physical properties, the two examined polymer films evoked the build-up of similar CaP layers upon mineralisation in a mixing chamber. PSBMA brush as well as ppH-ppMMA films produced a CaP layer, which most likely

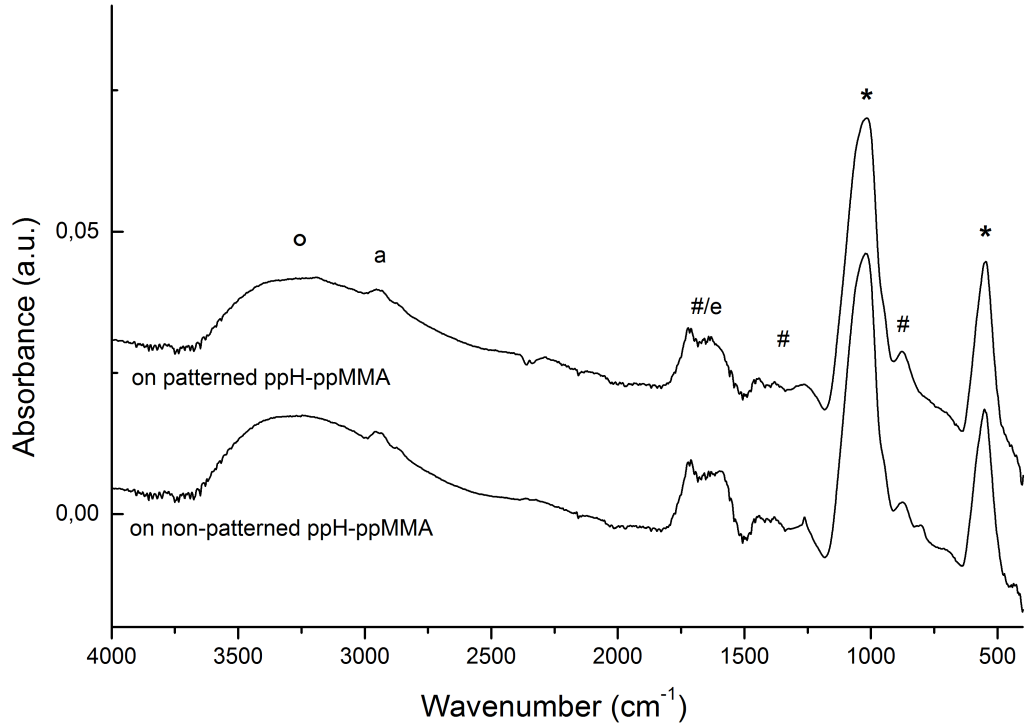

Figure 4.14: ATR-IR spectra of the mineral phase precipitated on patterned (top) and non-patterned (bottom spectrum) ppH-ppMMA coated samples. Bands labelled with ∘ are assigned to water, "a" to alkane moieties of the polymer, "e" to ester moieties of the polymer, # to CO_3^{2-} and $*$ to PO_4^{3-}.

Table 4.4: ATR-IR peak positions of the mineral precipitated on ppH-ppMMA samples in a mixing chamber after 1.5 h mineralisation with a 5 mM CaP solution at pH 7.4 in comparison with the position of IR vibration bands specified in literature.

	Measured band positions [cm^{-1}]		Band positions in literature [cm^{-1}]		
Substrate	Micropatterned ppH-ppMMA	Non-patterned ppH-ppMMA	ACP in ref. 65	ACP in ref. 63	ppMMA in ref. 81
Assignment					
PO_4^{3-}	551	546			
	804				
CO_3^{2-}	875	877	874		
PO_4^{3-}	1022	1018	1050		
CO_3^{3-}	1200–1500	1200–1500	1419	1400–1500	
CO_3^{3-}/ester	1550–1800	1550–1800	1587		1726
alkane	2960	2955			2800–3000
H_2O	3250	3250	3400		

comprised ACP1. Yet, the zwitterionic polymer brush carried charges on every polymer segment and was highly hydrated (comp. Section 2.2.2). The plasma polymer film with ppMMA as the topmost layer, on the other hand, was not as hydrophilic and had a surface energy with a high dispersive component (comp. Section 3.2.3). Despite the big difference between the surface properties of the two types of films, they nevertheless provoked the same reaction upon mineralisation. This and the ambiguous transfer of the polymer pattern to the mineral are signs that the mineralisation was not controlled by the template surface to a great extent. The charges of the PSBMA brush might have increased nucleation. The ppMMA film could also have carried charged carboxylate groups due to hydrolytic cleavage of the ester groups. However, prove of further influence on the mineralisation could not be elucidated.

In spite of the polymer films' lacking role as templates of the mineralisation, the results are not discouraging in terms of biomaterial properties. The ACP phase, which precipitated on all the substrates, is quite easily transferred into the thermodynamically most stable phase HA, for example by heat treatment. It is therefore a versatile starting point. As the experiments with the polymer brush coatings show, immersion in SBF is also likely to lead to a phase conversion resulting in biomimetic HA. The mineralisation therefore increased the bioactivity, promising also a more favourable cell reaction to mineralised substrates. If the mineralised plasma polymer films show the same favourable bioactivity in SBF is still to be elucidated.

Due to the polymer brushes lacking stability, cell culture experiments with these mineralised substrates were omitted. Still, the more stable plasma polymer films promise to show good biomaterial properties, as even the non-mineralised samples showed biocompatibility comparable to cell culture plastic control (comp. 3.2.3). Their biocompatibility might be even increased by the mineralisation and would be interesting to examine in future experiments.

5 Directed Nanoparticle Adsorption to Patterned Polymer Brush Surfaces*

5.1 Introduction to Nanoparticle Adsorption to Surfaces

To examine how not only a biomimetic implant surface with a polymeric matrix impregnated with CaP could be provided but also to deliver pharmaceutical agents, the adsorption of functionalised polymeric nanoparticles onto patterned polymer brush substrates was investigated. The nanoparticles were synthesised and kindly provided by Dr. Anke Zeller[366,367] during her time at the Max Planck Institute for Polymer Research in Mainz.

In implant medicine, a site specific drug release could be of great use to defeat implant site infections and to ameliorate bone growth around the implant. The nanoparticles have the potential to serve as carriers for antibiotics, bone growth enhancing agents such as BMPs[18,198] or the osteoclast inhibiting bisphosphonates.[216] This directed delivery is of considerable importance to attenuate the systemic side effects of many drugs. Thus, tailoring the interactions between polymeric nanoparticles – acting as drug delivery systems – and implant surfaces promises large improvements for next generation smart implants and biomaterials. Additionally, lab-on-a-chip systems may profit from the site specific delivery of reagents onto patterned surfaces to restrict reactions to certain areas of a chip.

Polymeric nanoparticles came into the focus of materials science as drug carrier systems since the 1980's.[368] They can lower the necessary amount of the applied drug or even make pharmaceuticals with inappropriate properties available by surrounding those drugs and masking their adverse pharmacokinetic properties. Although there are still a couple of issues, challenges and question to be solved concerning the carrier toxicity, carrier capacity, loading and release controlling mechanisms, specific targeting and

*Parts of this chapter (text, experimental details and figures) have been published recently in ref. 180: Annina Steinbach, Tobias Paust, Manuela Pluntke, Othmar Marti, Dirk Volkmer; "Selective Adsorption of Functionalized Nanoparticles to Patterned Polymer Brush Surfaces and its Probing with an Optical Trap" *ChemPhysChem*, **2013**, *14*, 3523–3531.

commercialisation, the micro- and nanoparticles seem to be promising drug delivery systems.[369]

Until now, only few studies are concerned with the assembly of polymeric nanoparticles on polymer modified substrates. In most cases, research focuses on the incorporation of inorganic material into a polymer material.[123,186,370–372] The interaction of polymeric nanoparticles with polymer coatings is – as one of the few – addressed by Chen et al.[373] During the deposition of Polystyrene (PS) nanoparticles on layer-by-layer deposited polyelectrolyte films, the authors observed a strong influence of pH, ionic strength and surfactants on the surface directed adsorption of the nanoparticles. Hereon, the group also published results on the assembly of polystyrene sulfate particles and amidine-terminated polystyrene microspheres on patterned polyelectrolyte layers, using pH, ionic strength and surfactants for the control of the assembly.[374] Jonas and Krüger[132] deposited polymer nanoparticles onto surfaces that were patterned by SAMs. They discussed in detail the forces that probably act between hydrophobic and hydrophilic, polar and non-polar, charged and non-charged particles and surfaces.

The interactions between nanoparticles and polymer brushes depend on several parameters:[186,370,372,375]

- strength of polymer/particle interaction
- polymer chain length
- polymer grafting density
- particle size
- solvent quality

Whereas smaller particles are able to penetrate into the brush and build several layers,[186,375] the particles used in this work were in the same order of magnitude as the polymer brush thickness in the hydrated state. Thus, the system here probably allowed nanoparticle binding to the surface with the nanoparticles dipping partly into the polymer brushes. In the here tested system, the last three points were also approximately constant. Therefore, the main parameter to influence the nanoparticles adsorption to the patterned polymer brush substrates was anticipated to be the strength of the interactions between the polymer (and its functional groups) and the functionalised nanoparticles.

To quantitatively describe these interacting forces, an appropriate method was sought. In cooperation with Pluntke and Paust of the Institute of Solid State Physics at Ulm

University, the probing of the nanoparticle/polymer brush interactions with an optical trap was tested.

Focused lasers are used to trap particles since the 1980s. The trapping is based on scattering and gradient forces of a strongly focused laser beam. The net force acting on the particle always points towards the laser focus, thus forming the trap. Hereby applies: the higher the optical intensity of the laser, the greater are the forces acting on the trapped particle.[376] A schematic of a particle in the laser focus is depicted in Figure 5.1. When a force from the outside is acting on the trapped particle, it is moved from its equilibrium position.[85] In a measurement, this displacement of the particle out of the focus is then measured in dependence on the distance to the surface. This displacement is directly proportional to the force acting on the particle, which is described by $F = -k_{\text{trap}}\Delta x$ with Δx being the displacement and $-k_{\text{trap}}$ as the trap stiffness, which is determined by calibration measurements of the particle movement without external forces applied.[85]

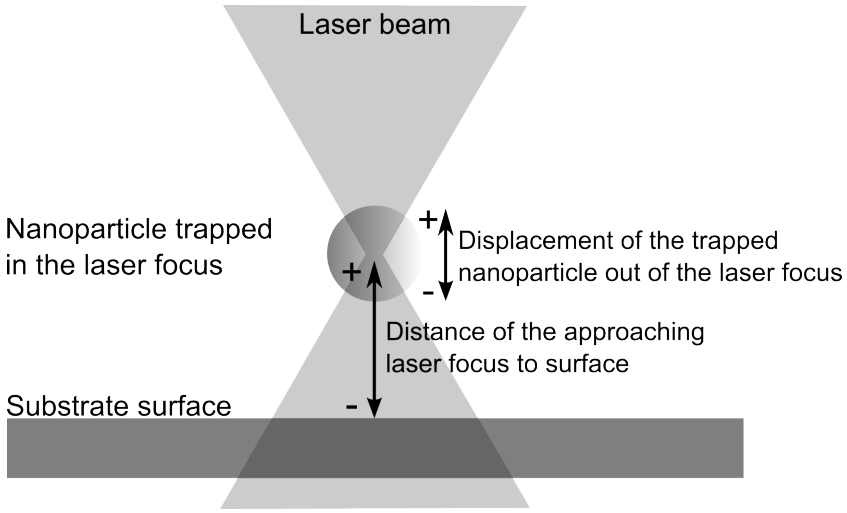

Figure 5.1: Schematic of a particle trapped in a focused laser beam. During measurements the displacement of the particle out of the focus is measured in dependence on the distance to the surface. Figure published in ref. 180.

Extremely small forces in the low pN range can be measured by optical traps. The interaction forces between particles and surfaces or between two particles have been measured. Optical traps were already used to examine the interaction between weak polyelectrolyte covered SiO_2 particles and deduce *via* theoretical models the polymer film height and its conformation switch between pancake and brush regime in dependence of pH and ion concentration.[85]

In this chapter, the optimisation of the selective deposition of phosphonate functionalised PS nanoparticles onto surfaces modified with linear micropatterned polymer brushes is described. The strong polyelectrolyte brushes PSPMA, PSBMA and PMETAC served as coatings to direct the phosphonate nanoparticles independently from the surrounding pH. The polycarboxylate PMAA brush was the means to introduce a pH-dependent interaction between the phosphonate nanoparticles and the surface. Figure 5.2 summarises the experiments conducted for this chapter.

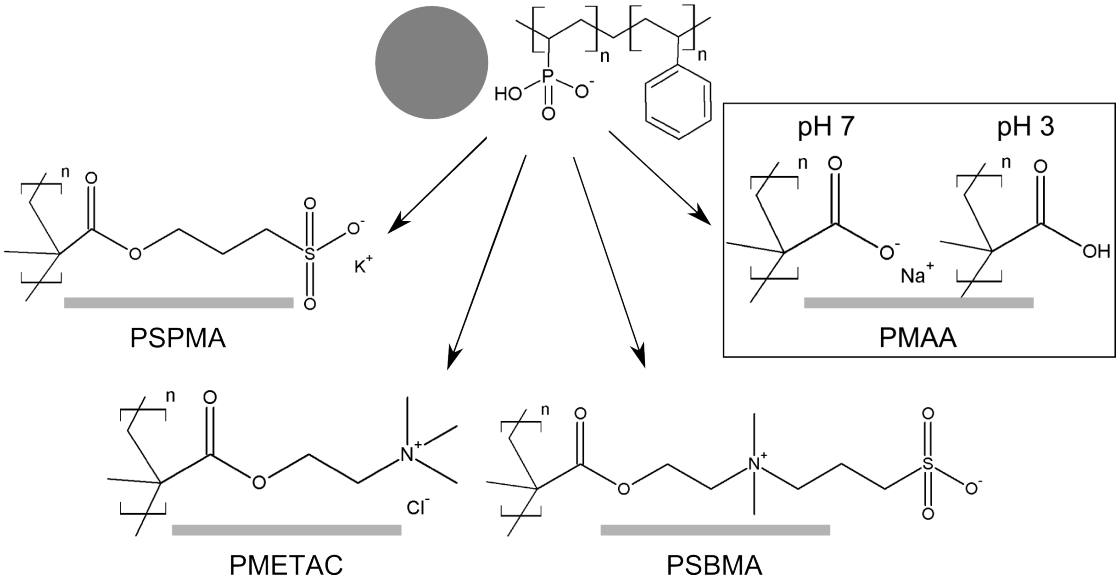

Figure 5.2: Schematic overview of the experiments in this chapter. Substrates with the four different polymer brush films already described in the previous chapters were coated with phosphonate functionalised nanoparticles. The micropatterned polymer brush substrates directed the nanoparticle adsorption in dependence on surface chemistry. Figure published in ref. 180.

To elucidate the interacting forces leading to the observed distribution patterns on the pH-dependent PMAA brush, the results of the optical trap measurements are included into this chapter. A model for the different forces causing the different distribution patterns is developed and discussed.

5.2 Results and Discussion of Nanoparticle Adsorption to Patterned Polymer Brush Surfaces

The first procedure that was tried to coat the polymer brush films was simply placing a drop of the colloid onto the glasses and rinse it afterwards to remove unbound or loosely bound nanoparticles. This method resulted in a thick layer of dried out nanoparticles

(Figure 5.3).

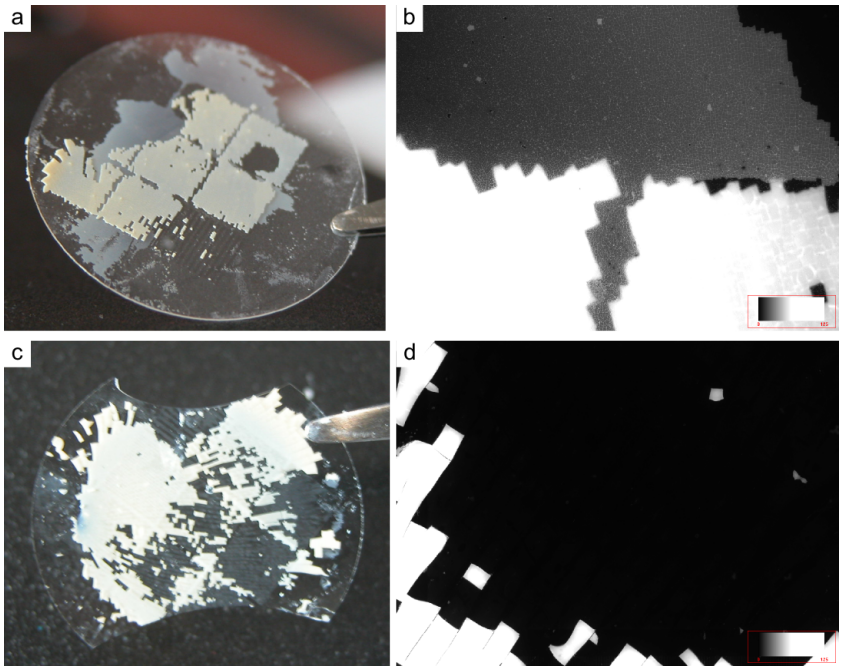

Figure 5.3: Dried out layer of nanoparticles that resulted from placing a drop of the colloid on patterned PSBMA (a, b) and PMETAC (c, d) coated samples.

Nevertheless, there was still a difference of distribution and adhesion visible after rinsing. On the PMETAC coated sample with the 9-fields pattern (comp. pattern to Figure 7.1e on p. 146), the nanoparticle layer (which resembled an armor plate more than a monolayer) adhered better to the polymer brush regions of the pattern (Figure 5.3c and d). The coating, which remained on the PSBMA sample after rinsing, adhered mainly to the patterned squares (Figure 5.3a and b), whereas on the PSPMA brushes no such coating was visible. These results were encouraging as the difference in distribution was anticipated and attributed to the different charges owing to the chemical functional groups of the polymers. The PS-co-Poly(Vinylphosphonic Acid) (PVPA) nanoparticles had a negative charge on their outside (for a schematic drawing see Figure 7.3 on page 150), so they should be attracted to the positive charge of the PMETAC brushes and repelled by the negative charge of the PSPMA brushes. The PSBMA brushes have no net charge and strong intra- and intermolecular interactions and no obvious functional groups to interact with phosphonate groups, but also do not repel these moieties. This lack of possible interactions gives leave to the assumption that the nanoparticles simply got caught in the pattern.

However, as the aim was having a clear distribution of a nanoparticle monolayer, other

possible coating procedures had to be tested. Simple immersion of up-right standing glasses hampered quick analysis with the fluorescence microscope, as with this method the glasses were coated from both sides. The fluorescence of the backside interfered with the analysis of the patterned side. Using a shaker or sonication during or after the coating procedure also did not lead to the desired result. These problems were the impulse for constructing a device that made coating of only one side of up-right standing glasses possible in a closed container to prevent the nanoparticle coatings from drying out. This device was custom-made by the workshop of the University Ulm and can be seen in Figure 7.4 on page 151.

With this device, there remained the task to optimise the parameters of the coating procedure: the solids content of the nanoparticles in the colloid and the pH during attachment and washing steps. The amount of nanoparticles in the colloid during immersion of the polymer brush substrates was determined to be 1 mg/ml. At a higher solids content, nanoparticles were stacking over each other in multiple layers (Figure 5.4). At a lower solids content, a clear distribution could not be perceived and the fluorescence was low.

Usually, the colloid was diluted with a HCl solution at pH 3. The nanoparticles were also suspended in a 0.1 M citric acid buffer at pH 3 to adsorb them to the substrates, but the fluorescence was low. Additionally, the distribution pattern of the nanoparticles had an overlay of crystal artefacts. When the substrates were rinsed with water to eliminate the crystals, there was no fluorescence perceived. The higher ionic strength of the buffer may have masked the electrostatic interactions, as interaction distances decreased with increasing ionic strength as was observed by Elmahdy *et al.* for SiO_2 colloids.[377]

With the optimised solids content of 1 mg/ml and diluted HCl as the right solvent for the adsorption step, the distribution pattern of the nanoparticles in dependence on the different polymer brush functionalisations was examined.

5.2.1 Charge-Dependent Adsorption of Phosphonate Nanoparticles to Strong Polyelectrolytes

The strong polyelectrolytes PSPMA, PSBMA and PMETAC were used to direct the nanoparticles independently of the pH (comp. Figure 5.2). The charged groups of these polymers, namely sulfonate groups and quaternary amines, were charged in the whole pH range applied here. The adsorption was always carried out at pH 3 and the washing procedure at pH 3 (in diluted HCl), at pH 5–6 (in water) or pH 7 (in Phosphate Buffered Saline (PBS)). The nanoparticle attachment showed no difference, regardless whether the washing steps were carried out at pH 3 or pH 7 (Figure 5.5). The resulting coatings, however, were more homogeneous, when the washing step was carried out at pH 7. It

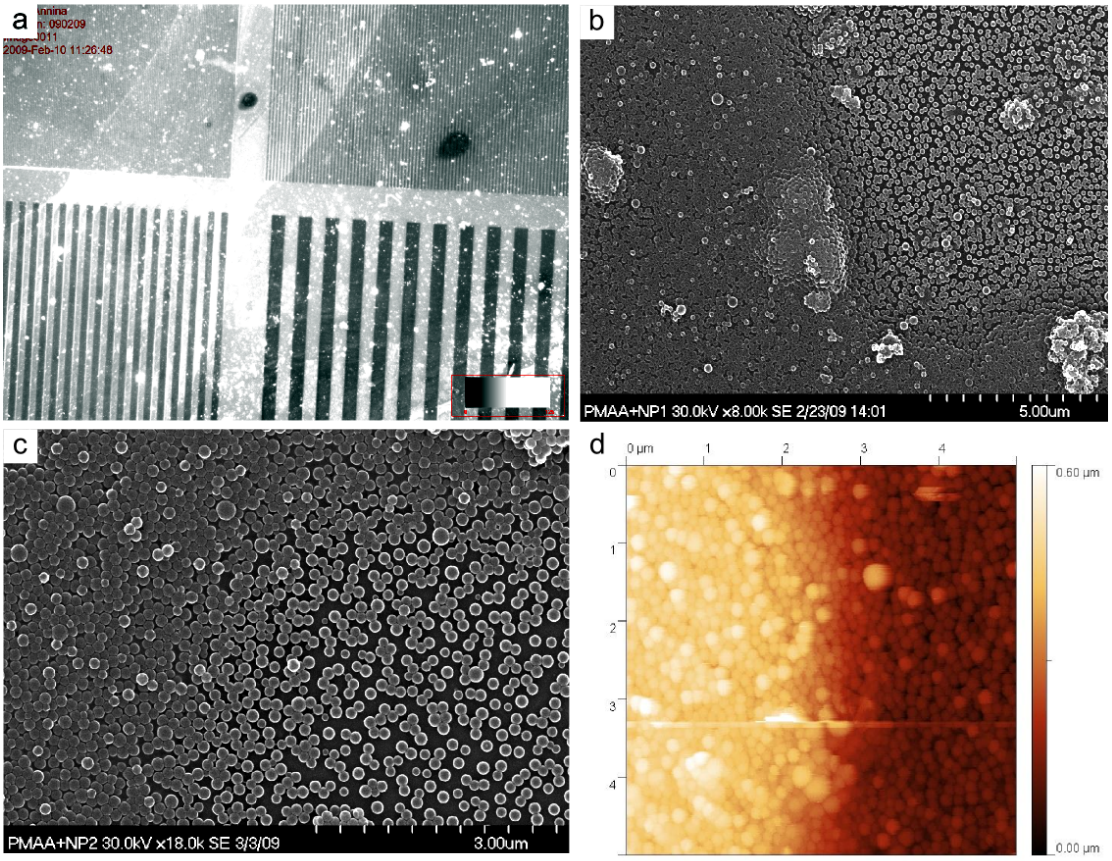

Figure 5.4: Nanoparticle adsorption on PMAA brush surfaces from a colloid of higher solid content (in this case 50 mg/ml) as seen through the fluorescence microscope (a), SEM (b, c) and by an AFM scan (d).

also turned out to be better to use PBS as the washing agent instead of deionised water, as this produced better and better reproducible results. The reproducibility may be due to the more stable pH, which is buffered at pH 7.4 in PBS. The pH of water in contrast varies between 5 and 6, depending on the content of CO_2 solved in the water.

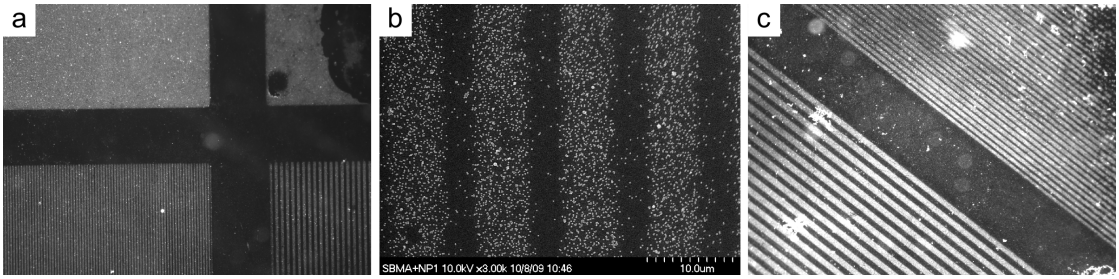

Figure 5.5: The distribution of the nanoparticles on PSBMA substrates did not change, when the washing step was carried out at pH 3 (c) instead of pH 7 (a, b), as seen by fluorescence microscopy (a, c) and SEM (b).

The distribution pattern of the nanoparticles on the three different polymer brush surfaces was clear and overall as expected. Attachment of phosphonate nanoparticles to the negatively charged PSPMA brush substrates was not observed, only bright spots of unspecific aggregated nanoparticles (Figure 5.6a). Here negative charges on the particle and the substrate even at pH 3 prevented any binding interaction. Jonas and Krüger[132] observed similar effects for the adsorption of SiO_2 and PS nanoparticles to sulfate carrying SAMs and accounted them to Coulomb repulsion and the strong hydration tendency of sulfate groups.

The polycationic PMETAC directed the nanoparticles preferably towards the brush areas (Figure 5.6b). Positive charge attracts negative charge, so the PMETAC brushes directed nanoparticle binding to the brush regions. This simple electrostatic interaction was exploited in several other studies for the interaction of polymer brushes with gold nanoparticles, *e.g.* ref. 186. However, here, in contrast to the works of Bhat *et al.*,[186] this ionic binding is independent of the pH because of the constantly charged quaternary amine.

The zwitterionic PSBMA in contrast prevented attachment onto the brush, but guided the nanoparticles into the grooves (Figure 5.6c). The PSBMA brushes had both negatively and positively charged groups. Thus, no charge could prevail for an electrostatic interaction with charged and hydrophilic nanoparticles. Instead of Coulomb interactions, other mechanisms might be responsible for the distribution of the phosphonate nanoparticles on the patterned PSBMA substrates. As described in Section 2.2.2, the PSBMA brush swelled to about double its dry height when immersed in water. This means that

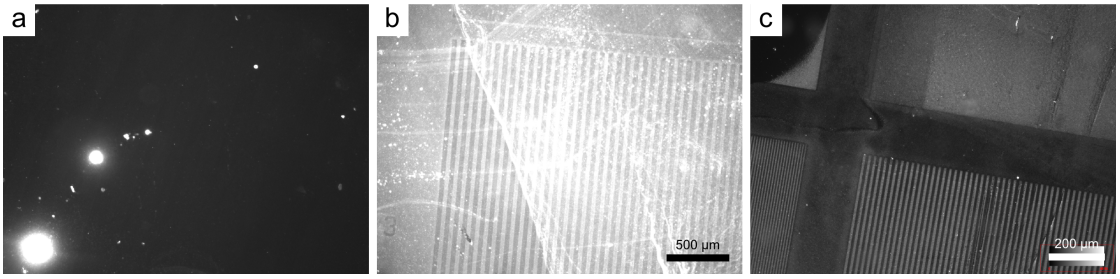

Figure 5.6: Fluorescence micrographs in grayscale with high fluorescence indicated by bright spots; (a) microstructured PSPMA sample after the adsorption and washing procedure, only unspecific aggregates of nanoparticles are visible; (b) nanoparticles on a microstructured PMETAC sample with preferred attachment to polymer brush regions, scale bar 500 µm; (c) nanoparticle adsorption on a PSBMA substrate with a strong preference to the grooves, scale bar 200 µm. Figure published in ref. 180.

in the swollen state, the height of the pattern is in the range of the phosphonate nanoparticles' diameter. Therefore, the nanoparticles could merely be trapped mechanically in the grooves surrounded by PSBMA brush "walls". The charged groups of the polymer brushes are also anticipated to be hydrated[51,130] hampering direct interactions between the charged groups of the brush and the nanoparticles. To interact with the nanoparticles, the functional groups of the PSBMA brush would have to strip off their hydration shell. The irradiated surface bound initiator, on the other hand, is hydrophilic (water contact angle 27°[181]) but not able to swell and therefore able to interact with the phosphonate nanoparticles. A combination of the two effects is probably the reason why preferentially in the grooves attachment could be observed.

Concluding, by coating substrates with patterned films of the three strong polyelectrolyte brush types PSPMA, PSBMA and PMETAC, it was possible to tailor the adsorption of phosphonate functionalised nanoparticles. The system enabled preventing adsorption or directing nanoparticles to the grooves or to the polymer brush regions.

5.2.2 pH-Dependent Adsorption of Phosphonate Nanoparticles to a Weak Polyelectrolyte

Next to the charge-dependent control of nanoparticle adsorption, a pH-dependent system was explored. The polycarboxylate PMAA promised to be a good candidate for a pH responsive polymer brush surface.

Nanoparticles with phosphonate groups on their surface indeed showed a very selective distribution on micropatterned PMAA brushes, which depended on the pH of the washing solvent. The adsorption always took place at pH 3, whereas the washing steps were again

carried out at either pH 7.4 in PBS or pH 3.0 in diluted HCl. Keeping the sample at pH 3 after attachment time, lead to an adsorption of the nanoparticles almost exclusively to the polymer brush regions (Figure 5.7a and b). In contrast to this, at changing the pH to 7.4, the attachment of the nanoparticles was restricted to the grooves (Figure 5.7c and d).

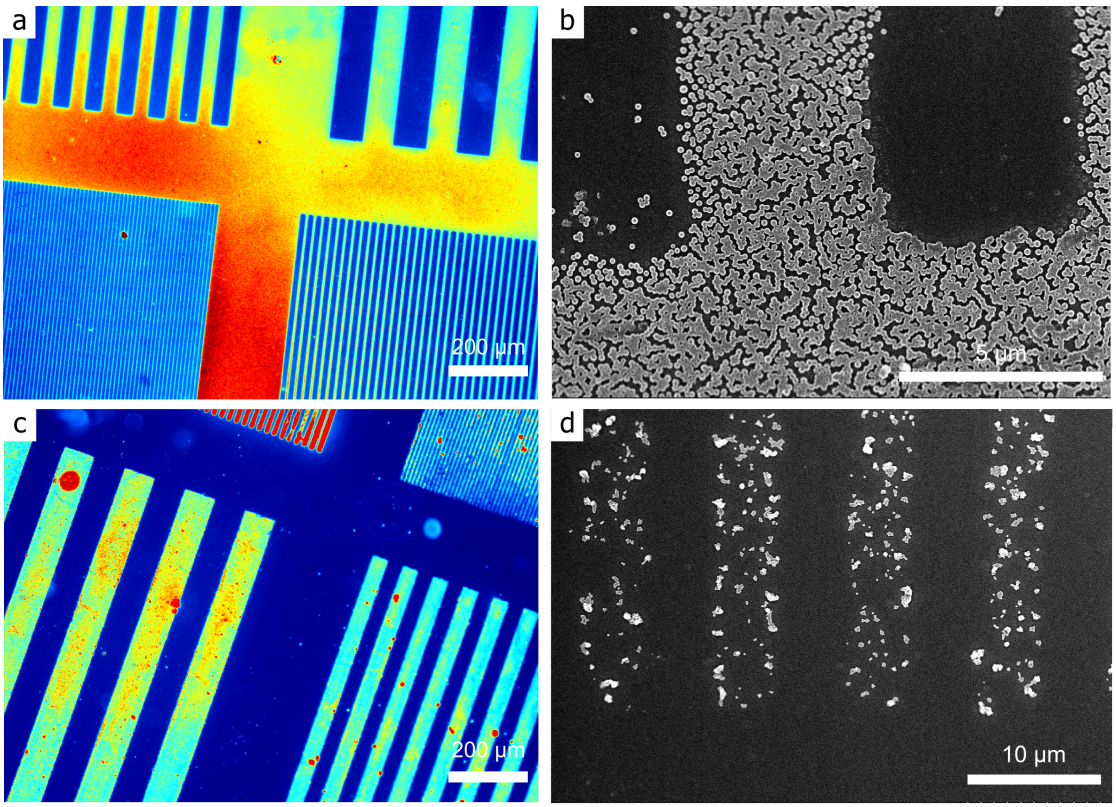

Figure 5.7: Pseudocolour fluorescence micrograph of nanoparticles loaded with fluorescence dye on PMAA brushes, adsorption and washing steps at pH 3 (a). Red colour indicates a high fluorescence intensity, blue a low intensity, scale bar 200 µm. Corresponding scanning electron micrograph (b), scale bar 5 µm. Fluorescence micrograph of a sample washed at pH 7 (c), scale bar 200 µm. Corresponding scanning electron micrograph (d), scale bar 10 µm.

To explain this behaviour, the surface potentials of the involved interaction partners were measured. The ζ-potential of the phosphonate functionalised nanoparticles varied only slightly in the pH region used: from −15.6 mV at pH 3 to −20 mV at pH 10.[367] Consequently, with the nanoparticles constantly carrying a negative surface potential, the major part for the switching behaviour was contributed to the polymer brush.

As streaming potential measurements showed (Figure 5.8), the polymer brush's ζ-potential dropped drastically from nearly 0 mV at pH 3 to around −30 mV at pH 7. The

measurements of the brush ζ-potential were quite unusual in that the curves did not have a proper plateau at higher pH and the measurements starting at the basic regime did not match the ones starting from the acidic regime.

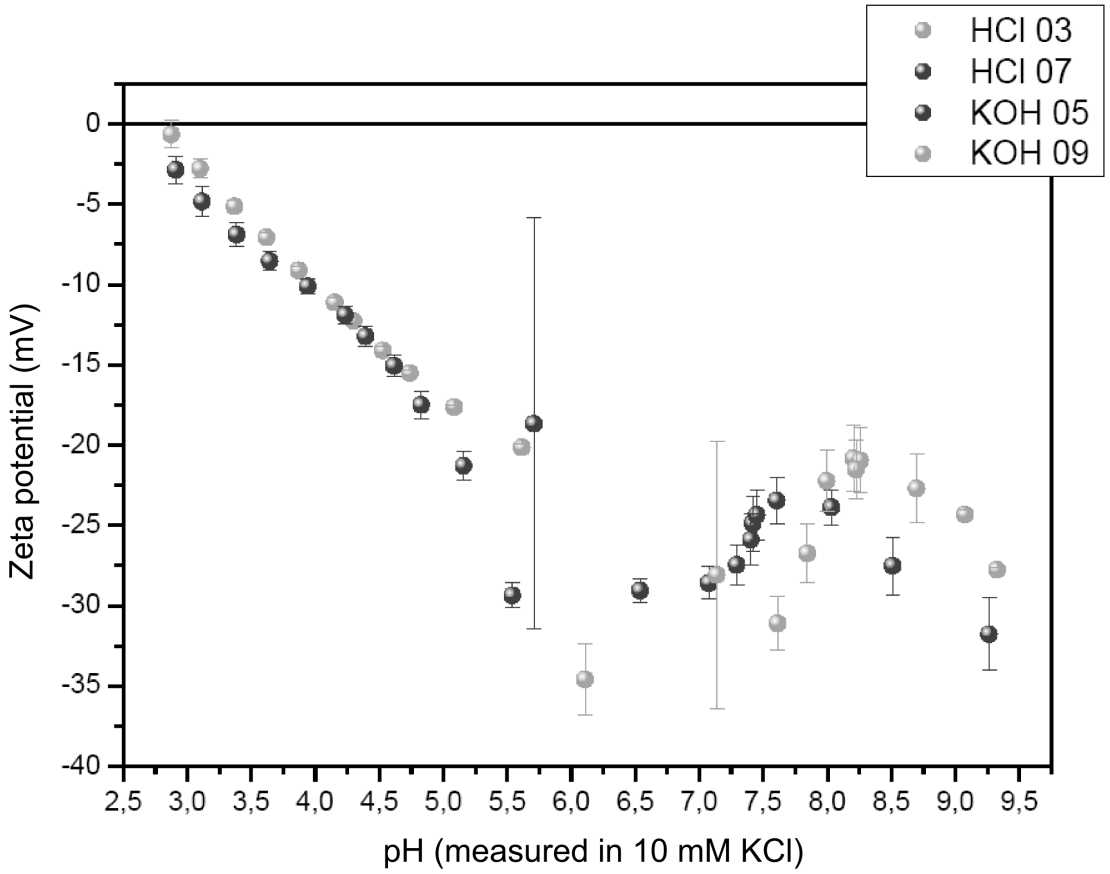

Figure 5.8: ζ-potential of the PMAA brushes *versus* pH measured by streaming potential measurements. Figure and measurements through the courtesy of the Bellmann group of the Leibniz Institute for Polymer Research Dresden.

One possible explanation for the unusual behaviour of the PMAA brush might be the pK_a dependence on the density of the respective functional group.[83] The degree of ionisation of a polymer's functional groups depends on the density of these charge baring moieties.[83,378] To avoid a charge density above a critical level, the degree of ionisation is lower, the higher the density of the charge bearing groups is.[378] Therefore, with a high polymer brush density, the pK_a should be higher – *i.e.* the acid less strong – than with a polymer brush of low density.

The unusual behaviour of the brush coating could be correlated to the brushes partly delaminating and thus lowering the carboxylic functional group density. It is well known

that the Si−O bonds hydrolyse in basic conditions.[266,379] Combined with the experience of a limited stability of the polymer brush films in aqueous surrounding this explanation seems quite feasible. The lower carboxylate density would again increase the degree of ionisation of the system and change the ζ-potential as the measurement goes along. On the one hand, this detachment would be quite striking, as it would mean that the brush stability was extremely low, not even surviving a measurement. On the other hand, the pH range gone through here is quite big, so the long term stability at pH 7.4 in cell culture experiments cannot be compared to the short term stability at a broad pH range here.

However the explanation of the unusual data of the ζ-potential measurements of the PMAA brush, it seemed nevertheless obvious that the polymer brush was the main cause for a surface potential or ionisation caused effect. At pH 3, ζ was 0 mV for the PMAA brush, so the major part of the carboxylate groups of the PMAA brush was protonated. In this state, the carboxylate groups could contribute their proton to hydrogen bonds. The phosphonic acid groups on the nanoparticles were partly deprotonated at pH 3 (comp. the ζ-potential and pK_{a1}=1.8, pK_{a2}=7.3), so they could equally contribute to hydrogen bonds with their lone pairs. Thus, hydrogen bonds as strong inter-molecular interactions may have contributed to the assembly of the phosphonate nanoparticles on the PMAA brush regions. This hypothetical interaction is depicted in Figure 5.9.

The reverse distribution pattern of the nanoparticles on the patterned PMAA film for pH 7 was observed compared to pH 3. At pH 7, the nanoparticles were arranged in the grooves of the pattern (Figure 5.7). At this pH, both the phosphonate and the carboxylic groups were highly negatively charged. The streaming potential measurements showed a drop of the polymer brushes' ζ-potential to about −30 mV at pH 7 and the ζ-potential of the nanoparticles was also measured to be clearly in the negative range.[367] To evade the Coulomb repulsion, the nanoparticles may have reassembled in the grooves. Additionally, the groove surface was hydrophilic (the water contact angle was 27°[181]) providing the possibility of interactions between the hydrophilic surface and the hydrophilic and charged nanoparticles.

However, note the lower density of the particle layer in Figure 5.7d compared with the nearly close packing in Figure 5.7b, which might be an effect of the repulsive forces acting. The immersion for attachment in the colloid had to take place in the acid regime, because this first step ensured an initial binding between the nanoparticles and the polymer brush coating. Thus, the first binding took place at pH 3 to adsorb the nanoparticles to the surface, whereas during the washing steps at pH 7, a rearrangement may have taken place and resulted in the observed adsorption pattern in the grooves. Otherwise, when

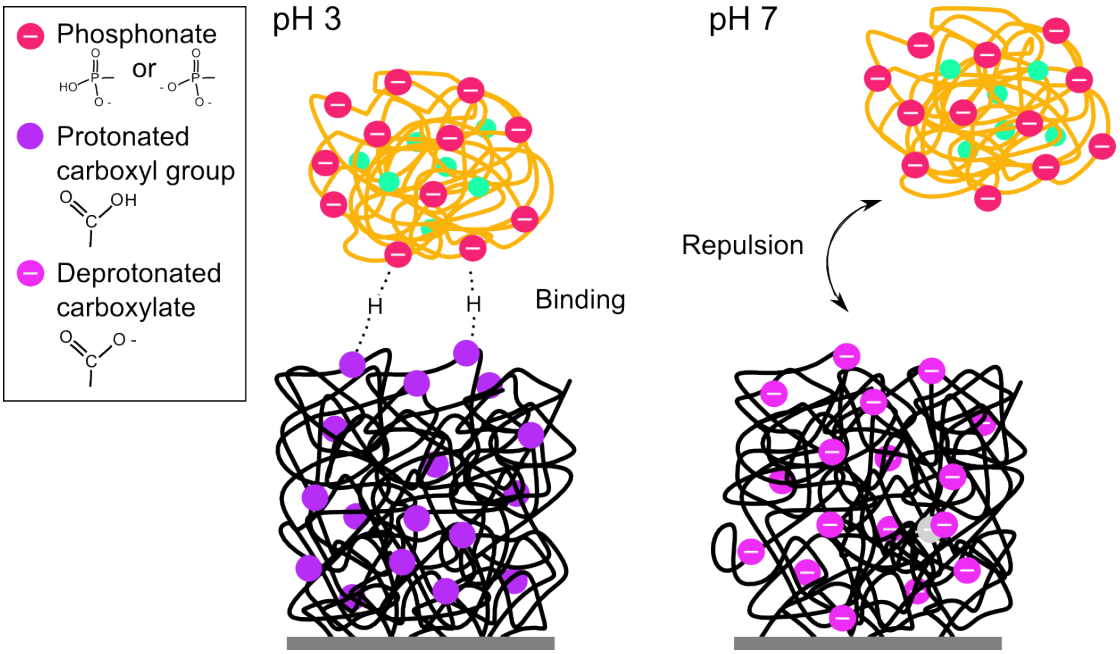

Figure 5.9: Sketch of the proposed binding model for pH 3 (left) and pH 7 (right). At pH 3 hydrogen bonds between the carboxylic acid of the brush and the only partially deprotonated phosphonic acid groups cause a strong preference of the nanoparticles for the brush regions; at pH 7 the charge repulsion of the phosphonate nanoparticles and the carboxylate brush prevent deposition on the brush area.

immersing the PMAA substrate in a basic nanoparticle suspension, the repulsive forces were stronger than the binding forces because of the negative charges and no binding occurred between the substrate and the particles in the first place. This case can be seen as an analogue to the interactions between the (almost) constantly charged PSPMA brushes and the phosphonate nanoparticles (Section 5.2.1).

5.2.3 Direct Measurement of the Interactions between Nanoparticles and PMAA Brushes

To actually measure the forces between the polymer brushes and the nanoparticles, an optical trap was used. With the optical trap set-up, it was possible to directly compare the areas covered with the PMAA brush with the groove surface. The experiments with the optical trap and the evaluation of their data were mainly conducted by Paust of the Institute of Experimental Physics at Ulm University. Details about the set-up and data analysis are given elsewhere.[180] In this chapter, I will merely discuss the results and their implications for the interacting forces between negatively charged nanoparticles and PMAA brushes in dependence on pH.

As the phosphonate nanoparticles with a diameter of 150 nm had a low contrast in the light microscope of the optical trap set-up, the measurements were conducted with larger nanoparticles. These particles had a negative surface potential as well as can be deduced from ζ-potential measurements (Figure 5.10). At pH 6 the ζ-potential increases parallel to the size values. This suggests that the unusual change of surface potential is due to agglomeration and should not have affected the optical trap measurements, as they were performed on single particles. As outlined above, the polymer brush's surface potential was anticipated to contribute the major part to the nanoparticle assembly effect. Consequently, the forces between the PMAA brush and the two different nanoparticles should not differ greatly and the substitute should be a valid model system for the measurements.

To visualise the principle of the optical trap and the measured parameter, compare Figure 5.1 and the respective paragraph in Section 5.1. Figure 5.11a and b show the displacement of the negatively charged nanoparticles during typical approaches to polymer brush areas (blue) and to groove surfaces (red) at pH 3 (Figure 5.11a) and at pH 7 (Figure 5.11b). During the approaches, there was a point where the nanoparticle was suddenly pulled towards the surface. This was the so-called snap-in, which is shown in the insets as a close-up.

The most striking difference between curves measured at pH 3 (Figure 5.11a) and the ones measured at pH 7 (Figure 5.11b) is the clear snap-in at pH 3. The nanoparticle was

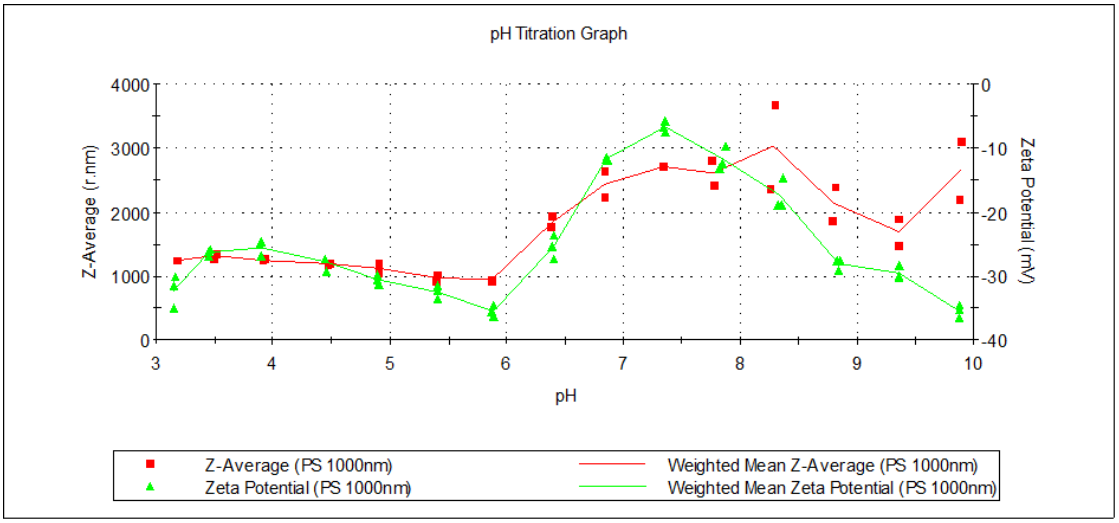

Figure 5.10: ζ-potential and particle size in dependence on pH. The particles used for optical trap measurements carried a negative surface potential over the entire pH range measured. The increase of surface potential at pH 6 correlates to the increase of particle size showing that agglomeration is the most likely cause for this behaviour.

suddenly displaced far from the focus towards the respective surface. This suggests that attractive forces were acting on the nanoparticle at pH 3 in close distance to the surface. The measurements also show that both types of surfaces attracted the nanoparticles, which seems to contradict the observed adsorption pattern in Figure 5.7.

The curves of the two surfaces, however, differ nevertheless in their behaviour after the snap-in: In the grooves, the rigid supporting material (glass) caused a steep rise of the curve as the nanoparticle was pressed against it and therefore displaced out of the laser focus, which was moved further downwards through the glass slides. On the polymer brush region, the nanoparticle had the possibility to at least partly enter the soft polymer brush material. The rise of the displacement was therefore slower.

At pH 7 (Figure 5.11b), the clear snap-in is missing for both curves indicating that the attractive forces were weaker. Again, the particles were displace when they were pushed against the surface. This was anticipated, the fact that the approaches towards the different surfaces did not differ, however, was not.

For a more in-depth analysis, the measured displacement data of the approaches were converted into potentials. The trap potential was substracted from the data to give the "net potential" representing only the interactions between nanoparticle and surface. This axial net potential was plotted as a potential landscape (Figure 5.11c–f) against the distance of the laser focus to the surface and the displacement of the nanoparticle out of

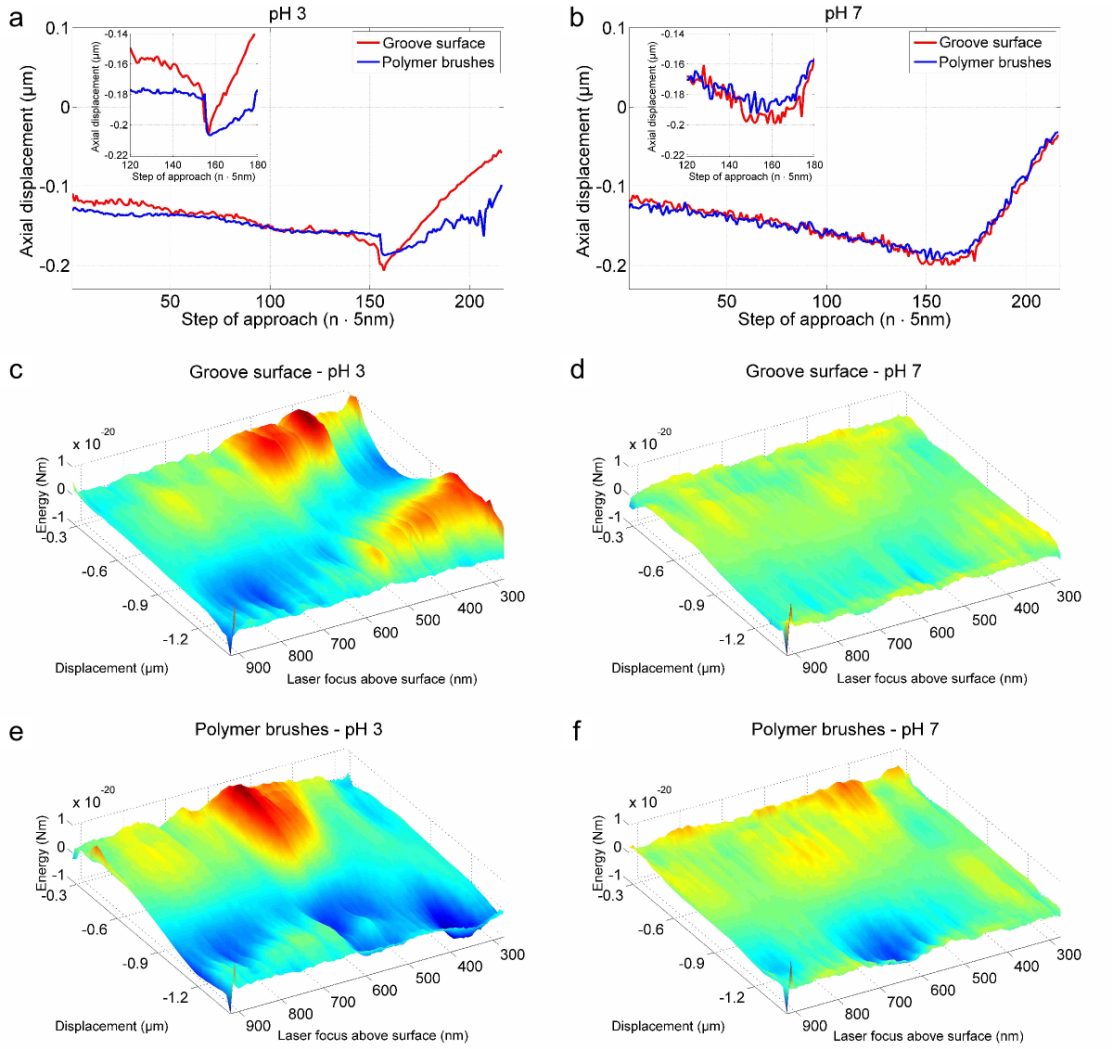

Figure 5.11: Interactions between negatively charged nanoparticles and a patterned PMAA brush surface in dependence on pH (left column pH 3, right column pH 7) as measured with an optical trap. In a and b, the displacement of the nanoparticles out of the laser focus is plotted against the approach of the laser focus to the surface (with the polymer brush areas in blue and the grooves in red). Attracting forces provoke a displacement towards negative values, repulsive forces towards positive values. The insets are close-ups of the respective snap-ins. The potential landscapes in c–f visualise the calculated net potentials for every step of several approaches. The optical trap's potential was substracted, therefore the plots show the influence of the respective surface on the nanoparticle in the trap. Over the distance of the laser focus to the surface and the displacement of the nanoparticles out of the laser focus the potential was plotted. A high potential (yellow to red) means that the probability of a nanoparticles taking up this state is low. The probability is in contrast high for nanoparticles to be located in a potential well (green to blue). Figure published in ref. 180.

the laser focus.

When measuring on groove surfaces at pH 3 (Figure 5.11c), the potential walls were quite steep reflecting forces restricting the nanoparticles movement. Upon approach, the potential well moved from more negative displacements (towards the surface) to more positive displacements (away from the surface). This reflects repulsive forces acting on the nanoparticle after the snap-in.

In contrast, the potential landscape of the measurements on polymer brush surfaces (Figure 5.11e) have a decided minimum at displacements towards the surface even upon close approach to the surface. At the same time, the potential walls are not as steep as over the groove surface reflecting the mobility and lower stiffness of the polymer brush. Therefore, the nanoparticles were drawn towards the PMAA brush surface over the whole approach, whereas they experienced repulsive forces upon closer approach over the groove surface. This reflects the distribution of the nanoparticles on the patterned substrate at pH 3 as seen in Figure 5.7

Looking at the potentials at pH 7 (Figure 5.11d and f) reveals completely different landscapes to the ones at pH 3. The potential walls are lower suggesting fewer spatial constrains. The potential minima run quite similar for groove and polymer brush surfaces upon approach. Only the polymer brush surface shows a pronounced potential well at the snap-in (Figure 5.11f). Overall neither surface seemed to interact strongly with the nanoparticles. Bringing these potentials together with the distribution pattern in Figure 5.7 reveals an apparent contradiction. The measurements with the optical trap did not show attractive forces between the grooves and the nanoparticles, but the nanoparticles seemed to have a decided preference for the grooves at pH 7 (Figure 5.7d).

If no specific forces could be measured with the optical trap, there had to be another effect that controlled the nanoparticle assembly. Lacking any strong interactions, the nanoparticles should have been easily moved and rearranged. It seems probable that a simple mechanical effect like the one discussed for the PSBMA brushes (Section 5.2.1) placed the nanoparticles in the grooves. The PMAA brushes were able to form even higher "walls" around the grooves that the PSBMA brushes. In equilibrium, after 1 h in PBS a height of about 300 nm was measured with an AFM.[173] This height is about double the diameter of the phosphonate nanoparticles and therefore a considerable barrier, which could easily retain the rearranging nanoparticles.

In summary, it was possible to show a switching behaviour of nanoparticle adsorption to the pH-responsive PMAA brushes. At pH 3, the PMAA brush were non-charged and able to bind phosphonate particles, very likely *via* hydrogen bonds. Measurements with the optical trap set-up comfirmed attractive forces acting between negatively charged

nanoparticles and the PMAA brushes. When the surrounding solvent was changed to PBS at pH 7, the nanoparticles rearranged and adsorbed preferrably in the grooves. As no specific forces could be measured with the optical trap, this clear distribution pattern was explained with the mechanical effect of high PMAA "walls" caging the nanoparticles in the grooves.

5.3 Conclusion

It was possible to direct phosphonate nanoparticles selectively to specific areas of a patterned substrate by a systematic choice of functionalisation with polymer brushes. Strong polyelectrolytes served as pH-independent modification, whereas PMAA controlled the nanoparticle adsorption in dependence of the pH. The interacting forces and effects leading to the selective nanoparticle assembly could be examined in more detail by an optical trap set-up. The here described system could find applications in the field of biosensors and lab-on-a-chip techniques.

6 Summary

Two different approaches towards the synthesis of thin polymer films and their applicability as biomaterials, especially as coatings for hard tissue implants, were tested. With SI-ATRP, it was possible to produce a range of surface-tethered polymers, which carried biomimetic functional groups: Sulfonates, amines and carboxylates. Three of the polymer brush coatings consisted of strong polyelectrolytes: the polysulfonate PSPMA, the polysulfobetaine PSBMA and the quaternary polyamine PMETAC. The fourth polymer brush comprised the weak polyelectrolyte PMAA carrying carboxylate groups. Additionally, polymer films of ppMMA with ppH or OTES as an adhesion promoting layer were synthesised by plasma polymerisation.

Micropatterning was achieved in both cases by employing UV-lithography through chrome coated quartz masks with the respective pattern. The polymer brush coatings were patterned before polymerisation by inactivating the surface-bound ATRP initiator in future groove areas. Plasma polymers were first synthesised and subsequently patterned by ablation of the polymer in the irradiated areas.

Synthesis of the polymer brush films proved to be quite elaborate making an industrial usage of this method for the production of implant coatings unlikely. The plasma polymer films were in contrast less chemically defined but the synthesis process seemed easier to scale up and was far less time and work consuming.

Analysis of the polymer brush films with AFM methods showed that these coating were able to swell in an aqueous environment about 2–5 times their dry height. This and the available literature suggest that the polymer brush films were highly hydrated.

The plasma polymers of this work, on the other hand, were less hydrophilic and were therefore not assumed to swell in this extreme way. However, the patterned plasma polymer coatings showed a strong wettability contrast between groove areas and ridges. XPS measurements confirmed that UV-irradiation caused oxidation of the polymer increasing the number of oxygen-bound carbon.

hMSCs and MC3T3-E1 cells were mostly growing in the grooves between the areas with polymer brush coating aligned along the pattern. As there were no signs of decreased viability of the cells, the restriction in cell distribution on patterned substrates

was attributed to the hydration of the polyelectrolytes preventing protein adsorption and cell adhesion. An exception were the positively charged PMETAC films on which cells colonised also the polymer covered areas. This unusual behaviour was ascribed to a favourable protein profile adsorbing to positively charged surfaces and to the small thickness of the polymer brush layer. A drawback was the observed instability of the polymer brush films under cell culture conditions.

MC3T3-E1 cell culture on the plasma polymer surfaces also showed alignment along the pattern and a preference to some degree for either the grooves or the ridges. As these cells are known to prefer hydrophilic over hydrophobic surfaces, a colonisation of the grooves was assumed. On the plasma polymers, viability of the cells was not hampered. In contrast to the polymer brush films, the plasma polymer coatings were stable under cell culture conditions promising good biomaterials properties.

Mineralisation of polymer brush substrates was accomplished in a set-up with an external pump and a mixing chamber under a constant flow of a 5 mM CaP solution. Other mineralisation methods such as immersion in SBF or dip coating in various Ca^{2+}, HPO_4^{2-} or CaP solutions, on the other hand were not successful. The mineral that built during the mineralisation in the mixing chamber reproduced the polymer brush pattern but was not formed specifically on groove or ridge surfaces. TEM and IR analysis suggested that the amorphous CaP phase ACP1 was formed. Immersion in SBF for 7 d caused a phase transformation likely towards a poorly crystalline carbonate containing HA-like phase. Longer immersion in SBF for 21 d lead to delamination of the mineralised polymer films.

When the non-mineralised plasma polymer films were immersed in SBF, no signs of mineralisation could be observed. Mineralisation of the coatings in the mixing chamber, however, following the protocol for the polymer brush mineralisation was successful. Again, the mineralisation was not exclusively on the irradiated or the non-irradiated surfaces and again, ACP1 was formed as evidenced by TEM and IR analysis.

For the polymer brush surfaces, it was additionally shown that they were a versatile tool to selectively deposit polymeric phosphonate functionalised nanoparticles. The constantly charged polymers PSPMA, PSBMA and PMETAC directed phosphonate nanoparticle adsorption independently of the pH. On PSPMA, adsorption was prevented, whereas on patterned SBMA substrates, the nanoparticles were assembled in the grooves. Positively charged PMETAC adsorbed the phosphonate nanoparticles to the brush areas.

The adsorption was also controlled by the pH when patterned PMAA brush surfaces were used. In this case, phosphonate nanoparticles were attracted to the brush when washing steps were carried out at pH 3, or in the grooves when washing at pH 7. This was explained by the protonation state of the polymer brush, which had its isoelectric

point at around pH 3 and was thus protonated at this point. At pH 7, it was completely deprotonated reflected by the zeta potential of around −30 mV.

Thus coating implant material with polymer brushes with these and other functional groups, can help to direct functionalised nanoparticles loaded with pharmaceuticals site-specifically. Another field for applications of these composite surfaces are biosensors, which need certain chemicals, proteins and/or cells to be strictly structured in the micron scale.

7 Experimental*

7.1 Chemicals and Materials

PBS, DMF p.a., SPMA, NaMA, bpy p.a., CuBr and CuCl were obtained from Sigma-Aldrich and used as recieved. METAC was obtained from Sigma-Aldrich and additionally treated with aluminum oxide to remove the inhibitor. SBMA, methanol p.a., $CuBr_2$, $CuCl_2$, H_2SO_4 p.a., H_2O_2 30 % p.a., 3-aminopropyltrimethoxysilane, 2-bromoisobutyryl bromide, Tetrahydrofuran (THF), triethylamine and methyl methacrylate (99 %) were obtained from Merck/VWR. THF was dried over Na before usage. *n*-Heptane (99 %) was obtained from J.T. Baker. Argon (5.0) and hydrogen (3.0) gas bottles were from Linde gas. Microscope glass slides were from Menzel, Germany, and deionised water was obtained using a TKA Smart2Pure Millipore machine.

7.2 Initiator Synthesis, Substrate Cleansing and Coating Procedure

To start the surface initiated polymerisation, the initiator 3-(2-Bromoisobutyramido)-propyl(trimethoxy)silane (see Scheme 2.1 on page 17) was chosen. Three methoxy groups served as linking groups to the glass surfaces by reacting with hydroxyl groups of the surfaces to siloxane linkers. The bromide acts as the ATRP initialising group. The procedure for the initiator's synthesis was adopted from Tugulu *et al.*[56] Briefly,

*Parts of this chapter (text, experimental details and figures) have been published in ref.s 47,48,81,180:
Sabine Letsche, Annina Steinbach, Manuela Pluntke, Othmar Marti, Anita Ignatius, Dirk Volkmer; "Usage of polymer brushes as substrates of bone cells" *Front. Mater. Sci. China*, **2009**, *3*, 132–144,
Annina Steinbach, Andrea Tautzenberger, Anita Ignatius, Manuela Pluntke, Othmar Marti, Dirk Volkmer; "Coatings from micropatterned sulfobetaine polymer brushes as substrates for MC3T3-E1 cells" *J. Mater. Sci. Mater. Med.*, **2012**, *23*, 573–579,
Annina Steinbach, Andrea Tautzenberger, Andreas Schaller, Andreas Kalytta-Mewes, Sebastian Tränkle, Anita Ignatius, Dirk Volkmer; "Plasma-Enhanced Chemical Vapor Deposition of *n*-Heptane and Methyl Methacrylate for Potential Cell Alignment Applications" *Appl. Mater. Interfaces*, **2012**, *4*, 5196–5203 and
Annina Steinbach, Tobias Paust, Manuela Pluntke, Othmar Marti, Dirk Volkmer; "Selective Adsorption of Functionalized Nanoparticles to Patterned Polymer Brush Surfaces and its Probing with an Optical Trap" *ChemPhysChem*, **2013**, *14*, 3523–3531.

3-aminopropyltrimethoxysilane and 2-bromoisobutyryl bromide were allowed to react, stirring for 3 h in anhydrous THF with triethylamine as the base. Triethylammonium bromide was removed and the solvent evaporated. After stirring the oily residue at 50 °C for 6 h, the product was further purified by distillation in a Büchi ball tube destillation oven. All steps were carried out under argon or nitrogen atmosphere. The product was verified by ^{1}H Nuclear Magnetic Resonance (NMR) and stored under nitrogen.

Prior to coating with the initiator, the substrates (*i.e.*, silicon wafers or glass slides) were sonicated in methanol and deionised water for 15 min, cleansed and oxidised with Piranha solution (7:3 mixture of H_2SO_4 and 30 % H_2O_2) at 120 °C for 30 min, rinsed with deionised water, methanol and – in the first experiments – dichloromethane, and finally dried in a stream of argon or nitrogen. The rinsing step with dichloromethane was omitted for later experiments, as there was no perceivable effect of this last step on the substrate.

To tether the initiator to the substrate, the cleansed substrates were immersed in a 10 mM initiator solution in anhydrous toluene under inert gas for 30 min, washed with anhydrous toluene, sonicated for 1 min in dichloromethane and acetone and dried in a stream of argon or nitrogen.

To produce patterned polymer brush substrates, the initiator coated glass slides were patterned at this point of the procedure employing UV-lithography as described in Section 7.5.

7.3 Atom Transfer Radical Polymerisation

For the synthesis of the polyelectrolyte brushes, ATRP was the first choice as outlined in 2.1.1. The polymerisation conditions were modified versions of Tugulu *et al.*[93] for NaMA, of Masci *et al.*[124] for SPMA and of the Huck group for SBMA[49] and METAC.[88,163] They were optimised for a Cu(I)/Cu(II)/bpy catalyst system at room temperature and under nitrogen or argon atmosphere.

7.3.1 Polymerisation of N-(3-Sulfopropyl)-N-methacryloyloxyethyl-N,N-dimethylammonium Betaine

SBMA was polymerised following the protocol of Azzaroni *et al.*[49] The monomer (15 g/ 54 mmol) was dissolved in 50 ml of a 1:4 methanol/water mixture and degassed with at least three freeze-pump-thaw cycles. With adding the catalyst system containing bpy, Cu(II) and Cu(I) ions in a ratio of 25:1:10 (420 mg/2.6 mmol bpy, 15 mg/0.11 mmol

$CuCl_2$ and 106 mg/1.1 mmol CuCl) and immersing the glass substrates in this solution the polymerisation was started and maintained for 2 h. To quench the polymerisation, the reaction solution was exchanged with water, the substrates rinsed with an excess of water and washed at least three times for 2 h with water and PBS, alternately, to remove unbound polymer and remaining catalyst.

7.3.2 Polymerisation of Potassium 3-Sulfopropylmethacrylate

For PSPMA, the protocol of Masci *et al.*[124] was adapted for a surface initiated reaction and optimised to yield thicker brushes.[181] 29.6 g (120 mmol) of SPMA were dissolved in 40 ml of a 1:1 mixture of DMF and deionised water. After three freeze-pump-thaw cycles, 1.25 g (8.0 mmol) of bpy and 215 mg (1.6 mmol) of $CuCl_2$ were added and two more freeze-pump-thaw cycles were conducted. 158 mg (1.6 mmol) CuCl was added to give a molar ratio of 5:1:1 for the catalyst system bpy, $CuCl_2$ and CuCl. The polymerisation was started by immersing the substrates and allowed to continue over night (14 h to 16 h). As described above, the reaction was stopped and the substrates rinsed and washed.

7.3.3 Polymerisation of 2-(Methacryloyloxy)ethyl Trimethylammonium Chloride

The guidelines for the PMETAC polymerisation was the work of Osborne et al.[88] and Zhou et al.[163] The METAC solution was first treated with aluminium oxide to remove the inhibitor and added to methanol to give 72 ml with a 1:1 mixture of the solvents. The monomer solution was degassed by three freeze-pump-thaw cycles, and bpy (886 mg/5.7 mmol) and CuBr (411 mg/2.9 mmol) were added as the catalyst system – in this polymerisation without the inhibitory Cu(II) ions, the molar ratio of METAC:bpy:Cu(I) being 100:4:2. Two further pump-freeze-thaw cycles were carried out and the substrates added to the polymerisation bath. After 24 h, the polymerisation was stopped and the substrates rinsed and washed, as outlined above.

7.3.4 Polymerisation of Sodium Methacrylate

As mentioned above, the procedure of Tugulu et al.[93] for the SI-ATRP of NaMA was the starting point for optimisation and resulted in the following procedure by Letsche:[172] 21.6 g (200 mmol) of NaMA and 780 mg (5 mmol) of bpy were dissolved at 50 °C in 25 ml deionised water. After allowing the solution to cool down to room temperature, the pH was adjusted to pH 9 with a 0.1 M solution of NaOH. After adding 90 mg (0.4 mmol) $CuBr_2$, the solution was degased by three freeze-pump-thaw cycles. The catalytic active

CuBr (287 mg/2 mmol) was added last to finally give a monomer:Cu^{+}:Cu^{2+}:bpy ratio of 200:2:0.4:5. Under inert gas, the solution was added to the substrates and allowed to polymerise for 30 min. Exchanging the polymerisation solution with water quenched the reaction and was followed by vigorous rinsing with water. To remove unbound polymer and remaining catalyst, the substrates were immersed in water at least three times for 2 h.

7.4 Synthesis of Plasma Polymer Coatings

The plasma polymerisation was carried out following a protocol by Andreas Schaller and Andreas Kalytta-Mewes as described in detail in ref. 81. For the coating procedure a Diener femto type I facility with a rectangular stainless steel vacuum chamber (103 mm x 103 mm x 600 mm), a RIE electrode with gas shower and a LFG40 40 kHz generator limited to 300 W was employed.

The first step in the coating procedure was the cleansing of the glass substrates. The cleansing was either achieved by the method described above (see 7.2) in the wet-chemistry approach or by etching the glasses in the plasma chamber in an Ar/H_2 plasma (82 %/18 %) at a pressure of 0.3 mbar for 1 h at 300 W output power. In the wet-chemical approach, a layer of OTES served as adhesive layer. It was applied to the surface by immersing the cleansed glass substrates in a 10 mM OTES solution in ethanol for 30 min. To remove excess OTES, the solution was exchanged for ethanol and the substrates sonicated for 15 min. The last step was repeated before the substrates were dried in a stream of nitrogen.

As an alternative all-plasma method to convey adhesiveness, heptane was plasma polymerised to give a PE-like layer (termed ppH) on the plasma-etched substrates. Here, not having to transfer every single substrate from the wet-chemical treatment to the plasma device is an obvious advantage, especially for a possible industrial application, where time and resources are scarce. To yield this ppH layer, *n*-heptane was transferred into the gas phase with an evaporator at 30 °C and fed into the vacuum chamber under feedback control to give an average pressure of 0.5 mbar. The reaction proceeded for 1 h at 90 W output power in a pulsed plasma. The pulsed mode was chosen for the plasma polymerisation steps to preserve the functional groups of the monomers for the polymer as possible and minimise the radical density. Pressure and output power had to be optimised to ensure an acceptable deposition rate but nevertheless yield a possibly undamaged polymer structure.

A top layer coating (ppMMA) was made by plasma polymerising MMA for 1 h at

0.5 mbar, 150 W output power and pulsed plasma. Again, the pressure was regulated by the evaporated MMA, which was vaporised at 30 °C as the heptane above.

7.5 Photolithography

For a patterned polymer brush coating, initiator-coated substrates were irradiated by deep UV-light using a photomask prior to polymerisation.[172] To pattern the plasma polymer films, the irradiation took place after the coating procedure in the plasma. The chrome-coated quartz masks were patterned with a variety of geometrical structures of different sizes in the micrometre range by Kohn, Kuster and Men of the Institute of Electron Devices and Circuits at the University of Ulm. Examples of the patterns are given schematically in Figure 7.1.

For irradiation, a Hamamatsu LC8 containing a 200 W 250 nm enhanced mercury lamp was employed.[380] Connected to the LC8 *via* a synthetic silica light guide (A10014-50-0110; with a 5 mm diameter and 1 m length), a E5147-06 beam distributor widened the beam to a square. The coated substrates were placed under the distributor at 17.5 cm distance, resulting in a beam widened to 4.5 cm. The manufacturer specifies the UV-light intensity at 365 nm at 4500 mW/cm^2 for the non-250 nm enhanced lamp measured at 10 mm distance from a different beam distributor (E5147-04) connected to a light guide with a smaller 3.5 mm diameter (A10014-35-0110).[380] In the same distance, but with our set-up, we measured with an Ophir power metre connected to an LP1-V1 absorber with a wavelength range of 250 nm to 2200 nm an integrated irradiance of 328 mW/cm^2 and an absolute value of 1.61 W. Measuring thus the intensity at the distance that the samples had to the beam distributor, the irradiance was 94 mW/cm^2 and 1.49 W, respectively. The lower absolute power measured at the greater distance is probably caused by the widening of the beam. Here, the square beam was too broad to hit the round absorber completely, which caused a small part of the energy not to be measured, but which was not relevant for the relative intensity that the samples received.

During the 20 min exposure time, direct contact between photomask and substrate was ensured. Exposure to deep UV-light resulted in the decomposition of the initiator molecule, removing the bromide group and obviating the polymerisation in the irradiated region. The non-exposed areas could subsequently be polymerised with different electrolyte monomers (NaMA, SPMA, SBMA and METAC) as described Section 7.3.

To pattern the plasma polymer coatings, again the Hamamatsu LC8 was used in a straightforward lithography procedure.[39] The plasma polymer coated substrates were placed under a photomask as outlined above and UV-irradiated for 20 min or for the

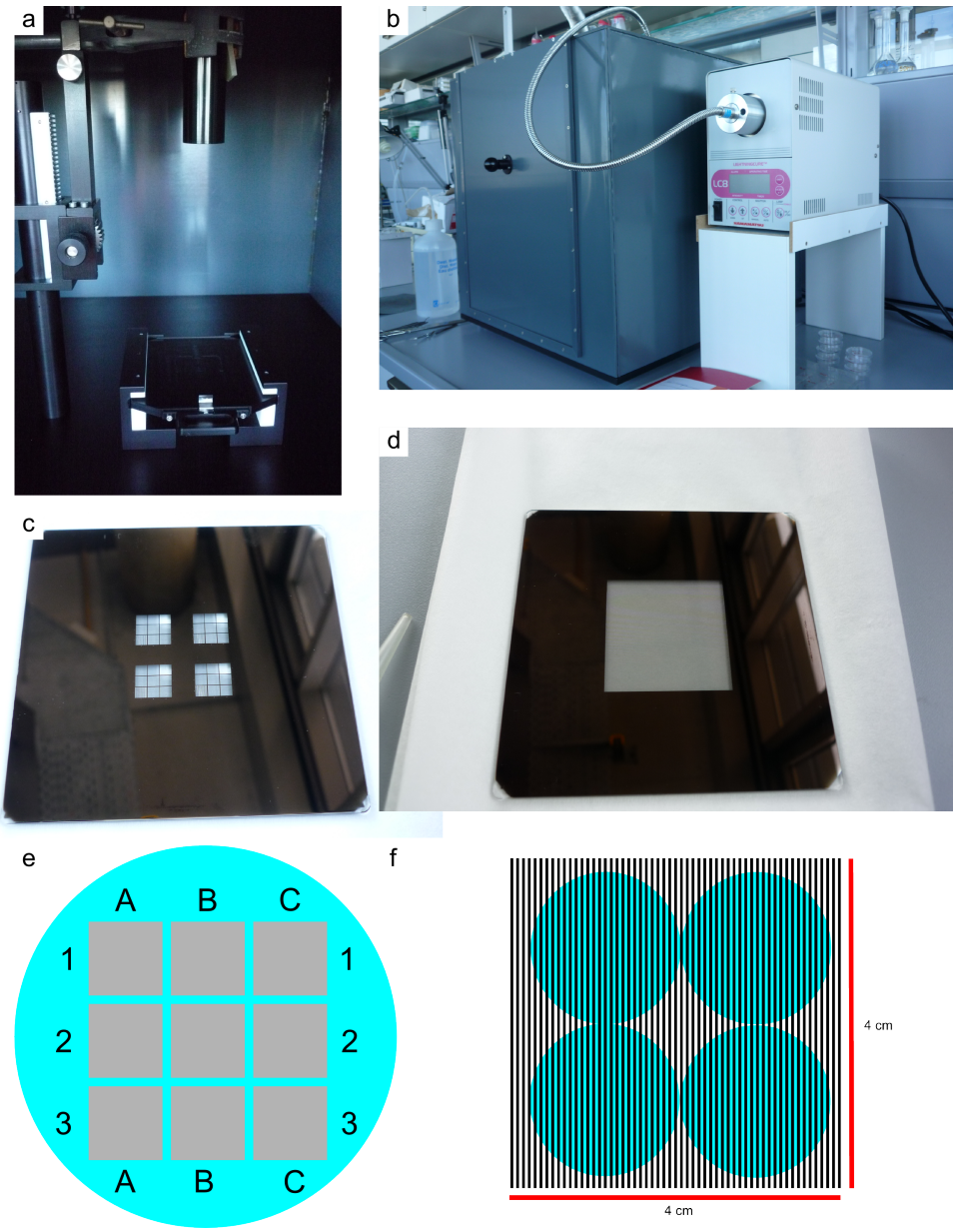

Figure 7.1: UV-lithography set-up, a: View inside the irradiation box, beam distributor placed at 12 cm distance to the samples. Samples were fixed by the sample holder, which also held the mask in the right position and in close contact to the samples; b: General view showing the grey irradiation box (left) and the Hamamatsu LC8 (right) connected by the light guide; c and d: Chrome coated quartz masks that enabled irradiation of four glass slides with a 18 mm diameter at the same time, the mask in c produced samples with nine fields with different pattern sizes shown schematically in e, whereas the mask in d produced samples continously patterned with one sized features, shown schematically in f; e: Scheme of the pattern in c, the nine fields produced patterns of the following feature sizes: A1: completely irradiated, B1: 1.25 µm, C1: 2.5 µm, A2: 5 µm, B2: 10 µm, C2: 20 µm, A3: 40 µm, B3: 80 µm, C3: 160 µm.

period described in the respective experiment. To remove degraded polymer from the irradiated regions, the samples were rinsed with deionised water and dried under a stream of nitrogen.

7.6 Mineralisation of Polymer Brush and Plasma Polymer Coatings

7.6.1 Dip Coating Mineralisation

Different procedures were tested for their ability to mineralise polymer brushes. Not many trials were successful, so the exact reaction conditions are given with the positive results in Section 4.2.1.

First, the plain approach of immersing the substrates in a CaP solution made of $CaCl_2$ and Na_2HPO_4 was tried for 0.5 mM, 5 mM and 10 mM solutions. The immersion time ranged from 1.5 h to 7 d with changing the solution at least every second day. This simple method did not mineralise the different polymer brushes.

The second method consisted of one to several cycles of immersion in $CaCl_2$ and Na_2HPO_4 solutions. To begin with, the polymer brush coated glasses were bathed in a 0.1 mM to 100 mM Ca^{2+} solution for 5 min to 5 d. After a rinsing step with deionised water, which was omitted in some experiments, the substrates were submerged in a 0.5 mM to 100 mM HPO_4^{2-} solution for 5 min to 7 d. In some cases, another rinsing step ended the procedure. In most experiments, further dip coating steps in either only HPO_4^{2-} or in Ca^{2+} and HPO_4^{2-} solutions with optional rinsing between the immersion steps.

A third approach was the dropwise addition of a HPO_4^{2-} solution to a Ca^{2+} solution, in which the coated glasses were immersed. For these experiments, 0.5 mM to 100 mM solutions of $CaCl_2$ and Na_2HPO_4 or K_2HPO_4 or $Ca(NO_3)_2$ and $(NH_4)_3PO_4$ were used. The immersion time in the Ca^{2+} solution at the beginning was supposed to serve as a doping period, to impregnate the Ca^{2+} binding sites. As soon as the addition of the HPO_4^{2-} solution started, the mineralisation bath was stirred to ensure a homogeneous distribution of the ions.

7.6.2 Mineralisation in a Mixing Chamber with an External Pump

A Harvard PHD 2000 syringe pump with gas tight 25 ml Hamilton syringes was used to pump a Ca^{2+} and a HPO_4^{2-} solution through a chamber in which the sample was placed upside down. The two solutions mixed shortly before entering the chamber (see Figure 7.2). After passing through the chamber, the liquid was drained *via* a tube (as

indicated in Figure 7.2) connected to a washing flask linked to a vacuum pump. The upside down position of the glass was meant to ensure that mineralisation was not simply a case of agglomerates build in solution falling down onto the sample unspecifically.

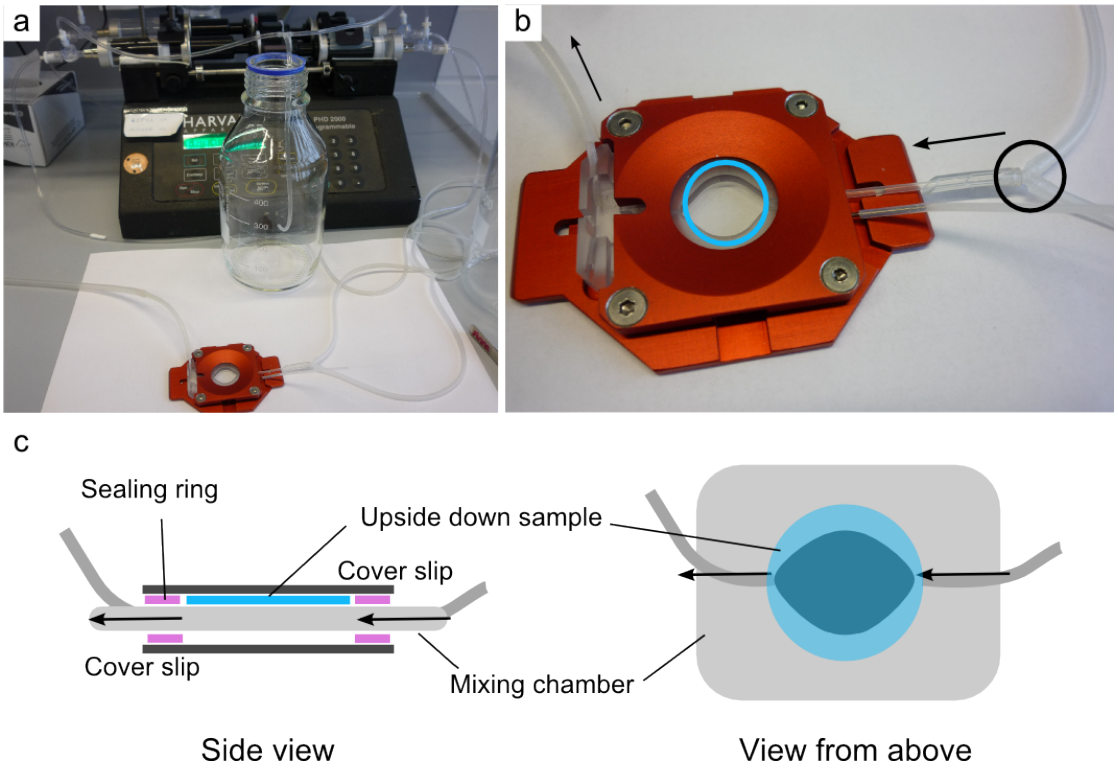

Figure 7.2: Mixing chamber and pump set-up used to mineralise polymer brush or plasma polymer coated glass slides. Overview of the mineralisation assembly with the Harvard pump in the background and the red mixing chamber (a). The $CaCl_2$ and Na_2HPO_4 solutions meet at the point indicated by the black circle in b. The flow direction of the solutions is indicated by arrows and the position of the sample by the blue circle. The schematic (c) shows the cross-section sideview (left) and top-down view (right) to visualise the assembly of the mixing chamber.

The solutions were buffered at pH 7.4 with a 50 mM TRIS-HCl buffer. Concentrations from 1 mM to 60 mM with flow rates from 0.2 ml/min to 4 ml/min and immersion periods from 45 min to 6 h were tried. As a short remark, the concentrations given here are the ones of the solutions *before* mixing. As the solutions mix with a ratio of 1:1, the volume is doubled and thus, the concentrations of the individual ions is halved. The flow rates specified here, on the other hand, are those that could be actually measured in the chamber, so they are the flow rates of both solutions added up.

As Ca^{2+} source, $CaCl_2$ solutions were used. For HPO_4^{2-} and PO_4^{3-} ions containing solutions, K_3PO_4, K_2HPO_4 or Na_2HPO_4 were employed. Prior to some experiments, the

samples were immersed in a 100 µM $CaCl_2$ solution to dope the polymer brushes with the cations and thus facilitate mineralisation. The very low concentration was chosen to avoid the brushes' collapsing.[123] Nevertheless, these pre-treated samples did not differ from those untreated.

The best mineralisation results were achieved by mineralising with 10 mM solutions (resulting in 5 mM CaP) for 90 min or with 2.5 mM solutions for 180 min and a flow rate between 0.6 ml/min and 1.0 ml/min. Thus, to compare different surfaces respecting their mineralisation behaviour without augmented time and effort, the higher concentration and a flow rate of 0.8 ml/min was chosen with a mineralisation period of 1.5 h.

7.6.3 Immersion in Simulated Body Fluid

SBF was used to evaluate preliminarily the bioactivity of the synthesised coatings as described in the pioneer work of Kokubo *et al.*[255] This method is generally used and described for several versions and modifications.[60,64,66,73,256–262] It also served as a test for the different coatings' stability in ion solutions, as dilamination was observed especially in solutions with bivalent ions. Therefore, SBF acted as a pre-screening before the samples were passed to the cell culture. Shortly, in a 50 mM TRIS-HCl buffer (pH 7.4), the salts listed in Table 7.1 were solved to give a supersaturated CaP solution in respect to HA. The SBF was autoclaved to avoid bacterial contamination, which could distort mineralisation results. For the same reason, the substrates and vessels were always treated with 70 % ethanol prior to the biomineralisation experiments and sterile conditions were generally sought.

Table 7.1: Salts and their concentrations used to create the ion composition of SBF.

	Ions and their concentrations [mM]							
	Na^+	K^+	Ca^{2+}	Mg^{2+}	HCO_3^-	Cl^-	HPO_4^{2-}	SO_4^{2-}
Salt	142	5.0	2.5	1.5	4.2	148	1.0	0.5
NaCl	137					137		
$NaHCO_3$	4.2				4.2			
KCl		3.0				3.0		
K_2HPO_4		2.0					1.0	
$MgCl_2$				1.5		3.0		
$CaCl_2$			2.5			5.0		
Na_2SO_4	1.0							0.5

The usual *in vitro* bioactivity test was run for 1, 2 or 3 weeks at 37 °C in tightly closed containers with the samples standing in an upright position. In the process, 3 glasses with a 18 mm diameter shared 15 ml SBF solution.

7.7 Immersion of Polymer Brushes in a Nanoparticle Dispersion

The phosphonate functionalised polystyrene nanoparticles loaded with the fluorescence dye *N*-(2,6-Diisopropylphenyl)Perylene-3,4-Dicarbonacidimid (PMI) were obtained from the Landfester group (Max Planck Institute for Polymer Science in Mainz). The assembly *via* free radical polymerisation in miniemulsion was published in ref. 367. The main polymer of the nanoparticles was PS, which had been copolymerised with 10 % Vinylphosphonic Acid (VPA), leading to copolymer nanoparticles, in which the phosphonate groups arranged at the particles' surface. The added fluorescence dye served as a label for a quick analysis of the distribution of the nanoparticles attaching to the structured substrates. Figure 7.3 shows a schematic of the fluorescence loaded copolymer nanoparticles.

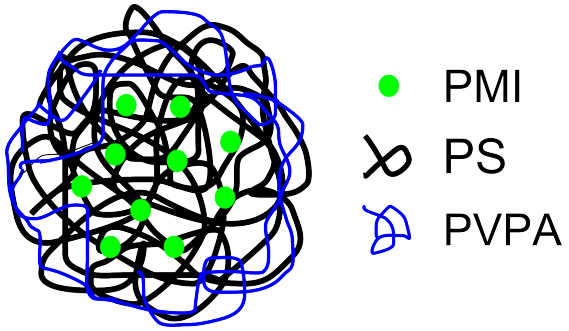

Figure 7.3: Schematic cross section of the nanoparticles showing the phosphonated part of the polymer arranging on the particle surface towards the hydrophilic solvent, in the hydrophobic inner part, consisting mainly of PS, the fluorescence dye PMI was located.

To yield a monolayer of the nanoparticles with a clear distribution pattern, the solids content of the dispersion had to be adjusted. Based on the original solids content of 112 mg/ml different dilutions were evaluated. A dilution to a solids content of 1 mg/ml was found to generate the desired monolayer with a clear adsorption pattern on the polymer brush surfaces. Higher solids contents resulted in multiple layers of nanoparticles stacking over each other (Figure 5.4 on page 125). However, the problems with aggregation of the nanoparticles other groups reported[381] were not observed.

After testing adsorption procedures with the samples lying horizontally unmoved, sonicated, or on a orbital shaker, two problems arose that had to be addressed. First, due to the high solids content at that time a thick, nearly armour-like layer of nanoparticles was build, which was only loosely bound. The distribution was additionally unspecific, probably owing to the nanoparticles sinking to the ground of the vessel in a non-specific

way. The second issue emerging was the colloid often being in contact with both sides of the substrates. The resulting fluorescence on both sides of the sample hampered the analysis of the coated substrates in the fluorescence microscope. To facilitate the analysis and coat the substrate only from one side and enable at the same time a procedure with the samples standing upright, a new container was designed. These vessels were custom-made by the Ulm University's workshop and can be seen in Figure 7.4. In these containers, the nanoparticle bath had a small volume, so colloid consumption was held low.

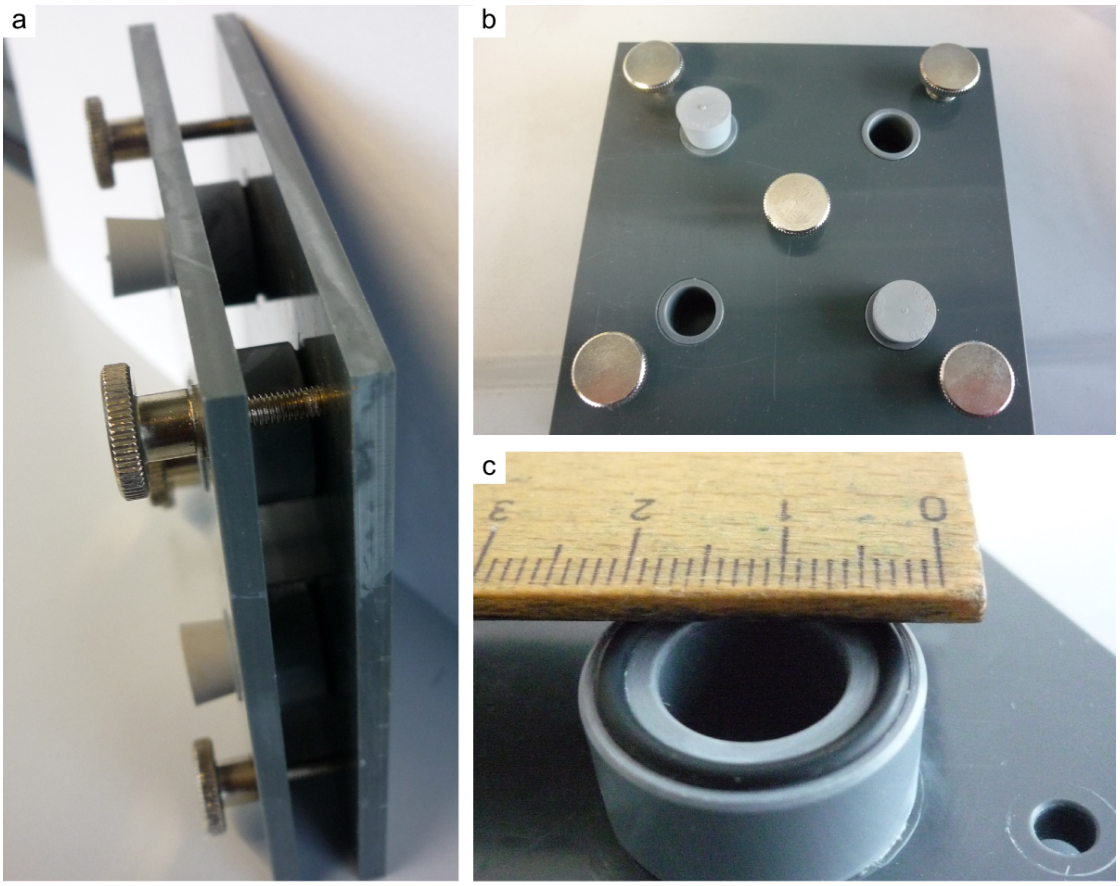

Figure 7.4: Custom-made container that was used to coat the polymer brush substrates with fluorescent nanoparticles and that made it possible to coat only one side of the substrate while the substrate was standing up-right. Side and front view (a and b) of the custom-made immersion device with the cylindrical miniemulsion bath, which can be plugged with rubber bungs. Five screws hold the back plate and the cover plate with the cylinders in place with an even pressure. Onto the back plate up to four substrates can be placed. At the meeting faces rubber gaskets seal the vessel (c).

To adjust the pH of the solution, hydrochloric acid was added until a pH of 3 was

achieved. Initially, a citric acid buffer was used to have a good control over the pH as the essential parameter and limit its fluctuations. Unfortunately, adsorption of the nanoparticles was poor under these conditions, so the buffer was replaced by diluted HCl.

The immersion time was optimised to allow for interaction between the polymer brushes and the nanoparticles, but avoid too much time being consumed or the solutions drying out.

For the final procedure to adsorb the nanoparticles to the patterned polymer brush coating, the substrates were immersed in the diluted colloid for 2 h for PMAA and 6 h for PSPMA, PSBMA and PMETAC. After immersion, the substrates were agitated shortly either in PBS for pH 7.4 or in diluted HCl (pH 3.0) and were bathed in the same solvent, stirring constantly over night.

7.8 Analytical Methods

7.8.1 Light Microscopy

The obtained coatings were always analysed optically for their surface morphology and successful patterning by employing the DIC mode of a Olympus IX70 microscope. This method is applicable to the low-contrast samples, as it visualises the material differences by converting differences in the optical path into contrast. The light micrographs of the mineralised samples were partly acquired in this mode but also in the bright field mode.

7.8.2 Fluorescence Microscopy

The above mentioned Olympus IX70 was additionally equipped with an Abrio fluorescence system. Fluorescence microscopy was used mainly as a fast and simple method to examine the adsorption pattern of the nanoparticles. As the fluorescence dye PMI with an excitation wavelength of 488 nm had been incorporated into these nanoparticles, they were visible, when a excitation filter at 470 nm to 490 nm was employed.

7.8.3 Height Profile Measurement

To measure the height of the plasma polymer pattern profile, a Bruker Dektak 8 profiler was employed. Height values are always given as the mean value with standard deviation and are based on 15 steps measured at three different spots on a sample.

7.8.4 Atomic Force Microscopy

The patterned samples were examined more closely with an Agilent 5500 Scanning Probe Microscope with a large multipurpose closed-loop scanner. Dry samples were measured for their surface morphology, pattern height and mechanical properties in the intermittent contact mode with a silicon cantilever (42 N/m spring constant; 7 nm to 10 nm tip radius). Swollen brushes in water or other solutions, on the other hand, were soft and deformable. Thus, very soft SiN-cantilevers (0.32 N/m spring constant) and tips with a large diameter (SiO_2 spheres with a 1 µm diameter) were necessary. To compare the height profiles in air with the ones in water, the brushes were scanned in contact mode with a force of 8 nN. For the swelling process to be in equilibrium during measurement, the samples were incubated in water for 20 min prior to scanning them. More details are given in ref. 47,48,173.

7.8.5 Scanning Electron Microscopy

For a detailed analysis of the nanoparticles' distribution on patterned polymer brushes, a Hitachi S-5200 High Resolution Scanning Electron Microscope (HR-SEM) was employed. The glass slides were cut to fit the sample holder, fixed to the holder and sputtered with a 4 nm platinum layer. Usually, the samples were examined at an acceleration voltage of 10 V.

The mineralisation results were observed in a Zeiss DSM 962, or in a Philips XL30 ESEM FEG Environmental Scanning Electron Microscopy (ESEM). Whereas the ESEM samples could be examined without additional treatment after gluing them on the holder, the samples for the Zeiss DSM 962 were sputtered with carbon for conductivity before analysis. Both instruments were equipped with a EDX detector, which data were evaluated with the EDAX Genesis software.

7.8.6 Transmission Electron Microscopy

To ascertain the mineral phase of the mineralisation experiments, the coatings were scraped off and dispensed in ethanol. After sonication, carbon coated TEM grids were agitated in the dispersion to confer the mineral phase. The dried samples were analysed with a JEOL JEM 2100F with a field emission gun as electron source, a accelerating voltage of 200 kV and a GATAN imaging filter with a CCD camera. Data sampled with an EDX detector were again evaluated with the EDAX Genesis software.

7.8.7 Infrared Spectroscopy

ATR-IR measurements were conducted using an Equinox 55 FT-IR-spectrometer (Bruker, Germany). For the measurements of the plasma polymer coatings, the samples were simply placed onto the sample holder without further preparation. To measure the CaP coatings after mineralisation and immersion in SBF, the coatings were scraped off, to prevent the SiO_2 signal to superimpose the PO_4^{3-} vibrations. The measured range was $400\,cm^{-1}$ to $4000\,cm^{-1}$ with a step width of $4\,cm^{-1}$, each measurement done with 64 scans.

7.8.8 X-Ray Photoelectron Spectroscopy

For XPS measurements, an Omicron system with an Al Kα X-ray source was employed. Data was analysed and fitted with pseudo-Voigt profiles using CasaXPS software or Origin 6.1 software. In case of the plasma polymer films, HOPG served as a conductive substrate. The initiator SAM was analysed on a Si surface.

7.8.9 Inductively Coupled Plasma Optical Emission Spectrometry

For ICP-OES measurements, a Varian Vista MPX Simultanous Spectrometer was employed by Mohs of the Chair for Chemical Physics and Materials Science, Augsburg University.

7.8.10 Optical Trap

Measurements of the interaction between nanoparticles and polymer brushes were conducted by Dr. Tobias Paust of the Institute of Experimental Physics, Ulm.[382] Details of the measurements and the set-up are given in ref.s 180,382.

7.8.11 Streaming Potential

The streaming potential was measured with an electrical analyzer (Anton Paar GmbH, Graz, Austria) by the Bellmann group, Leibniz-Institute for Polymer Research, Dresden.[383]

For the titration HCl and KOH in 10^{-3} M KCl solution were used at a flow rate of 150 ml/min.

7.8.12 Zeta Potential Titration

The ζ-potential of the PS nanoparticles used in the experiments with the laser trap was measured in a Zetasizer Nano set-up (Malvern) by Oliver Wiltschka, Institute of

Inorganic Chemistry II, Ulm. Measured were the particle size and the ζ-potential with a wavelength of 633 nm at an angle of 173°.

7.9 Cell Culture

Cell culture experiments were conducted in the Centre of Musculoskeletal Research, Ulm, mainly by Dr. Andrea Tautzenberger as described in detail in ref.s 47,48,81,181,267. Shortly, the hMSCs were obtained from the proximal tibia of two different healthy donors. Alternatively, MC3T3-E1 cells were used. Usually, the cells were cultivated at 8.5 % CO_2, 37 °C and 95 % humidity in expansion medium consisting of Dulbecco's Modified Eagle Medium (Biochrom) with 10 % Fetal Calf Serum (FCS) (BioWhittaker Cambrex), 1 % L-glutamine, 1 % penicillin/streptomycine and 0.5 % fungizon. At 80 % confluence the cells were passaged by 0.05 % trypsin/0.02 % EDTA treatment. For the biocompatibility experiments passage 2–4 cells were used at a density of 10 000 or 20 000 cells cm^{-2} and seeded on the different coated glass substrates in 12-well plates. Prior to experiments, all samples were sterilised with 70 % ethanol and dried overnight in the sterile flowbox. A detailed description of the quantitative RT-PCR experiments and SEM preparation is given in ref.s 48,81

8 Bibliography

[1] H. F. Hildebrand, Keynote Lecture, **2009**, Interface Biology of Implants, Symposium in Warnemünde.

[2] A. A. Campbell, G. E. Fryxell, J. C. Linehan, G. L. Graff, *J. Biomed. Mater. Res.* **1996**, *32*, 111–118.

[3] D. Williams, *J. Biomed. Eng.* **1989**, *11*, 185–191.

[4] M. Edgerton, M. J. Levine, *J. Prosthet. Dent.* **1993**, *69*, 406–415.

[5] T. J. Webster, E. S. Ahn, *Adv. Biochem. Engin./Biotechnol.* **2006**, *103*, 275–308.

[6] J. L. Arias, M. S. Fernández, *Chem. Rev.* **2008**, *108*, 4475–4482.

[7] S. Weiner, H. Wagner, *Annu. Rev. Mater. Sci.* **1998**, *28*, 271–298.

[8] A. Trüssel, R. Müler, D. Webster, *Ann. Biomed. Eng.* **2012**, *40*, 2475–2487.

[9] A. L. Boskey, R. Roy, *Chem. Rev.* **2008**, *108*, 4716–4733.

[10] United States Bone and Joint Decade: The Burden of Musculoskeletal Diseases in the United States, American Academy of Orthopaedic Surgeons, **2008**.

[11] S. G. Steinemann, *Periodontology* **1998**, *17*, 7–21.

[12] B. D. Ratner, *J. Mol. Recognit.* **1996**, *9*, 617–625.

[13] K. James, H. Levene, J. R. Parson, J. Kohn, *Biomaterials* **1999**, *20*, 2203–2212.

[14] F. Zhang, Z. Shi, P. Chua, E. Kang, K. Neoh, *Ind. Eng. Chem. Res.* **2007**, *46*, 9077–9086.

[15] K. Anselme, *Biomaterials* **2000**, *21*, 667–681.

[16] P. Layrolle, G. Daculsi, „Physicochemistry of Apatite and Its Related Calcium Phosphates“ in *Thin Calcium Phosphate Coatings for Medical Implants* (Hrsg.: B. León, J. A. Jansen), Springer Science+Business Media, **2009**, Kapitel 2, S. 9–24.

[17] W. Bonfield, *J. Biomed. Eng.* **1988**, *10*, 522–526.

[18] K. J. Burg, S. Porter, J. F. Kellam, *Biomaterials* **2000**, *21*, 2347–2359.

[19] T. Albrektsson, C. Johansson, *Eur. Spine J.* **2001**, *10*, S96–S101.

[20] M. R. Urist, B. F. Silverman, K. Büring, F. L. Dubuc, J. M. Rosenberg, *Clin. Orthop. Relat. Res.* **1967**, *53*, 243–283.

[21] J. A. Jansen, B. León, „Introduction“ in *Thin Calcium Phosphate Coatings for Medical Implants* (Hrsg.: B. León, J. A. Jansen), Springer Science+Business Media, **2009**, Kapitel 1, S. 1–8.

[22] S. V. Dorozhkin, M. Epple, *Angew. Chem. Int. Ed.* **2002**, *41*, 3130–3146.

[23] L. Liu, L. Zhang, B. Ren, F. Wang, Q. Zhang, *Artif. Cell Blood Sub.* **2003**, *31*, 435–448.

[24] E. K. Yim, K. W. Leong, *Nanomed. Nanotech. Biol. Med.* **2005**, *1*, 10–21.

[25] S. Goodman, P. Sims, R. Albrecht, *Biomaterials* **1996**, *17*, 2087–2095.

[26] S. Britland, H. Morgan, B. Wojiak-Stodart, M. Riehle, A. Curtis, C. Wilkinson, *Exp. Cell Res.* **1996**, *228*, 313–325.

[27] S. Faghihi, A. Zhilyaev, J. Szpunar, F. Azari, H. Vali, M. Tabrizian, *Adv. Mater.* **2007**, *19*, 1069–1073.

[28] H. Yoshimoto, Y. Shin, H. Terai, J. Vacanti, *Biomaterials* **2003**, *24*, 2077–2082.

[29] H.-J. Jin, J. Chen, V. Karageorgiou, G. H. Altman, D. L. Kaplan, *Biomaterials* **2004**, *25*, 1039–1047.

[30] S. Lossdörfer, Z. Schwartz, L. Wang, C. Lohmann, J. Turner, M. Wieland, D. Cochran, B. Boyan, *J. Biomed. Mater. Res. A* **2004**, *70A*, 361–369.

[31] O. Zinger, G. Zhao, Z. Schwartz, J. Simpson, M. Wieland, B. B. D. Landolt, *Biomaterials* **2005**, *26*, 1837–1847.

[32] D. Buser, R. Schenk, S. Steinemann, J. Fiorellini, C. Fox, H. Stich, *J. Biomed. Mater. Res.* **1991**, *25*, 889–902.

[33] B. Boyan, S. Lössdörfer, L. Wang, G. Zhao, C. Lohmann, D. Cochran, Z. Schwartz, *Eur. Cells Mater.* **2003**, *6*, 22–27.

[34] K. Anselme, M. Bigerelle, B. Noel, E. Dufresne, D. Judas, A. Iost, P. Hardouin, *J. Biomed. Mater. Res.* **2000**, *49*, 155–166.

[35] M. Lampin, R. Warocquier-Clerout, C. Legris, M. Degrange, M. Sigot-Luizard, *J. Biomed. Mater. Res.* **1997**, *36*, 99–108.

[36] P. Zapata, J. Su, A. J. García, J. C. Meredith, *Biomacromolecules* **2007**, *8*, 1907–1917.

[37] K.-W. Lee, S. Wang, M. J. Yaszemski, L. Lu, *Biomaterials* **2008**, *29*, 2839–2848.

[38] X. Walboomers, H. Croes, L. Ginsel, J. Jansen, *J. Biomed. Mater. Res.* **1999**, *47*, 204–212.

[39] L. Ploux, K. Anselme, A. Dirani, A. Ponche, O. Soppera, V. Roucoules, *Langmuir* **2009**, *25*, 8161–8169.

[40] E. S. Darley, A. P. MacGowan, *J. Antimicrob. Chemother.* **2004**, *53*, 928–935.

[41] A. A. Campbell, L. Song, X. S. Li, B. J. Nelson, C. Bottoni, D. E. Brooks, E. S. DeJong, *J. Biomed. Mater. Res.* **2000**, *53*, 400–407.

[42] J. F. Barrett, *Expert Opin. Ther. Targets* **2004**, *8*, 515–519.

[43] R. Iwata, P. Suk-In, V. P. Hoven, A. Takahara, K. Akiyoshi, Y. Iwasaki, *Biomacromolecules* **2004**, *5*, 2308–2314.

[44] R. R. Bhat, M. R. Tomlinson, J. Genzer, *J. Polym. Sci. Part B: Polym. Phys.* **2005**, *43*, 3384–3394.

[45] N. Singh, X. Cui, T. Boland, S. M. Husson, *Biomaterials* **2007**, *28*, 763–771.

[46] M. R. Tomlinson, R. R. Bhat, J. Genzer, *Polym. Preprints* **2005**, *46*, 44–45.

[47] S. A. Letsche, A. M. Steinbach, M. Pluntke, O. Marti, A. Ignatius, D. Volkmer, *Front. Mater. Sci. China* **2009**, *3*, 132–144.

[48] A. M. Steinbach, A. Tautzenberger, A. Ignatius, M. Pluntke, O. Marti, D. Volkmer, *J. Mater. Sci. Mater. Med.* **2012**, *23*, 573–579.

[49] O. Azzaroni, A. A. Brown, W. T. Huck, *Angew. Chem. Int. Ed.* **2006**, *45*, 1770–1774.

[50] Y. Chang, S. Chen, Z. Zhang, S. Jiang, *Langmuir* **2006**, *22*, 2222–2226.

[51] G. Cheng, Z. Zhang, S. Chen, J. D. Bryers, S. Jiang, *Biomaterials* **2007**, *28*, 4192–4199.

[52] A. Halperin, *Langmuir* **1999**, *15*, 2525–2533.

[53] C. de las Heras Alarcón, T. Farhan, V. L. Osborne, W. T. Huck, C. Alexander, *J. Mater. Chem.* **2005**, *15*, 2089–2094.

[54] A. Mizutani, A. Kikuchi, M. Yamato, H. Kanazawa, T. Okano, *Biomaterials* **2008**, *29*, 2073–2081.

[55] N. Singh, S. M. Husson, *Langmuir* **2006**, *22*, 8443–8451.

[56] S. Tugulu, A. Arnold, I. Sielaff, K. Johnsson, H.-A. Klok, *Biomacromolecules* **2005**, *6*, 1602–1607.

[57] B. P. Harris, J. K. Kutty, E. W. Fritz, C. K. Webb, K. J. Burg, A. T. Metters, *Langmuir* **2006**, *22*, 4467–4471.

[58] J. E. Raynor, J. R. Capadona, D. M. Collard, T. A. Petrie, A. J. García, *Biointerphases* **2009**, *4*, FA3–FA16.

[59] N. Costa, P. Maquis, *Med. Eng. Phys.* **1998**, *20*, 602–606.

[60] S. C. Leeuwenburgh, J. G. Wolke, M. C. Siebers, J. Schoonman, J. A. Jansen, „Electrosprayed Calcium Phosphate Coating for Biomedical Purposes“ in *Thin Calcium Phosphate Coatings for Medical Implants* (Hrsg.: B. León, J. A. Jansen), Springer Science+Business Media, **2009**, Kapitel 10, S. 263–300.

[61] B. León, „Pulsed Laser Deposition of Thin Calcium Phosphate Coatings“ in *Thin Calcium Phosphate Coatings for Medical Implants* (Hrsg.: B. León, J. A. Jansen), Springer Science+Business Media, **2009**, Kapitel 5, S. 101–156.

[62] B. León, J. A. Jansen, „Prospects for Future Applications“ in *Thin Calcium Phosphate Coatings for Medical Implants* (Hrsg.: B. León, J. A. Jansen), Springer Science+Business Media, **2009**, Kapitel 12, S. 315–316.

[63] R. Whitehead, W. Lacefield, L. Lucas, *J. Biomed. Mater. Res.* **1993**, *27*, 1501–1507.

[64] Q. Liu, J. Ding, F. K. Mante, S. L. Wunder, G. R. Baran, *Biomaterials* **2002**, *23*, 3103–3111.

[65] S. Rößler, A. Sewing, M. Stölzel, R. Born, D. Scharnweber, M. Dard, H. Worch, *J. Biomed. Mater. Res. A* **2002**, *64A*, 655–663.

[66] E. Thian, J. Huang, S. Best, Z. Barber, W. Bonfield, *J. Biomed. Mater. Res. Part B: Appl. Biomater.* **2006**, *76B*, 326–333.

[67] D. Scharnweber, S. Bierbaum, „Electrochemical Assisted Deposition of Thin CaP Coatings“ in *Thin Calcium Phosphate Coatings for Medical Implants* (Hrsg.: B. León, J. A. Jansen), Springer Science+Business Media, **2009**, Kapitel 9, S. 215–262.

[68] J. L. Ong, Y. Yang, S. Oh, M. Appleford, W. Chen, Y. Liu, K.-H. Kim, S. Park, J. Bumgardner, W. Haggard, C. M. Agrawal, D. L. Carner, N. Oh, „Calcium Phosphate Coating Produced by a Sputter Deposition Process“ in *Thin Calcium Phosphate Coatings for Medical Implants* (Hrsg.: B. León, J. A. Jansen), Springer Science+Business Media, **2009**, Kapitel 7, S. 175–198.

[69] M. Yoshinari, „Ion Beam Techniques for Thin Calcium Phosphate Coating Production“ in *Thin Calcium Phosphate Coatings for Medical Implants* (Hrsg.: B. León, J. A. Jansen), Springer Science+Business Media, **2009**, Kapitel 6, S. 157–176.

[70] M. Karpov, M. Laczka, P. S. Leboy, A. M. Osyczka, *J. Biomed. Mater. Res. A* **2008**, *84A*, 718–726.

[71] S. H. Maxian, J. P. Zawadsky, M. G. Dunn, *J. Biomed. Mater. Res.* **1993**, *27*, 717–728.

[72] P. Ducheyne, L. Hench, A. K. Il, M. Martens, A. Bursens, J. Mulier, *J. Biomed. Mater. Res.* **1980**, *14*, 225–237.

[73] O. D. Schneider, S. Loher, T. J. Brunner, L. Uebersax, M. Simonet, R. N. Grass, H. P. Merkle, W. J. Stark, *J. Biomed. Mater. Res. Part B: Appl. Biomater.* **2008**, *84B*, 350–362.

[74] D. Enlow, A. Rawal, M. Kanapathipillai, K. Schmidt-Rohr, S. Mallapragada, C.-T. Lo, P. Thiyagarajan, M. Akinc, *J. Mater. Chem.* **2007**, *17*, 1570–1578.

[75] F. Chen, Z.-C. Wang, C.-J. Lin, *Mater. Lett.* **2002**, *57*, 858–861.

[76] W. Linhart, F. Peters, W. Lehmann, K. Schwarz, A. F. Schilling, M. Amling, J. M. Rueger, M. Epple, *J. Biomed. Mater. Res.* **2001**, *54*, 162–171.

[77] L. Bjerre, C. E. Bünger, M. Kassem, T. Mygind, *Biomaterials* **2008**, *29*, 2616–2627.

[78] P. Chu, J. Chen, L. Wang, N. Huang, *Mater. Sci. Eng. R* **2002**, *36*, 143–206.

[79] L. Addadi, J. Moradian, E. Shay, N. Maroudas, S. Weiner, *Proc. Natl. Acad. Sci. USA* **1987**, *84*, 2732–2736.

[80] J. L. Arias, A. Neira-Carrillo, J. I. Arias, C. Escobar, M. Bodero, M. David, M. S. Fernandez, *J. Mater. Chem.* **2004**, *14*, 2154–2160.

[81] A. Steinbach, A. Tautzenberger, A. Schaller, A. Kalytta-Mewes, S. Tränkle, A. Ignatius, D. Volkmer, *Appl. Mater. Interfaces* **2012**, *4*, 5196–5203.

[82] F. Zhou, W. T. Huck, *Phys. Chem. Chem. Phys.* **2006**, *8*, 3815–3823.

[83] R. Konradi, J. Rühe, *Macromolecules* **2004**, *37*, 6954–6961.

[84] J. Rühe, M. Ballauff, M. Biesalski, P. Dziezok, F. Gröhn, D. Johannsmann, N. Houbenov, N. Hugenberg, R. Konradi, S. Minko, M. Motornov, R. R. Netz, M. Schmidt, C. Seidel, M. Stamm, T. Stephan, D. Usov, H. Zhang, *Adv. Polym. Sci.* **2004**, *165*, 79–150.

[85] M. M. Elmahdy, A. Synytska, A. Drechsler, C. Gutsche, P. Uhlmann, M. Stamm, F. Kremer, *Macromolecules* **2009**, *42*, 9096–9102.

[86] O. Prucker, R. Konradi, M. Schimmel, J. Habicht, I.-J. Park, J. Rühe, „Photochemical Strategies for the Preparation and Microstructuring of Densely Grafted Polymer Brushes on Planar Surfaces“ in *Polymer Brushes*, Wiley-VCH Verlag GmbH & Co. KGaA, **2005**, S. 449–469.

[87] Y. Mei, T. Wu, C. Xu, K. J. Langenbach, J. T. Elliot, B. D. Vogt, K. L. Beers, E. J. Amis, N. R. Washburn, *Langmuir* **2005**, *21*, 12309–12314.

[88] V. L. Osborne, D. M. Jones, W. T. Huck, *Chem. Commun.* **2002**, 1838–1839.

[89] S. Edmondson, V. L. Osborne, W. T. Huck, *Chem. Soc. Rev.* **2004**, *33*, 14–22.

[90] I. Luzinov, S. Minko, V. Senkovsky, A. Voronov, S. Hild, O. Marti, W. Wilke, *Macromolecules* **1998**, *31*, 3945–3952.

[91] M. D. Rowe-Konopacki, S. G. Boyes, *Macromolecules* **2007**, *40*, 879–888.

[92] S. Tugulu, H.-A. Klok, *Biomacromolecules* **2008**, *9*, 906–912.

[93] S. Tugulu, R. Barbey, M. Harms, M. Fricke, D. Volkmer, A. Rossi, H.-A. Klok, *Macromolecules* **2007**, *40*, 168–177.

[94] K. Matyjaszewski, P. J. Miller, N. Shukla, B. Immaraporn, A. Gelman, B. B. Luokala, T. M. Siclovan, G. Kickelbick, T. Vallant, H. Hoffmann, T. Pakula, *Macromolecules* **1999**, *32*, 8716–8724.

[95] N. Ballav, S. Schilp, M. Zharnikov, *Angew. Chem.* **2008**, *120*, 1443–1446.

[96] T. Wu, K. Efimenko, J. Genzer, *J. Am. Chem. Soc.* **2002**, *124*, 9394–9395.

[97] N. Cheng, O. Azzaroni, S. Moya, W. T. Huck, *Macromol. Rapid Commun.* **2006**, *27*, 1632–1636.

[98] N. Houbenov, S. Minko, M. Stamm, *Macromolecules* **2003**, *36*, 5897–5901.

[99] A. Ramakrishnan, R. Dhamodharan, R. Rühe, *J. Polym. Sci. A* **2006**, *44*, 1758–1769.

[100] Y. Lyatskaya, F. Leermakers, G. Fleer, E. Zhulina, T. Birshtein, *Macromolecules* **1995**, *28*, 3562–3569.

[101] E. Zhulina, T. Birshtein, *Macromolecules* **1995**, *28*, 1491–1499.

[102] Y. Tran, P. Auroy, L.-T. Lee, *Macromolecules* **1999**, *32*, 8952–8964.

[103] S. E. Moya, O. Azzaroni, T. Kelby, E. Donath, W. T. Huck, *J. Phys. Chem. B* **2007**, *111*, 7034–7040.

[104] S. Moya, O. Azzaroni, T. Farhan, V. L. Osborne, W. T. Huck, *Angew. Chem.* **2005**, *117*, 4654–4657.

[105] K. Lienkamp, L. Noé, M.-H. Breniaux, I. Lieberwirth, F. Groehn, G. Wegner, *Macromolecules* **2007**, *40*, 2486–2502.

[106] M. Biesalski, J. Rühe, *Macromolecules* **1999**, *32*, 2309–2316.

[107] J. Pyun, T. Kowalewski, K. Matyjaszewski, *Macromol. Rapid Comm.* **2003**, *24*, 1043–1059.

[108] K. Matyjaszewski, J. Xia, *Chem. Rev.* **2001**, *101*, 2921–2990.

[109] M. R. Buchmeiser, F. Sinner, M. Mupa, K. Wurst, *Macromolecules* **2000**, *33*, 32–39.

[110] B. Kong, J. K. Lee, I. S. Choi, *Langmuir* **2007**, *23*, 6761–6765.

[111] B. Zhao, W. J. Brittain, *Macromolecules* **2000**, *33*, 342–348.

[112] R. Advincula, Q. Zou, M. Park, S. Wang, J. Mays, G. Sakellariou, S. Pispas, N. Hadjichristidis, *Langmuir* **2002**, *18*, 8672–8684.

[113] X.-S. Wang, R. Jackson, S. Armes, *Macromolecules* **2000**, *33*, 255–257.

[114] D. M. Jones, W. T. Huck, *Adv. Mater.* **2001**, *13*, 1256–1259.

[115] A. Genua, J. Alduncín, J. Pomposo, H. Grande, N. Kehigias, V. Reboud, C. Sotomayor, I. Mondragon, D. Mecerreyes, *Nanotechnology* **2007**, *18*, 215301–1–215301–7.

[116] J.-B. Kim, M. L. Bruening, G. L. Baker, *J. Am. Chem. Soc.* **2000**, *122*, 7616–7617.

[117] J.-B. Kim, W. Huang, M. L. Bruening, G. L. Baker, *Macromolecules* **2002**, *35*, 5410–5416.

[118] W. Huang, J.-B. Kim, M. L. Bruening, G. L. Baker, *Macromolecules* **2002**, *35*, 1175–1179.

[119] B. Zhao, W. J. Brittain, W. Zhou, S. Z. Cheng, *Macromolecules* **2000**, *33*, 8821–8827.

[120] F. Limpoco, R. C. Advincula, S. S. Perry, *Langmuir* **2007**, *23*, 12196–12201.

[121] N. D. Treat, N. Ayres, S. G. Boyes, W. J. Brittain, *Macromolecules* **2006**, *39*, 26–29.

[122] S. Tugulu, M. Harms, M. Fricke, D. Volkmer, H.-A. Klok, *Angew. Chem.* **2006**, *118*, 7619–7623.

[123] W. S. Choi, H. Y. Koo, J. Y. Kim, W. T. Huck, *Adv. Mater.* **2008**, *20*, 4504–4508.

[124] G. Masci, D. Bontempo, N. Tiso, M. Diociaiuti, L. Mannina, D. Capitani, V. Crescenzi, *Macromolecules* **2004**, *37*, 4464–4473.

[125] M. M. Guerrini, B. Charleux, J.-P. Vairon, *Macromol. Rapid Commun.* **2000**, *21*, 669–674.

[126] Y. Li, S. P. Armes, X. Jin, S. Zhu, *Macromolecules* **2003**, *36*, 8268–8275.

[127] M. Ejaz, K. Ohno, Y. Tsujii, T. Fukuda, *Macromolecules* **2000**, *33*, 2870–2874.

[128] E. Ashford, V. Naldi, R. O'Dell, N. Billingham, S. Armes, *Chem. Commun.* **1999**, 1285–1286.

[129] K. A. Davis, K. Matyjaszewski, *Macromolecules* **2000**, *33*, 4039–4047.

[130] S. Chen, J. Zheng, L. Li, S. Jiang, *J. Am. Chem. Soc.* **2006**, *127*, 14473–14478.

[131] A. Goto, T. Fukuda, *Macromol. Rapid Comm.* **1999**, *20*, 633–636.

[132] U. Jonas, C. Krüger, *J. Supramol. Chem.* **2002**, *2*, 255–270.

[133] M. Ouchi, T. Terashima, M. Sawamoto, *Chem. Rev.* **2009**, *109*, 4963–5050.

[134] J.-S. Wang, K. Matyjaszewski, *J. Am. Chem. Soc.* **1995**, *117*, 5614–5615.

[135] H. Zhang, B. Klumperman, W. Ming, H. Fischer, R. van der Linde, *Macromolecules* **2001**, *34*, 6169–6173.

[136] K. Matyjaszewski, T. E. Patten, J. Xia, *J. Am. Chem. Soc.* **1997**, *119*, 674–680.

[137] H. Biederman, „Introduction“ in *Plasma Polymer Films* (Hrsg.: H. Biederman), Imperial College Press, **2004**, Kapitel 1, S. 13–24.

[138] R. Förch, Z. Zhang, W. Knoll, *Plasma Process. Polym.* **2005**, *2*, 351–372.

[139] H. Yasuda, *J. Polym. Sci. Macromol. Rev.* **1981**, *16*, 199–293.

[140] D. C. Guerin, D. D. Hinshelwood, S. Monolache, F. S. Dened, V. A. Shamamian, *Langmuir* **2002**, *18*, 4118–4123.

[141] T. Desmet, R. Morent, N. D. Geyter, C. Leys, E. Schacht, P. Dubruel, *Biomacromolecules* **2009**, *10*, 2351–2378.

[142] R. Daw, S. Candan, A. Beck, A. Devlin, I. Brook, S. MacNeil, R. Dawson, R. Short, *Biomaterials* **1998**, *19*, 1717–1725.

[143] R. B. Timmons, A. J. Griggs, „Pulsed Plasma Polymerizations“ in *Plasma Polymer Films* (Hrsg.: H. Biederman), Imperial College Press, **2004**, Kapitel 6, S. 217–245.

[144] D. E. Robinson, D. J. Buttle, J. D. Whittle, K. L. Parry, R. D. Short, D. A. Steele, *Plasma Process. Polym.* **2010**, *7*, 102–106.

[145] A. Holländer, J. Thome, „Degradation and Stability of Plasma Polymers“ in *Plasma Polymer Films* (Hrsg.: H. Biederman), Imperial College Press, **2004**, Kapitel 7, S. 247–277.

[146] R. Förch, A. N. Chifen, A. Bousquet, H. L. Khor, M. Jungblut, L.-Q. Chu, Z. Zhang, I. Osey-Mensah, E.-K. Sinner, W. Knoll, *Chem. Vap. Deposition* **2007**, *13*, 280–294.

[147] J. Alaerts, V. D. Cupere, S. Moser, P. van den Bosh de Aguilar, P. Rouxhet, *Biomaterials* **2001**, *22*, 1635–1642.

[148] H. Oonishi, H. Akiyama, M. Takemoto, T. Kawai, K. Yamamoto, T. Yamamuro, H. Oonishi, T. Nakamura, *Acta Orthop.* **2011**, *82*, 553–558.

[149] S. Santavirta, Y. T. Konttinen, V. Bergroth, M. Grönblad, *Acta Orthop. Scand.* **1991**, *62*, 29–32.

[150] T. B. Casserly, K. K. Gleason, *Chem. Vap. Deposition* **2006**, *12*, 59–66.

[151] M. Tanahashi, T. Yao, T. Kokubo, M. Minoda, T. Miyamoto, T. Nakamura, T. Yamamuro, *J. Appl. Biomater.* **1994**, *5*, 339–347.

[152] L. Brown, T. Koerner, J. H. Horton, R. D. Oleschuk, *Lab Chip* **2006**, *6*, 66–73.

[153] H. Varma, K. Sreenivasan, Y. Yokogawa, A. Hosumi, *Biomaterials* **2003**, *24*, 297–303.

[154] R. R. Shah, D. Merreceyes, M. Husemann, I. Rees, N. L. Abbott, C. J. Hawker, J. L. Hedrick, *Macromolecules* **2000**, *33*, 597–605.

[155] O. Prucker, M. Schimmel, G. Tovar, W. Knoll, J. Rühe, *Adv. Mater.* **1998**, *10*, 1073–1077.

[156] S. Schilp, N. Ballav, M. Zharnikov, *Angew. Chem.* **2008**, *120*, 6891–6894.

[157] A. I. Teixeira, G. A. Abrams, P. J. Bertics, C. J. Murphy, P. F. Nealy, *J. Cell Sci.* **2003**, *116*, 1881–1892.

[158] U. Schmelmer, A. Paul, A. Küller, M. Steenackers, A. Ulman, M. Grunze, A. Gölzhäuser, R. Jordan, *Small* **2007**, *3*, 459–465.

[159] H. Kitano, H. Suzuki, T. Kondo, K. Sasaki, S. Iwanaga, M. Nakamura, K. Ohno, Y. Saruwatari, *Macromol. Biosci.* **2011**, *11*, 557–564.

[160] A. E. Rapp, Diplomarbeit, Fakultät für Naturwissenschaften der Universität Ulm, **2010**.

[161] J. L. Charest, M. T. Eliason, A. J. García, W. P. King, *Biomaterials* **2006**, *27*, 2487–2494.

[162] M. Kaholek, W.-K. Lee, B. LaMattina, K. C. Caster, S. Zauscher, *Nano Lett.* **2004**, *4*, 373–376.

[163] F. Zhou, Z. Zheng, B. Yu, W. Liu, W. T.S.Huck, *J. Am. Chem. Soc.* **2006**, *128*, 16253–16258.

[164] W. Senaratne, L. Andruzzi, C. K. Ober, *Biomacromolecules* **2005**, *6*, 2427–2448.

[165] A. Jo, W. Joo, W.-H. Jin, H. Nam, J. K. Kim, *Nat. Nanotechnol.* **2009**, *4*, 727–731.

[166] H. Artelsmair, F. Kienberger, A. Tinazli, R. Schlapak, R. Zhu, J. Preiner, J. Wruss, M. Kastner, N. Saucedo-Zeni, M. Hölzl, C. Rankl, W. Baumgärtner, S. Howorka, D. Blaas, H. J. Grube, R. Tampé, P. Hinterdorfer, *Small* **2008**, *4*, 847–854.

[167] O. Azzaroni, S. E. Moya, A. A. Brown, Z. Zheng, E. Donath, W. T. Huck, *Adv. Funct. Mater.* **2006**, *16*, 1037–1042.

[168] A. Brock, E. Chang, C.-C. Ho, P. LeDuc, X. Jiang, G. Whitesides, D. Ingber, *Langmuir* **2003**, *19*, 1611–1617.

[169] H. Tu, C. E. Heitzman, P. V. Braun, *Langmuir* **2004**, *20*, 8313–8320.

[170] M. Lercel, H. Craighead, A. Parikh, K. Seshadri, D. Allara, *Appl. Phys. Lett.* **1996**, *68*, 1504–1506.

[171] F. Zhou, W. Liu, J. Hao, T. Xu, M. Chen, Q. Xue, *Adv. Funct. Mater.* **2003**, *13*, 938–942.

[172] S. A. Letsche, Dissertation, Fakultät für Naturwissenschaften der Universität Ulm, **2012**.

[173] M. Pluntke, Dissertation, Fakultät für Naturwissenschaften der Universität Ulm, **2012**.

[174] B. Kasemo, *Surf. Sci.* **2002**, *500*, 656–677.

[175] F. Xu, S. Zhong, L. Yung, E. Kang, K. Neoh, *Biomacromolecules* **2004**, *5*, 2392–2403.

[176] H. Yasuda, M. Gazicki, *Biomaterials* **1982**, *3*, 68–77.

[177] P. Favia, R. d'Agostino, *Surf. Coatings Techol.* **1998**, *98*, 1102–1106.

[178] Z. Yang, X. Lei, J. Wang, R. Luo, T. He, H. Sun, N. Huang, *Plasma Process. Polym.* **2011**, *8*, 208–214.

[179] W. Hinsberg, F. A. Houle, *J. Photopolym. Sci. Technol.* **2006**, *19*, 623–632.

[180] A. Steinbach, T. Paust, M. Pluntke, O. Marti, D. Volkmer, *ChemPhysChem* **2013**, *14*, 3523 – 3531.

[181] A. M. Steinbach, Masterarbeit, Fakultät für Naturwissenschaften der Universität Ulm, **2008**.

[182] K. Matyjaszewski, A. H. Müller, Naming of Controlled, Living and "Living" Polymerizations.

[183] K. Matyjaszewski, D. A. Shipp, J.-L. Wang, T. Grimaud, T. E. Patten, *Macromolecules* **1998**, *31*, 6836–6840.

[184] N. Cheng, A. A. Brown, O. Azzaroni, W. T. Huck, *Macromolecules* **2008**, *41*, 6317–6321.

[185] M. B. Huglin, M. A. Radwan, *Makromol. Chem.* **1991**, *192*, 2433–2445.

[186] R. R. Bhat, J. Genzer, B. N. Chaney, H. W. Sugg, A. Liebmann-Vinson, *Nanotechnology* **2003**, *14*, 1145–1152.

[187] S. Loschonsky, K. Shroff, A. Wörz, O. Prucker, J. Rühe, M. Biesalski, *Biomacromolecules* **2008**, *9*, 543–552.

[188] T. Farhan, O. Azzaroni, W. T. Huck, *Soft Matter* **2005**, *1*, 66–68.

[189] S. E. Moya, A. A. Brown, O. Azzaroni, W. T. Huck, *Macromol. Rapid Commun.* **2005**, *26*, 1117–1121.

[190] Y. Luo, F. J. Schork, *J. Polym. Sci. A* **2001**, *39*, 2696–2709.

[191] Z. Yan, Y. Luo, Y. Deng, J. Schork, *J. Appl. Polym. Sci.* **2004**, *91*, 347–353.

[192] D. M. Jones, A. A. Brown, W. T. Huck, *Langmuir* **2002**, *18*, 1265–1269.

[193] A. Schaller, personal communication, **2011**.

[194] P. Gijsman, G. Meijers, G. Vitarelli, *Polym. Degrad. Stability* **1999**, *65*, 433–441.

[195] S. Onari, *J. Phys. Soc. Jpn* **1969**, *26*, 500–504.

[196] A. H. Soeriyadi, V. Trouillet, F. Bennet, M. Bruns, M. R. Whittaker, C. Boyer, P. J. Barker, T. P. Davis, C. Barner-Kowollik, *J. Polym. Sci. A* **2012**, *50*, 1801–1811.

[197] O. Soppera, A. Dirani, A. Ponche, V. Roucoules, *Nanotechnology* **2008**, *19*, 395304–1–395304–9.

[198] A. I. Caplan, „Mesenchymal Stem Cells“ in *Handbook of Stem Cells*, *Bd. 2* (Hrsg.: R. Lanza, I. Weissman, J. Thomson, R. Pederson, B. Hogan, J. Gearhart, H. Blau, D. Melton, M. Moore, C. Verfaillie, E. D. Thomas, M. West), Elsevier Academic Press, **2004**, Kapitel 28, S. 299–308.

[199] M. F. Pittenger, A. M. Mackay, S. C. Beck, R. K. Jaiswal, R. Douglas, J. D. Mosca, M. A. Moorman, D. W. Simonetti, S. Craig, D. R. Marshak, *Science* **1999**, *284*, 143–147.

[200] A. Schäffler, C. Büchler, *Stem Cells* **2007**, *25*, 818–827.

[201] M. F. Pittenger, G. Mbalaviele, M. Black, J. D. Mosca, D. R. Marshak, „Mesenchymal Stem Cells“ in *Human Cell Culture*, *Bd. V* (Hrsg.: M. R. Koller, B. O. Palsson, J. R. Masters), Kluver Academic Publishers, **2001**, Kapitel 9, S. 189–207.

[202] M. Bernardo, M. Avanzini, C. Perotti, A. Cometa, A. Moretta, E. Lenta, C. del Fante, F. Novara, A. de Silvestri, G. Amendola, O. Zuffardi, R. Maccario, F. Locatelli, *J. Cell. Physiol.* **2007**, *211*, 121–130.

[203] S. Wakitani, T. Saito, A. I. Caplan, *Muscle Nerve* **1995**, *18*, 1417–1426.

[204] C. Capelli, M. Domenghini, G. Borleri, P. Bellavita, R. Poma, A. Carobbio, C. Micò, A. Rambaldi, J. Golay, M. Introna, *Bone Marrow Transpl.* **2007**, *40*, 785–791.

[205] E. Mackie, *Int. J. Biochem. Cell Biol.* **2003**, *35*, 1301–1305.

[206] J. Mahamid, A. Sharir, D. Gur, E. Zelzer, L. Addadi, S. Weiner, *J. Struct. Biol.* **2011**, *174*, 527–535.

[207] D. E. Cole, C. M. Gundberg, *Clin. Chim. Acta* **1985**, *151*, 1–7.

[208] M. D. McKee, A. Nanci, *Connect. Tiss. Res.* **1996**, *35*, 197–205.

[209] K. Horiuchi, N. Amizuka, S. Takeshita, H. Takamatsu, M. K. H. Ozawa, Y. Toyama, L. F. Bonewald, A. Kudo, *J. Bone Miner. Res.* **1999**, *14*, 1239–1249.

[210] J. Chen, H. S. Shapiro, J. L. Wrana, S. Reimers, J. N. Heersche, J. Sodek, *Matrix* **1991**, *11*, 133–143.

[211] J.-Y. Choi, B.-H. Lee, K.-B. Song, R.-W. Park, I.-S. Kim, K.-Y. Sohn, J.-S. Jo, H.-M. Ryoo, *J. Cell. Biochem.* **1996**, *61*, 609–618.

[212] H. Sudo, H.-A. Kodama, Y. Amagai, S. Yamamoto, S. Kasai, *J. Cell Biol.* **1983**, *96*, 191–198.

[213] H.-M. Kim, Y. Kim, S.-J. Park, C. Rey, H. Lee, M. J. Glimcher, J. S. Ko, *Biomaterials* **2000**, *21*, 1129–1134.

[214] K. Ogata, S. Imazato, A. Ehara, S. Ebisu, Y. Kinomoto, T. Nakano, Y. Umakoshi, *J. Biomed. Mater. Res. A* **2005**, *72A*, 127–135.

[215] K. M. Woo, V. J. Chen, P. X. Ma, *J. Biomed. Mater. Res. A* **2003**, *67A*, 531–537.

[216] T. Suda, I. Nakamura, E. Jimi, N. Takahashi, *J. Bone Miner. Res.* **1997**, *12*, 869–879.

[217] E. Eisenbarth, P. Linez, V. Biehl, D. Velten, J. Breme, H. Hildebrand, *Biomol. Eng.* **2002**, *19*, 233–237.

[218] J. H.-C. Wang, F. Jia, T. W. Gilbert, S. L.-Y. Woo, *J. Biomech.* **2003**, *36*, 97–102.

[219] F. Yu, F. Mücklich, P. Li, H. Shen, S. Mathur, C.-M. Lehr, U. Bakowsky, *Biomacromolecules* **2005**, *6*, 1160–1167.

[220] D. Zahor, A. Radko, R. Vago, L. Gheber, *Mater. Sci. Eng. C* **2007**, *27*, 117–121.

[221] R. Flemming, C. Murphy, G. Abrams, S. Goodman, P. Nealey, *Biomaterials* **1999**, *20*, 573–588.

[222] K. Chesmel, C. Clark, C. Brighton, J. Black, *J. Biomed. Mater. Res.* **1995**, *29*, 1101–1110.

[223] Y. Wan, Y. Wang, Z. Liu, X. Qu, B. Han, J. Bei, S. Wang, *Biomaterials* **2005**, *26*, 4453–4459.

[224] M. M. Stevens, J. H. George, *Science* **2005**, *310*, 1135–1138.

[225] J. Y. Lim, A. D. Dreiss, Z. Zhou, J. C. Hansen, C. A. Siedlecki, R. W. Hengstebeck, J. Cheng, N. Winograd, H. J. Donahue, *Biomaterials* **2007**, *28*, 1787–1797.

[226] K. L. Elias, R. L. Price, T. J. Webster, *Biomaterials* **2002**, *23*, 3279–3287.

[227] G. A. Dunn, *BioEssays* **1991**, *13*, 541–543.

[228] B. Zhu, Q. Lu, J. Yin, J. Hu, Z. Wang, *Tiss. Eng.* **2005**, *11*, 825–837.

[229] H. Kenar, A. Kocabas, A. Aydinli, V. Hasirci, *J. Biomed. Mater. Res. A* **2008**, *85A*, 1001–1010.

[230] M. Saito, S. Soshi, K. Fujii, *J. Bone Miner. Res.* **2003**, *18*, 1695–1705.

[231] C. Meier, M. E. Welland, *Biomacromolecules* **2011**, *12*, 3453–3459.

[232] M. J. Bühler, *Proc. ASME 2009 Int. Mech. Eng. Congress Exp.* **2009**, 795–798.

[233] S. Weiner, W. Traub, H. D. Wagner, *J. Struct. Biol.* **1999**, *126*, 241–255.

[234] P. Roach, D. Eglin, K. Rhode, C. C. Perry, *J. Mater. Sci. Mater. Med.* **2007**, *18*, 1263–1277.

[235] B. Kasemo, J. Gold, *Adv. Dent. Res.* **1999**, *13*, 8–20.

[236] B. G. Keselowsky, D. M. Collard, A. J. García, *J. Biomed. Mater. Res. A* **2003**, *66A*, 247–259.

[237] K. E. Healy, C. H. Thomas, A. Rezania, J. E. Kim, P. J. McKeown, B. Lom, P. E. Hockberger, *Biomaterials* **1996**, *17*, 195–208.

[238] Z. Zhang, S. Chen, Y. Chang, S. Jiang, *J. Phys. Chem. B* **2006**, *110*, 10799–10804.

[239] S. J. Sofia, V. Premnath, E. W. Merrill, *Macromolecules* **1998**, *31*, 5059–5070.

[240] T. McPherson, A. Kidane, I. Szleifer, K. Park, *Langmuir* **1998**, *14*, 176–186.

[241] M. E. Nash, D. Healy, W. M. Carroll, C. Elviry, Y. A. Rochev, *J. Mater. Chem.* **2012**, *22*, 19376–19389.

[242] M. D. Pierschbacher, E. Rouslahti, *Nature* **1984**, *309*, 30–33.

[243] K. Marcó, M. Ligeti, G. Mezö, N. Mihala, E. Kutnyánszky, É. Kiss, F. Hudecz, E. Madarász, *Bioconjugate Chem.* **2008**, *19*, 1757–1766.

[244] M. Navarro, E. M. Benetti, S. Zapotoczny, J. A. Planell, G. J. Vansco, *Langmuir* **2008**, *24*, 10996–11002.

[245] S. Tugulu, P. Silacci, N. Stergiopulos, H.-A. Klok, *Biomaterials* **2007**, *28*, 2536–2546.

[246] U. Geißler, U. Hempel, C. Wolf, D. Scharnweber, H. Worch, K.-W. Wenzel, *J. Biomed. Mater. Res.* **2000**, *51*, 752–760.

[247] K. Schröder, B. Finke, M. Polak, F. Lüthen, J. B. Nebe, J. Rychly, R. Bader, G. Lukowski, U. Walschus, M. Schlosser, A. Ohl, K.-D. Weltmann, *Mater. Sci. Forum* **2010**, *638–642*, 700–705.

[248] R. Daw, I. M. Brook, A. J. Devlin, R. D. Short, E. Cooper, G. J. Leggett, *J. Mater. Chem.* **1998**, *8*, 2583–2584.

[249] A. Grinevich, L. Bacakova, A. Choukourov, H. Boldyryeva, Y. Pihosh, D. Slavinska, L. Noskova, M. Skuciova, V. Lisa, H. Biederman, *J. Biomed. Mater. Res. A* **2009**, *88A*, 952–966.

[250] N. Krasteva, K. Hristova, E. Radeva, E. Pecheva, R. Dimitrova, L. Pramatarova, *AIP Conf. Proc.* **2010**, *1203*, 688–693.

[251] E. Radeva, L. Pramatarova, E. Pecheva, T. Hikov, E. Iacob, L. Vanzetti, R. Dimitrova, N. Krasteva, T. Spassov, D. Fingarova, *AIP Conf. Proc.* **2010**, *1203*, 949–954.

[252] H. Song, S. C. Jung, B. H. Kim, *Jpn. J. Appl. Physics* **2012**, *51*, 08HE01–1–08HE01–4.

[253] X. Cheng, H. E. Canavan, M. J. Stein, J. R. Hull, S. J. Kweskin, M. S. Wagner, G. A. Somorjai, D. G. Castner, B. D. Ratner, *Langmuir* **2005**, *21*, 7833–7841.

[254] D. Teare, D. Barwick, W. Schofield, R. Garrod, A. Beeby, J. Badyal, *J. Phys. Chem. B* **2005**, *109*, 22407–22412.

[255] T. Kokubo, H. Kushitani, S. Sakka, T. Kitsugi, T. Yamamuro, *J. Biomed. Mater. Res.* **1990**, *24*, 721–734.

[256] A. Dey, P. H. Bomans, F. A. Müller, J. Will, P. M. Frederik, G. de With, N. A. Sommerdijk, *Nat. Mater.* **2010**, *9*, 1010–1014.

[257] Y. Liu, E. B. Hunziker, „Biomimetic Coatings and Their Biological Functionalization“ in *Thin Calcium Phosphate Coatings for Medical Implants* (Hrsg.: B. León, J. A. Jansen), Springer Science+Business Media, **2009**, Kapitel 11, S. 301–314.

[258] E. S. Thian, S. M. Best, „Silicon-Substituted Hydroxyapatite Thin Films“ in *Thin Calcium Phosphate Coatings for Medical Implants* (Hrsg.: B. León, J. A. Jansen), Springer Science+Business Media, **2009**, Kapitel 8, S. 199–214.

[259] D.-M. Liu, Q. Yang, T. Troczynski, W. J. Tseng, *Biomaterials* **2002**, *23*, 1679–1687.

[260] S.-H. Oh, R. R. Finones, C. Daraio, L.-H. Chen, S. Jin, *Biomaterials* **2005**, *26*, 4938–4943.

[261] K. Tsuru, M. Kubo, S. Hayakawa, C. Ohtsuki, A. Osaka, *J. Ceram. Soc. Jpn* **2001**, *109*, 412–418.

[262] Q. Zhang, J. Chen, J. Feng, Y. Cao, C. Deng, X. Zhang, *Biomaterials* **2003**, *24*, 4741–4748.

[263] S. S. Sheiko, F. C. Sun, A. Randall, D. Shirvanyants, M. Rubinstein, H.-I. Lee, K. Matyjaszewski, *Nature* **2006**, *440*, 191–194.

[264] Y. Deng, X.-Y. Zhu, *J. Am. Chem. Soc.* **2007**, *129*, 7557–7561.

[265] A. Y. Fadeev, T. J. McCarthy, *Langmuir* **2000**, *16*, 7268–7274.

[266] M. J. Geerken, T. S. van Zanten, R. G. Lammertink, Z. Borneman, W. Nijdam, C. J. von Rijn, M. Wessling, *Adv. Eng. Mater.* **2004**, *6*, 749–754.

[267] A. Tautzenberger, Dissertation, Medizinische Fakultät der Universität Ulm, **2011**.

[268] U. M. Gross, D. Lassner, „In Vitro and In Vivo Evaluation of Thin Calcium Phosphate Coatings“ in *Thin Calcium Phosphate Coatings for Medical Implants* (Hrsg.: B. León, J. A. Jansen), Springer Science+Business Media, **2009**, Kapitel 4, S. 67–100.

[269] A. A. Deschamps, M. B. Claase, W. J. Sleijster, J. D. de Bruijn, D. W. Grijpma, J. Feijn, *J. Control. Release* **2002**, *78*, 175–186.

[270] A. J. Engler, S. Sen, H. L. Sweeney, D. E. Discher, *Cell* **2006**, *126*, 677–689.

[271] J. Zheng, L. Li, S. Chen, S. Jiang, *Langmuir* **2004**, *20*, 8931–8938.

[272] J. Zheng, L. Li, H.-K. Tsao, Y.-J. Sheng, S. Chen, S. Jiang, *Biophys. J.* **2005**, *89*, 158–166.

[273] L. Li, S. Chen, J. Zheng, B. D. Ratner, S. Jiang, *J. Phys. Chem. B* **2005**, *109*, 2934–2941.

[274] L. D. Unsworth, H. Sheardown, J. L. Brash, *Langmuir* **2005**, *21*, 1036–1041.

[275] N. Maroudas, *J. Theor. Biol.* **1975**, *49*, 417–424.

[276] R. Shelton, A. Rasmussen, J. Davies, *Biomaterials* **1988**, *9*, 24–29.

[277] R. Löbbicke, M. Chanana, H. Schlaad, C. Pilz-Allen, C. Günter, H. Möhwald, A. Taubert, *Biomacromolecules* **2011**, *12*, 3753–3760.

[278] D. Fischer, Y. Li, B. Ahlemeyer, J. Krieglstein, T. Kissel, *Biomaterials* **2003**, *24*, 1121–1131.

[279] D. M. Morgan, J. Clover, J. D. Pearson, *J. Cell Sci.* **1988**, *91*, 231–238.

[280] D. M. Morgan, V. L. Larvin, J. D. Pearson, *J. Cell Sci.* **1989**, *94*, 553–559.

[281] T. Ravikumar, H. Murata, R. R. Koepsel, A. J. Russell, *Biomacromolecules* **2006**, *7*, 2762–2769.

[282] H. J.-P. Ryser, *Nature* **1967**, *215*, 934–936.

[283] J. Davies, B. Causton, Y. Bovell, K. Davy, C. Sturt, *Biomaterials* **1986**, *7*, 231–233.

[284] C. H. Thomas, C. D. McFarland, M. L. Jenkins, A. Rezania, J. G. Steele, K. E. Healy, *J. Biomed. Mater. Res.* **1997**, *37*, 81–93.

[285] H. Winking, J. Gerdes, W. Traut, *Cytogenet. Genome Res.* **2004**, *105*, 251–256.

[286] N. Yahagi, H. Shimano, T. Matsuzaka, Y. Najima, M. Sekiya, Y. Nakagawa, T. Ide, S. Tomita, H. Okazaki, Y. Tamura, Y. Iizuka, K. Ohashi, T. Gotoda, R. Nagai, S. Kimura, S. Ishibashi, J. ichi Osuga, N. Yamada, *J. Biol. Chem.* **2003**, *278*, 25395–25400.

[287] C. M. Stanford, J. C. Keller, *Crit. Rev. Oral. Biol. Med.* **1991**, *2*, 83–101.

[288] Y. S. Kim, S. J. Birge, L. V. Avioli, R. Miller, *Calcif. Tiss. Int.* **1987**, *41*, 218–222.

[289] P. Schiller, G. d'Ippolito, W. Balkan, B. Roos, G. Howard, *Bone* **2001**, *28*, 362–369.

[290] T. Tsutsumimoto, S. Kawasaki, S. Ebara, K. Takaoka, *J. Bone Miner. Res.* **1999**, *14*, 1751–1760.

[291] D. Perizzolo, W. Lacefield, D. Brunette, *J. Biomed. Mater. Res.* **2001**, *56*, 494–503.

[292] M. Steenackers, R. Jordan, A. Küller, M. Grunze, *Adv. Mater.* **2009**, *21*, 2921–2925.

[293] F. Liu, B. Li, J. Sun, H. Li, B. Wang, S. Zhang, *Appl. Surf. Sci.* **2012**, *258*, 4322–4327.

[294] A. Meyer-Plath, K. Schröder, B. Finke, A. Ohl, *Vacuum* **2003**, *71*, 391–406.

[295] N. Marí-Buyé, S. O'Shaughnessy, C. Colominas, C. E. Semino, K. K. Gleason, S. Borrós, *Adv. Funct. Mater.* **2009**, *19*, 1276–1286.

[296] F. Anagnostou, A. Debet, G. Pavon-Djavid, Z. Goudaby, G. Hélary, V. Migonney, *Biomaterials* **2006**, *27*, 3912–3919.

[297] L. Wang, G. H. Nancollas, *Chem. Rev.* **2008**, *108*, 4628–4669.

[298] J. Christoffersen, M. R. Christoffersen, W. Kibalczyc, F. A. Andersen, *J. Cryst. Growth* **1989**, *94*, 767–777.

[299] F. Abbona, A. Baronnet, *J. Cryst. Growth* **1996**, *165*, 98–105.

[300] R. Boistelle, I. Lopez-Valero, *J. Cryst. Growth* **1990**, *102*, 609–617.

[301] F. Abbona, H. L. Madsen, R. Boistelle, *J. Cryst. Growth* **1986**, *74*, 581–590.

[302] M. S.-A. Johnsson, G. H. Nancollas, *Crit. Rev. Oral. Biol. Med.* **1992**, *3*, 61–82.

[303] V. R. Kodati, G. E. Tomasi, J. L. Turumin, A. T. Tu, *Appl. Spectrosc.* **1991**, *45*, 581–583.

[304] J. W. Murray, R. V. Dietrich, *Am. Miner.* **1956**, *41*, 616–626.

[305] L. J. Wang, J. W. Lu, F. S. Xu, F. S. Zhang, *Chinese Sci. Bull.* **2011**, *56*, 713–721.

[306] J. Mahamid, A. Sharir, L. Addadi, S. Weiner, *Proc. Natl. Am. Soc.* **2008**, *105*, 12748–12753.

[307] H. Yuan, Z. Yang, Y. Li, X. Zhang, J. de Bruijn, K. de Groot, *J. Mater. Sci. Mater. Med.* **1998**, *9*, 723–726.

[308] D. Volkmer, *Chem. Unserer Zeit* **1999**, *33*, 6–19.

[309] B. L. Smith, T. E. Schäffer, M. Viani, J. B. Thompson, N. A. Frederick, J. Kindt, A. Belcher, G. D. Stucky, D. E. Morse, P. K. Hansma, *Nature* **1999**, *399*, 761–763.

[310] A. Belcher, X. Wu, R. Christensen, P. Hansma, G. Stucky, D. Morse, *Nature* **1996**, *381*, 56–58.

[311] G. Falini, S. Albeck, S. Weiner, L. Addadi, *Science* **1996**, *271*, 67–69.

[312] S. Weiner, L. Addadi, *J. Mater. Chem.* **1997**, *7*, 689–702.

[313] J.-H. Bradt, M. Mertig, A. Teresiak, W. Pompe, *Chem. Mater.* **1999**, *11*, 2694–2701.

[314] A. L. Boskey, *Connect. Tiss. Res.* **1996**, *35*, 357–363.

[315] H. Cölfen, *Nat. Mater.* **2010**, *9*, 960–961.

[316] F. Nudelman, K. Pieterse, A. George, P. H. Bomans, H. Friedrich, L. J. Brylka, P. A. Hilbers, G. de With, N. A. Sommerdijk, *Nat. Mater.* **2010**, *9*, 1004–1009.

[317] A. Tsortos, G. H. Nancollas, *J. Colloid Interf. Sci.* **2002**, *250*, 159–167.

[318] G. K. Hunter, P. V. Hauschka, A. R. Poole, L. C. Rosenberg, H. A. Goldberg, *Biochem. J.* **1996**, *317*, 59–64.

[319] H. Jiang, X.-Y. Liu, G. Zhang, Y. Li, *J. Biol. Chem.* **2005**, *280*, 42061–42066.

[320] A.-W. Xu, Y. Ma, H. Cölfen, *J. Mater. Chem.* **2007**, *17*, 415–449.

[321] T. Gao, T. Lindholm, A. Marttinen, M. Urist, *Int. Orthop.* **1996**, *20*, 321–325.

[322] W. Traub, T. Arad, S. Weiner, *Proc. Natl. Acad. Sci. USA* **1989**, *86*, 9822–9826.

[323] S. Gajjeraman, K. Narayanan, J. Hao, C. Qin, A. George, *J. Biol. Chem.* **2007**, *282*, 1193–1204.

[324] G. He, S. Gajjeraman, D. Schultz, D. Cookson, C. Qin, W. T. Butler, J. Hao, A. George, *Biochemistry* **2005**, *44*, 16140–16148.

[325] H. Lowenstam, S. Weiner, *Science* **1985**, *227*, 51–53.

[326] A. Posner, F. Betts, N. Blumenthal, *Metab. Bone Dis. & Rel. Res.* **1978**, *1*, 179–183.

[327] L. B. Gower, D. J. Odom, *J. Cryst. Growth* **2000**, *210*, 719–734.

[328] M. J. Olszta, D. J. Odom, E. P. Douglas, L. B. Gower, *Connect. Tiss. Res.* **2003**, *44 (Suppl. 1)*, 326–334.

[329] W. Kibalczyc, K. Bondarczuk, *J. Cryst. Growth* **1985**, *71*, 751–756.

[330] J. Harries, D. Hukins, C. Holt, *J. Cryst. Growth* **1987**, *84*, 563–570.

[331] E. Eanes, J. Meyer, *Calcif. Tiss. Res.* **1977**, *23*, 259–269.

[332] J. Meyer, E. Eanes, *Calcif. Tiss. Res.* **1978**, *25*, 59–68.

[333] L. Gerstenfeld, J. Lian, Y. Gotoh, D. Lee, W. Landis, M. McKee, A. Nanci, M. Glimcher, *Connect. Tiss. Res.* **1989**, *21*, 215–225.

[334] D. H. Carter, P. V. Hatton, J. E. Aaron, *Histochem. J.* **1997**, *29*, 783–793.

[335] J. E. Aaron, *Calcif. Tiss. Res.* **1973**, *12*, 259–279.

[336] C. Gay, V. Gilman, T. Sugiyama, *Poultry Sci.* **2000**, *79*, 1005–1008.

[337] H. Zeng, W. R. Lacefield, *Biomaterials* **2000**, *21*, 23–30.

[338] Y. Yang, K.-H. Kim, J. L. Ong, *Biomaterials* **2005**, *26*, 327–337.

[339] C. Mao, H. Li, F. Cui, Q. Feng, C. Ma, *J. Mater. Chem.* **1999**, *9*, 2573–2582.

[340] M. Mastrogiacomo, A. Muraglia, V. Komlev, F. Peyrin, F. Rustichelli, A. Crovace, R. Cancedda, *Orthod. Craniofacial Res.* **2005**, *8*, 277–284.

[341] M. A. Hardenbrook, S. R. Lombardo, *Neurosurg. Focus* **2006**, *21*, E9/1–E9/5.

[342] C. L. Camiré, S. J. Saint-Jean, C. Mochales, P. Nevsten, J.-S. Wang, L. Lidgren, I. McCarthy, M.-P. Ginebra, *J. Biomed. Mater. Res. Part B: Appl. Biomater.* **2006**, *76B*, 424–431.

[343] E. Mueller, C. S. Sikes, *Calcif. Tiss. Int.* **1993**, *52*, 34–41.

[344] J. Birchall, R. Davey, *J. Cryst. Growth* **1981**, *54*, 323–329.

[345] J. Termine, A. Posner, *Arch. Biochem. Biophys.* **1970**, *140*, 307–317.

[346] S. Mann, B. R. Heywood, S. Rajam, J. D. Birchall, *Nature* **1988**, *334*, 692–695.

[347] H. Lu, C. Ma, H. Cui, L. Zhou, R. Wang, F. Cui, *J. Cryst. Growth* **1995**, *155*, 120–125.

[348] M. Fricke, D. Volkmer, *Top. Curr. Chem.* **2007**, *270*, 1–41.

[349] D. Volkmer, M. Fricke, C. Agena, J. Mattay, *Cryst. Eng. Comm.* **2002**, *4*, 288–295.

[350] D. Volkmer, M. Fricke, D. Vollhardt, S. Siegel, *J. Chem. Soc. Dalton Trans.* **2002**, 4547–4554.

[351] D. Volkmer, M. Fricke, *Z. Anorg. Allg. Chem.* **2003**, *629*, 2381–2390.

[352] D. Volkmer, M. Fricke, M. Gleiche, L. Chi, *Mater. Sci. Eng. C* **2005**, *25*, 161–167.

[353] D. Volkmer, M. Harms, L. Gower, A. Ziegler, *Angew. Chem.* **2005**, *117*, 645–650.

[354] D. Volkmer, M. Harms, L. B. Gower, A. Ziegler, *Angew. Chem. Int. Ed.* **2005**, *44*, 639–644.

[355] F. F. Amos, D. M. Sharbaugh, D. R. Talham, L. B. Gower, M. Fricke, D. Volkmer, *Langmuir* **2007**, *23*, 1988–1994.

[356] D. Volkmer, M. Fricke, T. Huber, N. Sewald, *Chem. Commun.* **2004**, 1872–1873.

[357] H. Gong, M. Pluntke, O. Marti, P. Walther, L. B. Gower, H. Cölfen, D. Volkmer, *Colloids Surf. A: Physicochem. Eng. Aspects* **2010**, *354*, 279–283.

[358] K. Malinova, M. Gunesch, S. M. Pancera, R. Wengeler, B. Rieger, D. Volkmer, *J. Colloid Interf. Sci.* **2012**, *374*, 61–69.

[359] O. Casse, O. Colombani, K. Kita-Tokarczyk, A. H. Müller, W. Meier, A. Taubert, *Faraday Discuss.* **2008**, *139*, 1–20.

[360] S. Suzuki, M. R. Whittaker, L. Grondahl, M. J. Monteiro, E. Wentrup-Byrne, *Biomacromolecules* **2006**, *7*, 3178–3187.

[361] O. Azzaroni, A. A. Brown, N. Cheng, A. Wei, A. M. Jonas, W. T. Huck, *J. Mater. Chem.* **2007**, *17*, 3433–3439.

[362] S. G. Boyes, B. Akgun, W. J. Brittain, M. D. Foster, *Macromolecules* **2003**, *36*, 9539–9548.

[363] P. Ngankam, P. Lavalle, J. Vögel, L. Szyk, G. Decher, P. Schaaf, F. Cuisinier, *J. Am. Chem. Soc.* **2000**, *122*, 8998–9005.

[364] J. Termine, R. Peckauskas, A. Posner, *Arch. Biochem. Biophys.* **1970**, *140*, 318–325.

[365] B. Fowler, E. Moreno, W. Brown, *Arch. Oral Biol.* **1966**, *11*, 477–492.

[366] A. Zeller, Dissertation, Fakultät für Naturwissenschaften der Universität Ulm, **2010**.

[367] A. Ziegler, K. Landfester, A. Musyanovych, *Colloid Polym. Sci.* **2009**, *287*, 1261–1271.

[368] V. Holzapfel, A. Musyanovych, K. Landfester, M. R. Lorenz, V. Mailänder, *Macromol. Chem. Physic.* **2005**, *206*, 2440–2449.

[369] T. M. Allen, P. R. Cullis, *Science* **2004**, *303*, 1818–1822.

[370] R. Gage, E. Currie, M. C. Stuart, *Macromolecules* **2001**, *34*, 5078–5080.

[371] K. C. Grabar, P. C. Smith, M. D. Musick, J. A. Davis, D. G. Walter, M. A. Jackson, A. P. Guthrie, M. J. Natan, *J. Am. Chem. Soc.* **1996**, *118*, 1148–1153.

[372] Z. Liu, K. Pappacena, J. Cerise, J. Kim, C. J. Durning, B. O'Shaughnessy, R. Levicky, *Nano Lett.* **2002**, *2*, 219–224.

[373] K. M. Chen, X. Jiang, L. C. Kimerling, P. T. Hammond, *Langmuir* **2000**, *16*, 7825–7834.

[374] H. Zheng, I. Lee, M. F. Rubner, P. T. Hammond, *Adv. Mater.* **2002**, *14*, 569–572.

[375] J. U. Kim, B. O'Shaughnessy, *Phys. Rev. Lett.* **2002**, *89*, 238301–1–238301–4.

[376] A. Ashkin, J. Dziedzic, J. Bjorkholm, S. Chu, *Opt. Lett.* **1986**, *11*, 288–290.

[377] M. M. Elmahdy, A. Drechsler, C. Gutsche, A. Synytska, P. Uhlmann, F. Kremer, M. Stamm, *Langmuir* **2009**, *25*, 12894–12898.

[378] T. Abe, S. Hayashi, N. Higashi, M. Niwa, K. Kurihara, *Colloids Surf. A: Physicochem. Eng. Aspects* **2000**, *169*, 351–356.

[379] S. R. Wasserman, Y.-T. Tao, G. M. Whitesides, *Langmuir* **1989**, *5*, 1074–1087.

[380] Hamamatsu, *Spot light source Lightningcure Series – LC8*.

[381] T. Serizawa, H. Takeshita, M. Akashi, *Langmuir* **1998**, *14*, 4088–4094.

[382] T. Paust, Dissertation, Fakultät für Naturwissenschaften der Universität Ulm, **2013**.

[383] H.-J. Jacobasch, F. Simon, P. Weidenhammer, *Colloid Polym. Sci.* **1998**, *276*, 434–442.

Danksagung

Zuerst gilt mein Dank Prof. Dr. Dirk Volkmer für die Möglichkeit, an diesem interdisziplinären und vielseitigen Thema zu arbeiten. Diese Art der Arbeit an der Schnittstelle der Disziplinen ist mir sehr entgegen gekommen, genauso wie die Freiheit und Eigenständigkeit, die ich dabei hatte. Ich habe während der Doktorarbeit viel gelernt und konnte mich auch persönlich weiter entwickeln.

Ebenso möchte ich Frau Prof. Dr. Anita Ignatius für die gute Kooperation über die gesamte Zeit meiner Doktorarbeit und für die Übernahme des Zweitgutachtens danken. Ohne sie wäre der Bezug zur biomedizinischen Anwendung der Materialien nicht möglich gewesen. Ihre konstruktive Kritik und Anmerkungen zu den gemeinsamen Veröffentlichungen waren immer äußerst hilfreich und zielführend.

Im Rahmen eines Projekts wurde ich durch die Landesstiftung Baden-Württemberg unterstützt. Vom Land Baden-Württemberg habe ich zeitweise großzügigerweise ein Stipendium im Rahmen des Landesgraduiertenförderungsgesetzes (LGFG) erhalten.

Vielen Dank an Anke Zeller und Andrea Tautzenberger für die immer gute und reibungslose Zusammenarbeit im Projekt. Besonderen Dank an Andrea, Kollega, für die große Unterstützung bei den gemeinsamen Veröffentlichungen, dafür, dass ich mich immer auf sie, ihre Pünktlichkeit und Gründlichkeit verlassen konnte, und vor allem für ihre Freundschaft (Dienstgespräche!).

Sabine Letsche möchte ich für die gute Laborgemeinschaft in Ulm danken, die vielen Sachen, die sie mir über die Bürstchen beigebracht hat und die lustigen Hitparaden-Tage. Manuela Pluntke danke ich für unzählige Messungen, nette Abende vor dem AFM mit viel Schokolade und ihre unkomplizierte, engagierte Art. Tobias Paust möchte ich für die Messungen mit der Laserfalle danken (vor allem weil es schwieriger und aufwändiger war als erwartet) die Unterstützung bei der gemeinsamen Veröffentlichung und die Bereitschaft, mir wirklich zu erklären, was und wie er gemessen hat. Natürlich gilt mein Dank auch der restlichen Ulmer Truppe, die hier nicht unerwähnt bleiben darf, weil sie ihren Beitrag geleistet haben, indem sie für Ausgleich gesorgt haben, ein offenes Ohr hatten, mich auf Yoga gebracht haben, Zeit für ein gemeinsames Bierchen oder zum Quatschen hatten oder einfach zu Blödsinn aufgelegt waren: Petra Murszat, Heidi Seitz, Kalina Malinova, Markus Tonigold, Stefan Henne...

Ein besonderer Dank geht an die Studenten, die bei mir Praktikum, Kochmagd oder Abschlussarbeiten gemacht haben: Larissa Miller, Jessica Thomas, Marwa Tallawi, Anna Rapp und Jacob Podschun. Larissa und Jessica verdienen ein riesiges Dankeschön für ihre Wochen an der Mineralisationspumpe, in denen sie mir ein gutes Stück weiter geholfen haben, den Parameterraum abzuklopfen. Anna und Jacob gilt mein Dank, weil es eine Freude war, sie bei ihren hervorragenden Arbeiten zu unterstützen – was ich hoffentlich getan habe. Ich hoffe, alle konnten etwas lernen. Ich konnte es auf jeden Fall.

Vielen Dank für die Unterstützung an die zentrale Einrichtung Elektronenmikroskopie in Ulm, an Oliver Wiltschka für ζ-Potentialmessungen, an Elisabeth Lachner und Ray Frenzel für XPS-Messungen, besonders für die in letzter Minute (also alle...).

Herzlichen Dank an die Augsburger Arbeitsgruppe: Jan Hanss, der in der Umzugs- und Eingewöhnungsphase in Augsburg eine unverzichtbare Hilfe war und einfach eine Institution und ein Original, Andreas Kalytta-Mewes für seine Arbeit an der Plasmaanlage, von der ich profitiert habe, und für seine ruhige, unkomplizierte Art, die immer gut getan hat. Vielen Dank an Sebastian Tränkle für AFM- und TEM-Messungen und an Benjamin Baumgärtner für ESEM-Aufnahmen. Danke für die gute Gemeinschaft an die bereits genannten, an Andreas Schaller, Stefan Braun, Sebastian Spirkl, Tamas Werner, Björn Bredenkötter, Maciej Grzywa, Phillip Schmieder, Dmytro Denysenko, Karolina Kazmierczak, Katharina Förg, Stephan Jantz, Peter Gross und Stefan Riegg (Uff, hab ich jemanden vergessen?). Die gemeinsamen Mittags- und Kaffee- oder besser: Schokolade-Pausen waren lustig und schön und ich habe sie genossen. Danke an alle! Vor allem an die Klugscheisser-Pubquiz-Runden (ja, Tamas! Ich hoffe, der Respektonen-Nachweis gelingt bald...) und die Trash-Videoabend-Crew! Besonders möchte ich Katha, Stuff und Andy danken, weil sie mit offenen Ohren und breiten Schultern (Also im übertragenen Sinn jetzt, Katha! Stuff, Andy, ihr könnt das wörtlich nehmen.) da waren, als es mir nicht gut ging.

Andy habe ich einen eigenen Absatz versprochen... Hat er auch verdient als Labor-Schatzi – für eine super Laborgemeinschaft, für seine Arbeit an der Plasmaanlage, für seinen guten (=rockigen) Musikgeschmack, für Sekretariat, für Gespräche über Kampfkunst und die Pflege langer Haare, über Probleme und alles, was uns gerade beschäftigt hat. Ich denke, wir waren ein gutes Team, was das Schreiben und Überarbeiten von Papern, Praktikumsvorbereitung und -Betreuung, Protokollkorrektur und die Organisation des Labors inklusive des Musikprogramms anging. Danke!

Ganz herzlich danken möchte ich hier auch dem Team von UniMento, vor allem Anna Lödermann und Katharina Scharrer, meiner Peer Group Christina Kunzmann, Jasmin Seitz und Karin Bee und meinem Mentor Prof. Anthony Unwin. Der Austausch und die Unterstützung haben mich weiter gebracht und mir die Augen geöffnet, in welche Richtung ich gehen möchte.

Ganz lieben Dank an alle Freunde, die da waren und sind. Danke auch Bene für die Strecke, die er mich begleitet hat.

Danke an meine Familie für die Unterstützung und die Sicherheit, dass trotz Höhen und Tiefen immer jemand da ist, auch wenn es nicht immer leicht ist.

Weiterhin gilt mein Dank PhD Comics, den Webradios fm4, rock nation, kx radio und 96,3 rock radio mit ihrer guten Musik und knuddeligen Sprachen, und anderen Wissenschaftlern, die in ihren Veröffentlichungen Humor zeigen und so den Labor- und Schreiballtag aufhellen. Stellvertretend seien hier Kitano *et al.*[159] genannt. (Herzchen!!!) Sie haben meine Moral und Motivation aufrecht gehalten.

Publikationsliste

Sabine A. Letsche, Annina M. Steinbach, Manuela Pluntke, Othmar Marti, Anita Ignatius, Dirk Volkmer; "Usage of polymer brushes as substrates of bone cells" *Front. Mater. Sci. China*, **2009**, *3*, 132–144.

Annina Steinbach, Andrea Tautzenberger, Anita Ignatius, Manuela Pluntke, Othmar Marti, Dirk Volkmer; "Coatings from micropatterned sulfobetaine polymer brushes as substrates for MC3T3-E1 cells" *J. Mater. Sci. Mater. Med.*, **2012**, *23*, 573–579.

Annina Steinbach, Andrea Tautzenberger, Andreas Schaller, Andreas Kalytta-Mewes, Sebastian Tränkle, Anita Ignatius, Dirk Volkmer; "Plasma-Enhanced Chemical Vapor Deposition of *n*-Heptane and Methyl Methacrylate for Potential Cell Alignment Applications" *Appl. Mater. Interfaces*, **2012**, *4*, 5196–5203.

Annina Steinbach, Tobias Paust, Manuela Pluntke, Othmar Marti, Dirk Volkmer; "Selective Adsorption of Functionalized Nanoparticles to Patterned Polymer Brush Surfaces and its Probing with an Optical Trap" *ChemPhysChem*, **2013**, *14*, 3523–3531